The Development of a Knowledge-Based Wax Deposition, Three Yield Stresses Model and Failure Mechanisms for Re-starting Petroleum Field Pipelines

Building on Chang and Boger's Yield Stresses Model, Bidmus and Mehrotra's Wax Deposition and Lee et al.'s Adhesive-Cohesive Failure Concepts to better Underpin Restart Operation of Waxy Crude Oil Pipelines

Abubaker Ahmed FAKROUN

Submitted for the Degree of Doctor of Philosophy

Faculty of Engineering and Informatics

University of Bradford

2017

ABSTRACT

Abubaker Ahmed Fakroun

The Development of a Knowledge-Based Wax Deposition, Three Yield Stresses Model and Failure Mechanisms for Re-starting Petroleum Field Pipelines

Building on Chang and Boger's Yield Stresses Model, Bidmus and Mehrotra's Wax Deposition and Lee et al.'s Adhesive-Cohesive Failure Concepts to better Underpin Restart Operation of Waxy Crude Oil Pipelines

Keywords; Elasticity, yield stresses model, wax deposition, effective yield stress, waxy crude oil, failure acceleration, pipeline restart, adhesive-cohesive failure, crystallisation, morphology.

Twenty years ago, Chang et al. (1998) introduced the three-yield stresses concept (dynamic, static and elastic limits) to describe yielding of waxy crude oils cooled below the wax appearance temperature (WAT). At the time, the limits in rheological instruments were such that they never actually measured the elastic-limit, a key fundamental property. Using modern instruments, this research succeeds in recording for the first time the entire yielding process down to stresses of 10^{-7} Pa and shear rate of 10^{-6} min^{-1} as a function of temperature, cooling rate and stress loading rate using two waxy oils of different origins and wax content. A four-yield stress model is established using derivative data (dynamic fluidity and failure acceleration). In addition, calorimetry (DSC) and microscopy (CPM) helped extract WAT, the gel and pour points and link gel crystal structure and its yielding and breakage to rheological properties.

The yielding stresses measured rheologically were tested in laboratory pipelines at two diameter scales, 6.5mm and 13.5mm to compare stresses in uniform and non-uniform cooling. It is demonstrated that rheological instruments can only predict gel breaking pressure when the cooling rate is low, i.e. yielding at

the pipe wall. A complementary heat transfer study was performed on a section of pipe statically cooled, both experimentally and theoretically to predict the gel front-liquid oil interface that develops in industrial pipeline where gel breaking occurs. This key information together with rheological data provide the means to predict accurately restart pressures of shut gelled pipelines that have eluded previous research.

ACKNOWLEDGEMENTS

I am grateful and would like to express my sincere gratitude and appreciation to my supervisor Professor H. Benkreira for his invaluable guidance and encouragement throughout my research study and teaching me to look for what is scientifically relevant. I am very thankful to him for his professional research philosophy; our discussions and his feedback have made me sure that we would accomplish a nice work.

I would like to thank Dr Tim Gough and Dr Raj Patel for their assistance with experimental aspects of this research.

I would like to thank in a special way my friends; Sudgi Elsadi, Atif Khan, Richard Alpin, Sree Sreedhara, Yusuke Shibata and Fathia Elbishti for their support and words of encouragement. We have had enlightening discussions with intelligent ideas to improve my work

I would like to thank the Ministry of Higher Education of the Libyan Government for sponsoring me for my PhD research study at the University of Bradford. I also would like to thank the National Oil Corporation (NOC) of Libya for providing me with the oil samples, necessary for this research.

Above all, I would like to thank my parents for their continuous support and prayers for me and many thanks for my wife, Sanbula, for her patience, love, encouragement and unlimited support.

Table of Contents

List of Figures

List of Tables

NOMENCLATURE

A	Cross sectional area, mm^2
CSR	Control Shear Rate Rheometer
CSS	Control Shear Stress Rheometer
CPM	Cross-polarised Microscope
C_p	Specific heat capacity, KJ kg^{-1} $^0C^{-1}$
C_{wax}	Wax concentration, wt. %
CCN	Critical Carbon Number
D	Diameter of pipeline, mm
DSC	Differential Scanning Calorimeter
EVP	Elastic-Visco-Plastic flow behaviour
F	Force, Pa
G'	Elastic modulus, Pa
G"	Viscous modulus, Pa
H_w	Latent heat of wax crystallised phase vs. dimensionless temperature
H	The Gap between two plates, mm
h	Heat transfer coefficient, W m^{-2} K^{-1}
ID	Internal diameter, mm
ICF	Incoming fluid
K	Thermal conductivity, W m^{-1} K^{-1}
L	Pipeline length, m
LVE	Linear Viscoelastic range
MCR	Modular Compact Rheometers
MPT	Model Pipeline Technique
N	Cone rotational speed
n	non-Newtonian index
Nu	Nusselt number
OGF	Outgoing fluid
P	Pressure, Pa or psi

PPT	Pour point temperature, ºC
Q	Volumetric Flow rate, ml/sec
R_a	Absolute roughness, mm
r_i	Radial location of the liquid–deposit interface, m
R_c	Cohesive strength radius, mm
R_{ye}	Effective yielding radius, mm
T	Temperature, ^oC
$\dot{T}$	Cooling rate, ^oC/min
T_s	Deposit layer temperature, ^oC
T_d	Liquid–deposit interface temperature interface, ^oC
T_l	Average liquid region temperature, ^oC
T_{wall}	Internal wall temperature, ^oC
T_L	Liquidus temperature, °C
t	Time, sec
T_{gel}	Gel point temperature, ºC
Ti	Initial temperature, ºC
V	Volume, mL
WAT	Wax appearance temperature, ºC
WDT	Wax disappearance temperature, ºC
$x_{w,s}$	Solid phase mass fraction in the deposit
$x_{w,l}$	Solid phase mass fraction suspended in the liquid
$x_{w,i}$	Mass fraction of solid-phase at liquid-deposit interface
$X_{w,s}$	Solid phase mass fraction in the deposit vs. dimensionless temperature
$X_{w,l}$	Solid phase mass fraction suspended in the liquid vs. dimensionless temperature
$X_{w,i}$	Mass fraction of solid-phase at liquid-deposit interface vs. dimensionless temperature

Greek Symbols

τ	Shear stress, Pa

τ_y	Yield stress, Pa
τ_e	Elastic-limit yield stress, Pa
τ_s	Static yield stress, Pa
τ_f	Fracture yield stress, Pa
τ_d	Dynamic yield stress, Pa
$\tau_{y,w}$	Adhesive yield stress, Pa
$\tau_{y,c}$	Cohesive yield stress, Pa
$\tau_{y,e}$	Effective yield stress, Pa
$\dot{\tau}$	Stress Loading rate, Pa/min
$\dot{\gamma}$	Shear rate, s^{-1}
μ	Newtonian viscosity, Pa.s
μ_p	Bingham plastic viscosity, Pa.s
δ	Deposit thickness, mm
α_l	Liquid phase thermal diffusivity, $m^2\ s^{-1}$
α_s	Deposit phase thermal diffusivity, $m^2\ s^{-1}$
α'	Apparent thermal diffusivity, $m^2\ s^{-1}$
ρ	Density, kg m^{-3}
λ	Latent heat of wax crystallised phase transformation, J g^{-1}

1. INTRODUCTION

1.1 Introduction

Crude oil or petroleum is a naturally occurring hydrocarbon which has over the past century completely transformed our way of life, providing fuels for cars, ships and planes as well as to generate electricity to run billions of homes and millions of industrial plants throughout the world. Crude oil is also the source of important chemicals that go in the manufacture of paints, adhesives, plastics, pharmaceuticals, pesticides, fertilizers, solvents and many other materials. The amount of crude oil the world consumes is staggering, 95 million barrels each day. As oil is buried underground, often in remote areas (under the sea in the North Sea, under the ice in northern Canada and Russia and in the deserts of the Middle East and North Africa), it has to be transported in very long pipelines (typical pipelines are over 1000 miles long). Pumping of oil is thus a big business and critical to the supply and cost of oil. *This is precisely the concern of this thesis- how to optimize pumping requirement in pipeline carrying oil, waxy crude oil in particular as explained later.*

Crude oil in its natural state is made up essentially (more than 93% typically) of hydrocarbons hot liquids, mostly alkanes (Paraffins), cycloalkanes (Naphthenes), aromatic and asphaltic hydrocarbons. The hot state is due to the fact that these hydrocarbons form deep into the earth where the temperature is high (on the average, the temperature rises 1°C for every 33 m of depth [1]). In some fields, some of the Paraffins and Naphthenes rather than being linear in conformation, form branched and cyclic structures, known as wax [2, 3]. Deep in the oil reservoirs, the wax is dissolved into the rest of the hydrocarbon mass, both of which are hot and in a liquid state. Waxy crude oils are found in many fields, the North Sea, China, Australia, the Middle East and Libya. *This thesis bases its work on waxy crude oils sourced from fields in the North Sea (BP) and Libya (Libyan Oil Corporation, the sponsor of this study*).

Now, waxy crude oils clearly have to be pumped hot, above what is known as WAT or the temperature at which the wax appears and precipitates out of the rest of the liquid hydrocarbons into a solid crystalline structure. When by accident for example following a break down in power that maintains the oil hot or during maintenance work of pipelines or new equipment installation when heating is turned off, the waxy crude oil, now static in the pipeline, will cool, causing the wax to precipitate first on the cool wall of the pipeline and then gradually across the section of the pipe. In time, through diffusion, wax crystals accumulate near the wall to eventually form a wax deposit core. If the pipeline is not re-started back, this core will age, becomes harder as crystal wax networks build reducing the pipe diameter and decreasing its flow efficiency as illustrated in Figure 1.1.1. In the extreme and when the wax content of the oil is large, the entire cross section is blocked. Such situations are frequent and very costly to the oil industry [4, 5, 6]. An example of this was reported by the UK Lasmo Company which abandoned a platform costing $100 million as a result of the frequent wax deposition problems in the pipelines [5]. A further example reports that in the Gulf of Mexico 14 pipelines had to be unplugged because of such problems [6].

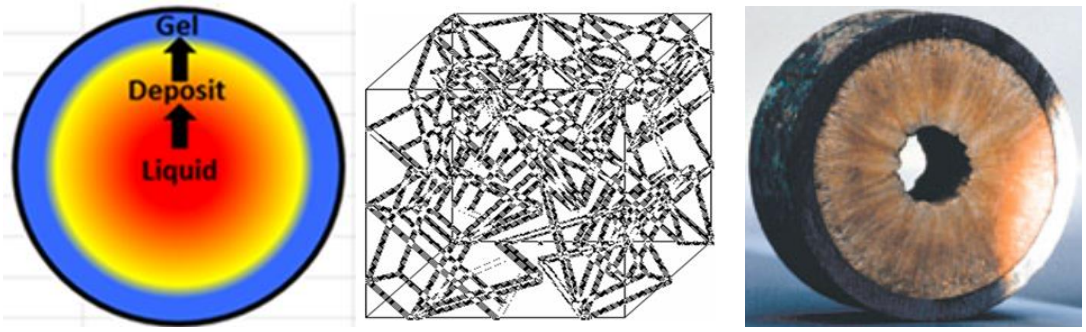

Figure 1.1.1: Wax dispersed, then crystallised and turning into a hard deposit in pipelines carrying waxy crude oils left to cool and cold for long times.

Clearly, the oil industry will look at ways to restart gelled pipelines as economically as possible- that is using the lowest re-start pressures. These will naturally depend on the type of waxy crude oil (how much wax it contains) and the

cooling scenarios that could happen (how quickly and down to which temperature). This is precisely the broad aim of the research described in this thesis.

As re-start pressures have to overcome the “strength” of the gel formed in the pipeline following cooling, clearly the nature of the research must have several dimensions, looking for example at:

- How the wax precipitates: at what temperature and in which proportion.
- The features of wax crystallisation (morphology).
- The rheological properties of waxy crude oils and how these vary with temperatures and cooling rates to inform us on the yielding and eventual flow of the gels.
- Measuring the re-start pressures of gelled pipelines in the laboratory with a view of linking them to rheological properties and other properties in order to guide operation at industrial scale.

Having given a broad overview of the aim and objectives of the research, we now define them more thoroughly.

1.2 Statement of Problem, Aim and Objectives

i. In pumping shutdown, initially hot waxy crude oil stops flowing and being heated. As the surrounding temperatures are usually much lower, the oils cools down *statically* (meaning it is not moving in the pipeline) at a certain cooling rate down to the surrounding temperature. A temperature profile develops radially across the pipe. We assume reasonably that there will be no variation along the pipeline.

ii. As a result of the drop in temperature, the wax, initially fully dissolved in the liquid hydrocarbons, precipitates at and below the wax appearance temperature, WAT, until it is totally out, forming a gel crystal composed of wax crystals.

iii. Because a radial temperature distribution prevails in the pipeline, cooler at the wall than towards the centre, diffusion will cause the wax to migrate

towards the wall and form a core deposit the size of which depends on the wax content of the oil as cooling rate, final temperature and pipe diameter.

iv. Eventually, when this process is complete, the pipe section will be composed of a central plug of liquid hydrocarbons containing no wax surrounded by a core of wax crystals.

v. The problem we are required to solve ultimately is to predict the minimum (economical) pressure required to re-start the pipeline. This forms the practical aim of the research.

vi. Our hypothesis is this minimum pressure must balance the “yield” stress at the wax core / liquid plug interface.

In order to investigate this problem comprehensively (the broad aim of the research), we propose the following objectives:

1. A critical literature survey to review prior work in this area and build on the gaps to advance knowledge in this important field of Transport Phenomena.
2. Use in the experiments, two suitably chosen waxy crude oils of widely different origins and wax content, North Sea oil sourced from BP and a Libya oil sourced from the Libyan Oil Corporation. These oils will be labelled BPO and LO respectively.
3. A thermal characterisation of these oils using a Differential Scanning Calorimeter (DSC) to measure the wax appearance temperature (WAT) and subsequent thermo-grams to enable relating wax precipitation amount with temperature and total wax content. This is to be measured as a function of cooling rate, the critical parameter throughout this study.
4. Knowing WAT and how it varies with cooling rate, use this information to guide the range of operating conditions for the rheological studies to be undertaken. Rheology here is at the heart of the research as it will enable obtaining the deformation and flow curves of the gelled crude oil as they are subjected to a range of rheological tests, including (a) constant stress, (b) oscillatory, (c) creep and recovery, (d) thixotropy. At the outset, it is recognised that these gels will have complex yielding stresses, initially deforming elastically, and then creeping before eventually fracturing and

flowing. Again, temperature and cooling rates will critically affect the yielding processes and stresses.

5. Microscopic observations of waxy crude oils as they gel below WAT using a Cross Polarised Microscope (CPM) to assess crystal formation and growth as a function of cooling rate and other critical parameters. This information will help to form hypothesis on how these gel break upon the application of stresses.
6. Investigate and measure the temperature profiles that develop in a laboratory section of pipeline containing static oil that cools under defined cooling rates at the wall (to be design in our lab). This will enable locating the gel fronts as it develops in a pipeline. This is important information, required to extract the corresponding rheological data (at the temperature and cooling rate that prevail in the pipeline.)
7. Investigate and measure re-start pressures in laboratory pipelines (to be designed here) that replicate the situation in the field not just near isothermal cooling as it would occur when the laboratory pipeline diameters are very small.
8. Correlate all the information above so that knowledge based model is developed to guide the prediction of re-start pressure in large scale operations informed by heat transfer, gel morphology and rheological data.

1 .3 Structure of the Thesis

This thesis is organized in the classical way. It begins with an introductory chapter setting the context of the problem in relation to industrial problems and academic research. This has been presented succinctly above without over-emphasising the importance of oil (its geological origin, historical exploration, supply and demand, properties, usage, composition, etc.), rather focussing on the research issue considered. A literature review then follows in Chapter 2 to critically appraise previous works, finding gaps in knowledge to inform the direction of the present research. Chapter 3 is then presented, describing the experimental methodology including the analytical instruments used and the pipeline rigs

designed. The results and discussion are placed in Chapter 4, following the sequence of work packages described in the objectives. The thesis concludes with a chapter that summarises the main conclusions, states the contributions of the thesis, and gives recommendations for future research.

2. LITERATURE REVIEW

2.1 Introduction

The previous chapter introduced and explained the importance of waxy crude oils and the challenges in handling and processing this type of crude oils in today's industry, and highlighted the aim and objectives of this research program. The aim was formulated as a continuance of the latest works done by previous researchers but bringing in a step change in characterising the rheology of these oils with a view of re-starting gelled pipeline with the least pressure, i.e. more economically.

This chapter presents a detailed review of the essentials and up to date advancements for a good understanding of the rheological properties of waxy crude oils; their different transitional phases during the cooling process; the yielding process and the mechanisms involved in restarting the flow of a waxy crude oil in a gelled pipeline following static cooling during a production shutdown period, as well as the remediation techniques proposed in previous studies.

Many research papers have been published on the different aspects of wax flow assurance problems. However, very few efforts have been made to give a full summary of the various aspects of the problem. Prominent reviews available in the literature are by Wardhaugh and Boger [7] and by Chang and Boger [8] and have been referenced in most previous works.

At the outset, this chapter was considered as one of the key objectives towards achieving the aim of this research. In order to address the important research issues, this literature survey considers the following aspects:

- Introduction to the rheology of waxy crude oil.
- Rheological parameters of waxy crude oils.
- Morphological structure and crystallisation of waxy crude oil gel.
- Viscoelastic behaviour of waxy crude oil gels.

- Yielding of gelled waxy crude oil and pipeline restart.
- Factors affect the structure and yielding process of gelled waxy crude oil.
- Static cooling and wax deposition of waxy crude oil in pipelines.
- Wax deposition modelling.
- Theoretical modelling of pipeline start-up.

2.2 Introduction to the Rheology of Waxy Crude Oil

Waxy crude oils typically exhibit a Newtonian fluid behaviour at high temperature and pressure (reservoir conditions). When crude oil flows out of the reservoir into pipelines it becomes exposed to cold environment. Normally, waxy crude oils are pumped warm for reasons that will become clear below. In conditions of unwanted cooling (accidental stoppage of heating following electrical failure for example), the oil temperature drops below its wax appearance temperature (WAT), wax crystals begin to precipitate out of solution and a very rapid increase in viscosity occurs indicating the beginning of non-Newtonian flow behaviour [7]. Non-Newtonian fluids can be classified into three types: time-independent, time-dependent and visco-plastic.

2.2.1 Time-Independent non-Newtonian Behaviour

The viscosity of time-independent non-Newtonian fluids is dependent on the shear rate at any point and the shear rate is a function of the magnitude of the shear stress only, the time of application of shear stress being immaterial. Such fluids can be subdivided into pseudo-plastics, dilatant and viscoplastic plastic fluids [7, 8]. There are many of viscoplastic fluids/yield stress materials. Bingham plastic is one type of viscoplastic/yield stress materials as illustrated in Figure 2.2.1.

2.2.1.1 Pseudo-Plastics Fluids

These models are a part from power-law and also described as shear thinning because their apparent viscosity decreases with increasing shear rate, typically described by the power law model:

$$\tau = K|\dot{\gamma}^{n-1}|\dot{\gamma} \qquad (2.1)$$

where *K* is the consistency index, *n<1* is the power law exponent or the flow-behaviour index and $\dot{\gamma}$ is the shear rate. The higher the value of *K* the more viscous is the fluid and the greater the change of *n* from unity, the more the non-Newtonian behaviour (the variation of apparent viscosity with shear rate). Pseudoplasticity is typical of most non-Newtonian fluids, including waxy crude oils.

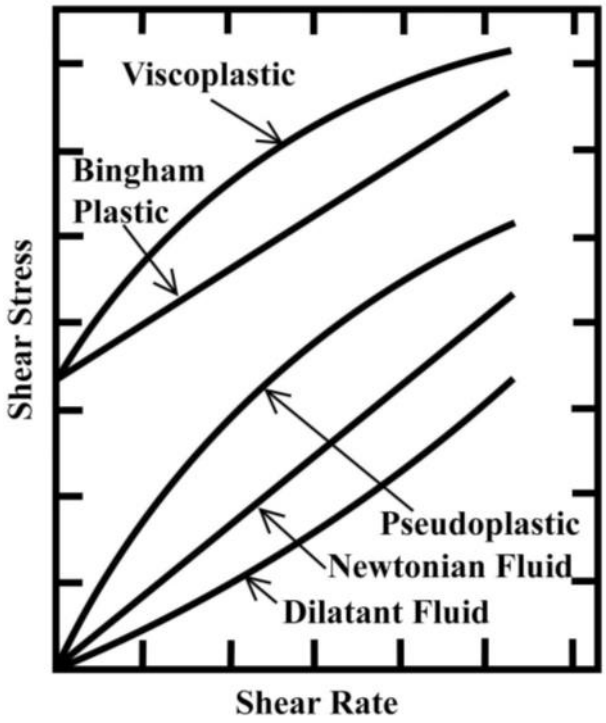

Figure 2.2.1: Newtonian and non-Newtonian behaviours.

2.2.1.2 Dilatant Fluids

These fluids also described as shear-thickening exhibit increasing apparent viscosity with increasing shear rate. The power law equation (2.1) still holds but with *n* > 1. Clay suspensions typically show dilatancy; waxy crude oils do not.

2.2.1.3 Plastic Fluids

A plastic fluid (viscoplastic) will not flow until the applied shear stress (τ) exceeds a certain minimum value (τ_y) known as the yield stress. Beyond the yield

point, the fluid may behave as a Newtonian fluid and such behaviour is described by the Bingham plastic model:

$$\tau = \tau_y + \mu_p \dot{\gamma}, \qquad \tau \geq \tau_y \tag{2.2}$$

$$\dot{\gamma} = 0 \qquad \tau < \tau_y$$

where μ_p is known as the plastic viscosity.

When above the yield stress, the fluid displays shear thinning behaviour a combination of Eq. (2.1) and (2.2) is appropriate, typically:

$$\tau = \tau_y + K|\dot{\gamma}^{n-1}|\dot{\gamma}$$

$$\eta = \frac{\tau_y}{\dot{\gamma}} + K\dot{\gamma}^{n-1} \tag{2.3}$$

Eq. (2.3) is known as the Hershel-Bulkley model one of many models coined to describe a particular non-Newtonian behaviour, another one for example being the Casson model:

$$\sqrt{\tau} = \sqrt{\tau_y} + \sqrt{\eta_c \dot{\gamma}} \qquad \tau > \tau_y \tag{2.4}$$

$$\dot{\gamma} = 0 \qquad \tau < \tau_y$$

Waxy crude oils as will be discussed throughout this thesis require a yield stress before they can flow by the fact that they turn into a gel below a certain temperature. Therefore, many researchers have assigned to them the simple Bingham plastic model such as; Harvey et al. [9], Ells and Brown [10], Irani and Zajac [11]. Other researchers such as; Barry [4] observed that this may be applicable only in a limited range of shear rates. He also suggested that the Casson model (which is an adjustment of the Bingham plastic model as stated earlier) provided a better fit. Ronningsen [12] went further, proposing a *time-dependent* Bingham plastic behaviour on account that the breakage of a gelled structure may be induced at a lower stress but over time [13,14,15]. We shall

return to this important point of discussion, indeed the crux of the research, later on. It was mentioned here merely to illustrate the point about plastic behaviour.

2.2.2 Time-Dependent non-Newtonian Behaviour

This behaviour reflects on the importance of the time of application of shear. In essence, lower stresses over time can be just as efficient at breaking structure as a higher stress applied over a very short time. Conversely, once the shear stress is removed, the apparent viscosity gradually increases and returns to its original value. This is described as thixotropy as illustrated in Figure 2.2.2. As with dilatancy, the opposite behaviour (rheopexy) can also occur with the apparent viscosity increasing with time after the shear rate is increased to a new constant value. When the shear stress is removed, the structure of the fluid gradually breaks down. However this behaviour is only noted at moderate rates of shear [4]. At rapid shearing rates, structure does not form. Examples of rheopectic liquids include gypsum pastes and printer inks. Figure 2.2.2 shows graphically the behaviour of a rheopectic fluid.

Rheopexy is not observed with waxy crude oils; however thixotropy is as observed by Chang and Boger [8].

2.2.3 Viscoelastic Behaviour

This behaviour is best understood with reference to polymer melts which have long molecules imparting the melt with both solid deformation and liquid flow, hence the term visco-elastic or liquid-solid. Waxy crude oils contain long polymeric molecules, paraffin or wax and will naturally exhibit such behaviour as will become evident later in the thesis.

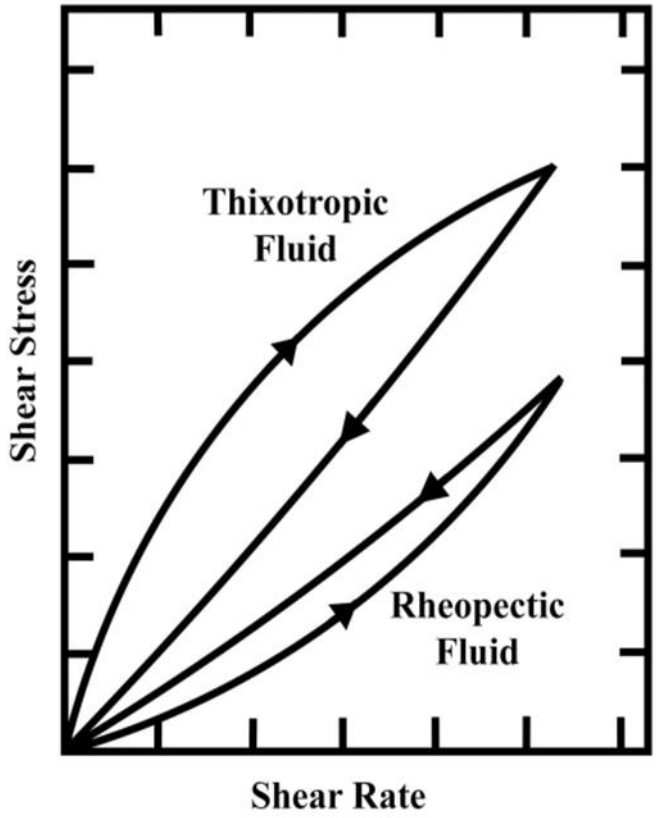

Figure 2.2.2: Behaviours of thixotropic and rheopectic fluids.

2.3 Rheological Parameters for Waxy Crude Oils Properties

A number of critical properties are important in describing the complex behaviour of waxy crude oil and its yielding process. These are the wax appearance temperature (WAT), the wax disappearance temperature (WDT), the gelation temperature (T_{gel}), the pour point (PPT), viscosity, gel strength and thixotropy.

Gel strength and yielding process of waxy crude oil are particularly important for this research and will be reviewed in details in subsection 2.6.

2.3.1 Wax Appearance Temperature (WAT)

The WAT, also called the cloud point temperature (CPT) indicates wax precipitation as it is the temperature at which the first wax crystals appear in a clear solution. No wax precipitation or deposition will occur as long as the crude oil

temperature is above the WAT, but once the temperature drops below the WAT, wax molecules will begin to crystallize out of solution and wax deposition can occur. However, there is a clear distinction between the wax appearance temperature (WAT) and the wax disappearance temperature (WDT). Wax disappearance temperature is the temperature at which the last wax crystals are in equilibrium with the wax liquid phase [16]. Typically, WAT values for high paraffinic crudes range from 38^{o}C to 66^{o}C [17].

2.3.1.1 WAT Measurement Techniques

The WAT of waxy crude oils can be measured using a number of techniques including Differential Scanning Calorimetry (DSC), Cross-Polar Microscopy (CPM), Viscometry, Filter Plugging and Nuclear Magnetic Resonance (NMR). The first two techniques used by Ronningsen et al. [18], Hamouda et al. [19], Pan et al. [20], Elsharkawy et al. [21], Cazaux et al. [22], Thomason [17], Calange et al. [23], Davidson et al. [14], Alboudwarej et al. [16], and Bordalo et al. [24], both techniques will be described below.

2.3.1.1.1 Cross Polar Microscopy (CPM)

The CPM is considered as one of the most accurate methods [18] and is based on the theory that all crystalline materials rotate the plane of polarization of transmitted light while liquid hydrocarbons do not. This method requires a light source, an infrared filter, a polarizer, a temperature controller and a microscope. The sample is enclosed in glass cover slides that are placed on the variable thermal microscope stage and viewed through the crossed polarizer. The microscope is equipped with a video digital camera and connected to a computer where the growth of wax crystals during cooling and disappearance during heating can be monitored directly on screen. When a waxy crude sample is cooled down on the temperature controlled slide under the microscope, wax crystals form and rotate the polarization plan of light i.e. light will be transmitted as paraffin crystals form. These crystals appear as white dots on the dark background. The first white

dot, i.e. the first wax crystals appear when the temperature reaches the wax appearance temperature [25, 26, 27], as shown in Figure 2.3.1.

Figure 2.3.1: An image of wax crystals obtained at wax appearance temperature (WAT) of BPO crude oil from CPM.

2.3.1.1.2 Differential Scanning Calorimetry (DSC)

Differential Scanning Calorimeter (DSC) measures the difference in the heat released between a reference and a test sample during crystallisation. It is thus a fundamentally precise method. As with the CPM method, only a small quantity of sample is required. The test sample is heated to a certain temperature, usually 30^{o}C above WAT of waxy crude oil, and cooled at a given cooling rate. The reference sample has known properties and it is held in static thermal state over the temperature range used for the measurement. At the WAT, the test sample begins to cool slower than the reference sample due to the release of heat of crystallisation. This is controlled by an analyser which calculates the difference in heat inputs required to maintain the temperature of both samples equal. The temperature at which a melting peak occurs in the heat flow-temperature curve (thermo-gram) is taken to be the WAT [21], (see Figure 2.3.2). This point is seen as a deviation from the straight line trend above the WAT measured on the thermo-gram.

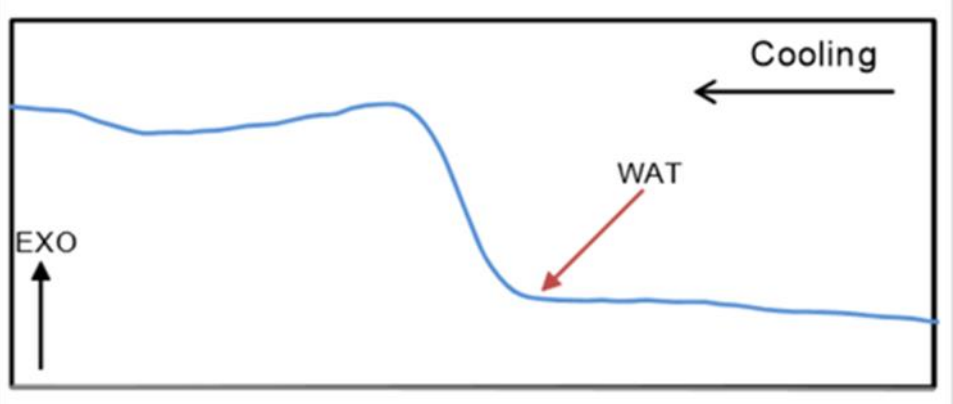

Figure 2.3.2: DSC thermo-gram of a Middle East Crude (Elsharkaway et al.) [21].

This technique will be used in our research to measure WAT and the concentration of crystalline wax as a function of temperatures and cooling rates. The enthalpy of fusion (Q_{oil}) of a sample can be obtained from the DSC (see Figure 2.3.3), and the weight fraction of crystallized wax can be calculated according to the model introduced by J. Chen et al., 2003 [28] as expressed in Equation 2.6. This solid weight fraction as a function of temperature defines the solubility curve for the given sample [26]:

$$C_{wax} = 0.75Q_{oil} + 0.20 \tag{2.6}$$

where C_{wax} (wt.%) is the wax content of crude oil, Q_{oil} (J/g) is the total heat used between WAT and −20◦C.

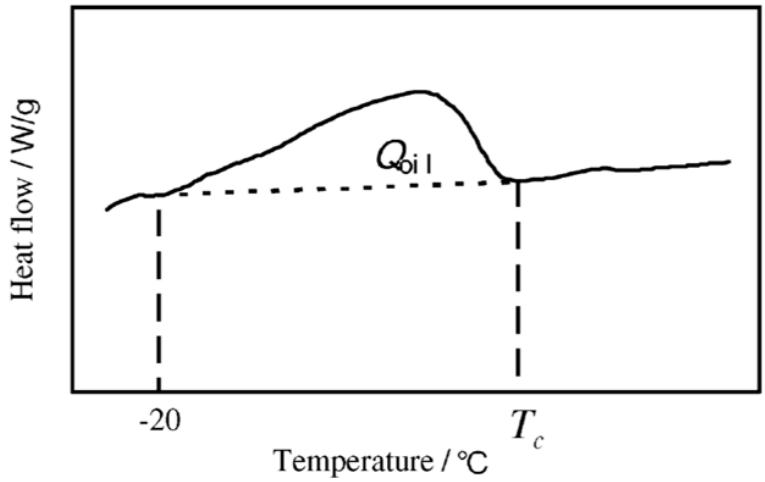

Figure 2.3.3: A sample of DSC curve of crude oil (J. Chen et al., 2003).

2.3.2 Pour Point Temperature (PPT)

The pour point is the temperature at which the flow of a waxy crude oil stops and the crude oil becomes a frozen solid. The PPT indicates that an interlocking gel structure is completely formed as a result of crystallization of wax crystals from the oil under static conditions, causes the viscosity and flow properties of the oil to change dramatically. This property of waxy crude oil increases with increasing wax content [29, 30].

The pour point temperature can be measured using ASTM D5853-95 and D-97 procedures. It can also be determined by cooling a sample in steps of 1°C and determining the lowest temperature at which the liquid sample is able to move [31, 32].

2.3.3 Viscometry

From most literature, waxy crude oil is observed to behave as a Newtonian fluid when its temperature is above WAT and non-Newtonian below this temperature. This behaviour is essentially tracked by the key rheological parameter called *viscosity*. When the temperature of crude oils drops to its gel state, its viscosity increases towards very high values (infinity). In general, viscosity can be *Newtonian*, *apparent* or *plastic* depending on the flow behaviour of the waxy crude at a given temperature. In all cases it is the ratio of shear stress/shear rate:

$$\mu = \tau/\dot{\gamma} \tag{2.7}$$

$$\mu_a = \frac{\tau}{\dot{\gamma}} \tag{2.8}$$

$$\eta_p = \frac{\tau - \tau_y}{\dot{\gamma}} \tag{2.9}$$

2.3.3.1 Viscosity Measurement

As with other fluids, the viscosity of crude oil can be determined using a rheometer (or viscometer) of the vane, cone and plate, concentric cylinder, or capillary type. The description, merits and limitations of these techniques have

been presented in detail by Wardhaugh and Boger [8]. For the purposes of this work, a Controlled Stress Rheometer, Anton Paar MCR 301, fitted with cone-plate or plate-plate geometries was employed. This rheometer will be described in detail in the Experimental Methods chapter.

2.4 Structure, Crystallisation and Gelation of Waxy Crude oil

Gelation of crude oil takes place when 1 to 6% of wax particles have separated from the oil fluid [6, 18, 33, 34, 35]. Using NMR and X-ray diffraction, the solid phase of gelled waxy crude oils is described as mainly crystalline, with only a small unstructured fraction [36, 37]. As explained earlier in the Introduction Chapter, the macro-crystalline particles are composed mostly of *n*-paraffins needle shaped crystals classified as fractal structures [25, 38, 39]. On the other hand, iso-paraffin fractions in waxy crude oil are related to the microcrystalline formation [18]. Generally, sheet or needle-like crystals are commonly found with dimensions of few micrometres or less [36, 37].

Wax crystallisation and gelation processes occur through several stages. At the WAT, the short-range intermolecular attractive forces are greater than the energy of molecular motion and the molecules are bound together into a crystal. The first stage is the formation of lamellar sub-crystals with thicknesses of about 1.5-3 nm [36, 37, 40], corresponding roughly to the length of a linear C_{20} paraffin, and inter lamellar distances from 30 to 100 nm [36]. These sub-crystals grow in two dimensions as sheet-like crystals. The next stage is the aggregation of these sub-crystals to form the large space filling network seen in photomicrographs. This interaction between the wax crystals leads to the formation of a network of crystals resulting from the strong contact and attraction between crystals [25].

These platelet crystals interlock into structured systems which are observed by the microscope as the waxy crude oil gel [33, 34]. This view was confirmed by Kane et al. who used Transmission Electron Microscopy (TEM) and interpreted the results as providing evidence for the growth of sub-crystals.

The behaviour of waxy crude oil gels has been compared to other structured systems. Ronningsen [12] compared them to polymer gels and likened the yielding

behaviour to the break of bond linkages within the network. Wardaugh and Boger [7] thought that these gels behave more like fractal solids while Henaut et al. [41] suggested that they belong to the class of thermo reversible strong gels. Visintin et al. [39] described the compatibility of waxy crude oil gels with colloidal gels where gelation developed from attractive interactions between the crystals which lead to network formation.

However, others studied gel forming colloidal systems for waxy gels and stated that the associating particles are not present in the fluid initially, but rather form and increase in size at a rate which is fixed by crystal growth, as it is a physical mechanism which is totally different from the diffusion-limited gelation of the system [42]. The more interesting issue by Vignati et al. [42] is that clusters are formed by the aggregated wax solids.

2.5 Viscoelastic Behaviour and Gelation Temperature (*Tg*) of Waxy Crude Oils

As stated above, waxy crude oils exhibit non-Newtonian behaviour at temperatures below the WAT. However, crude oils go through a rheological transition over a narrow temperature range to a gel-like phase characterized by a significant yield stress. This temperature is referred to as the pour point (PPT) and below this point the crude oil no longer flows [42]. At this temperature, the whole waxy crude oil literarily solidifies into a wax. The transition from the weak structure in the temperature region between the WAT and PPT (slurry region) to a solid-like structure at temperatures below the PPT will be discussed in this section.

Van Tempel [43, 44], noted that a waxy crude oil suspension at low temperature shows strong similarity to other gel systems containing a network of solid particles, such as fat and aqueous clay particle suspensions which display viscoelasticity at small deformations. He suggested that the elastic component likely occurred from the presence of a network of bonds formed as a result of weak attractive forces.

Many other researchers studied the rheological behaviour of waxy crudes using oscillatory tests on controlled-stress rheometers [5, 7, 8, 39, 42, 45, 46, 47,

48]. These tests conducted for the purpose of understanding waxy crude gelation under static conditions were carried out at very low frequencies and dynamic stresses (typically 0.1 – 1Hz and 0.01 – 1Pa respectively). The choice of low frequency oscillations and low dynamic stresses is to ensure the experiment is conducted within the linear viscoelastic region of the gel i.e. below the point where the gel loses its elasticity. For gelation under flow conditions, a shear stress is imposed on the sample and this strongly weakens the structure of the gel formed and decreases its gelation temperature [46]. The results from all these tests show identical observations regarding the behaviour of the storage or elastic (G') and loss or viscous (G'') modulus during the cooling of a waxy crude oil sample. For example, Figure 2.5.1 shows a typical result obtained by Venkatesan et al. [49].

Generally, at temperatures higher than the WAT, the moduli are constant with G'' higher than G' indicating that the solution behaves like a viscous fluid [5]. When the temperature of the sample is slightly below the WAT, G'' and viscosity begin to increase and over a temperature range around the PPT, both viscoelastic modules and the viscosity increase several orders of magnitude [42]. For uniformly waxy crude oil gel, the gel point or gelation temperature is defined as the temperature at which the ratio of the storage modulus to loss modulus is unity. Therefore, gelation temperature is the point where the storage modulus becomes equal to the loss modulus [5, 46, 47, 49]. However, Singh et al. [5] added that for the samples that separate into two layers (viscous gel layer and liquid layer) during testing as experienced on a cone and plate rheometer, the gel point is defined as the temperature at which the ratio of elastic and viscous modulus is less than unity. Below the gelation temperature, for a uniformly formed gel, the elastic modulus increases faster than the viscous modulus indicating a transformation into a solid-like structure. All these behaviours can be noted in Figure 2.5.1.

Venkatesan et al. stated that the gel temperature of a waxy crude oil determines the initiation of the deposition process. The pour point as defined by the standard ASTM test method is not sufficient to describe the deposition of waxy crudes. The gelation temperature explained in their study is found to be an appropriate measure of the onset of gelation under static as well as flow

conditions. Li et al. [50] also defined the gelation temperature as the temperature at which the amount of precipitated wax crystals changes the oil behaviour from viscous to viscoelastic during a static cooling.

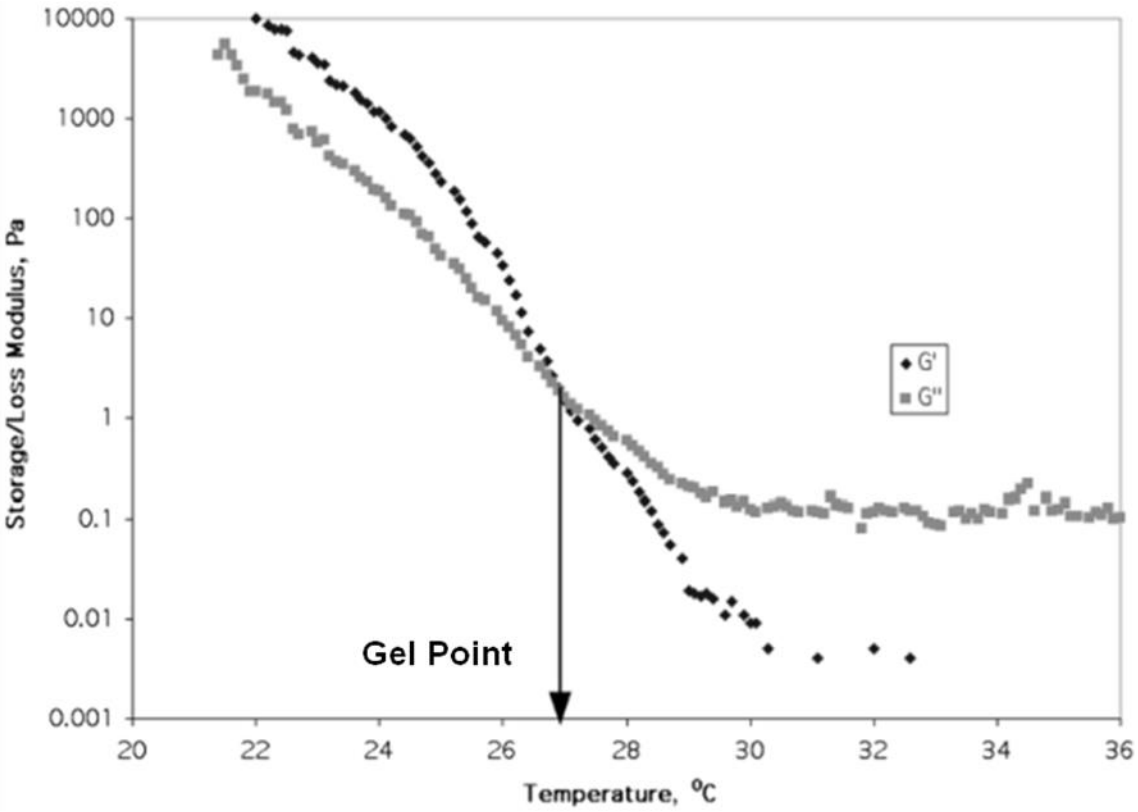

Figure 2.5.1: Viscoelastic Modules with temperature, Venkatesan et al. [49].

2.6 Yielding of Gelled Waxy Crude Oils

2.6.1 Yield Phenomenon and Pipeline Restart

In general, yield stress is considered as a measure of gel strength. It is defined simply as the minimum stress to be applied for the fluid to start flow. Cooling waxy crude oil form solid-like gels to below its yield stress value, the gelled waxy crude oil does not flow due to the solid lattice formed by the waxy crystals [7, 8]. The gelled waxy crude oil exhibits time-dependent Bingham plastic flow behaviour during a restart situation when a constant pumping pressure is imposed on the fluid in pipeline [12].

The yield stress concept was first introduced by Bingham and Green [51] for a class of fluids known as viscoelastic fluids. The yielding process of a gel is a complicated process and various researchers have proposed various models to explain this phenomenon. The first important and qualitative research to describe the yielding of waxy crude oils was in 1991 by Wardhaugh and Boger [7] who defined yield stress as the "shear stress at which the gelled oil ceases to behave as a Hookean solid". They used the vane technique to measure yielding of waxy crude oils which they characterised by three deformation regions: the elastic response, creep and fracture, as shown in Figure 2.6.1. From this figure, three critical points can be identified: point A termed the elastic-limit yield stress (τ_e), representing the change from elastic deformation to creep, point B termed the static yield stress (τ_s), representing the change from creep to fracture and a third point c described as the dynamic yield stress (τ_d) but not determined by Wardhaugh and Boger in 1991. Chang et al. [8] stated that the dynamic yield stress can be extrapolated after the structure of the sample is completely destroyed with continued shear i.e. after point C. Chang et al (1998) introduced a three-yield stresses concept: elastic limit, static and dynamic stresses.

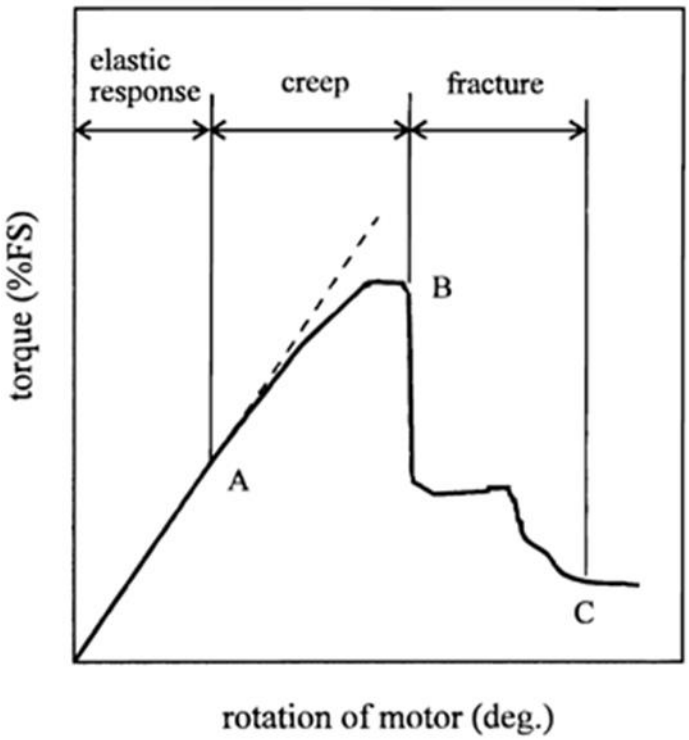

Figure 2.6.1: Yielding process of waxy crude oil: vane technique (Jackson-Hutton crude oil at 10 °C; Wardhaugh and Boger, 1991).

The *elastic limit yield stress* defines the start of viscoelastic creep i.e. the shear stress below this stress causes recoverable deformation only; the *static yield stress* is the shear stress where fracture of the wax structure occurs while the *dynamic yield stress* describes the broken down structure after yielding and this yield value was obtained by extrapolating the dynamic shear stress-shear rate data to the zero shear rate limits as shown in Figure 2.6.2 a and b. Chang et al. [8] also added that engineers are most interested in the static yield stress as this stress value effectively determines the pump capacity required to initiate flow and ensure pipeline restart.

It is important here to note that in Chang and Boger (1998)'s work, the elastic-limit yield stress and initial creep regions were not recorded directly by the controlled stress test due to the resolution limit of the rheometer (Carri-Med CSl 100) used in their research, as the shear rate in those regions is very low as shown in Figure 2.6.2b. In the research carried here, the advanced rheometer used (Anton Paar MCR 301) is capable in operating at very small stresses, thus

enabling an accurate determination of the elastic-limit yield stress and the initial creep region. This is the critical and added-knowledge aspect of this research- the capability of measuring accurately the onset of yielding, all the way from near zero deformation to fracture and then flow whilst accurately varying temperature and cooling rate.

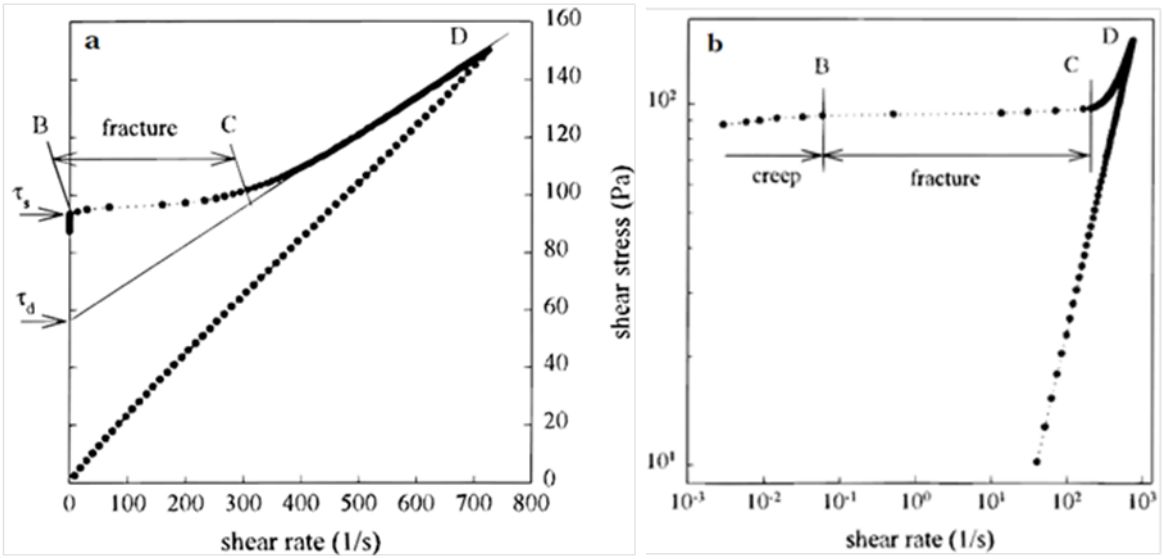

Figure 2.6.2: Controlled stress test: **(a)** difference between the static and dynamic yield stresses (DH19, 16 °C); **(b)** fracture process (DH19, 16 °C) [8].

2.6.2 Yield Stress Measurement Techniques

Many types of equipment and different direct and indirect techniques have been used by previous researchers to determine the static yield stress of wax gel. Their results and conclusions regarding the validity and usefulness of the data obtained differ widely. For examples:

- Capillary U-tubes used by Gill and Russell [52], Davenport and Russel [53] and Russell [54].
- Large pilot pipeline facilities used by Davenport and Somper [55] and Veschuur et al. [56].
- Lab-scale model pipelines used by Ronningsen [12], Carniani et al. [57], Borghi et al. [58], Lee et al. [59] and A.I. Amhamed [60].

- Controlled-stress or shear rotational rheometry instruments used by Wardhaugh and Boger [7], Ronningsen [12], Chang et al. [8], Henaut et al. [41], Borghi et al. [58], Lee et al. [59] and Ekweribe [26].

The capillary tube and large pilot scale pipeline measurement techniques have been criticised as being unsuitable for understanding the yielding behaviour of statically cooled waxy crude oils due to nonlinear pressure distribution, pipe compressibility effects, porosity of wax structure and contraction effects [7]. However, the researchers added that an "exception to this conclusion is the excellent work of Ronningsen (1991), who reported that reasonable good estimates of the yield stress as compared to model pipeline results can be obtained with a constant stress rheometer". Similar success was reported by Lee at al. (2007) using small diameter model pipeline and low cooling rate. In fact, the model pipeline test is the most common laboratory method to measure gel yielding because of its geometrical similarity with the real pipeline.

However, comparisons of the yield stress data from both techniques, at the same testing conditions, have shown that the yield stress measured by the Controlled Stress Rheometer (CSR) is in general much higher than the one obtained from the Model Pipeline Technique (MPT) [8, 7, 12, 17, 55, 56, 58 61]. The reproducibility of the measurement of the yield stress obtained from controlled stress rheometers and model pipelines was very poor, thus, the prediction of the pressure required to restart gelled waxy crude oil pipelines is poorly achieved and inconsistencies appear between yield strength measuring techniques [7, 8, 55, 60, 61, 62].

In model pipeline tests, the gel is formed under controlled conditions (cooling rate, temperature, etc.) and pressure is then slowly applied at one end of the pipe until flow is observed at the other end. The failure yield stress or gel strength (τ_y) is then calculated from force balance as:

$$\tau_y = \Delta P D / 4L \tag{2.10}$$

where ΔP is the minimum pressure differential across the pipeline; D is the pipe internal diameter; L is the pipe length.

This model assumes linear pressure and shear stress distributions throughout the model pipeline regardless of the total length. This model has been described by Borghi et al. (2003) as “over simplistic and not able to give reliable results”. The researchers also stated that a safely factor of approximately 2 is normally recommended. Lee et al. (2007) concluded that this implies an error of 100% would occur quite often.

Lee et al. (2007) used a rheometer and a cross polarised microscope and stated that the gel strength failure mechanism (yield stress) in cooled pipelines is dependent on cooling rate: it can be an adhesive failure when the cooling rate is low or cohesive failure when the cooling rate is high. In other words, the restart of the gelled oil may result from the breakdown of the gel structure itself (cohesive failure) when the applied stress exceeds the mechanical strength of the gel structure maintained by the mechanical interlock of wax crystals, or it may occur because of the breakage at the interface between the gel and the pipeline wall (adhesive failure), as shown schematically in Figure 2.6.3. In their study, they revealed that the controlled stress rheometer and the classical restart pressure drop equation (Eq. 2.10) can successfully predict the required gel breaking pressure of a gelled pipeline when *only* the cooling rate is low and breaking occurs between the gel and the pipe wall (adhesive failure). This was also reported by other researchers such as Thomason, W.H. [17].They also stated that in large diameter pipelines, waxy oil gels formed may not be homogeneous because of thermal gradients in the axial and radial locations pipeline directions. For example, because of the faster cooling rate near the wall, the size and shape of wax crystals near the pipe wall will be different from those at the centre of the pipeline. This affects the homogeneity of wax crystallisation across the pipeline diameter. This morphology influences the strength of the gel and the failure mechanism [59]. *However, it is important to mention here that no further experimental investigation has been done by Lee et al. such as heat transfer experiments, which need to be done to enable the location of the wax core-oil plug interface throughout a pipeline cross-section and then predicts the mechanism conditions for failures in pipelines. In this research, this important point will be addressed.*

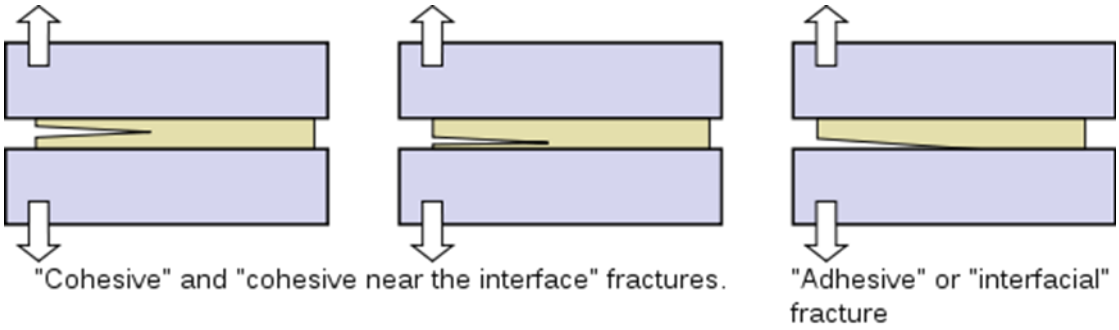

Figure 2.6.3: Schematic diagram of various strength failures of gelled waxy crude oil in pipeline.

Chang et al (1998) stated that “it is important to note that no standard test for determining the yield stress of waxy crude oils has been adopted by the petroleum industry. This is due to the very poor repeatability in any given instrument and the poor reproducibility between the different tests and techniques”. They attributed poor repeatability and reproducibility of the yield stress measurements to their strong dependence on not only what the sample is experiencing, i.e., temperature, cooling rate and shear rate, but also on what the sample has experienced, i.e., thermal and shear history. Furthermore, yield stress might also be affected by further several factors, including: composition, aging (shutdown holding time), shrinkage, compressibility, and gelation pressure [26].

One of the objectives of this research is to clarify this inconsistency by providing an agreement between the model pipeline and the controlled stress rheometer if the gel fails adhesively and the gel has been formed as a homogenous gel structure across the pipeline. Experimental investigations will also be done in this research to mimic the cooling process in real pipelines to find out the reasons behind cohesive failure in pipelines.

2.6.3 Factors affecting the yielding of waxy crude oil gels

During the 1970s, many researchers, [54, 56, 63, 64, 65], started to investigate the factors affecting the yield strength of waxy crude oils after they realized that the yield stress value was a better measure of pump-ability than the pour point.

A critical review for the most important reports done in this point of research is presented in the following subsections. These factors will be reinvestigated in this research using real waxy crude oils, but in more details and concentrating on the effect of temperature and cooling rate which have showed inconsistency between many previous studies.

2.6.3.1 Effect of Shear History

The effect of shear history on gel strength has been studied by many researchers since 1965. The shear history includes both shearing before cooling and shearing during cooling. The effect of shear is only obvious before the waxy crude becomes gel, because after gelation, the viscosity becomes very high and the shear rate in the gel phase becomes zero [5].

Perkins and Turner [63] observed that subjecting oil to high shear conditions at temperatures below about 100^{o}F will increase the yield stress of the gel after it is subsequently cooled to a low testing temperature. Many other researchers reported a considerable decrease in yield stress as a result of pre-shear or dynamic cooling. Verschuur et al. [56] observed 85% gel strength reduction when shear was applied during certain portion of the cooling process. Visintin et al. [39] concluded that if the pre-shear duration is longer, the static yield stress is lower. The gel strength for a crude oil with a pour point of 21^{o}C was found to be lower by a factor of 2 to 4 when wax crystallization occurred while the crude was in movement. Paso [46] commented that gelation tests conducted in rheometers under applied stress simulated the formation of wax deposits in oil pipelines under flowing conditions, with the exception that a thermal gradient was not present. Results from his work indicated that small amounts of shear during gelation results in an increase in crystal sizes, which correlates with an increase in the yield stress of the gel. Chang et al. [8] found from oscillatory test that a lower static yield stress is obtained with higher frequency, while Vignati et al. [42] investigated the time evolution of the storage modulus of a model crude oil under quiescent and shear conditions. Their results indicate that the strongest gel was formed under quiescent conditions. They concluded that “during an oscillatory test, very small perturbations

would cause weak zones to collapse internally, preventing fully developed gel behaviour".

2.6.3.2 Effect of Stress Loading Rate

Stress loading rate is the change of the applied shear stress with time (Pa/min). Chang et al. [8] attributed the difficulties of applying measurements of static yield stress from the controlled stress rheometer directly to pipeline design, to the stress loading rate which essentially is the time scale of the measurement. They stated that the dependence of static yield stress on the stress loading rate may be due to the viscoelastic creep process in yielding.

While studying eight waxy North Sea crudes, Ronningsen [12] observed that increase in stress loading rate resulted in an increase in yield stress for tests run on controlled stress rheometer. Similar effects were reported by Chang et al (1998) who found that reducing stress loading rate by a factor of 8 caused a factor of 2 reductions in static and dynamic yield stress. As shown in Figure 2.6.3, for BO crude oil tested at 20^{o}C, when the stress loading rate decreases from 26 to 6.5 Pa/min, the static yield stress decreases from 17.1 to 7.2 Pa while the dynamic yield stress decreases from 14.1 to 6.9 Pa. They also reported a power-law relation between yield stress and stress loading rate. Visintin et al. [39] measured yield stress of 56, 46 and 37 Pa for stress loading rates of 21, 11 and 2.6 Pa/min at 15^{o}C testing temperature.

However, other researchers reached different conclusions. For example, Perkins and Turner [63] found that "gel strength was a point function of shear strain and apparently not a sensitive function of the path by which the shear strain is imposed". The difference in these observations may lie in differences in the fluids used in the tests.

In conclusion, the yield strength measurement of waxy crude oil is strongly dependent on the stress loading rate. Thus, a practical recommendation for pipeline restart based on these results is that the pump pressure in starting or restarting a pipeline transporting waxy crude oil should be increased as slowly as possible, since a slower operation will require a lower pump pressure not only in

initiating the flow but also in transporting the oil in the final broken state after the restart [8].

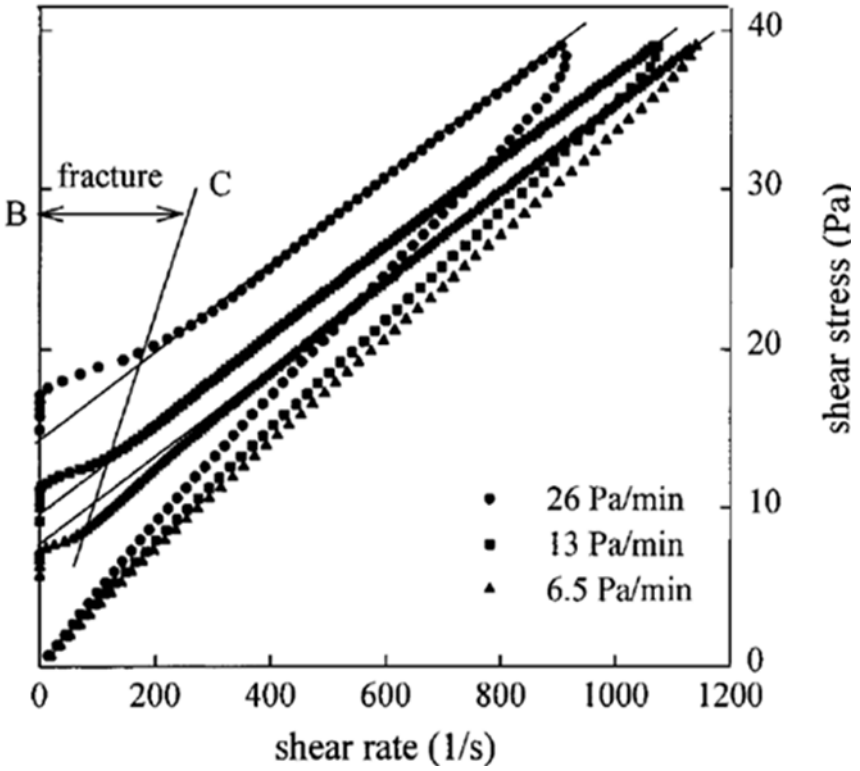

Figure 2.6.3: Controlled Stress Test: effect of stress loading rate on yield stress of BO crude oil at 20 °C (Chang et al.) [8].

2.6.3.3 Effect of Ageing Time

Aging is the isothermal holding time after the gel is formed at a final minimum temperature. Similarly with cooling rate, previous works have observed different aging effects on gel strength from different experiments on different fluids.

Perkins and Turner [63] reported that during yield stress measurements, the equilibrium condition is apparently reached after about 48 hours and for stabilised waxy crude oil, gel strength may increase for 8 – 12 hours after reaching the testing temperature. They also noted that partially degraded gels rebuild gel strength upon stationary aging at testing temperature for a number of hours. Visintin et al. [39] measured a higher yield stress for longer holding time at 15 and 20^{o}C (6 and 1^{o}C below PP), the maximum strength was obtained after 4 hours. However, Cawkwell and Charles [66] observed in a model pipe that the two

Canadian arctic crude oil gels they studied got at maximum strength after about 12 hours. Singh et al. [5, 6] and Paso and Fogler [67] explained the aging effect as a counter diffusion process where paraffin components having a number of carbon atoms more than a supposed critical carbon number (CCN) distribute from the bulk oil into the gel deposit, subsequently precipitating while paraffin components containing a number of carbon atoms less than the CCN distribute out of the deposit with time. Another mechanism for ageing was proposed by Coutinho et al. [68] who showed that in the absence of temperature composition gradients, the hardening of waxy deposits is related to growing of the paraffin crystals, a mechanism by which the large crystals grow at the expense of the melting of smaller crystals of higher energy.

On the other hand, some researchers have reported different observations. Wardhaugh and Boger [7] did not find any significant difference in gel strength after hours of aging. They added that “in the reported cases of the structure development in waxy crude oil on standing, it is most probable that either an equilibrium or steady-state condition was not established or a (very slight) temperature reduction occurred”. Pedersen et al. [69] found from their Nuclear Magnetic Resonance experiments that the same amount of wax was precipitated at a given temperature regardless of whether the sample was cooled at a rate of 10^{o}C/hr. or was equilibrated for 24hrs. Ronningsen [12] and Chang et al. [25] also observed the absence of ageing effects, often insignificant effect on gel structure. These disagreements were attributed to poor temperature control during the experiments or to the different composition of the oils [25].

However, Lopes da Silva and Coutinho [47], after conducting their tests on three different oils under careful control of shear and thermal history and showing that “the ageing and strengthening of the waxy crude oil gels do occur, especially for more initial crystal networks at temperatures close to the gelation temperature”. They concluded that the apparent disagreement can be attributed to the different degrees of super cooling used in different studies.

2.6.3.4 Effect of Composition

The yield stress of waxy crude oil gels is also a function of the composition of the waxy crude oil. Gill and Russell [52] found that the removal of light components would increase gel strength, with consideration of the other factors. A similar observation was made by Perkins and Turner [63] who noted that "weathering or removal of light ends can lead to significant increases in gel strength". Thomason [17] reported that dissolved gas has a very small impact on wax appearance temperature (WAT) of waxy crude but a considerable impact on gel strength and even a larger impact on viscosity. Dissolved gas reduces the gel strength, hence for a shut-in pipeline filled with waxy crude oil with considerable amount of light components, and recommended that to maintain pressure on the line as this would be beneficial during pipeline restart.

Paso and Fogler [67] showed on a cold finger apparatus that *n*-paraffins were mainly responsible for aging. The more these components distribute into the gel deposit, the stronger the gel becomes. The asphaltene content of a waxy crude oil can also have a significant impact on the strength of gels formed at cold shutdown conditions. Venkatesan [45] observed a depression of gelation temperature and yield stress with increase in asphaltene content in a model waxy crude oil mixture. Kriz and Andersen [70] reported a "critical asphaltene concentration in the wax network". In their case study, this value was 0.01%wt., below this value, the yield stress increased with asphaltene concentration, and above this value, the yield stress reduced with increasing asphaltene concentrations.

The presence of water in the composition of waxy crudes is also important since oil is always produced with some water. Recently, Visintin et al. [71] studied oil emulsion gels with various water cut volume percentages. They observed an increase in viscosity and yield stress when the water content exceeded 30% vol. These results are in agreement with Perkins and Turner [63] who noted that "the presence of only a fraction of one percent of emulsified water had little effect on yield strength, but a high percentage led to a decided increase".

2.6.3.5 Effect of Cooling Rate and Thermal History

The presence of wax crystals gives particular rheological behaviour to the oil under steady shear flow and formation of strong thermo-reversible gels. This behaviour is highly dependent on the shear and thermal histories of the sample. The thermal history of a waxy crude oil makes reference to the different heating and cooling pre-treatments that the fluid has been subjected to. This includes the initial crude oil temperature at reservoir conditions, cooling rate, final crude oil temperature and isothermal holding time prior to production shutdown and resuming pipe flow [7, 8, 25].

Perkins and Turner [63] in their studies of Prudhoe Bay oil samples identified three aspects of thermal history which could significantly impact yield strength: temperature cycling, testing temperature and cooling rate. They observed that cycling temperature to an intermediate value, back to a higher value and finally to a low testing temperature, could lead to significant increase in yield strength. From their studies, the yield strength increased with decrease in testing temperature and higher cooling rates.

Chang et al. [25] studied the effect of thermal history on the waxy structure of two statically cooled waxy crude oils. This experimental study was carried out at various cooling rates and isothermal holding times by using a controlled stress rheometer for the rheological measurements and a microscope for the wax crystals morphology. The results lead to the conclusion that thermal history strongly affects the waxy structure. The results of their work can be concluded as follows

- Larger wax particles are observed at low cooling rates, which results in higher yield stress values.
- The isothermal holding time does not result in significant effect on wax structure.
- Structure recoverability of the waxy structure is negligible after breakdown.

These results are in agreement with the experimental studies presented by Ronningsen [12] carried out in a model pipeline and a controlled stress rheometer,

Visintin et al. [39] carried out in a controlled stress rheometer, Abdelrahim [62] carried out in a model pipeline and a controlled stress rheometer and R. Venkatesan et al. [27] carried out by Cross Polar Microscopy for the wax crystals morphology.

On the other hand, these results were in disagreement with other studies such as those by Barry [4], Russell and Chapman [64], Perkins et al. [63], Petrellis et al. [72], Cawkwell et al. [66], Henaut et al. [41] and Amhamed [60], as they stated that higher cooling rate results with higher yield stress and vice versa.

Figure 2.6.4 (a) and (b) show typical results of the statements above and their disagreements. However, Ronningsen [12] concluded that "the longer time available for the wax crystals to grow together into a rigid network structure under slow cooling, outweighed the effect of larger crystal size". Paso [46] attributed this disagreement to the likely presence of non-*n*-paraffin hydrocarbon components and impurities, such as branched and cyclic paraffins, asphaltene and resins, in the crude oils observed by these researchers. Chang et al. [25] opined that "the distinct characterization of different waxy crude oils could be the main reason for the confusion" and recommended that each waxy crude oil should be characterized individually to determine its yielding properties as a function of cooling rate and thermal history before any design or computation is carried out for start-up prediction.

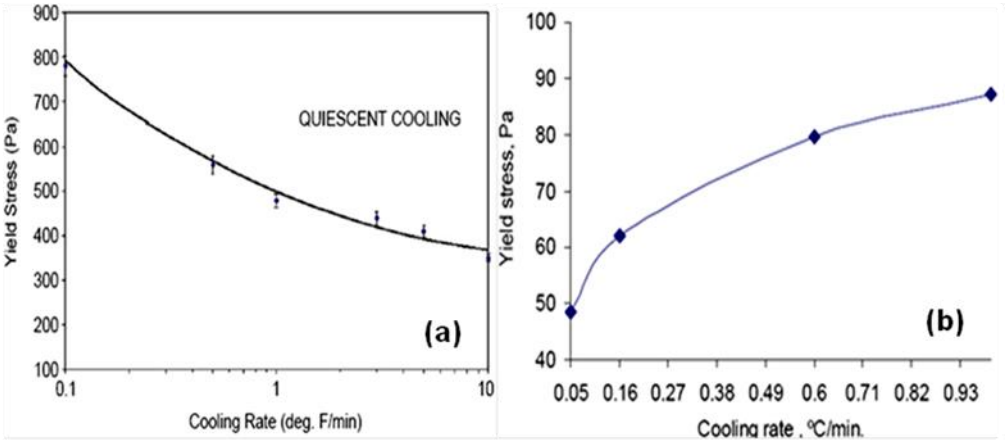

Figure 2.6.4: Effect of cooling rate: **(a)** lower yield stress with higher cooling rate (R. Venkatesan et al.) [27] **(b)** lower yield stress with lower cooling rate (A.I. Amhamed) [60].

More recently, Lee et al. [59] used a constant stress rheometer and experimentally showed that there exists a delineation point between cohesive and adhesive failures when the measured gel strength is plotted as a function of cooling rate as shown in Figure 2.6.5.

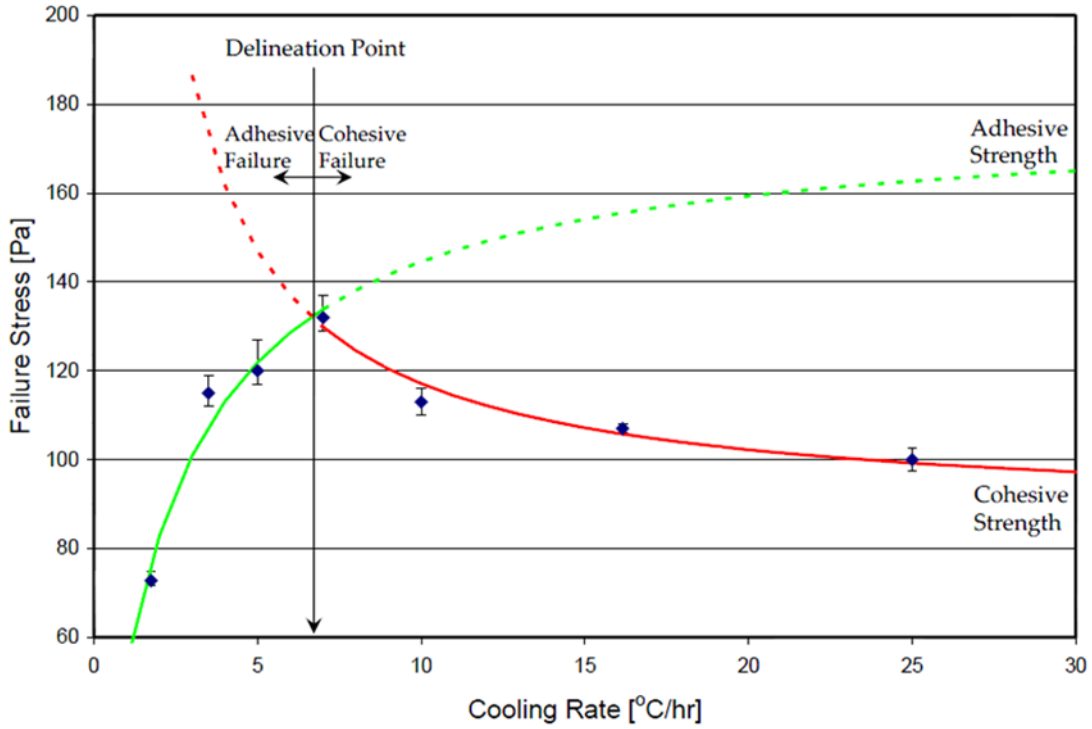

Figure 2.6.5 Gel failure stress vs. cooling rate (Lee et al. [59]).

The results in Figure 2.6.5 show that the gel failure strength increases with increasing cooling rates at low cooling rates and decreases at high cooling rates. Using the controlled stress rheometer and the cross-polarized microscope experiments, their study has also investigated the possible reasons why there exists a delineation point between cohesive and adhesive failures. They explained that when the cooling rate is below the delineation point (about 7°C/hour in their system), the cohesive gel strength is much larger than adhesive failure strength, and the gel breaks adhesively at the interface between metal surface and gel network. If the cooling rate is higher than the delineation point, the cohesive strength becomes smaller than the adhesive strength, the gel breaks within the gel structure cohesively.

2.7 Static Cooling and Wax Deposition of Waxy Crude Oils in Pipelines

2.7.1 Static Radial Cooling Process

When a production shutdown happens due to a planned maintenance or an emergency situation, the waxy crude oil phase transforms from liquid state exhibiting Newtonian flow behaviour above WAT to a gel-like state exhibiting non-Newtonian flow behaviour below WAT [17, 73].

The deposit evolution process throughout a pipeline cross-section under static cooling was summarised by Ekweribe [26] in five stages starting from full liquid phase and ending to solid-like gel phase. The transformation process was described by three regions; Liquid (*L*), Precipitate (*P*) and Deposit (*D*) regions, as shown schematically in Figure 2.7.1. At low temperature below the WAT of waxy crude oil, the solubility of wax decreases and wax molecules precipitate out of liquid phase in a static condition. In the absence of flow, the precipitation of wax molecules leads to the formation of a wax-oil gel. The phase transformation process of the wax in oil involves three main stages; wax precipitation, wax deposition and wax gelation [25].

Singh et al. [6] stated that once the gel layers start to form at the pipe wall, they act as insulators reducing the thermal gradient. Consequently, diffusion effect begins to reduce as more crystals are deposited. Therefore, a stronger gel would be formed at the wall and a weaker one at the pipe centre. It is logically to assume that the rate of precipitation at the liquid-gel interface would be faster than the rate of diffusion of the crystals through the gel layer to the pipe wall. Practically the result is that it would take a longer time after shut down for restart issues to become a problem [6]. Accurate modelling of cooling process hence becomes an important idea to the operator who can estimate the time needed before serious restart issues could be anticipated.

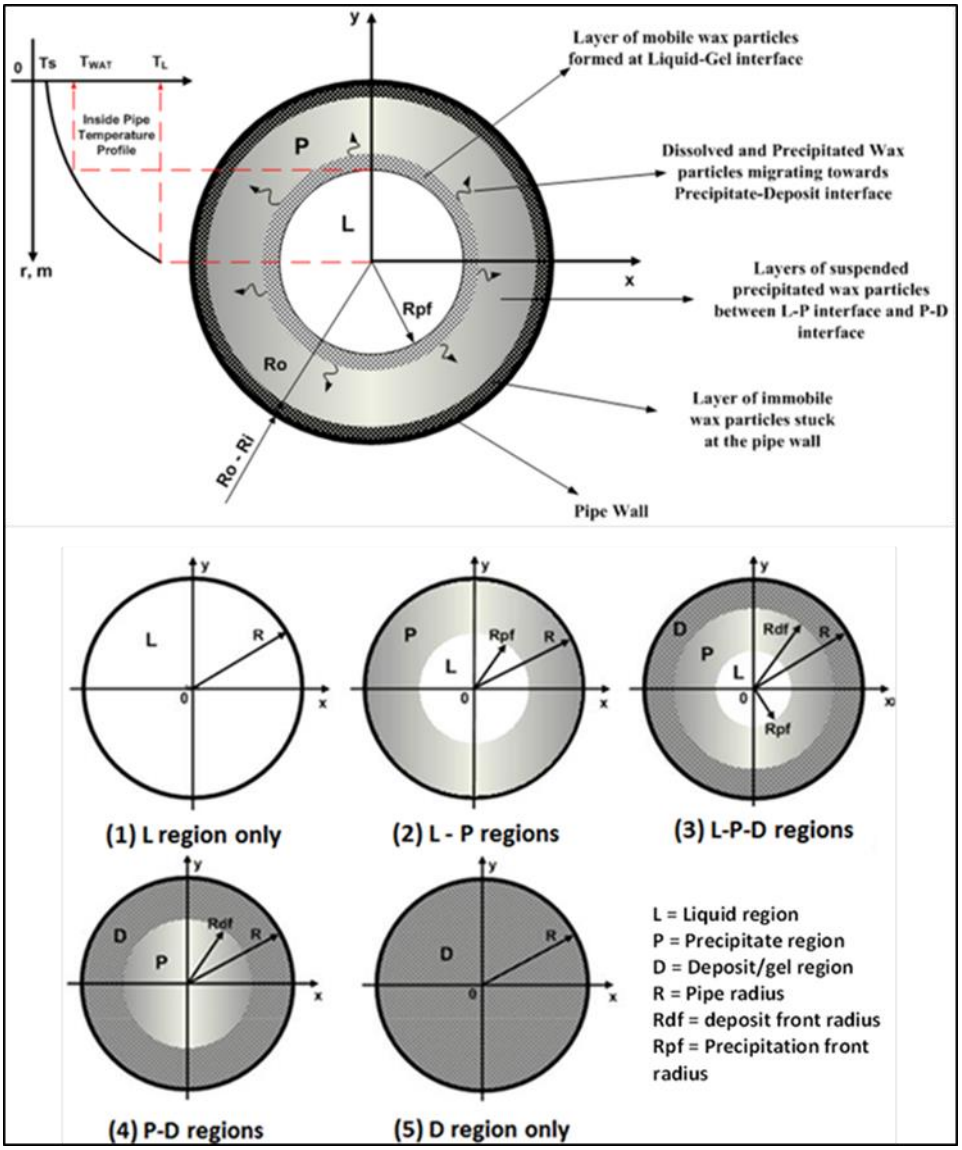

Figure 2.7.1: Schematic of the wax deposit evolution inside a cross-section of a waxy crude oil pipeline under static cooling, (Ekweribe [26]).

2.7.2 Wax Deposition Mechanisms

Previous studies suggested many mechanisms describing the wax deposition process: molecular diffusion, shear dispersion, Brownian diffusion, gravity settling and heat transfer. Molecular diffusion and heat transfer are currently considered as the most relevant mechanisms.

2.7.2.1 Heat Transfer

For the heat-transfer mechanism of wax deposition process, the deposit formation and growth is considered to be a fractional solidification process including crystallization [74-93]. The rate of heat transfer through the deposit layer is dependent on the thermal driving force between the bulk waxy oil temperature and the pipe wall temperature. The overall rate of heat transfer is affected by the convective and the conductive thermal resistances.

Mathematical models based on the moving boundary problem formulation for heat transfer associated with phase transformation were developed by Bhat et al. [83-85]; Mehrotra et al. [86, 87]; and Arumugam et al. [90, 91]. For the models based on this heat-transfer approach, the release of the latent heat of phase changes with changing of the growth of a wax deposit layer close to the pipe wall as it is held at a temperature lower than the WAT of the waxy crude oil. An assumption made in the heat-transfer mechanism is that the liquid–deposit interface temperature is equal to the WAT of the crude oil during the deposition process.

2.7.2.2 Molecular Diffusion

The molecular diffusion mechanism is based on the assumption of a radial temperature gradient. This occurs when the pipeline wall temperature becomes lower than the WAT of waxy crude oil. This increases the concentration gradient which causes the diffusion of wax from the region of higher concentration within the bulk oil, towards the wall where the concentration of dissolved wax in oil phase is lower.

Many of the recent models in describing wax deposition assume that molecular diffusion is the controlling mechanism [6, 94, 95, 96, 97]. This modelling approach is based on estimating the amount of wax deposited from the radial transport of wax molecules that is caused by a radial concentration gradient. The concentration gradient is assumed to be induced by the temperature gradient resulting from the difference between the coolant temperature (lower than WAT) and bulk-crude-oil temperature (higher than WAT). For the molecular-diffusion

modelling approach, the amount of wax deposit is obtained from the rate of mass transfer at the liquid–deposit interface, and the liquid-deposit interface temperature is back-calculated from an energy balance, which predicts a gradual increase in its initial value from being close to the pipe wall temperature to the WAT at steady-state [59]. An essential assumption in the molecular diffusion modelling approach is that the deposit–liquid interface temperature is variable. The prediction is an increase with deposit growth from an initial value close to the pipe-wall temperature and ultimately to the WAT at steady state. This mechanism of wax deposition is the most widely studied and has been reported as a principal mechanism [6, 94, 95, 97-102]. Singh et al. [6] presented a plot of predicted changes in the liquid-deposit interface temperature with time but the predictions were not validated with any experimental measurements. Merino-Garcia et al. [103] suggested that molecular diffusion may not be the controlling mechanism for the deposition process because it is a relatively slow process.

2.7.3 Structure of the Wax Deposits

The structure of wax deposits formed in pipelines during the deposition process is lamellar in nature and is similar to that of pure n-alkanes except for a conformational disorder that occurs in the interfacial region. The packing of the sub-cell is orthorhombic at room temperature and hexagonal at higher temperatures [104]. Observation of the deposits with a cross-polarized microscope by Holder et al. [33, 34] revealed that the wax crystallites have structures of platelets that overlap and interlock. The crystallization of the paraffins thus leads to the formation of gel deposits with a complex morphology [6]. Gelling occurs when a sufficient amount of solid paraffin crystals allows the formation of a solid network structure. Wax deposits are therefore liquid oil entrapped in a network of solid paraffin wax. Wax-oil gelation is due to the flocculation of orthorhombic wax crystallites that appear in solution during cooling [37]. The conditions at which the gel is deposited affect the composition of the gel. Studies have shown that as little as 2% of precipitated paraffin wax is sufficient to form a gel deposit [33, 34, 6].

2.7.4 Factors Affecting Wax Deposition

2.7.4.1 Effect of Composition

Clearly, the lower the paraffin content in the crude oil, the less likely deposition will occur. For the single phase wax deposition, it was shown that when different wax-solvent mixture compositions are exposed to similar temperature conditions with respect to their respective WAT, the same amount of deposition occurs [32, 81, 88]. However, when all the mixtures were exposed to identical operating conditions, those with a higher wax composition produced more solid deposits. Increasing the wax content of a crude oil increases its WAT, which sequentially increases the possibility of deposition. Hammami et al. [105] suggested that while both n-paraffins and iso-paraffins tend to cluster together and precipitate from crude oil as wax solids, the iso-paraffins tend to delay the formation of wax nuclei and usually form unstable solids. Naphthenes or cyclo-paraffins tend to disrupt the wax nucleation process because they are stiff and bulky in nature, while aromatics are good solvents for paraffin waxes. Patton et al. [106] observed that an oil mixture containing lighter paraffin waxes formed unstable deposits which easily flaked off the deposition surface while the oil mixture with heavier waxes formed structurally stronger deposits. A reduction in paraffin deposition from crude oil, in the presence of asphaltenes has been reported by Woo et al. [107] and Misra et al. [108]. Deposited asphaltenes could serve as nucleation sites for additional wax deposition. The presence of impurities and other amorphous solids in the oil might lower the energy barrier required for the formation of the critical wax nucleus [105]. Meray et al. [109] reported that on adding light fractions to crude oil, the WAT of the crude decreased by as much as 15°C depending on the amount of light component added. Similar results were obtained by adding solution gas to the oil [100].

2.7.4.2 Effect of Temperatures Difference

Many previous studies supposed that the temperature difference between the bulk oil and the pipeline wall temperature is the driving force required for wax

deposition to occur [95, 110, 111]. However, recent studies have shown that having a higher overall temperature difference does not necessarily turn into greater amount of deposition in wax deposition [81, 82, 88]. Wax deposition decreases as the temperatures of the waxy crude oil and pipeline wall increase relative to the WAT.

Bidmus et al. [81] showed that the temperature difference between the oil-deposit interface and the pipeline wall is an essential parameter for wax deposition. When the thickness of the wax deposit increases, this creates a thermal insulation that limits the rate of heat transfer and reduces further increases in the deposit mass [112].

2.7.4.3 Effect of Surface Roughness

Wax deposition is affected by the material and properties of the pipeline inner surface. Many studies suggest that the adhesion of the deposit onto a surface is a function of roughness; the deposition surface is responsible for the adherence of the deposit onto the surface. Jorda [113] carried out wax deposition experiments using a cold spot test apparatus and concluded that the quantity, adhesion and the mean molecular weight of the paraffin that accumulates on the deposition surface increases as the surface roughness increases. Jorda attributed the lower amount of wax observed on plastic coated surfaces when compared to metallic surfaces to the smoother surface of the plastic coated surfaces. However, Patton et al. [106], performed similar experiments and concluded that there was no correlation between surface roughness and amount of deposit. They found that paraffin waxes of lower molecular weight slid off or flaked off smooth surfaces while high molecular weight paraffins did not. The lower amount of deposit observed for plastic-coated surfaces was attributed to thermal insulation provided by the plastic layer.

2.7.5 Measurement of the Liquid-Deposit Interface Temperature

Recently, Bidmus et al. [78] performed deposition experiments to measure the changes in the liquid-deposit interface temperature during transient cooling of

wax-solvent mixtures in a cylindrical vessel using fixed temperature coolant under the WATs of wax-solvent mixtures. Two designs for the static cooling were used in their experiments. In the first design, mimicking the typical pipeline geometry, the cold surface was the vessel wall. The deposit layer in the first design started at the vessel wall and its growth was radially inward, causing the liquid-deposit interfacial area to decrease with time. In the second design, mimicking the cold finger deposition experiment, the cold surface was a cylindrical copper tube located concentrically at the centre of the vessel such that the flow of thermal energy from the wax-solvent mixture was radially inward. The deposit-layer in the second design started at the centre (i.e., on the outer surface of the cold finger tube) and its growth was radially outward such that the liquid-deposit interfacial area increased with time. Bidmus et al. stated that the deposit-layer thickness increased more rapidly with a larger heat-transfer and a lower coolant temperature. The interface temperature was observed to be equal to the WAT of the wax-solvent mixture, and it decreased slightly when the liquid-region temperature became less than the WAT of the original mixture (causing the precipitation of wax crystals). The results of this study support the constant-interface temperature assumption made in the heat-transfer approach for modelling solids deposition from waxy mixtures, but not the increasing interface temperature assumption in the molecular-diffusion approach [78].

2.7.6 Theoretical Modelling of Wax Deposition

Some researchers have used the molecular diffusion approach to model the wax deposition process from waxy oils such as Burger et al. [94]; Majeed et al. [114]; Svendson [99]; Singh et al. [5, 97]; Kok and Saracoglu [115]; Ramirez-Jaramillo and Lira-Galeana [96]. In this approach, the rate of wax deposition is modelled using a modified form of Fick's diffusion equation. The wax deposition variation was estimated in this way by Burger et al. (1981) in terms of the wax solubility coefficient for the oil, dC/dT, and the radial temperature gradient, dT/dr, given as;

$$\frac{dm_d}{dt} = D_m A \left(\frac{dC}{dT}\right)\left(\frac{dT}{dr}\right) \tag{2.11}$$

where m_d is the mass of the deposit, *C* is the wax concentration, and D_m is the mass diffusivity. Singh et al. [5, 6, 97] used a form of equation 2.11 to model wax deposition and aging in wax–solvent mixtures. In their approach, the liquid–deposit interface temperature was back calculated from an energy balance, which predicted a gradual increase in its initial value from close to the pipeline wall temperature to the WAT at steady state.

Other researchers have used the heat transfer approach to model the wax deposition process from waxy crude oil mixtures. Mehrotra [116] suggested the use of a heat transfer correlation for wax deposition and assumed that the heat transfer resistances due to the pipe wall and coolant flow were negligible, and developed the following correlation;

$$\frac{hx_d}{k_d} = \frac{2x_d}{D-2x_d}\left(ln\frac{D}{D-2x_d}\right)^{-1}\frac{(T_d-T_c)}{(T_h-T_d)} \tag{2.12}$$

The $(\frac{hx_d}{k_d})$ parameter was plotted against the temperature differential and flow rate results from the experiments performed by Agrawal et al. (1990) and was found to give an average value of 0.29 ± 0.19. This was suggested as a possible parameter for scale up.

Bidmus and Mehrotra (2004) examined the pseudo-steady state conditions of wax deposition. They suggested a dimensionless scale up parameter (θ_d) defined as the thermal resistance offered by the wax deposit relative to the overall thermal resistance. It also represented the ratio of the temperature difference across the deposit layer to the overall temperature difference, given as:

$$\theta_d = \frac{R_d}{R_h+R_d+R_m+R_c} = \frac{T_d-T_{wi}}{T_h-T_c} \tag{2.13}$$

where T_d is the temperature at the liquid-deposit interface, T_{wi} is the inner wall temperature of the pipeline, and T_h and T_c are the average oil and coolant temperatures respectively. θ_d , has been related to the amount of wax deposited for various process variables [32, 81, 88, 89, 92].

Bhat and Mehrotra (2005, 2006) presented a transient mathematical model based on heat transfer considerations for solids deposition from waxy mixtures in both radial and axial directions for established laminar flow in a pipeline. They modelled the solids deposition using a moving boundary problem formulation, and found that the rate of heat transfer at the liquid–deposit interface, as well as those in the liquid region and the deposit layer, influenced the growth of the deposit layer. At steady state, a smaller deposit thickness was predicted with pipeline length for higher mixture temperature, pipe wall temperature, and inlet Reynolds number. Recently, Arumugam et al. (2013) modified the model of Bhat and Mehrotra (2005), by including a correlation proposed by Kasumu et al. (2013), to predict wax deposition in a waxy mixture in a pipeline in both the flow and static conditions. They were able to match their predictions with the trends in laboratory experimental data reported by Bidmus and Mehrotra (2009).

2.8 Theoretical Modelling of Pipeline Start-up

The minimum pressure required to restart flow in fully gelled pipeline can be calculated from the mechanical force equilibrium that exists between the force pushing the gel in the pipe ($P\frac{\pi D^2}{4}$) and the shear resistance at the pipe wall ($\pi DL\tau 4$), as follows:

$$\Delta P = \frac{4\mathrm{L}\tau_{\mathrm{y}}}{\mathrm{D}} \tag{2.14}$$

where ΔP is the minimum pressure differential across the pipeline; D is the pipe internal diameter; L is the pipe length; and τ_y is the fracture (failure) yield stress.

Equation (2.14) is based on the assumption that the yield stress is constant along the entire pipeline length and it takes only the start-up stage into account and fails to describe the entire yielding process [41]. However, many studies have shown that yield stress varies throughout the pipeline cross-section such as; Henaut et al. [41]; Borghi et al. [58]; Verschuur et al. [56]; Lee et al. [59]; Cawkwell et al. [66]. Furthermore, as previously mentioned, Lee et al (2007) stated that Equation 2.14 is based on an assumption that the gel breaking occurs at the

pipeline wall by means of the adhesive failure mechanism. For this type of failure, there is agreement with the restart pressure based on yield stress measurements by the rheometer experiments. *However, if the gel breaking occurs at somewhere across the pipeline section by means of the cohesive failure mechanism, the pressure drop predicted by the controlled stress rheometer and Equation 2.14 would be larger than that of model pipeline experiments because of a cohesive failure in the pipeline.*

Wardhaugh and Boger (1991) gave a good overview of the situation of a full pipeline in operation from start-up to flow. Their diagram represented by Figure 2.8.1 illustrates exactly the point by splitting the progress of pumping into time zones and corresponding stresses and viscosities. In zone 1, the waxy oil leaves the well head or reheating station at overhead temperature where the wax is dissolved and the oil behaves as a Newtonian fluid. The oil enters zone 2 where due to cooling below the pour point, the wax crystallizes thus increasing both stress and viscosity. In zone 3, the wax is being broken, steady state is reached, medium stresses and viscosities prevail. Such zoning together with simple modelling (zone 1, the flow is Newtonian, Zone 2 and 3 require models with yield stress) is useful and is used in pipeline to estimate the pressure requirements for a given overall duty [7].

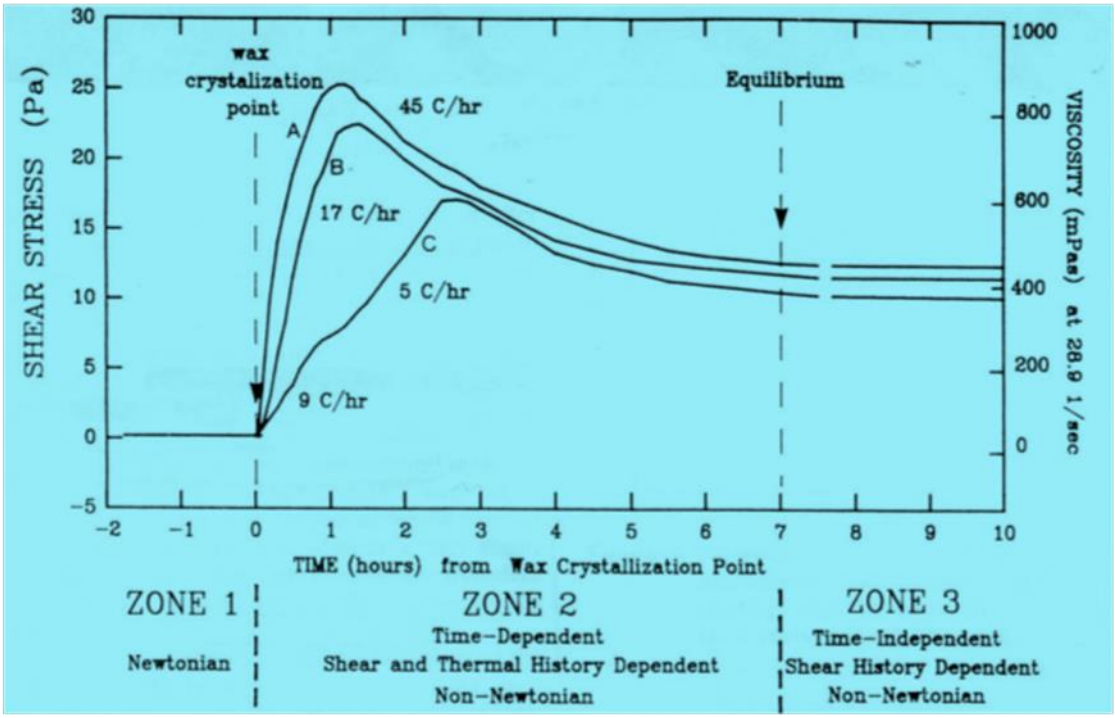

Figure 2.8.1: Zone mapping of flow in an operating pipeline, [7].

More recently, Chang et al. (1999) developed a more refined model for the start-up phase by including a rheological model that contains more than 1 yield stress value. They used a three yield stress model. This model proposed by Kraynik [117], who added a dynamic yield stress for describing behaviour after yielding to the model to develop a two yield stress model forwarded by Houwink [118].

The three yield stress model used an elastic-limit yield stress (τ_e), a static yield stress (τ_s) and a dynamic yield stress (τ_d) which is extrapolated from the flow curve, as we explained earlier in our description of how the waxy structure may deform. Chang et al. (1999) used this model to describe the three possible results of applying constant pressure to a pipeline, containing gelled waxy crude oil, in terms of the relationship between the wall shear stress (τ_w) applied to the pipeline and the initial gel strength of the oil, as following;

- **Start-up without delay** ($\tau_w > \tau_s$): Flow begins immediately with three different regions, as shown in Figure 2.8.2, where *R* is the total radius of the pipeline and r_f and r_c represent the boundaries of the following regions:

Flow area: ($R > r > r_f$), consisting of a sheared annulus. The local stress is higher than the static yield stress ($\tau_r > \tau_s$). The gel structure in this region is instantly destroyed and the oily gel becomes liquid-like, exhibiting a *dynamic yield stress*. The inside radius of the annular flow area (r_f) can be determined by the values of the wall shear stress and the static yield stress as;

$$r_f = R\frac{\tau_s}{\tau_w} \tag{2.15}$$

Creep area*:* ($r_f > r > r_c$), the local stress is lower than the static yield stress, but higher than the elastic-limit yield stress ($\tau_s > \tau > \tau_e$). The gel structure in this region starts to degrade with *a viscoelastic deformation*. The inside radius of the annular creep area (r_e) can be determined by the elastic-limit yield stress as;

$$r_c = R\frac{\tau_e}{\tau_w} \tag{2.16}$$

Elastic deformation area: ($r < r_c$)*,* the local stress is lower than the elastic-limit yield stress ($\tau < \tau_e$). There is a solid-like core, where the oily gel only has elastic deformation and will initially move in a creep region as an un-sheared plug of radius (r^*).

- **Start-up with delay** ($\tau_s > \tau_w > \tau_e$): Flow begins after a delay time. An external creep region and a core elastic deformation area are present, and initially, no flow occurs. Flow only starts when the gel in the creep region has sufficiently degraded, starting at the wall, allowing for movement of an un-sheared plug with uniform velocity through the pipe. The radius of the plug area (r^*) will decrease as degradation in the creep region continues.
- **Unsuccessful start-up** ($\tau_w < \tau_e$): Flow will not start under this condition. The oil gel only deforms elastically and gel structure is unaffected by shear.

Chang et al. (1999) suggested that for a successful start-up, the gelled oil in a cross-section of pipe will become *heterogeneous* because of differences in the rate of structural breakdown caused by differences in local shear stress. Therefore, their model considers the time-dependent rheology of the waxy crude oils. They used a time-dependent Bingham-style equation, as represented in Equations

(2.17a), (2.17b) and (2.17c), for an approximation of the time-dependent non-Newtonian behaviour of a gelled waxy crude oil under constant stress conditions:

$$\tau = \tau_y(t) + \eta(t)\dot{\gamma}, \tau > \tau_y(t) \quad (2.17a)$$

$$\tau_y(t) = \frac{\tau_y(0) - \tau_y(\infty)}{1+kt} + \tau_y(\infty) \quad (2.17b)$$

$$\eta(t) = constant \quad (2.17c)$$

where, η is the plastic viscosity, $\dot{\gamma}$ is the shear rate, τ_y is the apparent yield stress, and *k* is a rate constant. $\tau_y(0)$, and $\tau_y(\infty)$ are the apparent yield stress at times,$t = 0$, and $t = \infty$, respectively. Here, $\tau_y(0)$ is equivalent to $\tau_s(0)$, with an initial wall stress above this value resulting in an immediate finite flow rate, and $\tau_y(\infty)$ corresponds with $\tau_e(0)$, with wall stresses below this value resulting in reversible deformation and no possible flow.

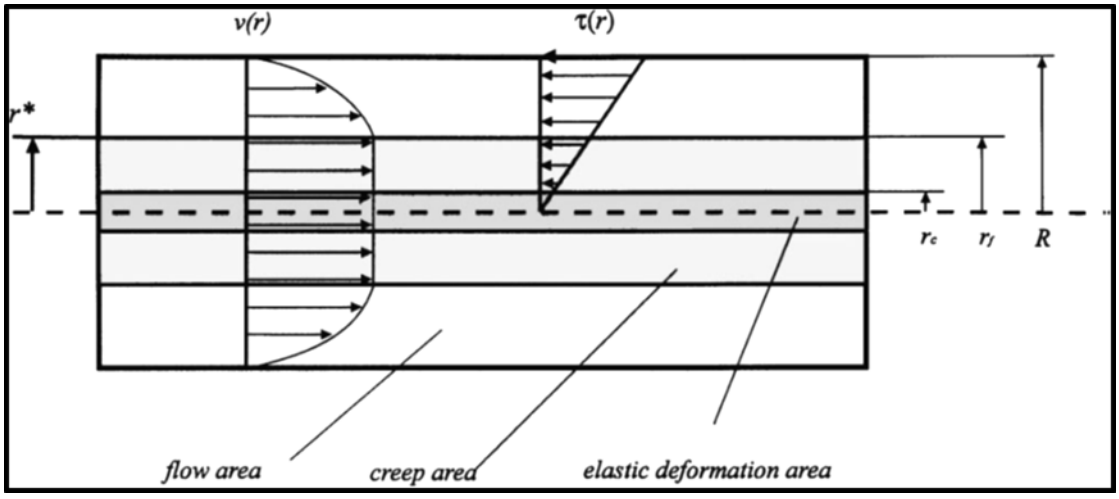

Figure 2.8.2 Schematic diagram of start-up without delay ($\tau_w > \tau_s$ when *t* = 0).

In the same work, Chang et al. (1999) also described the start-up process using a basic physical model as the pumping of an incoming fluid (ICF) into a pipe of length, *L*, and inside diameter, *D*, to displace the outgoing fluid (OGF), as shown in Figure 2.8.3(a) and (b). Here *Z(t)* is the length of the pipe occupied by the ICF, $r_I^*(t)$ and $r_0^*(t)$ are the un-sheared plug radius of the ICF and OGF respectively at

time, t, P_1 is the inlet pressure, P_2 is the outlet pressure, and P_Z is the interface pressure. The radius of the un-sheared plug in the flow was given by equation;

$$r^*(t) = R\,\frac{\tau_y(t)}{\tau_{w0}} \tag{2.18}$$

where, $\tau_{w0}(t)$ is the wall shear stress in the OGF at time *t*. For the case of start-up without delay or start-up with delay at time, $t > t_{delay}$, Chang et al. (1999) defined the initial wall shear stress in terms of the pressure drop. They used a finite differences method to model the time and position dependent changes in the flow properties of the OGF. M time intervals were used to divide the duration of the flow from start-up ($\Delta t = t_i - t_{i-1}$), and the flow was treated as approximately steady in each time interval for adequately small (Δt). The sheared annulus ($r^* < r < R$) was divided, for each instant (t_i) into *N* radial elements of thickness (Δr) and distance (r_j) from the centre of the pipe ($r_j = r_{j-1} + \Delta r = r^* + j\Delta r$). The volumetric flow rate (Q_i) at time t_i was given by following equation;

$$Q_i = \sum_{j=1}^{N} Q_j + Q_{plug} \tag{2.19}$$

where, Q_{plug} is the flow rate of the un-sheared plug and Q_j is the volumetric flow rate of the *j*th annular element.

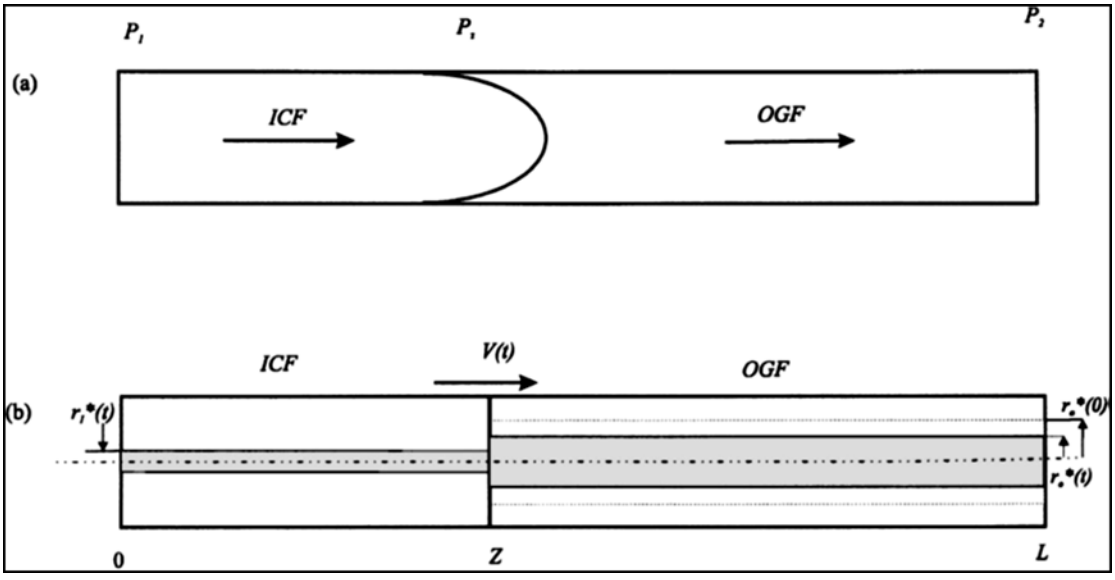

Figure 2.8.3 Schematic diagram of two-fluid displacement model: **(a)** True interface; **(b)** simplified interface (Chang et al, 1999).

Chang et al. (1999) used their model to calculate the plug radius (r^*) for each time interval using equations (2.17b) and (2.18) with a known wall stress. The flow rate could then be calculated from *j* = *N* at the pipe wall to the un-sheared plug at *j* = *0*. The beginning of turbulent flow was predicted by calculation of a critical Reynolds number, with the appropriate adjustment to the friction factor used in the model. For these calculations the pipe dimensions (*L* and *R*), pump pressure (ΔP_c), properties of the OGF ($\tau_y(0), \tau_y(\infty), \eta(t), k$ and ρ_o) and properties of the ICF (τ_B, η_B and ρ_I) need to be known. Here ρ_I and ρ_o are the fluid densities of the ICF and OGF; τ_B is the Bingham yield stress; and η_B is the Bingham plastic viscosity. Therefore, the accuracy of this model in predicting the time-dependent flow properties during start-up and the time needed to clear a blockage depended on complete knowledge of the system, requiring accurate experimental measurements.

2.9 Summary

To date, the previous works that are of relevance to our research area can be summarised as follows:

- **Effect of thermal history on wax crystallization and wax-oil gel formation**

The characteristics of wax crude oil gels depend on the crystal morphology and structures of the crystal networks, which are strong functions of both thermal (including cooling rate and final temperature) and shear histories [6]. As explained earlier, the crystallization of wax molecules below the wax appearance temperature (WAT), which is the rheological key parameter for waxy crude oil under static cooling, results with the formation of gels with a complex morphology. The structure of the waxy crude oil gel is an interlocking of various wax forms such as needles, plates and orthorhombic wax crystals, dependent on cooling rate, temperature, wax concentration and thermal and shear history [6, 37]. Cazaux et al. (1998) investigated the gel structure using X-ray diffraction (XRD), Small-angle X-ray scattering (SAXS), a cross-polarized microscopy (CPM) and a controlled

stress rheometer (CSR). They reported that the key parameters that determine the structure of waxy crude oil gel are the crystal shape and number density of wax crystals and both of which depend on the temperature and cooling rate. Chang et al. (1999) reported that the morphology of the paraffin crystals strongly depends on both the cooling rate, temperature and the shear stress applied to the mixture [27, 36]. Recently Visintin et al. (2005) and Vignati et al. (2005) reported that waxy crude oil gels have the characteristics of colloidal gels and the radius of gyration of the waxy oil gel changes with cooling rate.

- **Yield stress measurement of waxy crude oil**

The yielding behaviour of waxy crude oil gel is very complex process due to the effect of many factors, including stress loading rate, cooling rate and temperature. All these parameters can result in difficulty to determine accurate yield strength of waxy crude oil gel and ultimately to predict the pressure required to restarting the gelled pipelines. This is precisely the problem that formulates the aim of this research.

To date, there appears to have been no other reported yield stress measurements of waxy crude oil and restart of the gelled waxy crude pipeline. The only previous works relevant to our investigation are those by Chang and Boger [8], Chang et al. [13, 25], Venkatesan et al. [27] and Lee et al. [59]. Although, the main attention of Chang and Boger (1998) was to qualitatively describe and measure the yielding process of waxy crude oil as a model of three yield stresses by using the controlled stress rheometer, but in their work, the elastic-limit yield stress and initial creep regions were not recorded directly by the controlled stress test due to the resolution limit of their rheometer, as the shear rate in those regions is very low. Furthermore, Chang and Boger (1998) stated that no standard measurements can be proved by the industry for real pipelines applications because of the very low reproducibility of the measurements. Chang et al. (1999), used the idea of the three yield stress model to describe the three possible results of applying a constant pressure to a pipeline, containing gelled waxy crude oil, in terms of the relationship between the wall shear stress applied to the pipeline and the initial gel strength of the oil.

Chang et al. (2000), using a cross polarized microscope, attributed the poor reproducibility between the rheometer and pipeline to the effect of cooling rate on the gel structure of waxy crude oil, and observed large crystals with low cooling rate and small crystals with high cooling rate. Chang et al. (2000) analysed their observations and stated that a lower cooling rate results with higher yield stress, but no practical applications for these conditions have been applied to pipelines. Venkatesan et al. (2005) also used a cross polarised microscope, partially agreed with Chang et al.'s statement and concluded that the yield stress decreases with an increasing cooling rare, but added that when the gel is formed under a high gelation stress, the yield stress of the gel increases with an increasing cooling rate. However, many other studies were in complete disagreement and stated the opposite of the statements highlighted above.

- **Restart of non-uniformly gelled pipeline**

The radial cooling system of pipelines results with different radial cooling rates and temperatures. This affects the structure of waxy crude oil gels, which may result inhomogeneous structures and gel strength throughout the cross-section of pipeline during quiescent cooling. As stated earlier, the morphology and structure of cooled waxy crude oils are strong functions of cooling rate and temperature, thus, gel strength also depends on these factors [27, 36, 41, 59]. If the cooling rate is low, wax molecules have sufficient time and mobility to form large crystals and as a result the number density of crystals decreases. From the literature, this is said to affect the yielding mechanism of the gel in the pipeline resulting in inconsistencies in the yield strength values between the model pipeline and rheometer techniques. Consequently, these conditions should be consistently applied for both the model pipeline and rheometer experiments.

The reasons behind the inconclusive contradicting experiments results between rheometer and model pipeline techniques have not been fully explained by pervious researches, thereby further confusing the prediction of restart pressure of gelled pipeline using the controlled stress rheometer.

The most recent study which has looked at similar aspects in relation to this problem was undertaken by Lee et al. (2007). They used the rheometer, cross

polarised microscope and model pipeline and stated that the gel strength (yield stress) failure mechanism in a pipeline is dependent on cooling rate. It can be an adhesive failure when the cooling rate is low or a cohesive failure when the cooling rate is high. Their study has also revealed that the controlled stress rheometer and classical restart pressure drop equation can successfully predict the required gel breaking pressure of a gelled pipeline if only the cooling rate is low and the gel breaking occurs at the pipe wall (adhesive failure).

In real pipelines which have a big diameter, the waxy oil gels formed may not be homogeneous because of thermal gradient in the axial and radial locations inside the field pipelines. For example, because of the faster cooling rate near the wall, the size and shape of wax crystals near the pipe wall will be different from those at the centre of the pipeline, affecting the homogeneity of wax crystallisation across the pipeline diameter. This crystal morphology affects both the strength of the gel and the failure mechanism of the gel in the pipeline. For example, the restart of the gelled oil may result from the breakdown of the gel structure itself (cohesive failure) or it may occur because of the breakage at the pipeline-gel interface at the wall of pipeline (adhesive failure) depending on the cooling rate and wax content [59, 119]. The cohesive yielding of the gel occurs when the applied stress exceeds the mechanical strength of the waxy oil gel structure maintained by the mechanical interlocking of wax crystals [27, 39, 42, 59].

3. EXPERIMENTAL METHOD

3.1 Introduction

Following the introduction chapter aims and objectives and the gaps knowledge as established in the literature review, the experimental methodology is now presented. It describes a series of complementary work packages building towards being able to address the principal aim – that of being able to predict the re-start pressure of gelled pipelines in real situations, where the pipe diameter is large and a temperature gradient prevails across the diameter leading to a liquid plug surrounding by a core deposit as described earlier. These work packages are:

i. A presentation of the waxy crude oils and their preparation for the experiments. As reviewed earlier, waxy crude oils elasto-plasto-viscous materials which “remember” past deformations, particularly after cooling. A base line has to be set so that, “clean” (of past history) samples are used and their deformation and flow under various cooling and deformation conditions are studied. This base line is to be referred to as “conditioning” as it will be explained later. Thus all the experiments will use conditioned oils from the start.
ii. A thermal characterisation of these oils so that their wax appearance temperature and their wax content are established accurately as a function of the principal parameters that are cooling rates and temperatures. This will be achieved using a differential scanning calorimeter (DSC).
iii. A microscopic characterisation of gel formation under various cooling rates and temperatures so that the crystal structure is understood and its possible failure inferred. This will be carried out using a cross polarised microscope (CPM).

iv. A rheological characterisation of these oils at various states (liquids, gels near WAT and gels below WAT) at various temperatures, cooling rates and stresses so that their yielding and flow curves are measured accurately. As explained in the literature review, this part is at the heart of this research and advanced control stress rheometry capable of operating at very low stress will be the main tool but supported also by oscillatory and creep-recovery tests.

v. The measurement of re-start pressures of gelled small scale pipelines at two sizes, one 6.5mm diameter so that near isothermal conditions are achieved in the pipe and one twice as large to establish variation from isothermal conditions, mimicking in the laboratory large scale operation. A full description of the pipeline rig is given.

vi. The measurement of temperature profiles that occur in typical pipelines carrying waxy crude oils, using a section of pipes and the two conditioned oils, cooled under controlled conditions. A full description of this instrumented set-up will be given.

3.2. Samples Presentation and Conditioning

This experimental study was carried out using two waxy crude oils; one originating from the North Sea and supplied by BP and one originating from Libya and supplied by AOC (Agip Oil Co). These samples will be referred throughout this thesis as BPO and LO, respectively. They were chosen to give universality to the research as they differed widely in the total paraffinic content, wax appearance temperature (WAT) and pour point temperature (PPT). Table 3.2.1 taken from the results chapter show the wax content to be 15.7% for BPO and 39.6 % for LO, WAT about 31^0C and 61^0C respectively and PPT about 18^0C and 35^0C respectively. Further details on these values and how they vary with cooling rates will be given in the DSC thermal characterisation section. The important information is that these waxy crude oils are very different from one another.

As explained earlier, waxy crude oils are elasto-plasto-viscous materials which “remember” past deformations, particularly after cooling. A base line has to be set so that, “clean” (of past history) samples are used and their deformation and

flow under various cooling and deformation conditions are studied. This base line is set by the following “conditioning” treatment:

1. Samples of the crude oils which arrived to the laboratory in 20 L drums were transferred to 2 L aluminium pots. These pots had a cover drilled with a hole to insert a stirrer. The cover was designed so that apart from the hole it would seal the oil from the atmosphere as shown in Figure 3.2.1.
2. The oils in these pots were heated from room temperature to 100^{o}C and then stirred at 80 rpm raising the stirrer vertically at different height (5cm, 10cm and 15cm). This heating- stirring continued for 2hrs with BPO and 3hrs for LO. Temperature of 100^{o}C chosen was considered high enough to remove all the thermal waxy structure memory since this is the average reservoir temperature of BPO and LO. Also as will be shown in the thermal characterisation results, the wax disappearance temperatures (WDT) are about 40^{o}C and 70^{o}C for BPO and LO crude oils, respectively.
3. The samples were then cooled in a water cooled bath (shown in Figure 3.2.1) down to 50^{o}C in 50 min for BPO and to 80^{o}C in 20 min for LO. These temperatures were chosen because the wax appearance temperatures (WAT) measured are around 30^{o}C and 60^{o}C for BPO and LO, respectively.
4. The samples were then stored at these temperatures in the water bath ready for testing.
5. In what follows, these samples will be referred to as conditioned samples.
6. It is important to note that this conditioning method had to be evaluated to assess repeatability of data and deviation from measurements using non-conditioned samples. This was performed in the rheological measurements (described later) and was shown to be appropriate.

Table 3.2.1: Content of wax in the crude oils investigated, their Wax Appearance Temperatures (WAT) and Pour Point Temperatures (PPT).

Crude oil	PPT (°C)	WAT (°C)	Wax content (%wt.)
BPO	18±1	30-31.5	15.7
LO	35±1	60-61.5	39.6

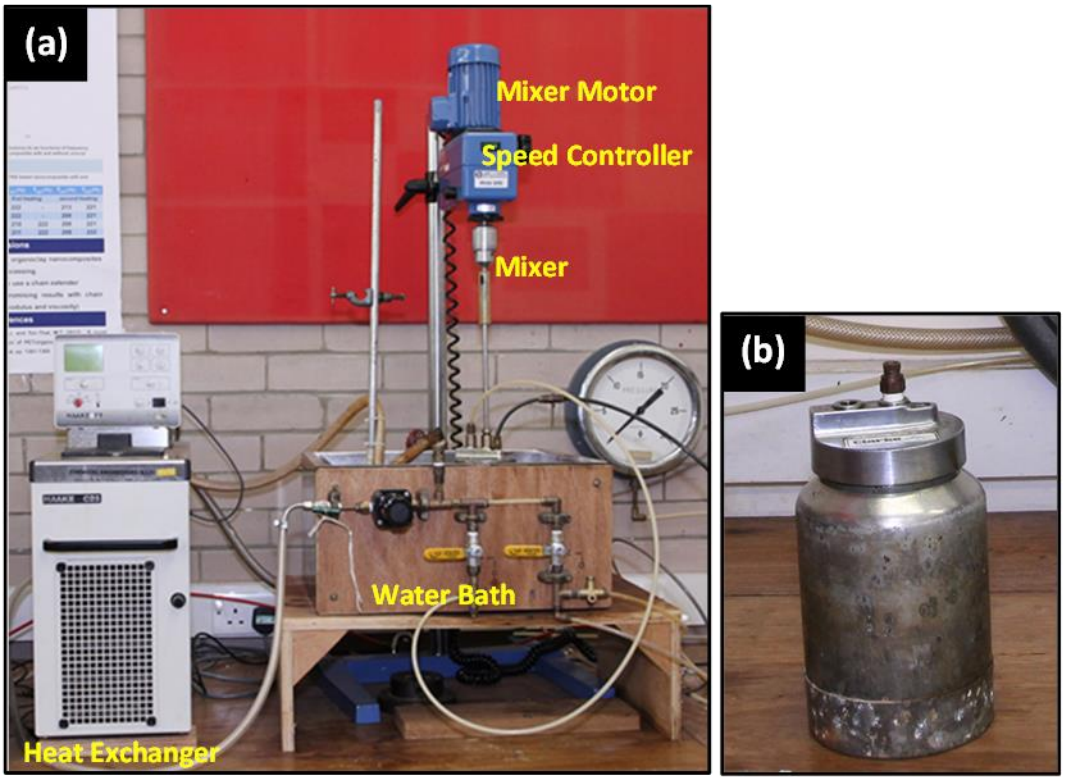

Figure 3.2.1 (a) Picture of the rig used for conditioning the oils **(b)** The sealed pot.

3.3 Differential Scanning Calorimetry (DSC) Experiments

Differential Scanning Calorimeters measure temperatures and heat flows associated with thermal transitions in a material. It was used here to measure the wax appearance temperature, WAT, the total wax content of the oils and the wax fraction precipitating at any temperature below WAT. The DSC also allows measuring the effect of cooling rate on WAT and the wax fraction precipitated.

The DSC used in this study was the Thermal Analysis DSC Q20 from TA Instruments shown in Figure 3.3.1. This instrument, with the cooling accessories, can operate in a very large temperature range (-180^{o}C to 725^{o}C) with a fine temperature and calorimetric accuracy of +/-0.1^{o}C and +/-0.05%. Here the lowest temperature used was -20^{o}C using dry nitrogen gas purged through the DSC cells. The instrument is equipped with a 50-position auto sampler and Platinum software, which allows for automated calibration and verification runs during off-work hours. The entire procedure is automated and computer controlled once the oil samples (4-8mg) are loaded into Tzero^{TM} hermetic pans and sealed. The thermal measurements are then performed by heating the samples to a temperature 20^{o}C above WAT (60^{o}C for BPO and 80^{o}C for LO), then maintained at these temperatures for 5 min to ensure all the paraffin wax was in a liquid state, fully dissolved in the oil. Subsequently, the samples were cooled down to -20^{o}C at a set cooling rate and the heat flow measured. Two parallel runs were made to check repeatability of the results. The cooling rates tested were 1, 5, 10 and 15^{o}C/min for LO and at cooling rate of 5, 10 and 15^{o}C/min for BPO

Figure 3.3.1: Picture of the Differential Scanning Calorimeter (DSC) used in this study.

3.4 Microscopic Observations

Microscopy viewing of the gelled oil was conducted using a Cross Polarised Microscope (CPM) made up of the following set-up as depicted in Figure 3.4.1:

(i) A hot stage microscope (THMS600, Zeiss, Thornwood, USA) connected to a Peltier temperature programmed heating/cooling unit operational from from -100^{o}C to 200^{o}C with 0.1^{o}C temperature precision, a minimum heating/cooling rate of 0.1^{o}C/hr. and a maximum heating/cooling rate of 130^{o}C/min.

(ii) A cross-polarized light source to identify crystals and co-crystals and,

(iii) An Axio-cam camera (MRC 5 Zeiss, Tv2/3"c, 0.63x, 1069-414) to obtain pictures of the structures observed. This camera is a 12-bit camera which employs a single-chip charge-coupled device (CCD) sensor with Bayer RGB primary colour filtration. The two-thirds-inch CCD chip incorporates 1.45 million effective pixels, which can be shifted during image getting to obtain a maximum effective resolution of 12.5 million pixels. Images may be obtained at resolution as high as 4080 x 3072 pixels.

(iv) A measurement cell fitted with a lid on the top with a window for the front view of the lens to keep the sample thermally insulated. For good viewing, the window and the sample carrier were kept clean of any particles of dust.

For the measurements, the oil samples were first heated to a temperature at least 20^{o}C above the WAT (60^{o}C for BPO and 80^{o}C for LO) for 30 min before being loaded in a Quartz Crucible and placed in the measurement cell of the thermal stage. The advantage of using a crucible are that it is suitable for liquids such as crude oils and can load a sample through the side loading door of the stage without removing the lid or disturbing the lens set up. The crucible is made from fused quartz and has small lip around the top. Then the crude oil sample was covered with 16 mm glass cover slip over the top of the crucible and cooled to the test temperature at identified cooling rate. The microscope is connected to the

computer where the growth of wax crystals of crude oils during cooling and disappearance during heating can be monitored directly on the screen. The oil samples were photographed with the digital camera and then images were sent to the computer.

The following series of CPM observations were performed:

(i) At cooling rates of 0.5, 1 and 5^{o}C/min from 60^{o}C down to 30, 25, 20 and 15^{o}C for BPO and from 80^{o}C down to 63, 50, 40 and 30^{o}C for LO.

(ii) At aging time of 5 minute and 4 hours. By aging time, it is meant keeping the structure after cooling at the test temperature and observing if any changes occur over time (isothermally) to the crystal structure.

(iii) As in (i) but to determine WAT by video recording observations a few degrees above WAT first (35^{o}C for BPO and 65^{o}C for LO) then gradually zooming towards WAT in steps of 1°C with a minimum of 10 minutes holding time between temperature setting until the first crystals appear. The temperature is then reduced in steps of 0.1^{o}C with 5 minutes holding time between temperatures until 5 to 10 additional crystalline material spots can be seen.

As for the actual photographs obtained, Figure 3.4.2 is taken from the result section show typical observations with the wax crystals appearing as white dots on a dark background. This results from the fact that on formation the wax crystals rotate the polarization plan of the light (i.e. the light will be transmitted as crystals), the liquid oil does not.

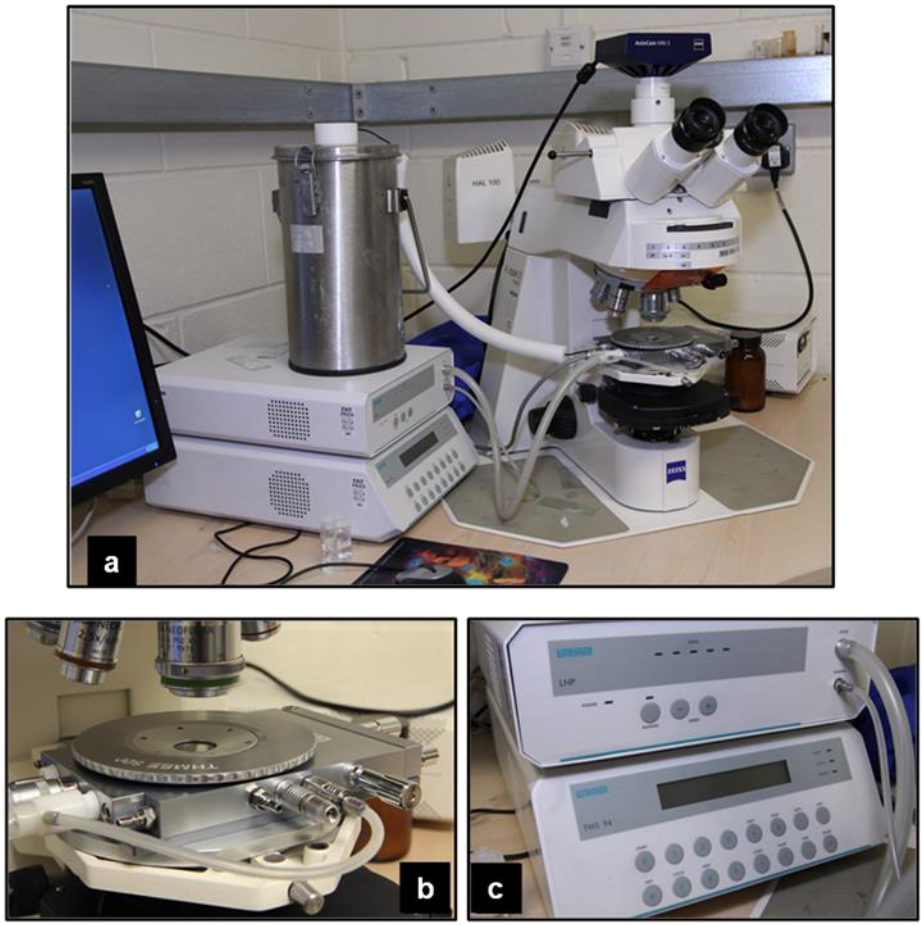

Figure 3.4.1: CPM Set-up used in this study: **(a)** the Zeiss Cross Polar Microscope, **(b)** the INSTEC TS62 Peltier thermal stage and **(c)** the pumped cooling /heating programmer.

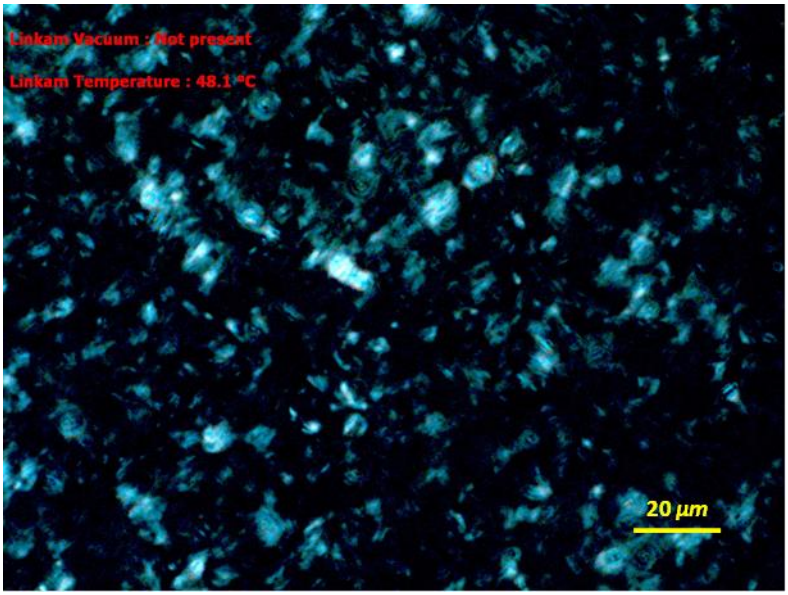

Figure 3.4.2: Typical CPM photograph for LO crude oil at 48.1^{o}C.

3.5 Rheological Measurements

Rheology forms an important part of the work carried out in this research, the aim being to measure as precisely as possible the yield stress necessary to restart flow of gelled waxy crude oils. As these oil gels are elasto-visco-plastic below the wax appearance temperature, they will first behave as solids, deforming elastically first, then undergoing creep and eventually fracturing before flowing as viscous liquids. Such complex deformation occurs over a very small range of stresses and will depend on the rate at which the stresses are increasing. Also, the elastic yield stress of these oil gels (soft solids) will be relatively small (compared to solids). The rheological instruments to be used will thus have to be capable of operating precisely at very low stresses. It is only recently that such devices have been developed. This study uses such state of the art instrument (Anton Paar Modular Compact Rheometer, MCR 301) that can operate in controlled stress, creep-recovery and oscillatory shear modes with temperatures, cooling rates and stress loading rates controlled to a very good accuracy.

As emphasised and described in Section 3.2, all the samples used for rheological measurements were conditioned prior to the tests which only required around 0.70ml pre-conditioned sample to be deposited on the rheometer plate the temperature of which was set at the pre-conditioned temperature of the oil, 60^{o}C for BPO and 80^{o}C for LO. Thereafter, the sample was cooled statically (plate or cone stationary) to a temperature near its WAT but above it by 5^{o}C. This cooling was performed at 5^{o}C/min. Following this start point, a cooling rate was set, a temperature was set, a stress loading rate was set- all programmed-and the measurement performed and testing the effect of these parameters on the flow curves was obtained, hence the yield stresses were measured.

Three repeat tests were carried out using a fresh sample to test repeatability. The variation in yield stresses values between the measurements was deemed acceptable only when it did not exceed 1%.

3.5.1 The MCR 301 Rheometer

The essential capabilities of the MCR 301 Rheometer (Figure 3.5.1) are twofold (i) it is provided with an air bearing with technology for digitally controlled shear stress CSS and controlled shear rate CSR extending down to 10^{-7} Pa and 10^{-6} min^{-1} respectively and (ii) it is provided with a peltier device which controls the temperature to an accuracy within $\pm 0.5^{o}C$ at programmable cooling rate in the range $0.01^{o}C$/min to $6.5^{o}C$/min. There is also flexibility in the flow geometries that can be accommodated, plate and plate and cone and plate. Here work was carried out using plates of diameters 25mm/25mm and 50mm/50mm (for the plate-plate flow geometry) and a cone angle of 1^{o} (for the cone-plate flow geometry). These various conditions were used to cross-check that the data were independent of the flow geometry used. In addition, a calibration check was executed prior to this experimental programme (see Table 3.5.1) and the error in viscosity measurement was found to be less than 1%. Figure 3.5.2 shows these geometries, their advantages and disadvantages and the pertinent equations relating shear stress (τ), shear rate ($\dot{\gamma}$) with the measured torque (M) and cone rotational speed (N) or plate angular velocity (ω) and flow geometry (plate radius R, cone angle α and plate-plate gap H).

Table 3.5.1: Calibration of the rheometer (MCR301) with a standard oil (2700-V07)

Temperature (^{o}C)	Specific viscosity (mPa.s)	Measured viscosity (mPa.s)	% Error
20	35.35	35.06	0.81
25	27.72	27.55	0.61
40	14.74	14.84	0.34

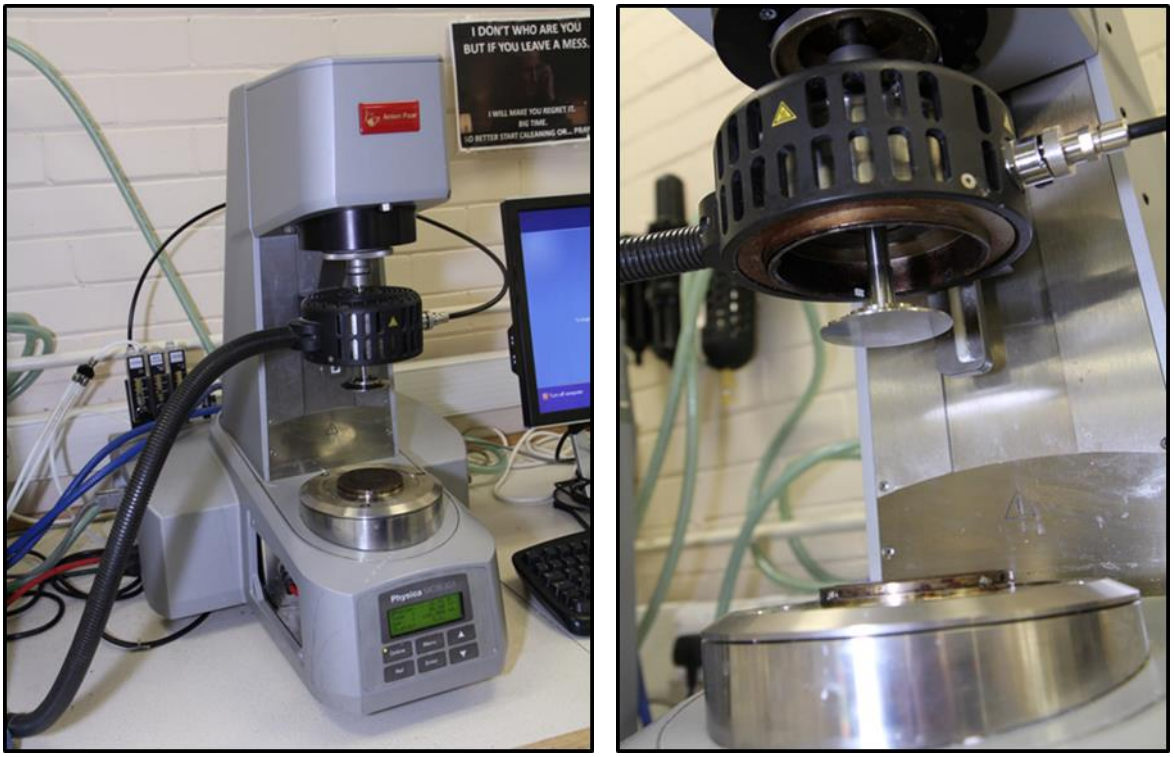

Figure 3.5.1 The Controlled Stress Rheometer used in this study (Anton Paar MCR 301).

3.5.2 Controlled Stress Measurements

Controlled stress test is a hysteresis loop method mostly used in the study of thixotropic fluids. It was used here to measure the yielding behaviour by increasing the stress from 0 to 150 Pa in the case of BPO and from 0 to 1500 Pa for LO and thixotropy by decreasing the stress back to 0. A good range of temperatures, cooling rates and stress loading rates were tested to arrive at a sound comparison between the oils and develop a good understanding of yielding develop with each of the two oils. The conditions tested are shown in Table 3.5.2.

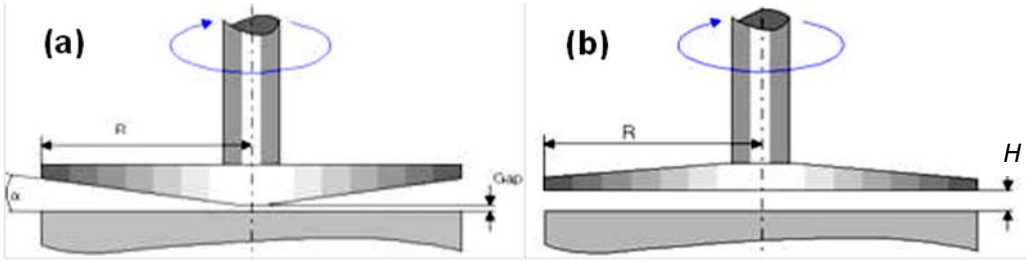

$\tau = \frac{3M}{2\pi R^3}; \quad \dot{\gamma} = \frac{2\pi N}{tan\,\alpha}$	$\tau = \frac{2\,M}{\pi\,R^3}; \; \dot{\gamma} = \frac{r\,\omega}{H}$

Advantages & Disadvantages of Flow Geometries

	Cone-plate geometry	Plate-plate geometry
Advantage	• High rate and homogenous shear conditions. • Any present air bubbles are pressed out of conical shear gap before the test start.	• Suitable for very viscous sample. • Large shear rate can be applied. • Allows presence of slip to be easily detected. • Allows attaching different roughness surfaces to study effect of pate roughness on measurements.
Disadvantages	• Particle size is limited. A three dimensional material cannot be measured. • For high viscosity materials, a long period is required before the equilibrium state is reached.	• Shear rate is not the same over the diameter • Solid-like material can be measured.

Figure 3.5.2: Rheometric flow geometries **(a)** Cone-plate **(b)** Plate-plate.

Table 3.5.2: Controlled Stress measurements range of testing conditions.

Control Parameters	BPO (WAT= 35°C)	LO (WAT= 61°C)
Initial temperature	60°C	80°C
Temperatures tested	Between 13 and 30°C	Between 15 and 45°C
Cooling rates tested	0.5, 1 and 2°C/min	0.5, 1 and 2°C/min
Stress Loading rates tested	10, 30, 80 Pa/min	30 Pa/min

3.5.3 Creep Recovery Measurements

Creep recovery tests were used to check that the yield stress measured using the controlled stress method lay within the correct range of stress values. Indeed, previous workers [7, 8] used this technique to zoom into the yield values. Thus they were performed for one crude oil only, in this case for BPO, the one whose values are the most sensitive (being of lowest) strength. Thus the elastic-limit yield stress and static yield stress were determined by applying different constant stresses on BPO samples at 18°C cooled from 60°C at cooling rate of 2°C/min and holding time for 10 min at test temperature for a creep time of 1 min and then removing the stress suddenly, and the strain recovery over time was recorded.

In the creep recovery test, the time scale of the measurement is presented as the creep time. The elastic-limit and static yield stresses are determined as a range of values of two applied stresses for time of 1 min. The creep time on the two measured yield stresses can be observed by studying the creep curves at different applied stresses.

3.5.4 Oscillatory flow Measurements

In rheology, oscillatory shear flow is most useful at extracting the viscoelastic behaviour of materials. Typically, a strain γ that varies sinusoidally with time at a frequency ω is applied and a stress σ which also varies sinusoidally with time at the same frequency but lagging behind is measured. These are described typically by the following equations:

$$\gamma = \gamma_0 \sin\omega t \qquad (1)$$

$$\sigma = \sigma_0 \sin(\omega t + \delta) \qquad (2)$$

In order to probe the structure of soft materials such as waxy crude oils gels, the application of strains at low amplitudes γ_0 is most desirable as the structure is initially conserved and only marginally deformed that is elastically and linearly. At these low amplitudes, the stress response Eq. (2) can then be expressed as:

$$\sigma = G'(\omega)\sin\omega t + G''(\omega)\cos\omega t$$

G' (the storage modulus) and G'' (the loss modulus) being the ratio of stress and strain amplitudes, G' being based on the amplitude of in-phase stress and G'' being based on the out-of-phase stress. These moduli express the relative contribution of the viscous and elastic response of such material and they are the parameters measured in oscillatory tests as a function of the frequency ω. As explained in the literature review chapter, such a method has been used extensively by previous researchers to measure yielding and subsequent fracture as the stress amplitude is increased.

Note that the measurements were carried out with the plate-plate geometry which providing a well roughened surface to avoid any slip during the test. Plates of diameter 50 mm diameters gave better repeatable data than the 25 mm plates for liquids such as the crude oils used in this investigations. The gap between the plates should be selected carefully to produce a uniform flow. For selecting the appropriate gap, trial tests were first conducted with BPO (chosen as it is the most sensitive in that it has comparatively lower yield stresses than LO) at fixed frequency of 0.3 Hz, changing the gap from 0.065 mm to 0.2 mm. The stress-strain

relationship of the different gaps experiments is shown in Figure 3.5.3. From the figure, it can be noticed that when the gap is increased, the longer the horizontal segment between the start of fracture (point B) and the end of the fracture (point C) is obtained with the testing gap of 0.12mm, indicating that is the best steadied behaviour allowing a variety of frequency values over a large range without affecting the overall trend between points B and C, thus a clear comparison in this region can be still obtained.

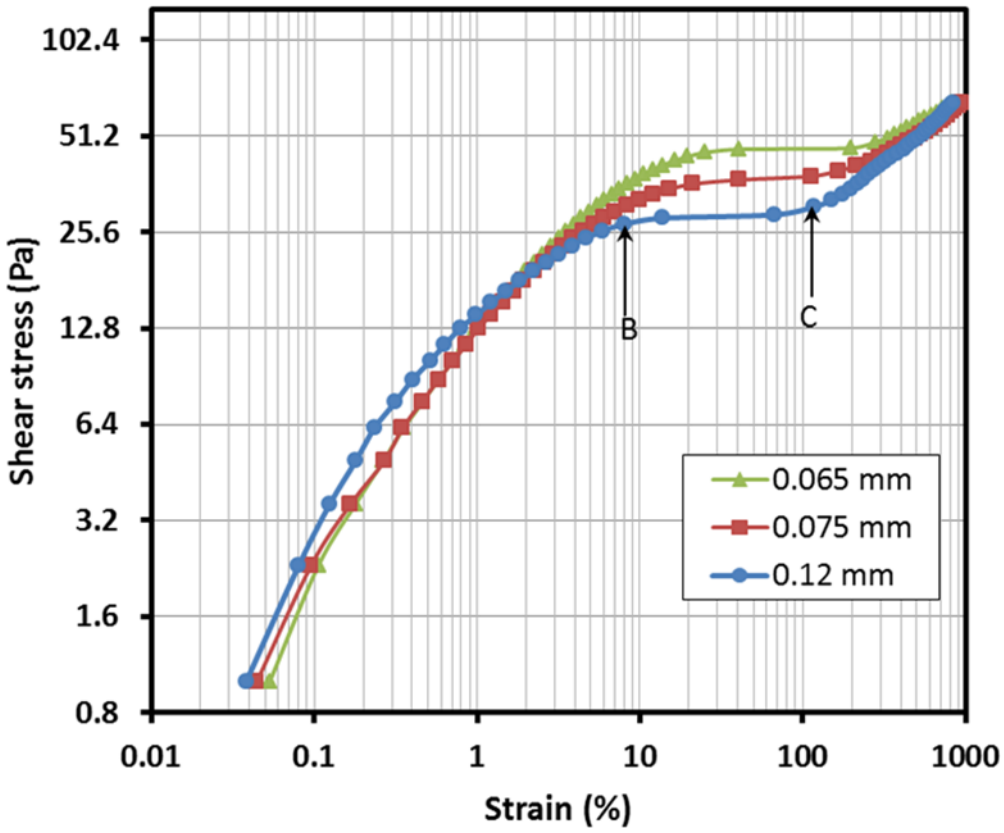

Figure 3.5.3: Oscillatory test: effect of testing gap on stress vs. strain curve during and after the yielding process for fresh BP crude oil samples tested at temperature 18^{o}C, cooling rate of 2^{o}C/min and frequency of 1 Hz.

As for the actual tests, they were performed on BPO and LO samples, preconditioned as in all cases in the range of conditions shown in Table 3.5.3 below.

Table 3.5.3: Oscillatory Shear Measurements Range of Conditions

Control Parameters	**BPO (WAT= 35°C)**	**LO (WAT= 61°C)**
Initial temperature of pre-conditioned oil	60°C	80°C
Temperatures tested	18°C	35°C
Cooling rates tested	2°C/min	2°C/min
Amplitude of oscillations and frequency tested	1 to 75 Pa 0.3, 1 and 6 Hz	1 to 120 Pa 0.3, 1 and 6 Hz

In order to measure the gel point, the same experiments (measuring G' and G'') were carried out but over a range of temperatures near the pour point, from 23°C down to 14°C for BPO and from 40°C down to 31°C, in steps of 3°C. This conducted at various cooling rates (0.5, 1 and 5°C/min) to assess the effect of cooling rate on the gel point. The gel point is obtained when a tested sample behaviour changes from viscous (G''>G') to elastic (G''<=G'), indicating wax precipitation upon cooling. Again three repeat experiments were carried out to ascertain the data.

3.6 Model Pipelines Restart Pressures Measurements

As stated in the introductory chapter, the ultimate aim of the research is to enable an accurate prediction of the minimum restart pressures of shut pipelines holding waxy crude oils which have been left to cool and form a gel as illustrated in Figure 3.6.1. As cooling is non-uniform, higher at the wall than in the centre of the pipe, there will be a corresponding gradient in temperatures and in the sizes of the wax crystals that form. As, the waxy crude oil is not entirely made of wax this differential cooling will induce diffusion of dissolved wax molecules from the centre towards the wall region where they will precipitate. As a result, an oil plug will form in the centre surrounded by a wax crystals core. Many smaller crystals will thus have formed on the cooler pipe wall, increasing in size towards the pipe centre. The tiny crystals will create a large interfacial wax-metal area resulting in strong adhesive forces between the wax and the metal. In the centre region, at the interface between the liquid oil plug and the wax core, the crystals will be larger in size, offering a correspondingly smaller interfacial area resulting in comparatively weaker cohesive liquid-wax crystal forces. The minimum restart pressure is thus equivalent to the force that must overcome the cohesive rather than the adhesive yield stress termed here $\tau_{y,c}$, given from force balance:

$$\Delta p \pi R_c^2 = 2\pi R_c L \tau_{y,c}$$

Naturally, this yield stress is obtained from the rheological measurements described above at the temperature that prevails at the oil plug-wax core interfacial area.

The model pipeline that is required must thus be one that can create differential cooling across its section and the plug-core structure rather than a uniform cooling and a uniform gel structure (see Figure 3.6.1). In other words, the diameter of the pipe must be large enough.

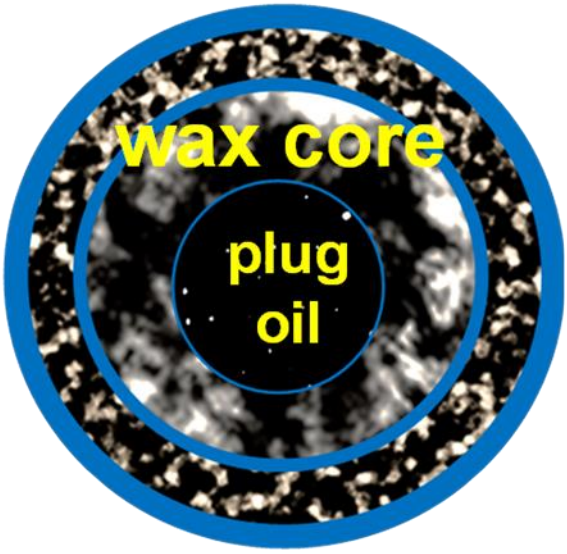

Figure 3.6.1: Schematic of a pipeline cross-section holding waxy crude oil under static cooling. The different thicknesses of the blue line circles represent various radial cooling rates, resulting in different radial crystal structure and thus different radial gel strength.

3.6.1 Design and Description of the Pipelines Rig

Following from the discussion above, the design of the rig is simple in principle- a pipe of diameter and length that can mimic the situation in the field with controlled heating (uniform along the entire length of the pipe) followed by controlled cooling (uniform along the entire length of the pipe) and a means to restart flow, observe its start point accurately and measure the corresponding restart pressure accurately.

As for the purpose of the rig, it is not merely to mimic the situation in the field, it also offers the opportunity to measure yield stresses that may correspond to those measured using rheological instruments, when a uniform cooling across the pipe is generated. Then the effects of cooling rates and temperatures can be assessed in similar way as done using rheological instruments. Effectively, the model pipeline rig can serve as a capillary rheometer when the pipe diameter is so small that cooling can be assumed to be uniform throughout the pipe cross section as it is uniform in the plate-plate or cone-plate viscometer.

On the basis of the above principle, the pipeline rig was built with the accessory components as shown schematically in Figure 3.6.2 using two 10m long

copper pipelines, one of internal diameters of 6.5mm (deemed to provide uniform cooling across the pipe diameter and one of internal diameter twice the size, 13.5mm. A third 13.5mm internal diameter pipe made of stainless steel, to investigate effect of the internal wall roughness and comparing to the 13.5mm copper pipeline. These pipes were jacketed (concentric pipes construction) by other copper pipes of the same length, 22mm internal diameter for the 13.5mm pipe and 12mm for the 6.5mm pipe, for controlled cooling or heating (from 0.16 to 5^{o}C/min) with water circulation throughout the annulus between the pipes. The pipes were fixed in the central position inside and along the pipes of the jackets using 18 star-rings with 0.5m distance between each other. All the external pipes were insulated with K-Flex® LS PVC as shown in Figure 3.6.2. The pipe temperature was measured and controlled to within ±0.5ºC using thermocouples distributed every 1m along the pipeline. The pressure drop along pipe length was measured using a manometer.

The oil sample was contained in a 2-litre aluminium pot, conditioned as previously described and then kept in the water bath at a temperature around 20^{o}C above the WAT of each crude oil (i.e. 60^{o}C for BPO and 80^{o}C for LO crude). After that, the oil sample was pumped into the heated pipeline by pressurising the pot with nitrogen gas taken from a cylinder at a controlled pressure. Once inside the pipe, the hot oil was left a few minutes to ensure a steady state base point then a controlled cooling rate was applied down to the desired test temperature. Once the test temperature was reached, the oil was held at that temperature to develop its gel structure. This time period will be referred to as the holding time period. The pipeline was then restarted by the application of a pressurized nitrogen gas applied at increments of 0.25 psi every 2 min until flow was deemed to have started when the free meniscus in the glass end of the pipeline outlet moved up as viewed using a video camera connected to a monitor. The pressure at which the oil started to move was considered as being the yield pressure, the equivalent of the yield stress.

No observations were made of the pipe interior; thus there was uncertainty on whether the gel broke at the wall or at the centre.

Using the set up and methodology just described, restart pressures were measured to establish the effects of cooling rate, test temperature and holding time on the yield stress of BPO and LO. Parallel experiments were carried out in the rheometer (see above) in order to make comparison. Table 3.6.1 describes the range of conditions covered, the important objectives being:

1) To demonstrate the hypothesis that in a case when the cooling is uniform, the yield stress calculated on the basis that the force balance is applied on the wall as $\Delta p\pi R^2 = 2\pi RL\tau_{y,w}$, rather than at the oil plug-wax crystals core interface as $\Delta p\pi R_c^2 = 2\pi R_c L\tau_{y,c}$, in such case the yield stress will not correspond to the one measured in the rheometer as the sample in the rheometer is uniformly cooled.
2) To demonstrate that as the pipe diameter is increased, the formation of the oil plug-wax crystals core is more likely to happen.
3) To demonstrate the importance of the adhesive force that develops at the wall between the wax crystals and the metal interface as reflected in the restart pressure (yield stress) measured with different roughness plate surfaces in the rheometer and two model pipelines differ in internal wall roughness, the rough pipe providing larger interfacial area. Copper pipeline with absolute roughness (*Ra*) = 0.002mm and stainless steel pipeline of absolute roughness (*Ra*) = 0.03mm were used in this study. In addition to using the original measuring parallel plate of the rheometer with finished stainless steel surface of roughness (*Ra*) = 0.002mm, different roughness surface was attached to the measuring parallel plate using a sandpaper with roughness (*Ra*) = 0.03mm, which the same roughness of the model stainless steel pipeline used as shown in Figure 3.6.3. Plate and pipe roughness was measured using a mechanical tester (Taylor Hobson Precision, AMETEK Inc., USA) which essentially a diamond-tipped stylus travelling across the surface and measuring the profile from which the amplitude (R_a) of the roughness is measured (see Figure 3.6.4).

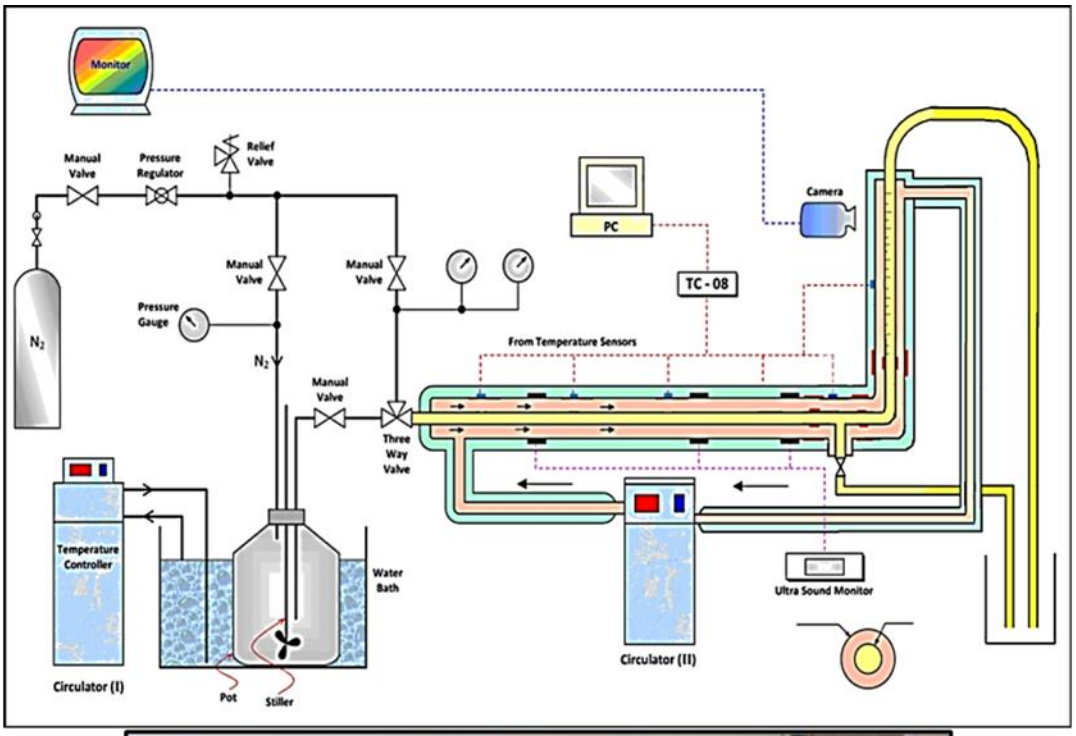

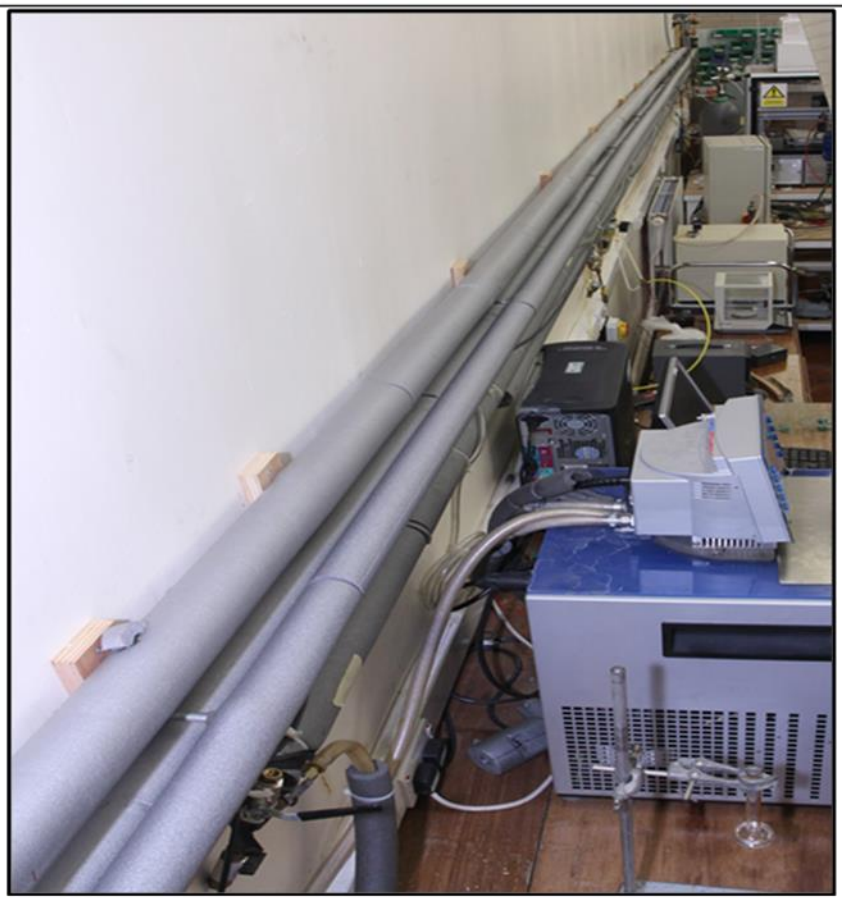

Figure 3.6.2: The simplified schematic of the laboratory model start-up pressure pipeline rig and picture of the laboratory model start-up pressure pipelines.

Table 3.6.1: Pipelines and Rheometer measurements range of testing conditions.

<table>
<tr><th>Control parameters tested</th><th>Crude oil tested</th><th colspan="8">Techniques</th></tr>
<tr><td rowspan="4">Cooling rates</td><td rowspan="4">LO</td><td colspan="2">Rheometer</td><td colspan="2">6.5mm ID pipe</td><td colspan="2">13.5mm ID pipe</td><td colspan="2"></td></tr>
<tr><td colspan="2">Ra (mm)</td><td colspan="2">holding time</td><td colspan="2">holding time</td><td colspan="2">Ra (mm)</td></tr>
<tr><td>0.002</td><td>0.03</td><td>5min</td><td>4hrs.</td><td>5min</td><td>4hrs.</td><td>0.002</td><td>0.03</td></tr>
<tr><td colspan="8">0.05, 0.1, 0.2, 0.5, 1, 2, 5 °C/min</td></tr>
<tr><td rowspan="5">Temperatures</td><td rowspan="2">LO</td><td colspan="3">Rheometer</td><td colspan="2">6.5mm ID pipe</td><td colspan="2">13.5mm ID pipe</td></tr>
<tr><td colspan="7">Ra = 0.002mm, holding time = 5min, 0.2 °C/min</td></tr>
<tr><td colspan="8">15, 25, 35, 40 °C</td></tr>
<tr><td rowspan="3">LO and BPO</td><td colspan="7">6.5mm ID pipe</td></tr>
<tr><td colspan="7">2°C/min, holding time 3hrs., R_a= 0.002mm</td></tr>
<tr><td colspan="4">LO</td><td colspan="3">BPO</td></tr>
<tr><td colspan="4">15, 25, 35, 40 °C</td><td colspan="3">15, 20, 25, 30 °C</td></tr>
</table>

Figure 3.6.3: The 50mm measuring parallel plates of different surface roughness.

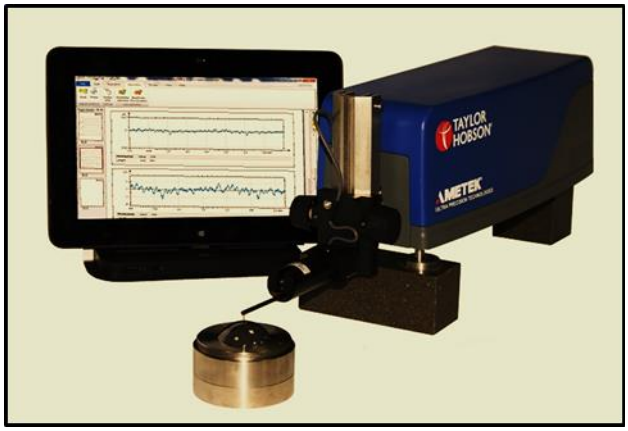

Figure 3.6.4: The roughness tester (Taylor Hobson) used in this study.

3.7 Temperature and Deposition Profiling Measurements

3.7.1 The "Static Cooling" Rig

It follows from the previous section that in order to predict the correct yield stress from the restart pressure measurements, the location of the oil plug-wax crystals core interface is required ($\Delta p \pi R_c^2 = 2\pi R_c L \tau_{y,c}$). As the oil core-wax crystals deposit structure derives from the differential cooling in the pipe and the corresponding diffusion of the wax molecules towards the wall, the measurement of the temperature profile across the pipe holding the cooling oil is necessary. A "static cooling" rig was thus constructed for these measurements. It consisted of two concentric glass pipe heat exchanger type 150 mm height (double glazing), one 60mm internal diameter and one 120mm internal diameter. The inner pipe held the oil and the outer annular held the heating/cooling fluid (water), thus enabling the replication of the situation of a hot waxy crude oil being held stagnant in a pipe and allowed to cool and form an oil core-wax crystals deposit structure. Figure 3.6.5 shows the experimental set-up composed of the concentric glass pipe (shown here un-insulated), the water heater/cooler, a data logger and a pc controlling and logging the operating parameters. Figure 3.6.6 gives a cross section of the inner pipe holding the oil with 4 pre-calibrated K-type thermocouples positioned across the pipe radius, at an angle of 30^0 from each other (see Table 3.6.2). The 4 thermocouples immersed in the oil were fixed on steel rods dipped halfway into the oil. To minimize any heat loss by conduction, the exposed surfaces of all thermocouples were covered with a tight-fitting tygon tube, except for their tips for temperature measurement.

To ensure that the heat transfer took place only between the waxy crude oil and the coolant in the radial direction, appropriate steps were taken to insulate all other surfaces. A circular disk of Styrofoam insulation, 4 cm in thickness was placed on the bottom of the pipe vessel, fixed and covered with silicone, and the top of the vessel was covered by Styrofoam lid, 5 cm in thickness as shown in Figure 3.6.5. All inlet and tubes and the vessel body were covered with thermal insulation to minimize heat loss.

3.7.2 The Static Cooling Rig Mode of Operation

During the experiments, preconditioned samples of the crude oil (BPO and LO) were put in the vessel heated to 80^{o}C and held isothermally for 1 hour to achieve thermal equilibrium across the diameter of the vessel. The oil was then cool down to an initial temperature, 20^{o}C above WAT. This temperature was controlled via the 4 thermocouples as described above and constituted the initial uniform temperature of the oil. Then a cooling rate was applied at the wall of the vessel and temperatures across the vessel radius recorded by the 4 thermocouples until the lowest temperature recorded reached a value below the pour point of the oil. Cooling rates in the range 1 to 0.05^{o}C/min were tested.

Prior to these tests, calibration experiments were performed to ensure that the inner wall temperatures were the same around the vessel and that there was symmetry in the temperatures measured. For this, heating-cooling experiments were carried out with additional thermocouples placed in the opposite side of the main measuring thermocouples and distributed at the same diameters with the same distances and angles as shown in Figure 3.6.7. This calibration method was implemented in both the 120mm and 60 mm vessels.

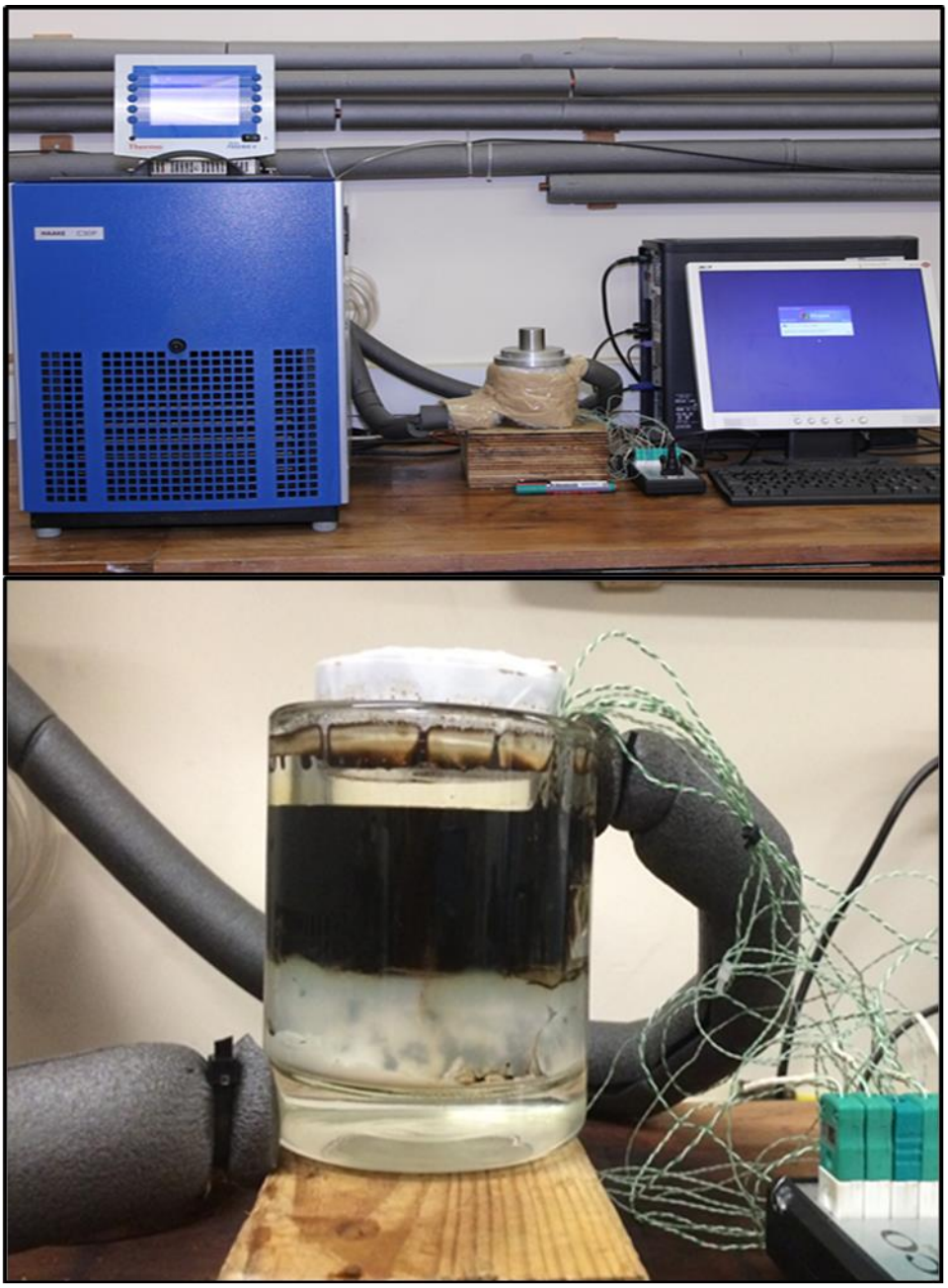

Figure 3.6.5: Experimental setups for static cooling in the cylinderical vessel.

Table 3.6.2: Radial locations of thermocouples in the cylindrical vessels for static deposition experiments

120 mm diameter vessel		60 mm diameter vessel	
Thermocouple label	**Radial distance from the vessel wall (mm)**	**Thermocouple label**	**Radial distance from the vessel wall (mm)**
TC1	10	TC1	5
TC2	20	TC2	10
TC3	40	TC3	20
TC4	60	TC4	30

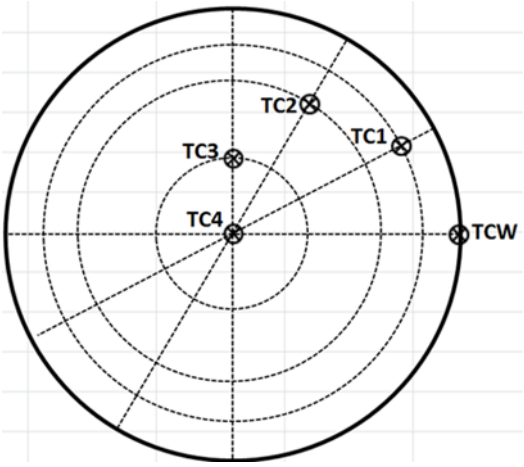

Figure 3.6.6: Radial distribution of thermocouples in the vessels for static cooling experiments.

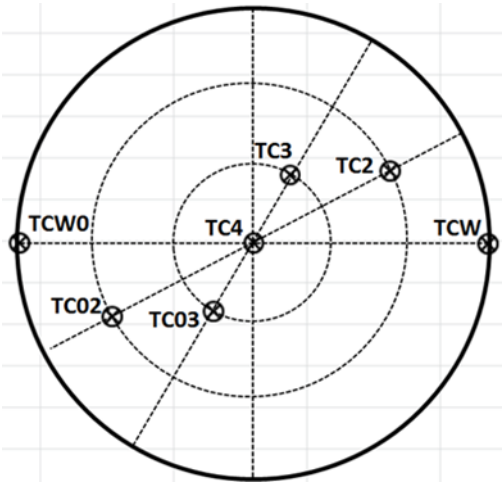

Figure 3.6.7: Radial distribution of thermocouples in the vessels for measurement calibration experiments.

4. RESULTS AND DISCUSSION

4.1 Introduction

In this chapter, the results obtained from the experimental programme are presented and analysed. As stated in the introduction, the aim here is to develop a technique that enables precise prediction of start-up pressures of waxy crude oils that have gelled upon cooling in pipelines. Clearly this requires a comprehensive multi-aspects package of experiments which consider not only the fundamental properties of the oils but also the way they gel upon cooling in shut-down pipelines. Two real, as obtained from the oil fields, waxy crude oils of different origins (Libya and North Sea, denoted LO and BPO respectively) and wax content were considered and the following package of experiments were carried out:

(1) Calorimetry- using a Differential Scanning Calorimetry (DSC) to measure the fundamental properties of the oils as they are heated then cooled at controlled heating and cooling rate. The properties measured include wax appearance temperature (WAT), wax disappearance temperature (WDT), and wax total concentration, and mass fraction of wax precipitating at any temperature below WAT. *These basic data will inform the critical temperatures to consider in the rheological studies*.

(2) Rheology- using a state of the art rheometer, capable of operating at very low constant stress to zoom into the yield region of gelled oils. As noted in the literature survey, the novelty of the work resides in being able to operate at low stresses, a feature not available to earlier researchers. Constant shear stress, constant shear rate, oscillatory shear and creep modes of measurements were carried out in order to obtain comprehensive data on the yielding, creep and fracture of gelled oils as well as cross checking the data. In the rheological investigations, the effects of temperature and cooling rate were measured as well as the rate of the applied stress. *The data so collected should provide the*

yield stress(s) and the rheological model that are necessary to predict the start-up pressures of gelled oils. *In addition, the rheological data will also provide an indication of the gel point as it will be shown.*

(3) Microscopy- using a Cross Polarised Microscopy (CPM) to observe the gelation, crystallisation processes and morphology of oils that have been heated then cooled at controlled heating and cooling rate. *Such information will help unravel the mechanism of gels breakage in shutdown cooled pipelines- that is whether they break at the wall or at the gel front.*

(4) Static cooling temperatures profile- using a small scale cylindrical vessel, reproducing the conditions of an actual pipeline suddenly shut and allowed to cool; this to measure the formation and development of gelling across the pipe cross section. This data will enable to locate precisely the gel front that separates the wax deposit region and the still-fluid central section. *This information is critical in the calculation of the start-up pressure using rheological data. Remember that the start-up pressure derives from a force balance using the yield stress and the location of the gel front.*

(5) Start-up pressure- using model, small scale pipelines of various diameters and roughness. As described in the previous chapter, these model pipelines were design to reproduce under static cooling mimicking the conditions of actual pipelines during shutdown, i.e. under static cooling conditions. *The data so collected will provide a check on the predicted start-up pressures using rheological data.*

4.2 Calorimetry or Fundamental Properties of Gelled Waxy Crude Oils

As explained at the outset, waxy crude oils are hydrocarbons which contain dissolved wax (alkenes). When hot, the wax is completely dissolved in the solvent hydrocarbons but upon cooling below a critical temperature, it begins to precipitate. The temperature at which wax begins to precipitate out from waxy crude oil is called Wax Appearance Temperature (WAT). Flow assurance study for waxy crude oil systems often require measurement of at least two keys from crude oil properties, the WAT and the gel point (T_{gel}). Using the WAT and gel point, the

rheological and behaviour problems of waxy crude oil can be represented into three regions on a temperature scale; *first region* is identified by the temperatures above the WAT where the crude oil acts as a Newtonian fluid and there is no possibility of wax deposition, *second region* is identified by the temperatures between the WAT and the T_{gel} where the crude oil acts as light behaviour of non-Newtonian fluid, and *third region* is defined by temperatures below the gel point where the crude oil behaves as highly non-Newtonian fluid and the oil behaviour changes from viscous to viscoelastic and may gelled under static conditions. Clearly whereas WAT is a well-defined transition temperature, a fundamental property, gel point (T_{gel}) is a subjective property, albeit a useful one in practical terms. When considering rheology, it should be possible to give a better defined condition for the gel point; the temperature at which a waxy crude oil gels is an important property that determines the initiation of the deposition process.

Here are described WAT measurements obtained with the two oils considered, using a DSC device which measures the heat flow in or out as temperature is increased or decreased at identified cooling rates. Clearly, upon wax precipitation, a phase change will occur causing a sharp change in the isotherm. Figure 4.2.1 presents such a feature and the ensuing data for the two oils considered in this study, cooled down to -20^{o}C at cooling rate of 0.5^{o}C/min, from 60^{o}C in the case of the North Sea oil (BPO) and 80^{o}C in the case of the Libyan oil (LO). As shown in the figures, the WAT is determined from the sudden increase in heat flow, 31.8^{o}C for BPO and 65.7^{o}C for LO under the condition of 0.5^{o}C/min cooling rate. Figure 4.2.2 presents data for a series of increasing cooling rates, 1, 5, 10 and 15^{o}C/min, the effect of which is to decrease the WAT (63.3, 62.7, 61.8 and 60.4^{o}C for LO and 30.3, 27.5 and 26.4^{o}C for BPO). The reverse temperature (at which the wax formed dissolves again in the oil), the Wax Disappearance Temperatures (WDT) presented in Figure 4.2.3 showed an increase rather than a decrease with cooling rates (60.7, 61.9, 62.4 and 64.2^{o}C for LO and 36.3, 37.8 and 39.9^{o}C for BPO). This can be explained as follows. As the cooling rate is increased, wax precipitates at lower temperatures (WAT) and networks with smaller crystals (not allowed to grow) are formed suggesting a weaker structure

compared to larger crystals which requires higher temperatures (WDT) to break down). For the purpose of comparison, Figure 4.2.4 shows the opposing variations of WAT and WDT with cooling rate. This assertion will be checked via microscopy (see Section 4.5) that large cooling rates produce smaller crystals than low cooling rates.

At a set cooling rate, it is clear that the DSC will deliver not only the WAT and WDT but also the total heat (heat of crystallisation) out of the system upon the precipitation of all the wax. The total heat (the area measured under the curve shown in Figure 4.2.1) together with the heat flow curve enable the calculation of the wax fraction being precipitated at a given temperature using Eq. 2.6 by Jun Chen et al, 2003). Taking the example of Figure 4.2.1, the total heat as being 21.481 Jg^{-1} for BPO and 61.605 Jg^{-1} for LO, the total wax content of BPO can be computed as being 16.3 wt % and 46.4 wt % for LO. Clearly, LO has much larger wax content than BPO, (a reason these two oils were chosen). Using the same reasoning, the fraction being precipitated at a set temperature will be the total heat (the entire area under the curve) divided by the area under the curve from its left (hot) beginning to the temperature at which it is being cooled. Figure 4.2.5 present such data for BPO and LO at a cooling rate of 0.5^{o}C/min. To emphasise the importance of the cooling rate on the precipitated wax fraction, Figure 4.2.6 presents the data measured for a series of cooling rates.

In conclusion, the DSC measurements have provided the necessary data to guide the rheological work in that the critical temperature at which the wax begins to precipitate (WAT) is obtained unequivocally. Also, the DSC data demonstrated how WAT and WDT show opposite variation with cooling rate indicating the importance of cooling rate on the structure (strength) of the wax network (crystal size and by implication number). In principle this should tally with the rheological measurements on the yielding of these structures.

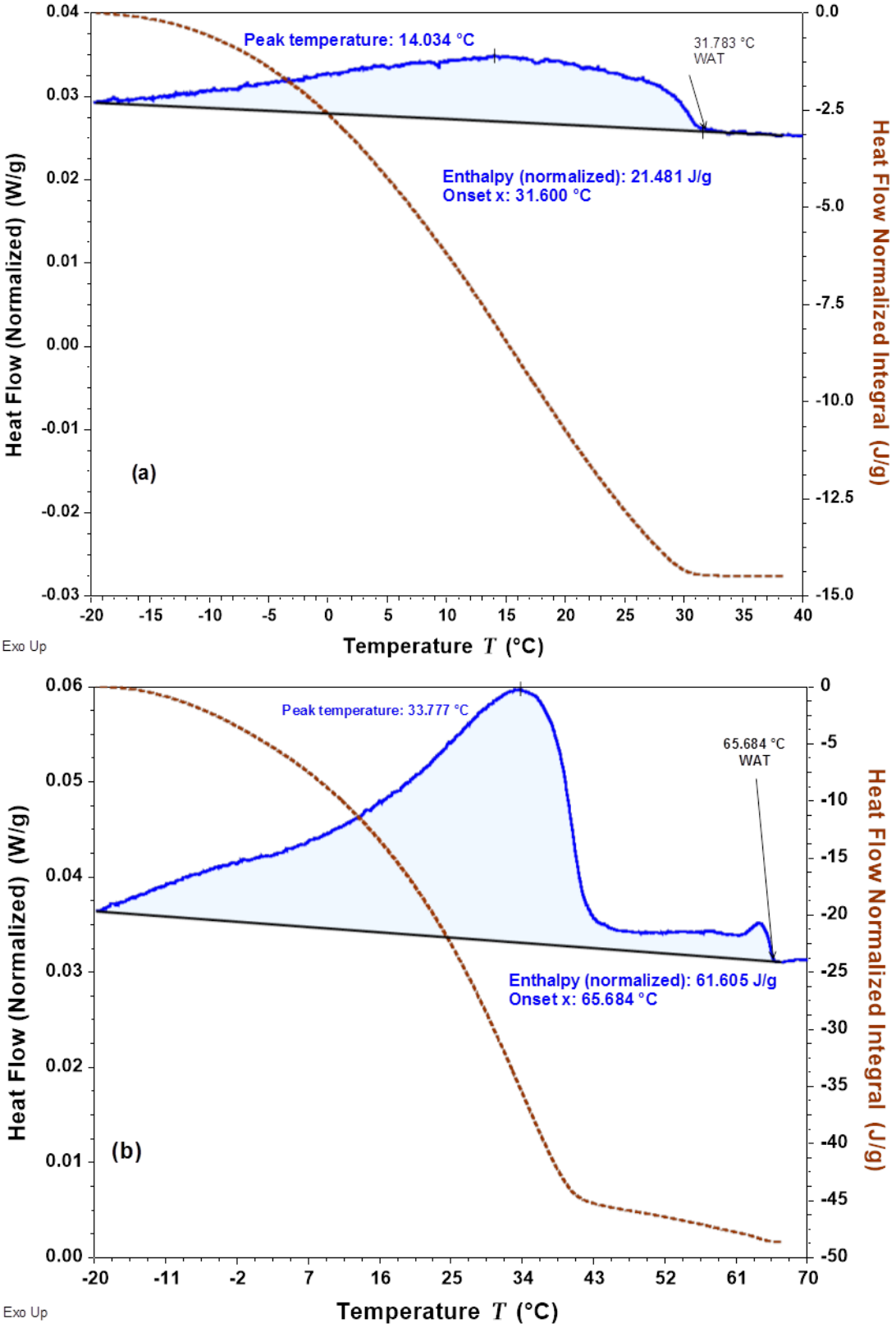

Figure 4.2.1: Heat flow vs. temperature measured by DSC at cooling rate of 0.5°C/min for **(a)** BPO and **(b)** LO.

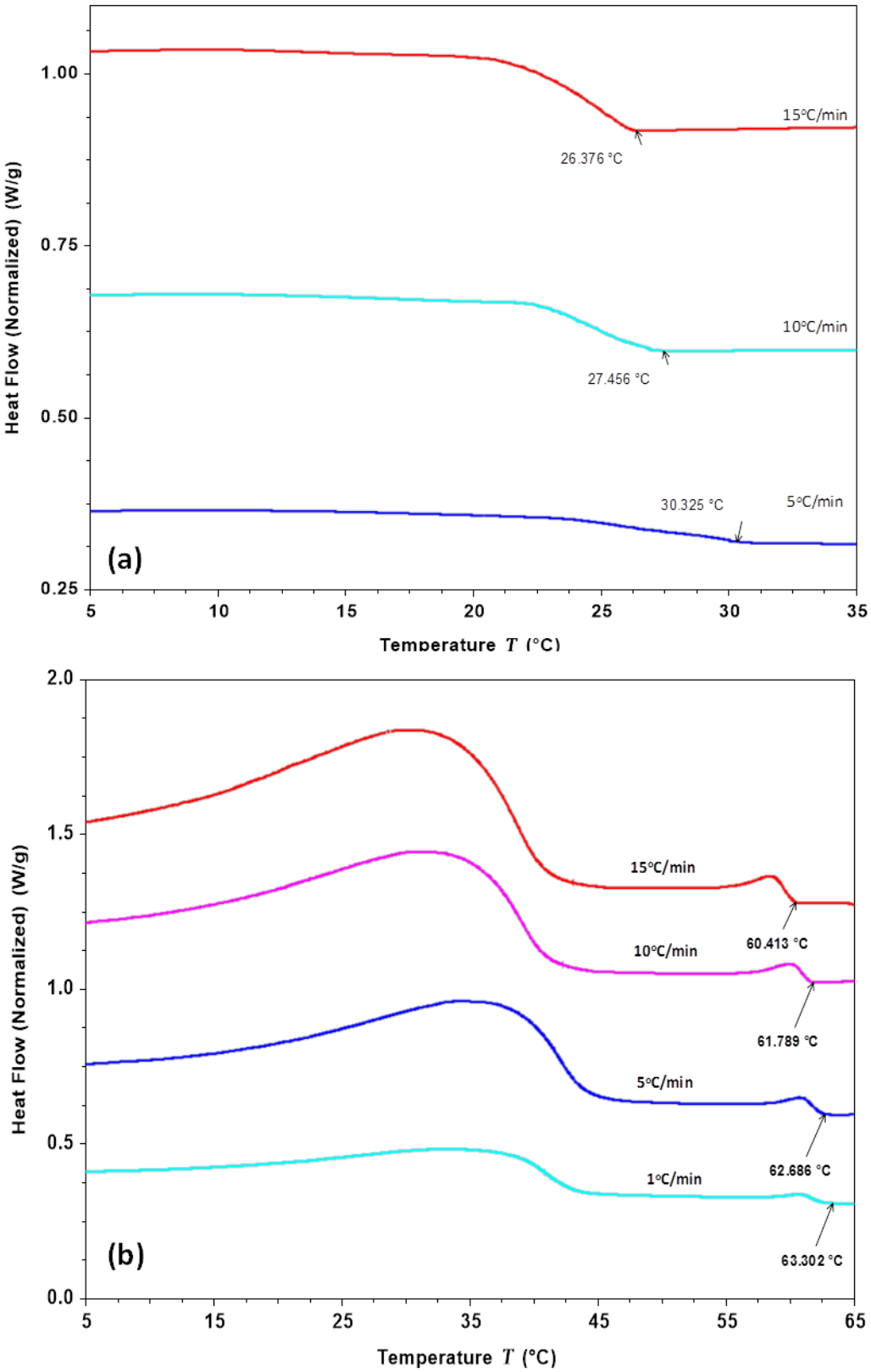

Figure 4.2.2: Effect of cooling rate on WATs for **(a)** BPO and **(b)** LO.

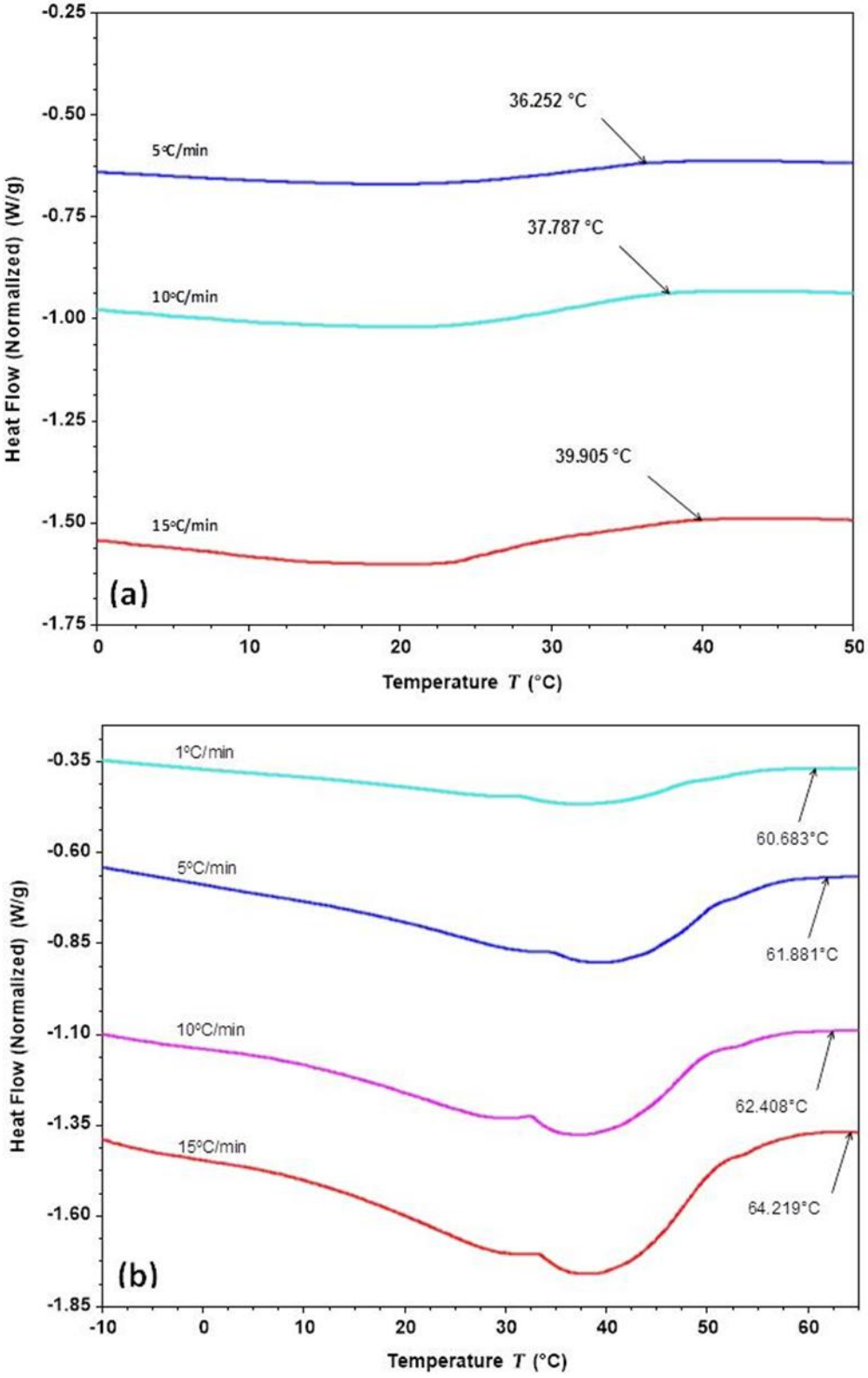

Figure 4.2.3: Effect of cooling rate on WDT of for **(a)** BPO and **(b)** LO.

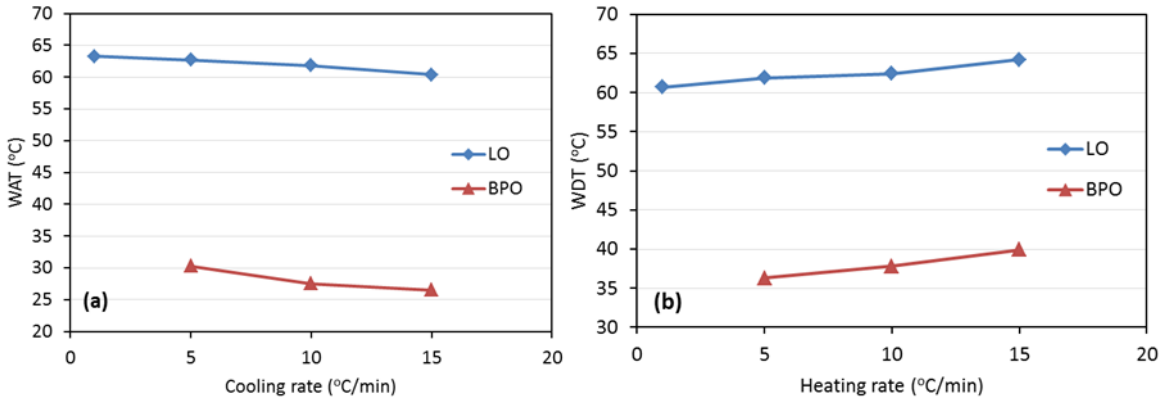

Figure 4.2.4: The opposing variation of (a) WAT and (b) WDT.

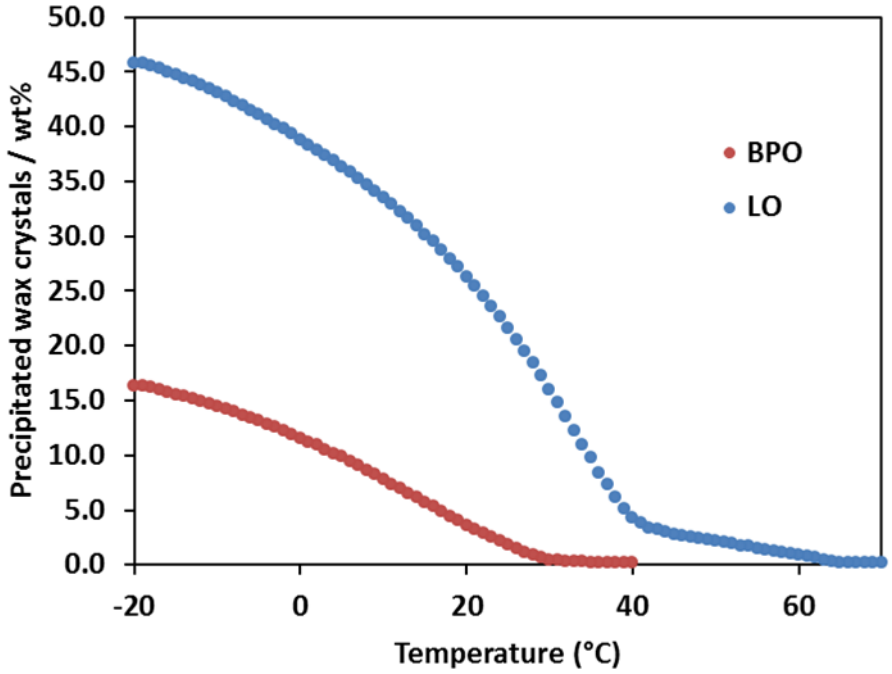

Figure 4.2.5: Precipitated wax as a function of temperature for BPO and LO crude oils under cooling at cooling rate 0.5°C/min.

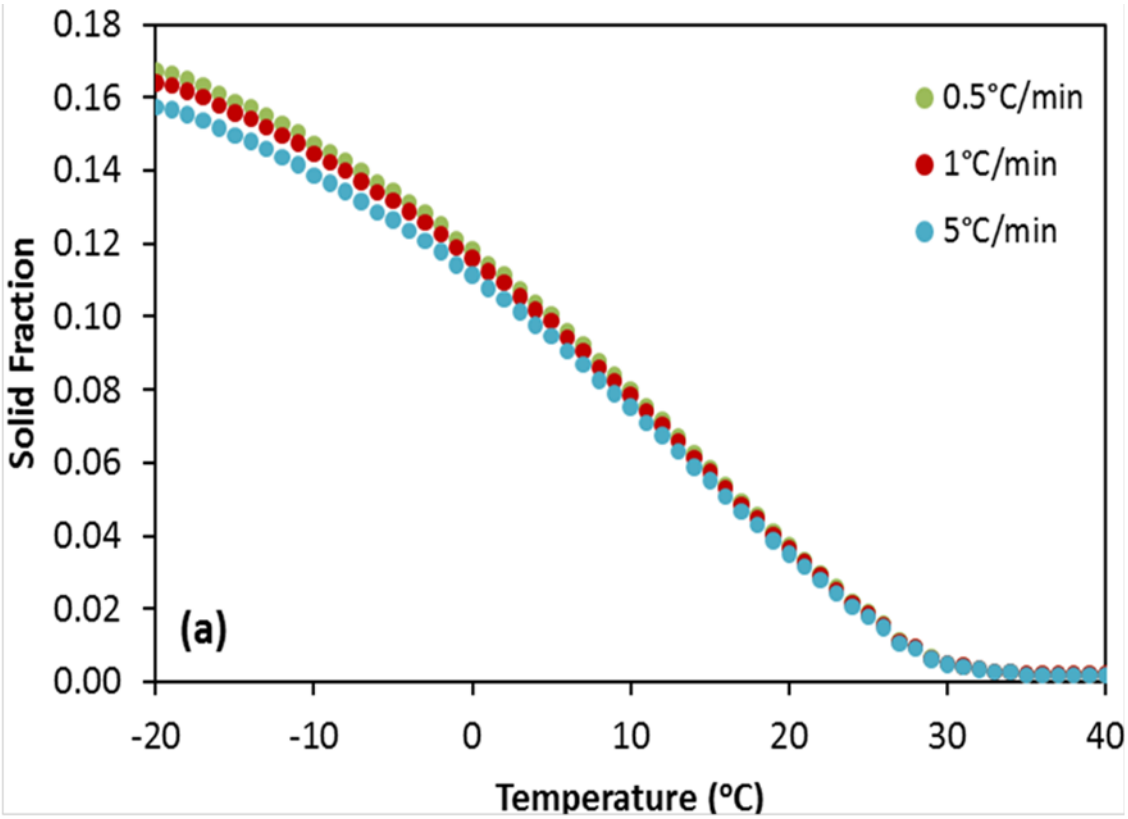

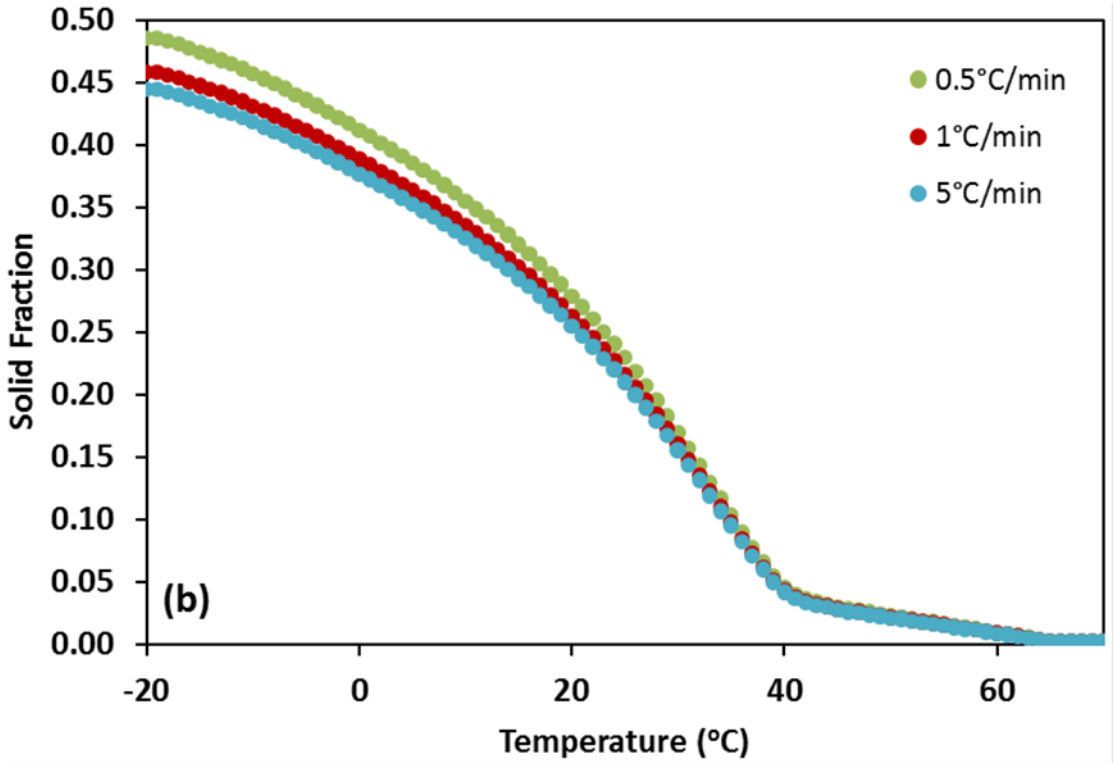

Figure 4.2.6: Effect of cooling rate on solid fraction in **(a)** BPO crude oil **(b)** LO crude oil.

4.3 Rheology of Gelled Waxy Crude Oils

Following from the DSC measurements, here are presented data that probe into the yielding and subsequent deformation that occurs before a gelled waxy crude oil can flow. These measurements are central to this research and as explained in previous chapters.

With regard to the range of conditions tested, remember from the DSC measurement that the WAT was about 32^{o}C for BPO and 65^{o}C and decreased by a few degrees as the cooling rate was increased, 4^{o}C at most when the cooling rate was increased from 0.5 to 15^{o}C/min. Clearly the temperatures to be tested will be near and below WAT. Remember also that our ultimate interest is to use the rheological data to predict start-up pressures of shut-down pipelines which have been allowed to cool because of pump and heating power failure. Thus the lowest temperatures reached upon cooling will be ambient temperatures. However, because of the high risk associated with leaving a shut-down pipeline cool, start-up will be carried out as soon as possible, that is at marginally higher than ambient temperature. For this reason, a base line cooling rate of 0.5^{o}C/min and cooled temperatures of 15^{o}C and 35^{o}C were chosen for BPO and LO respectively to reflect on the fact that BPO is a North Sea crude oil and LO is a Libyan crude oil. However, data for a range of temperatures and cooling rates are also presented as shown in Table 4.3.1 below. The other important parameter to consider is the stress loading rate as for start-up, it is required to know how to increase the pump power (is low better than large?) and the rheological data will help guide us. The range of stress loading rates considered is also presented in Table 4.3.1.

Table 4.3.1 Parameters conditions used in this study for the rheological measurements.

Crude oil	Temperature (^{o}C)	Stress Loading Rate (Pa/min)	Cooling Rate (^{0}C/min)
BPO	13, 15, 20, 25, 30	10, 30, 80	0.5, 1, 2
LO	15, 25, 35, 40, 45	10, 30, 80	0.5, 1, 2

Finally, and importantly, the presentation of a sample with no memory to the rheometer is an important aspect as explained earlier. In the section below it is shown how prior conditioning of the oils is the first consideration in the rheological measurements to ensure the gathering of meaningful and repeatable data.

4.3.1 Prior Conditioning & Repeatability of data

The procedure for conditioning the oils prior to rheological measurements was described in the previous chapter. Essentially, any prior memory is removed to ensure an appropriate base line by heating and mixing the oil well above its WAT over a sufficient time period and maintaining it at this high temperature, 60^{o}C for BPO and 80^{o}C for LO, the same start temperature of the plate rheometer. Figure 4.3.1 compares controlled stress data carried out for two BPO samples, one conditioned as just explained and one left unconditioned. Figure 4.3.1 presents also results from repeat experiments. The controlled stress experiments were carried out at 18^{o}C after the oil was brought down to this temperature from its initial temperature of 60^{o}C at a cooling rate of 2^{o}C/min under a stress loading rate of 30Pa/min. The difference in the results is striking showing:

(i) Large differences in the magnitude of the flow curves, the unconditioned samples showing much higher yield stresses than the conditioned samples;

(ii) Unrepeatable flow curves with the unconditioned samples and;

(iii) Repeatable flow curves with the conditioned samples.

Thus although the two samples, unconditioned and conditioned, were tested in the rheometer under the same conditions (cooled from 60 to 18^{o}C at a cooling rate of 2^{o}C/min on the rheometer plate), their prior history was very different, the unconditioned samples having its precipitated wax not destroyed through mixing prior to testing. Similar experiments carried out for conditioned and unconditioned LO samples and showed similar behavior.

Clearly prior conditioning is pre-requisite for meaningful and repeatable results and was adopted throughout the program.

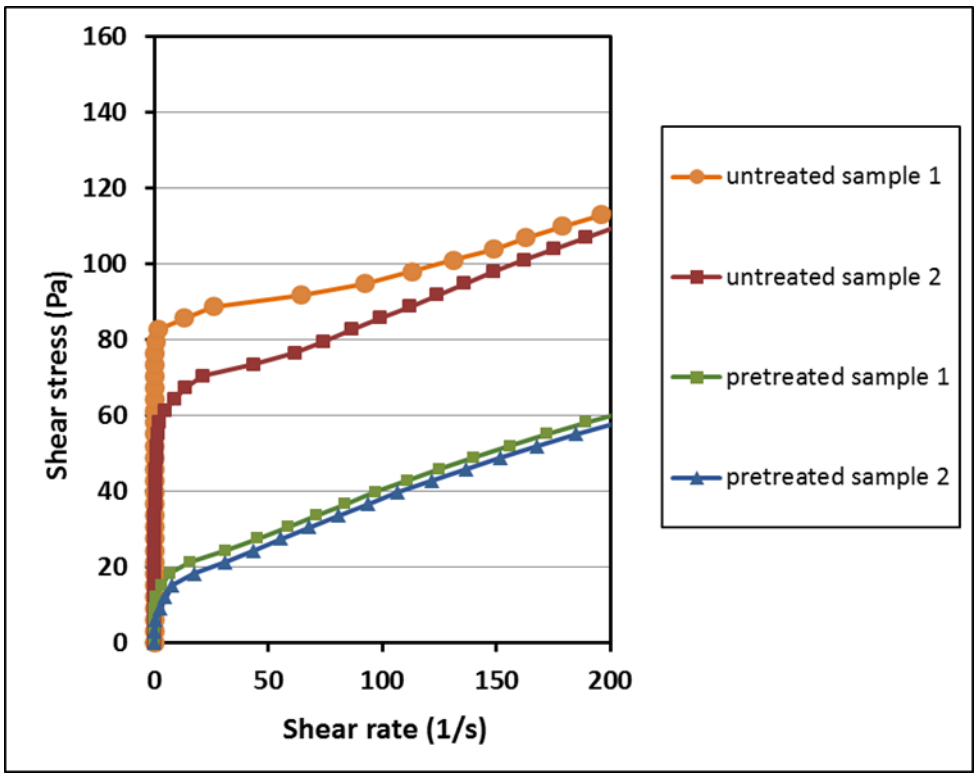

Figure 4.3.1: Comparison of controlled stress experiments of unconditioned and conditioned BPO samples (T=18^{o}C, cooling rate=2^{o}C/min from 60^{o}C, stress loading rate= 30Pa/min).

4.3.2 Controlled Stress Rheology

As previously described in the experimental design chapter, the controlled stress test is a hysteresis loop method mostly used in the study of thixotropic fluids. The data are obtained by applying a shear stress sweep at a predetermined rate from 0 to an upper value and back and measuring the corresponding shear rate. Such method is very appropriate at measuring the entire deformation process, here the initial elastic deformation up to yielding and subsequent creep and fracture followed by viscous flow. As the sweep goes from zero shear stress into the viscous flow region and back to zero, the approach enables also the measurement of thixotropic behaviour. With advanced rheometers such as the one used in this study capable of applying measurable very low stresses (here starting at 10^{-7} Pa and resolving shear rates down to 10^{-6} min^{-1}) to capture the entire rheology of waxy crude oil in very small increment, the technique can deliver in principle a precise

foot-print of the entire deformation and pin point exactly the end of elastic deformation when yielding begins denoted by an *elastic-limit yield stress* (τ_e) or the beginning of creep; the end of creep or the beginning of fracture denoted by a *static yield stress* (τ_s); the end of fracture or the beginning of viscous flow denoted by *a fracture yield stress* (τ_f). Assuming the ensuing viscous flow to be Newtonian (as the wax would have been completely destroyed and dispersed into the hydrocarbon base), this linear part of the flow will be then defined geometrically by extrapolating to a *dynamic yield stress* (τ_d). Such elasto-visco-plastic (EVP) flow behaviour, illustrated schematically in Figure 4.3.2, is described here by 4 yield stresses, two well-defined, τ_e and τ_d (end point of the linear elastic region and extrapolated point of the linear viscous region, respectively) and two less well-defined, τ_s and τ_f as they define the end of creep and fracture respectively. Both τ_s and τ_f have to be estimated somehow, most suitably by the scale of change in the stress-strain curve as explained in Figure 4.3.2. Clearly, whereas τ_e and τ_d can be expected to be independent of the stress loading rate, τ_s and τ_f will not be as they describe the deformation of the net gel work between the elastic and viscous regimes where the rate of creep and fracture will depend on the rate of stress loading. The lower the stress loading rate, the easier the bonds holding the gel crystal will creep and break. To complete the picture of the behaviour expected, it is clear also that temperature and cooling rate will affect deformation and subsequent flow. This is because temperature dictates the amount of wax that will precipitate and cooling rate the structure of the gel network, i.e. the size and number of the crystals and by implication the strength of the bonds that hold them together.

In conclusion, prior to presenting the results, we have explained how complex the rheological behaviour is expected to be and have presented the corner stones of the rheological model that should ensue- one that will be defined by 4 yield stresses that will depend on temperature, T, cooling rate, $\dot{T}$, stress loading rate, $\dot{\tau}$ and wax concentration, w_c (to reflect on differing waxy crude types) as follows:

$$\tau_e = \tau_e(T, \dot{T}, w_c)\ ;\ \tau_d = \tau_d(T, \dot{T}, w_c);\ \tau_s = \tau_s(\dot{\tau}, T, \dot{T}, w_c)\ ;\ \tau_f = \tau_f(\dot{\tau}, T, \dot{T}, w_c) \qquad (4.1)$$

Guided by these considerations, the various data collected are now presented in order to measure these yield stresses and how they vary with operating conditions.

4.3.2.1 Elastic, Static, Failure and Dynamic Stresses

Typical data (at one set of temperature, cooling rate and stress loading rate) for BPO and LO as shown in Figures 4.3.3-4.3.4 broadly first to show the similarity with Figure 4.3.2 then zooming into the yield areas of interest to resolve the values of τ_e , τ_s , τ_f by monitoring the change of slope $d\dot{\gamma}/d\tau$ or *fluidity* as shown in Figures 4.3.5. As can be noted that τ_d is obtained by extrapolating the linear viscous region at zero shear rate, as shown in Figure 4.3.3a and 4.3.4a. The dotted red line in Figures 4.3.3b - 4.3.4b shows the only possible minimum limit shear rate was obtained by Chang and Boger (1998), in comparison to our obtained data.

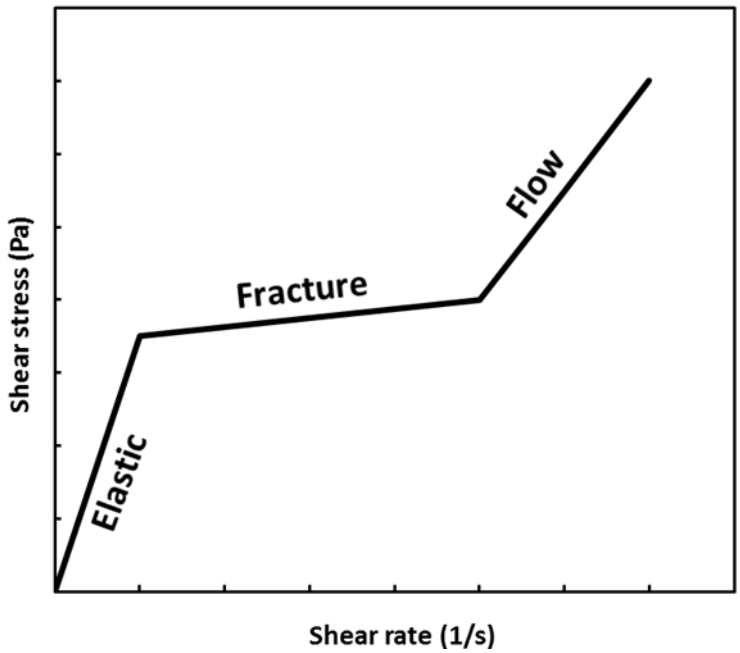

Figure 4.3.2: Illustration of the yielding characteristics of waxy crude oils.

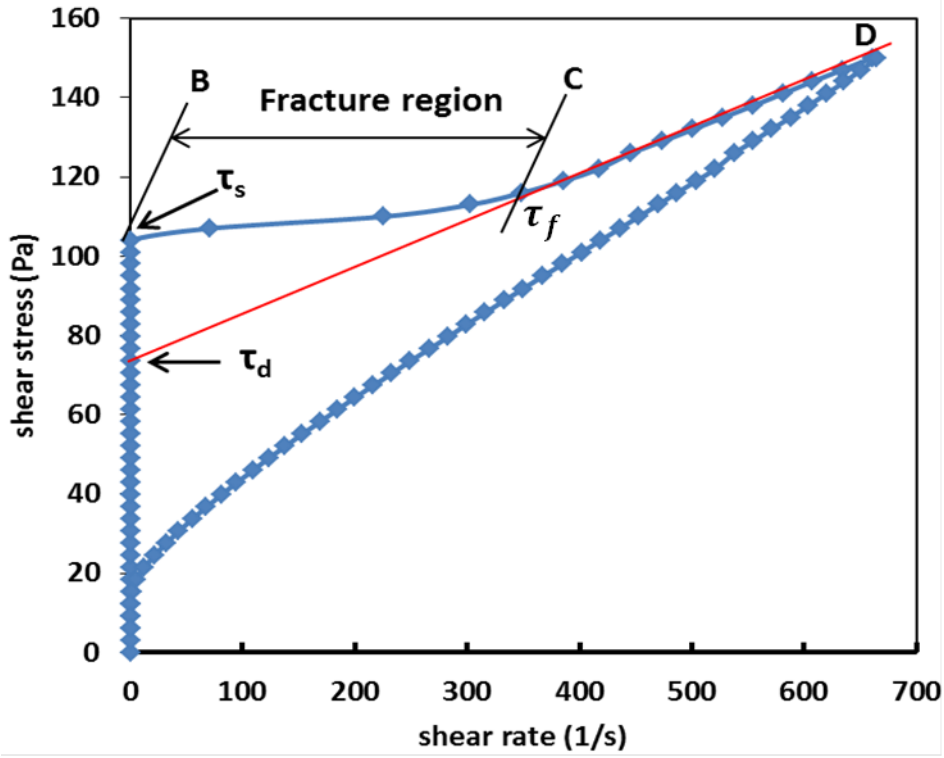

Figure 4.3.3a: Controlled stress sweep for BPO at 15°C, cooling rate 0.5°C/min, stress sweep 0-150Pa and stress loading rate 30Pa/min.

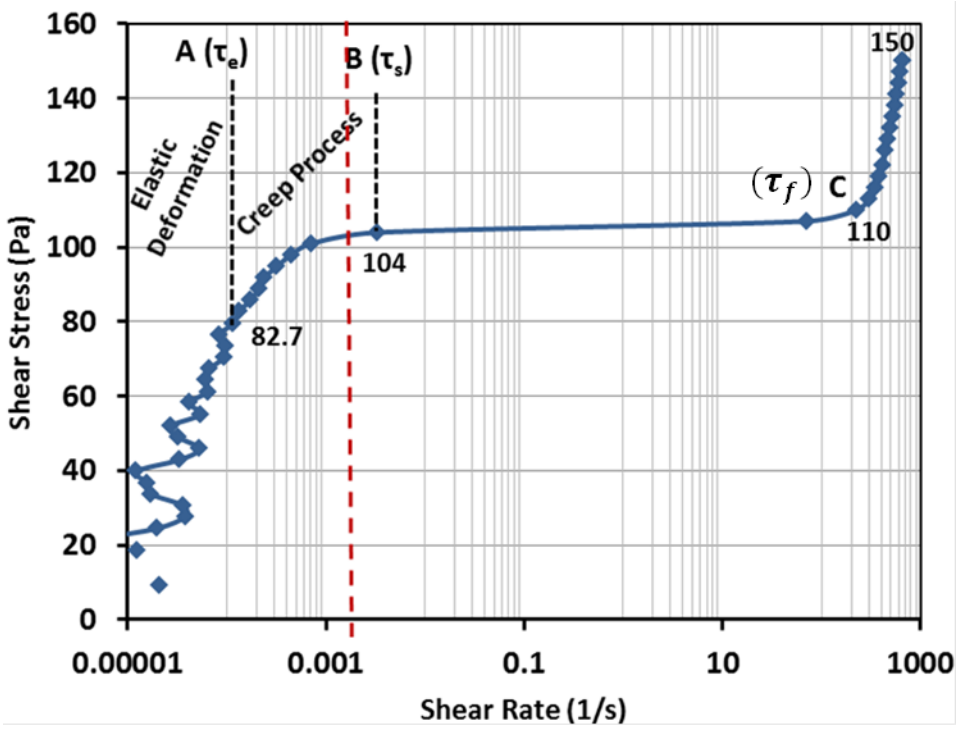

Figure 4.3.3b: A log-log zoom into the controlled stress data for BPO at 15°C, cooling rate 0.5°C/min, stress sweep 0 -150 Pa for 5 min at stress loading rate 30Pa/min.

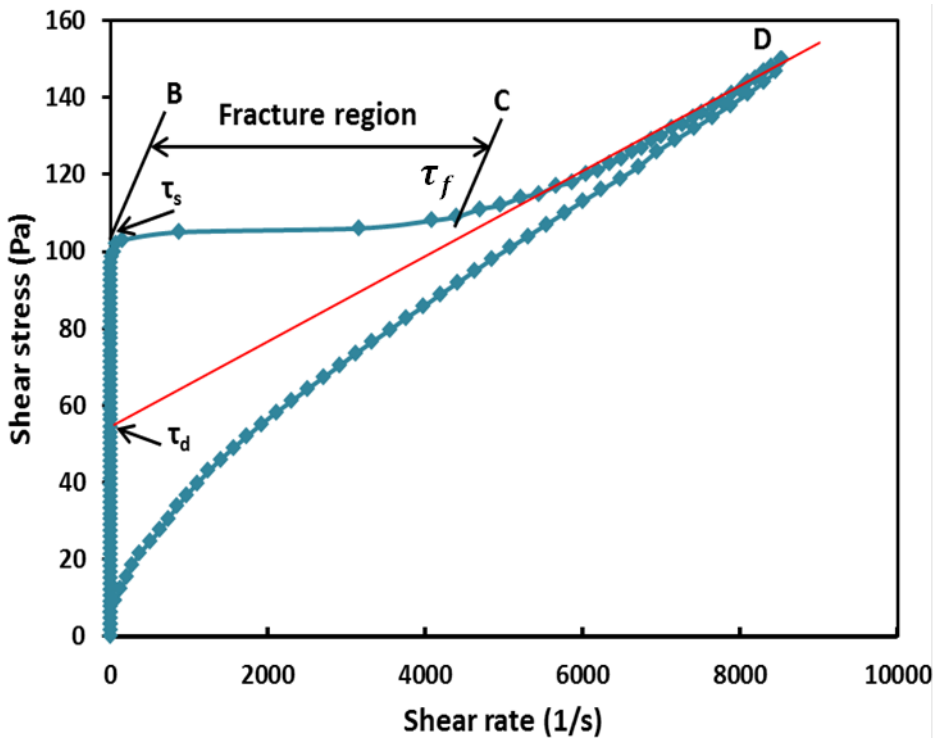

Figure 4.3.4a: Controlled stress sweep for LO at 35°C, cooling rate 0.5°C/min, stress sweep 0-150Pa and stress loading rate 30Pa/min.

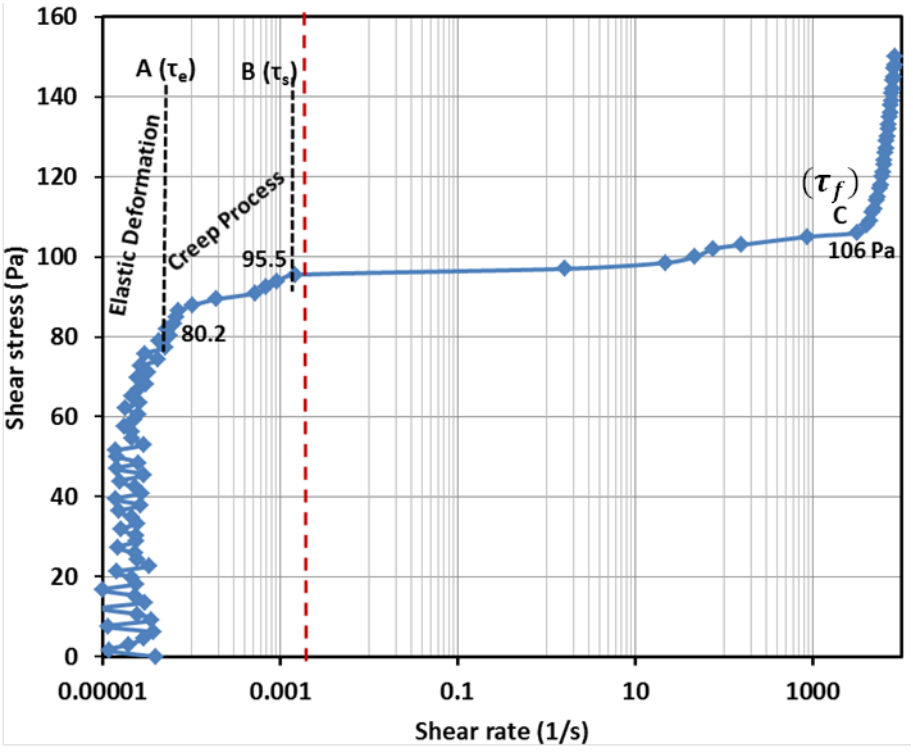

Figure 4.3.4b: A log-log zoom into the controlled stress data for LO at 35°C, cooling rate 0.5°C/min, and stress sweep 0-150 Pa for 5min at stress loading rate 30Pa/min.

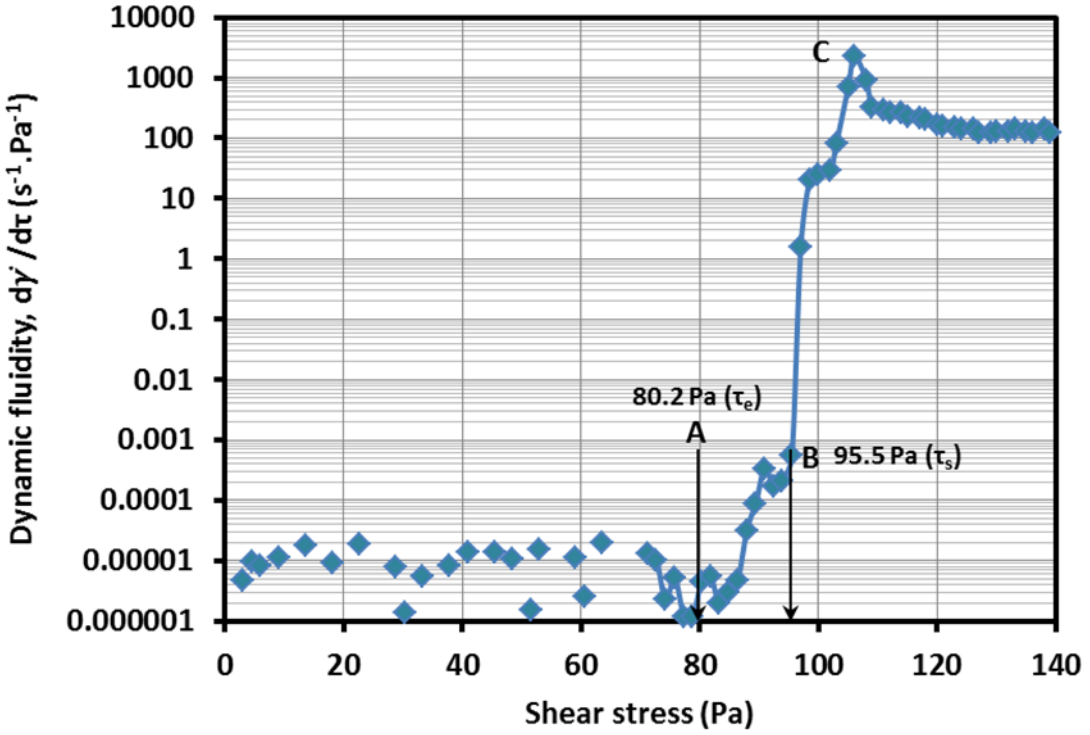

Figure 4.3.5a: Controlled stress data processing method to obtain; τ_e, τ_s , τ_f for BPO at 15°C, cooling rate 0.5°C/min, and stress sweep 0-150 Pa for 5 min at stress loading rate 30Pa/min.

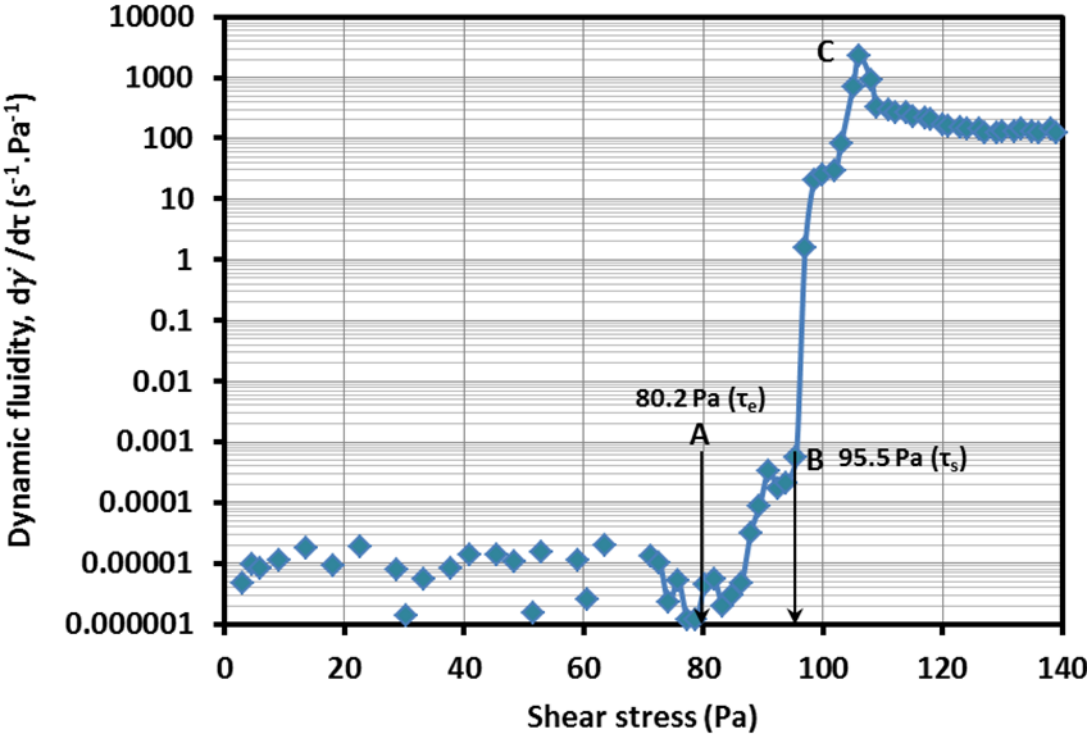

Figure 4.3.5b Controlled stress data processing method to obtain; τ_e, τ_s , τ_f for LO at 35°C, cooling rate 0.5°C/min, and stress sweep 0-150 Pa for 5 min at stress loading rate 30Pa/min.

The observations that can be made from this first set of data are that:

1. The behaviour corresponds precisely to that of an EVP model material as described schematically at the outset of this section by Figure 4.3.2.
2. The deformation and subsequent flow of the waxy crude oils can be obtained by carefully tracking and resolving the flow curve data and extract precise values of the 4 yield stresses of interest, τ_e , τ_s , τ_f and τ_d.
3. The several types of yield stresses have been identified as: elastic-limit yield stress, end of creep-beginning of fracture yield stress, end of fracture-beginning of viscous flow. At this juncture, the yield stress that demarks the end of fracture-beginning of viscous flow appears to be the most appropriate. It is the stress at which failure of the gel network is complete is the parameter of practical interest as far as start-up is concerned. Until this value is reached, *oil flow will not begin, rather it will simply first deform as a solid (when $\tau < \tau_e$), then creep between τ_e and τ_s, then break between τ_s and τ_f. So unlike Boger's suggestion, restart should be predicted on the basis of τ_f not τ_s.*

In addition, the same data just presented can be processed to describe the speed at which the yielding-creep-failure processes develop depending on the conditions tested (temperature, cooling rate, stress loading rate). This is obtained by plotting the data in the form of *shear acceleration* or *failure acceleration* (change of shear rate/change of time = $d\dot{\gamma}/dt$) as a function of time as shown in Figures 4.3.6. Again and as expected, it is observed that after the elastic yield point (τ_e), the deformation increases in speed, accelerating as we move from creep into fracture, breaking in the process the gel network. A maximum occurs indicating the end of failure (the complete breakdown of the gel network) or the beginning of viscous flow. In magnitude terms, Figures 4.3.6 shows that the maximum failure acceleration of BPO is 154.9 s^{-2} under the particular conditions tested (15^{o}C, cooling rate 0.5^{o}C/min, stress sweep from 0-150 Pa over 5 min, stress loading rate 30Pa/min). LO on the other hand exhibits a higher maximum failure acceleration of 2284 s^{-2} under the particular conditions tested (35^{o}C, cooling rate 0.5^{o}C/min, stress sweep from 0-150 Pa over 5 min, stress loading rate 30Pa/min). Such information

is useful in quantifying the gel network speeds of breakage, giving good indication of difference in structure (stacking of the gel crystals, may be their shapes and other features that support high or low speed of failure).

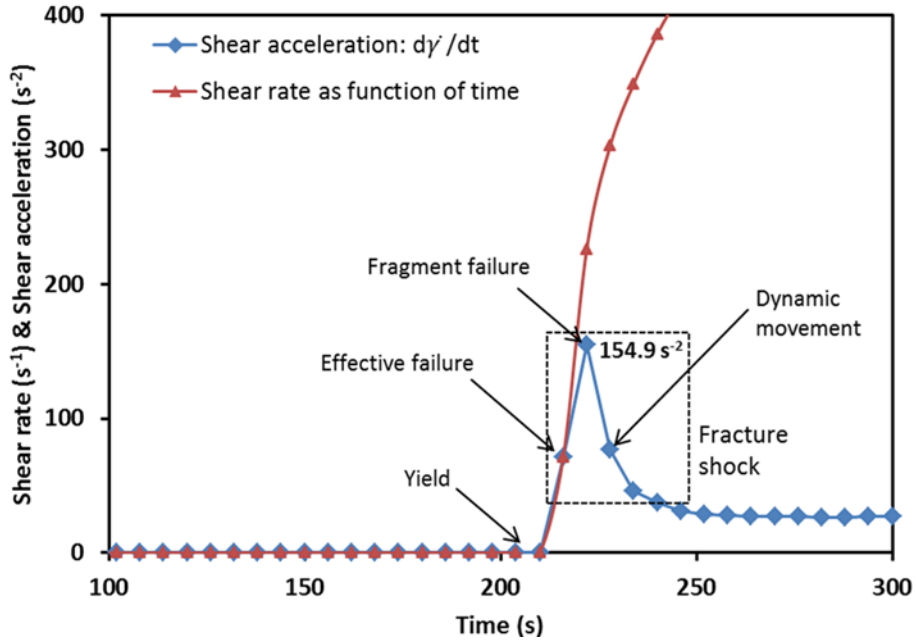

Figure 4.3.6a: Controlled stress test: Shear acceleration and shear rate with respect to time for BPO crude oil tested at 15°C and cooling rate 0.5°C/min under stress sweep from 0 to 150 Pa for 5 min at stress loading rate 30Pa/min.

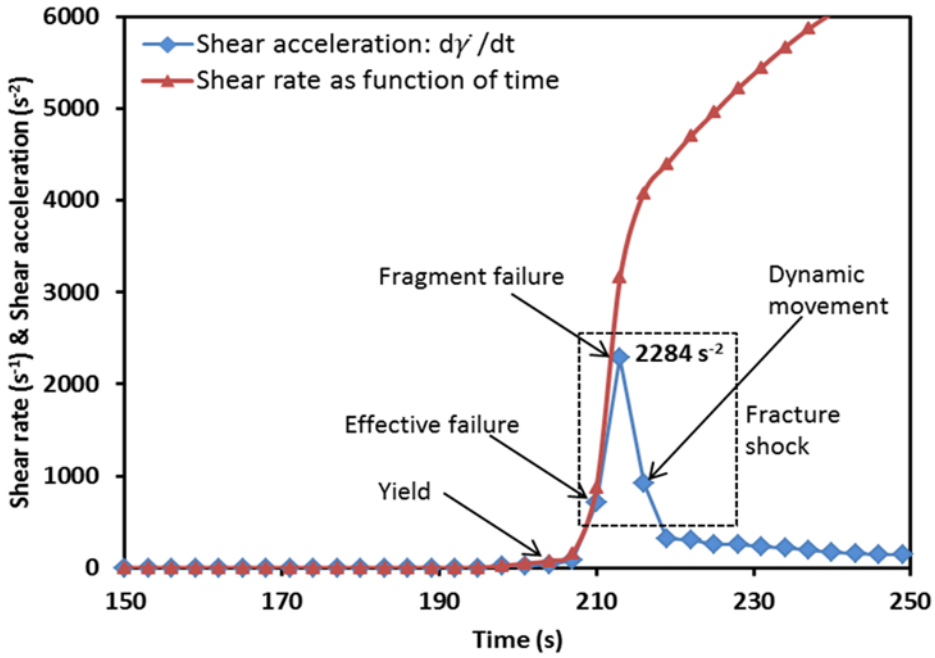

Figure 4.3.6b Controlled stress test: Shear acceleration and shear rate with respect to time for LO crude oil tested at 35°C and cooling rate 0.5°C/min under stress sweep from 0 to 150 Pa for 5 min at stress loading rate 30Pa/min.

4.3.2.2 Comparing the yielding proceses of the oils at constant temperature

The previous section provided the main features of the yielding-creep and failure processes leading to flow. Data for BPO and LO were given for one set of conditions typical of those encountered in practice. Inevitably, these conditions (temperature) were not the same for both because BPO and LO differ in their WAT and wax content so their gelling will occur at different temperatures. Here are presented data under similar conditions where possible to probe deeper into the rheological properties.

Figures 4.3.8- 4.3.9 provide such data with both BPO and LO tested at 15^{o}C after being cooled from 80^{o}C at cooling rate 0.5 ^{o}C/min under stress loading rate at 30 Pa/min.

To begin with, Figure 4.3.8 gives a broad comparison of the yielding process that show a large difference in the static yield stress values for BPO and LO, 104 Pa for BPO crude oil compared with 1210 Pa for LO crude oil. This difference can be attributed to the larger wax content of LO (39%) compared with that of BPO (15%) and probably also to the wax types not being the same. Such large difference in wax content explains that upon gelling the network of crystals will be denser in LO compared with BPO. Immediately, it can be understood why in practice LO is transported at higher temperatures.

When transforming the data in the form of failure acceleration as in Figure 4.3.9, we observe the very large failure acceleration of LO crude oil, 12510s^{-2} compared with 154.9s^{-2} explaining the ease with which BPO breaks.

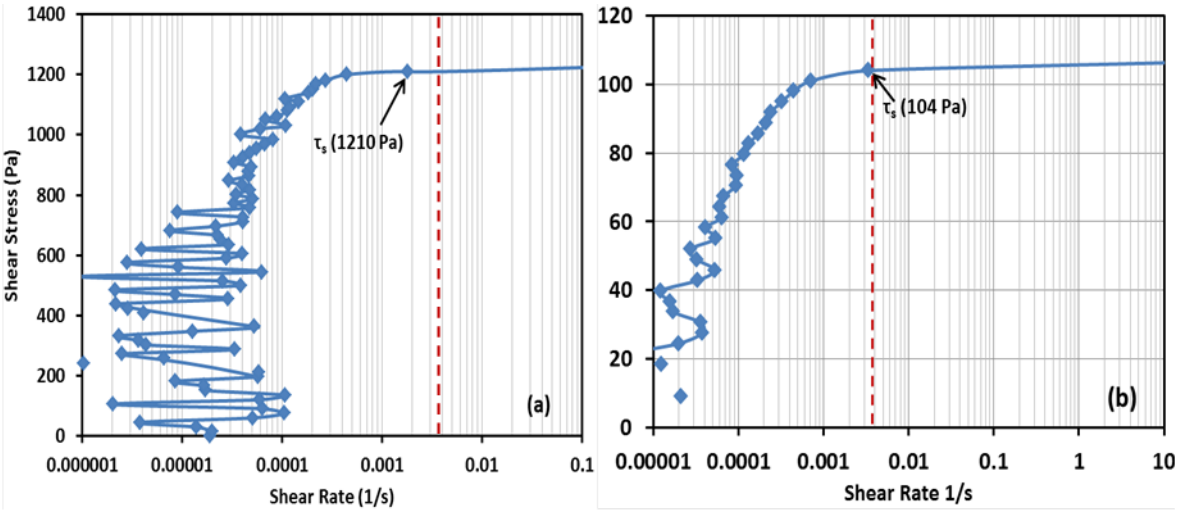

Figure 4.3.8: Controlled stress test: Comparison between the yielding process the static yield stress of **(a)** LO and **(b)** BPO tested under the same conditions at temperature 15^{o}C and cooling rate at 0.5^{o}C/min and stress loading rate at 30Pa/min.

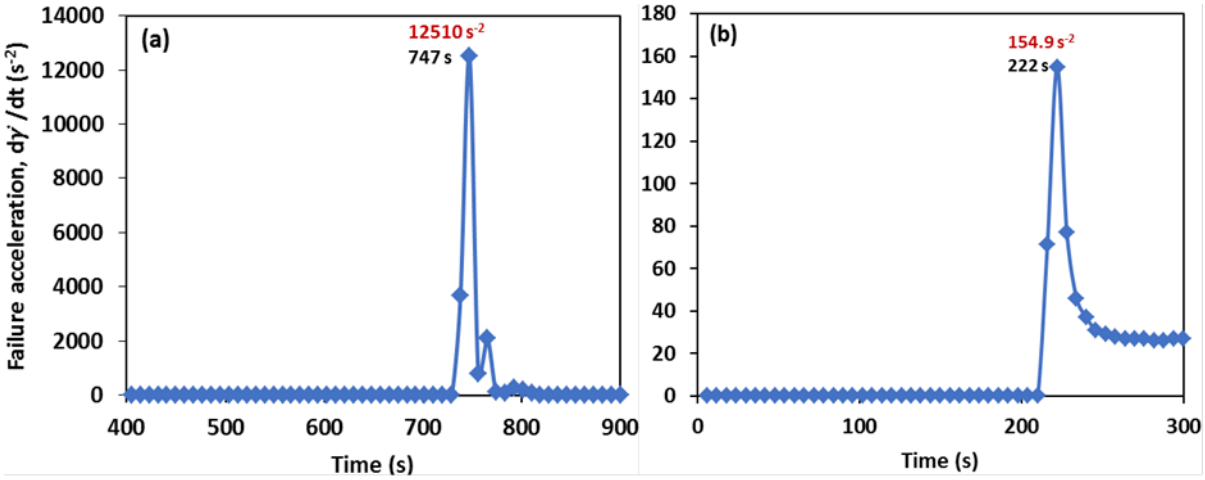

Figure 4.3.9: Controlled stress test. Comparison between the failure accelerations of the fracture shocks of **(a)** LO crude oil and **(b)** BPO tested under the same conditions at temperature 15^{o}C and cooling rate at 0.5^{o}C/min and stress loading rate at 30Pa/min.

4.3.2.3 Effect of stress loading rate on yielding, creep and fracture processes

An observation made earlier is the importance of the stress loading rate on the deformation after yielding. As stated in Section 4.3.2, from Eq. (4.1), the static τ_s and fracture τ_f yield stresses are expected to be stress loading rate dependent unlike the elastic τ_e and dynamic τ_d yield stresses. This is because yielding and breakage (failure) are expected to be stress loading rate dependent unlike elastic deformation and viscous flow. Figure 4.3.10 shows this to be the case. The data here are for BPO deformed at 20^{o}C and cooling rate of 1^{o}C/min at three different stress loading rates 10, 30 and 80 Pa/min applied from 0 to 120 Pa. The elastic yield rate is unchanged at 18 Pa but both the static and fracture yield stress change, increasing interestingly with increasing stress loading rate as shown in Figure 4.3.11 and Table 4.3.2. This data suggest that creep and failure is more effective at lower stress loading rate. In other words, the application of a stress from 0 to a set value over a longer time is more effective at breaking a gelled crude oil than "brutal" force. This observation is important when it comes to restart pressures of gelled pipelines. Again, the dotted red line in Figures 4.3.10b shows the only possible minimum limit shear rate was obtained by Chang and Boger (1998), in comparison to our obtained data.

Table 4.3.2 Controlled stress test; the four yields stress values of BPO crude oil at testing temperature 20^{o}C and cooling rate 1^{o}C/min, and under different loading rates.

Stress loading rate (Pa/min)	Elastic-limit yield stress, τ_e (Pa)	Static yield stress, τ_s (Pa)	Fracture yield stress, τ_f (Pa)	Dynamic yield stress, τ_d (Pa)
10	18	29	38	25
30	18	36	47	32
80	18	49	57	45

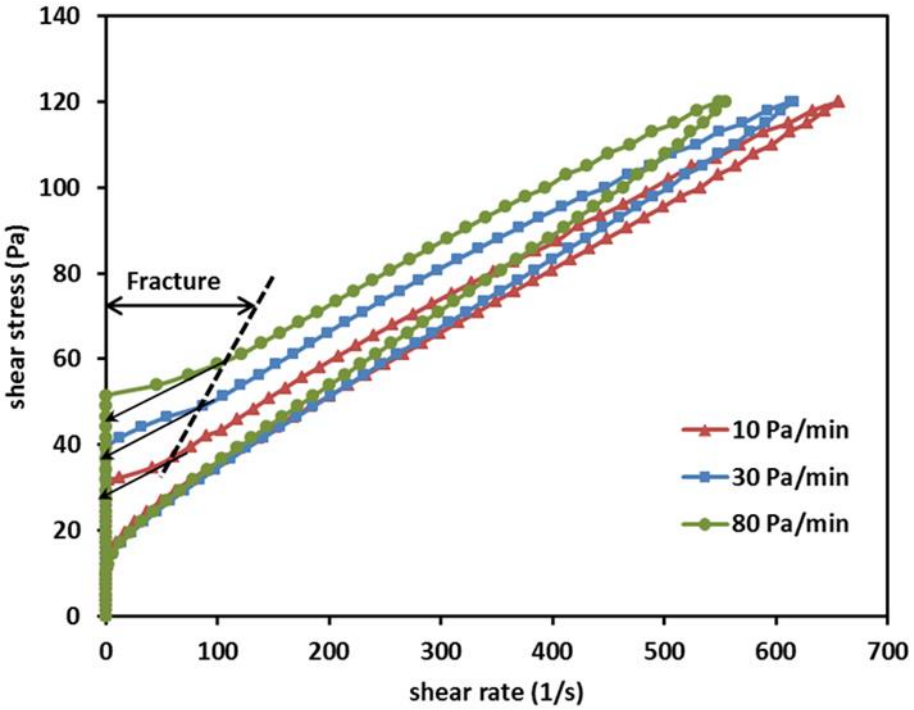

Figure 4.3.10a: Controlled stress deformation of BPO test at 20°C, cooling rate 1°C/min and stress loading rates 10, 30 and 80 Pa/min.

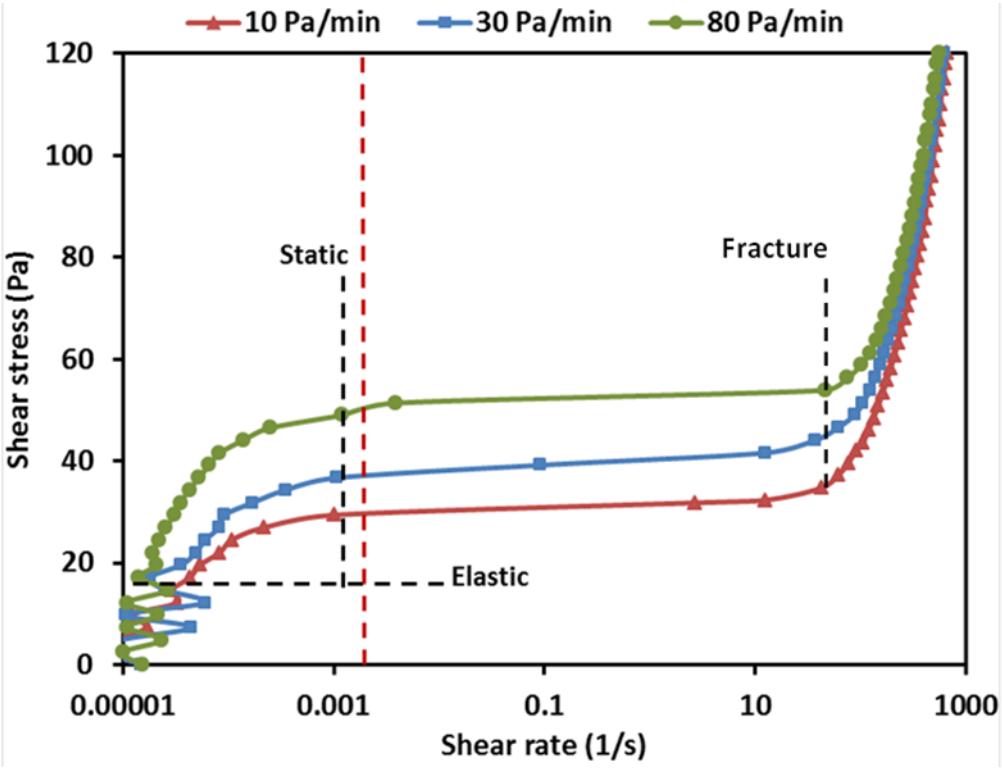

Figure 4.3.10b: Controlled stress deformation of BPO test at 20°C, cooling rate 1°C/min and stress loading rates 10, 30 and 80 Pa/min.

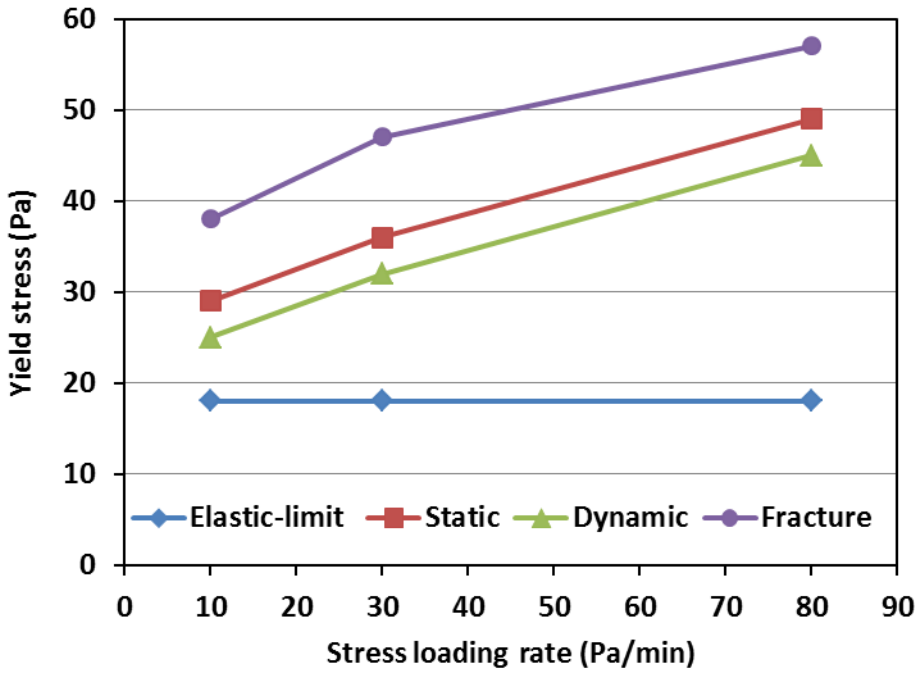

Figure 4.3.11: Dependence of the four measured yield stresses on stress loading rate for BPO crude oil at 20°C and cooling rate 1°C/min under different stress loading rates 10, 30 and 80Pa/min.

Although unable to measure the elastic yield stress because of the limitation of the old controlled stress rheometers, Ronningsen (1992) and Boger et al. (1998) noted that the static yield stress might become very low at sufficiently low rates of stress loading.

It is important to observe from the data presented in Figures 4.3.10 that the return behaviour in the flow curves gives different yield stresses. This is because of the thixotropic behaviour of the gels. Once they are broken, they will remember the past deformation, here differing when the stress loading rate is not kept constant.

As discussed earlier, a further insight can be obtained by examining the data in the form of dynamic fluidity $d\tau/d\dot{\gamma}$ (the ease of deformation) versus shear stress at the different stress loading rates experimented. Figure 4.3.12 gives such data, showing clearly that a lower stress loading rate produces a higher dynamic fluidity. Figure 4.3.12 also enables a better resolution of the values of the static yield stress at the different loading rates, confirming the values tabulated earlier (see Table 4.3.2). Finally this figure shows clearly, that the gel once broken

completely show the same fluidity independently of the stress loading rate (merger of the curves beyond the fracture stress).

In conclusion, we can state from this data that a lower stress loading rate produces a lower static yield stress, a lower fracture yield stress, a lower dynamic yield stress, and as a result a higher dynamic fluidity and a lower apparent viscosity. The dependence of the static yield stress and fracture yield stress on the stress loading rate may indicate that the pressure required to restart a pipeline flow is also dependent on how quickly the pipeline is started, in addition to that it being already controlled by the strength of the wax structure of the oil in the pipeline. It is then for a best operation, the pump pressure in restarting a gelled waxy crude oil pipeline should be increased as slowly as possible, since a slower operation will need a lower pump pressure not only in starting the flow but also in transporting the oil in the final broken state after the pipeline restart and this can reduce the costs of the operations.

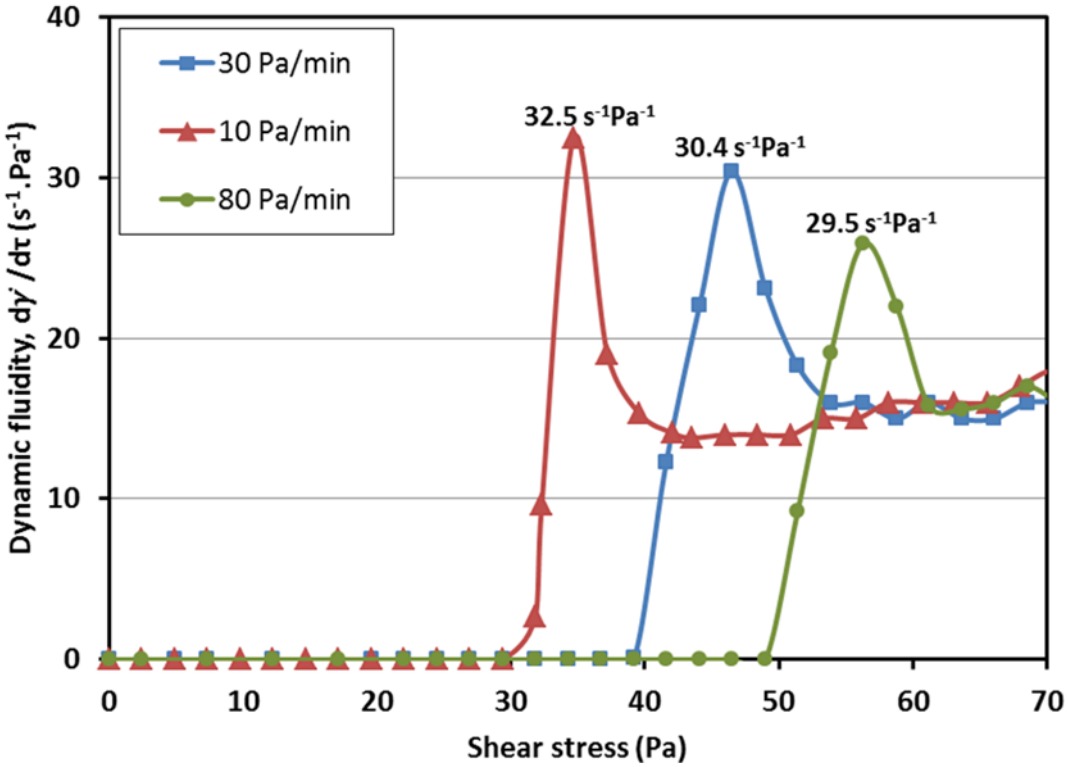

Figure 4.3.12 Controlled stress test. Effect of stress loading rate on fracture process and dynamic fluidity for BPO crude oil tested at temperature, 20°C and cooling rate, 1°C/min under different stress loading rates.

4.3.2.4 Effect of Cooling Rate on yielding, creep and fracture processes

As explained at the outset, cooling rate is the parameter that controls the formation of the gel structure, once the wax precipitates below WAT. It is a physical fact, born out by experiments and supported by theories that with crystalline materials high cooling rates produce smaller size crystals than at low cooling rates which allow crystals to grow. In the situation where a material is crystalline in its entirety or in large proportion of its contents, then high cooling rates will produce structures with small crystals throughout the entire material. Waxy crude oils are however only partly crystalline as in many cases the wax content is much less than 100%, BPO is here 16.3 wt % and LO 46.4 wt %. In such situations, allowing crystals to grow allows them to form a network throughout the oil. Small crystals on the other hands will create pockets of aggregates in the material rather than a network. Thus, on this basis, low cooling rates should produce stronger networks than high cooling rates. Higher yield stresses should thus derive at low cooling rates, be them elastic-limit, static, fracture and dynamic stresses. Figures 4.3.13 (flow curves over the entire shear range), Figures 4.3.14 (a zoom on the flow curves to pinpoint the yield stresses) and Figures 4.3.15 (a comparison on the variation of the elastic-limit, static, fracture and dynamic yield stresses with cooling rates) and Tables 4.3.3 (a summary of the data) show this to be the case for both BPO and LO when the cooling rates was increased from 0.5 to 1 and then 2 ^{o}C/min.

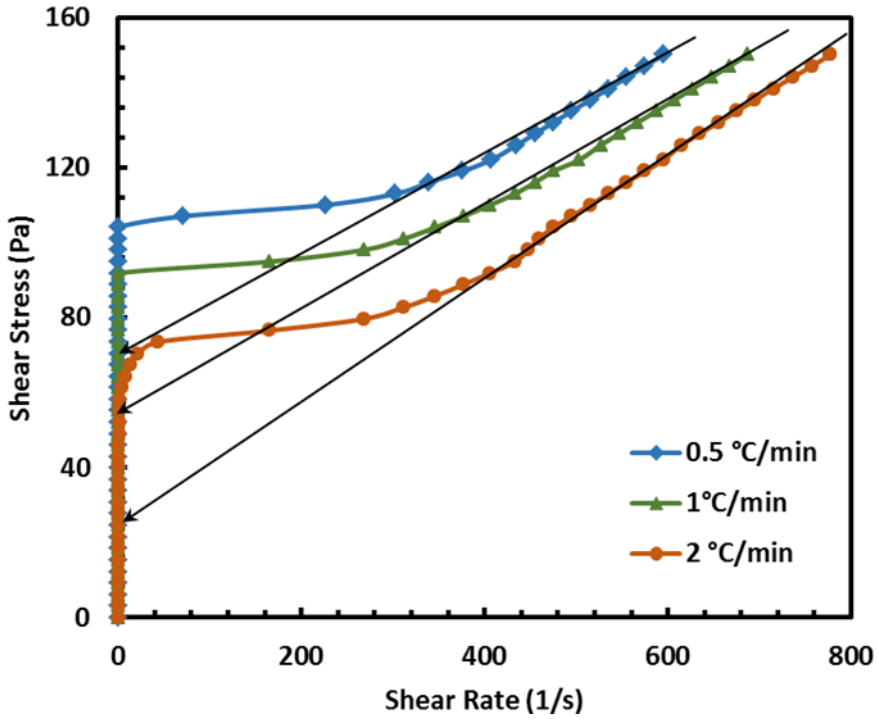

Figure 4.3.13a: Controlled stress test. Yield stress measurements for the three BPO samples tested under the same conditions at testing temperature 18°C and different cooling rates.

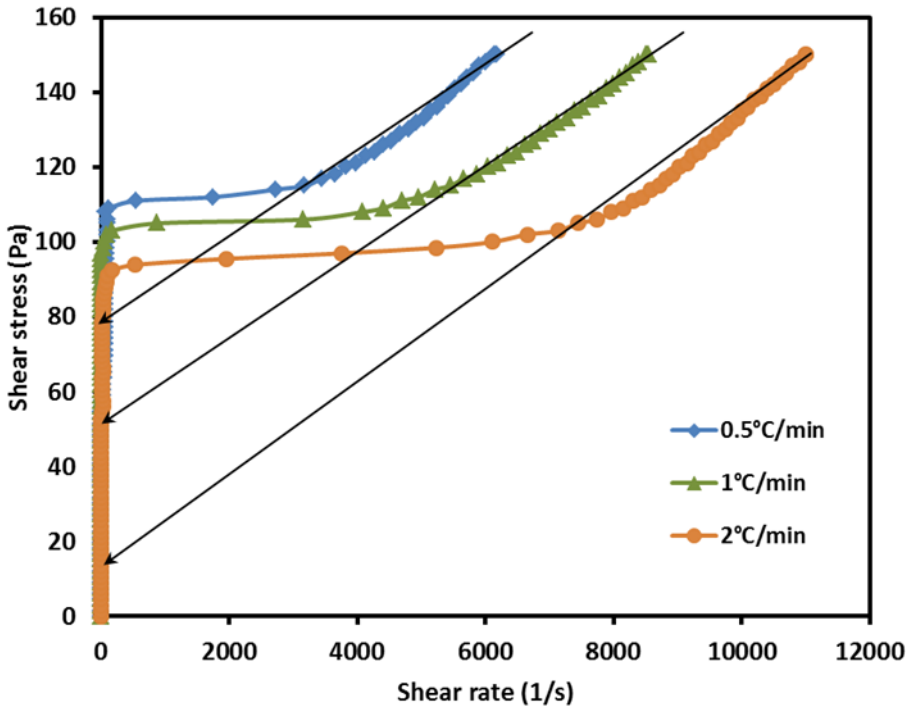

Figure 4.3.13b: Controlled stress test. Yield stress measurements for the three LO samples tested under the same conditions at testing temperature 35°C and different cooling rates.

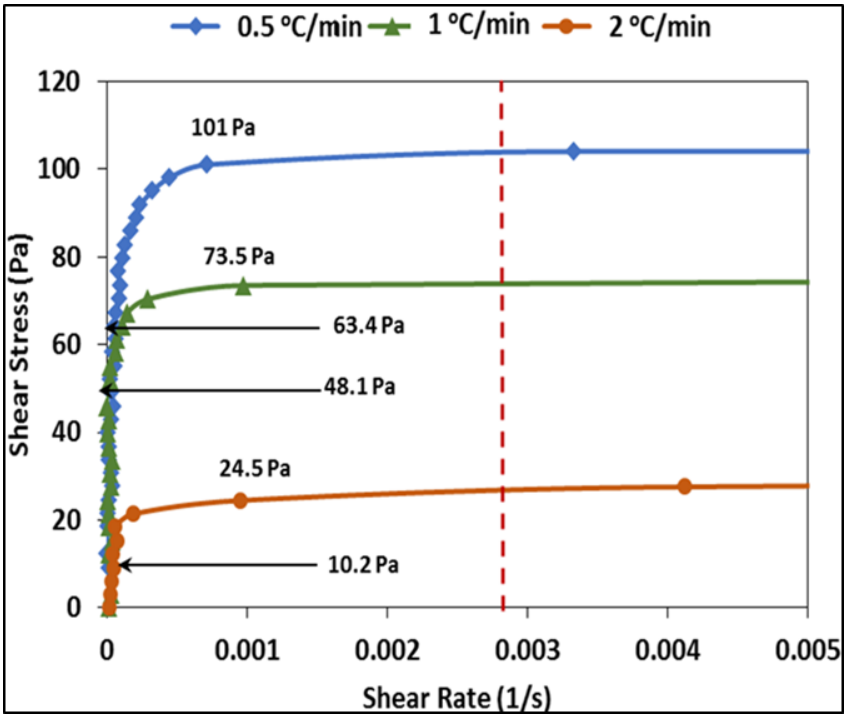

Figure 4.3.14a: Controlled stress test. Difference between the elastic-limit yield stress and static yield stress of the three BPO crude oil samples tested under the same conditions at testing temperature 18^{o}C and different cooling rates.

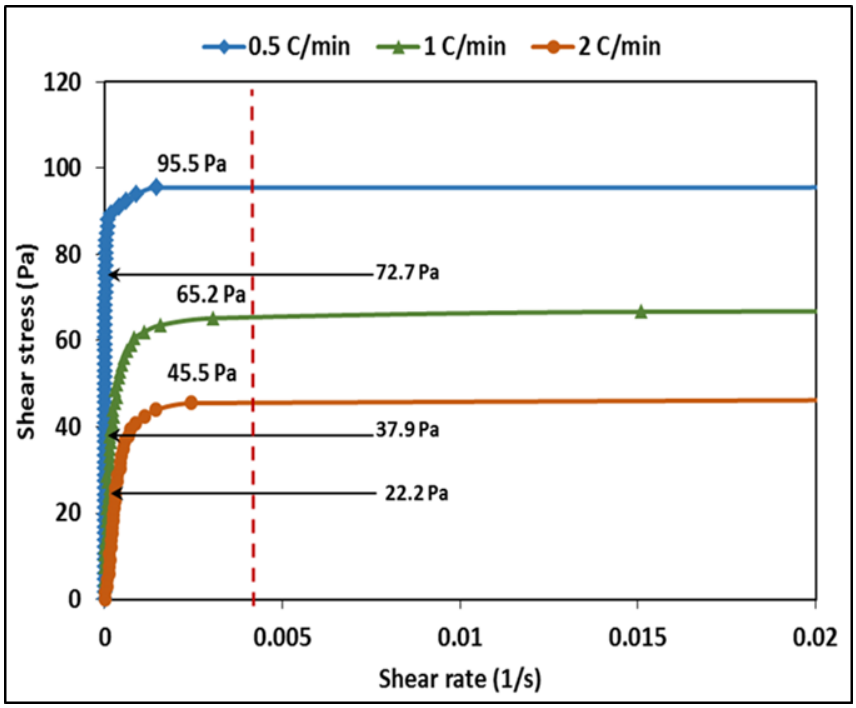

Figure 4.3.14b: Controlled stress test. Difference between the elastic-limit yield stress and static yield stress of the three LO crude oil samples tested under the same conditions at testing temperature 35^{o}C and different cooling rates.

Table 4.3.3a Controlled stress test. Results of the four yield stresses of BPO crude oil tested under the same conditions at testing temperature 18°C and different cooling rates.

Cooling rate (°C/min)	Fracture acceleration $d\dot{\gamma}/dt$ (s^{-2})	Fracture time (s)	Elastic-limit yield stress (Pa)	Static yield stress (Pa)	Fracture yield stress (Pa)	Dynamic yield stress (Pa)
0.5	155	222	63.4	101	113	73.6
1	123	192	43.1	73.5	96	57.3
2	43	150	**10.2**	24.5	74	21.4

Table 4.3.3b Controlled stress test. Results of the four yield stresses of LO crude oil tested under the same conditions at testing temperature 35°C and different cooling rates.

Cooling rate (°C/min)	Fracture acceleration $d\dot{\gamma}/dt$ (s^{-2})	Fracture time (s)	Elastic-limit yield stress (Pa)	Static yield stress (Pa)	Fracture yield stress (Pa)	Dynamic yield stress (Pa)
0.5	2284	497	72.7	95.5	108	67.8
1	1810	455	37.9	65.2	101	47
2	1212	287	**22.2**	45.5	93	15.1

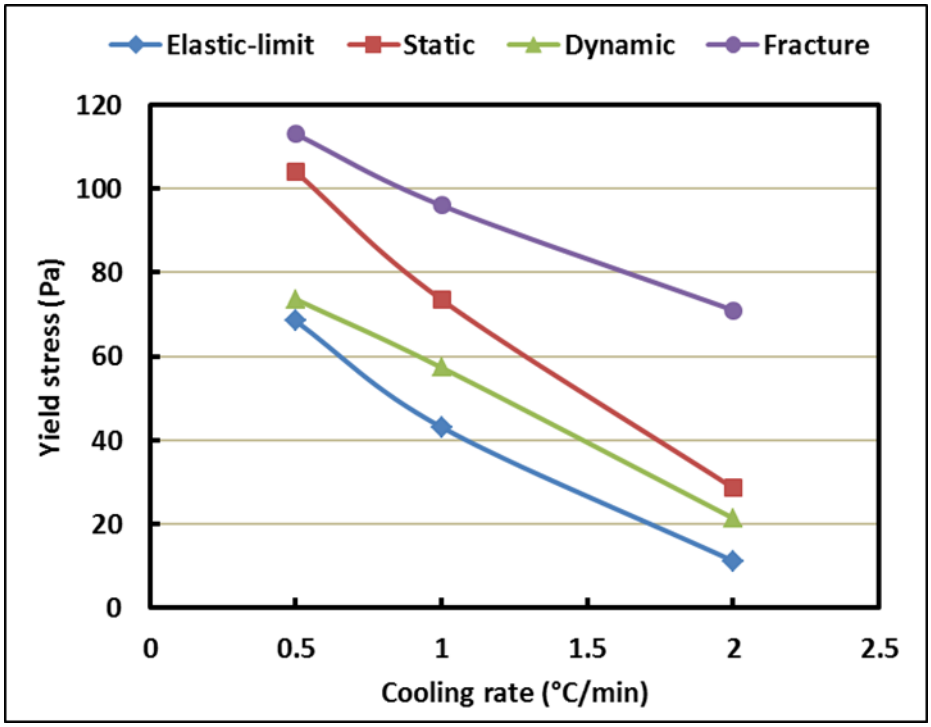

Figure 4.3.15a: Effect of cooling rate on the four yield stresses of gelled BPO crude oil samples tested under the same testing conditions at testing temperature 18°C and different cooling rates.

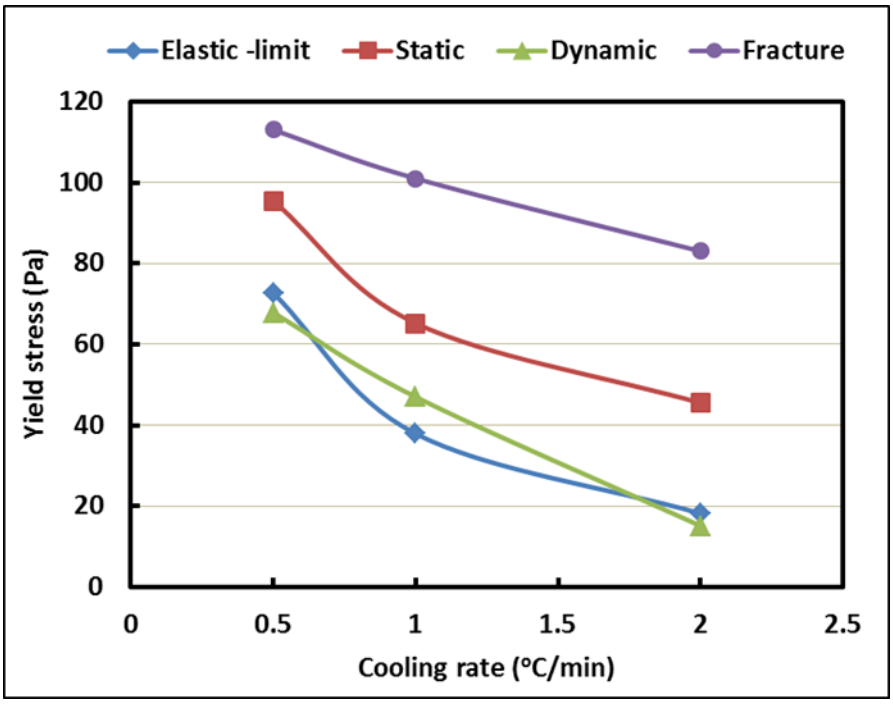

Figure 4.3.15b: Effect of cooling rate on the four yield stresses of gelled LO crude oil samples tested under the same testing conditions at testing temperature 35^{o}C and different cooling rates.

As carried out with previous data, the data on the effect of cooling rate were processed to study this effect on failure dynamics (acceleration) and pinpoint further the values of the yield stresses. Figures 4.3.16 give this data for both oils showing the failure acceleration at the fragment failure point increasing from 43 to 155s^{-2} for BPO and from 1212 to 2284s^{-2} for LO when the cooling rate was reduced from 2 to 0.5^{o}C. Figures 4.3.17 shows how the failure time decreases with increasing cooling rates suggesting that rapid drop in temperatures in the field lead to weaker, easier to break gel structures. Bearing in mind the explanation given earlier, this is not as surprising as it may appear.

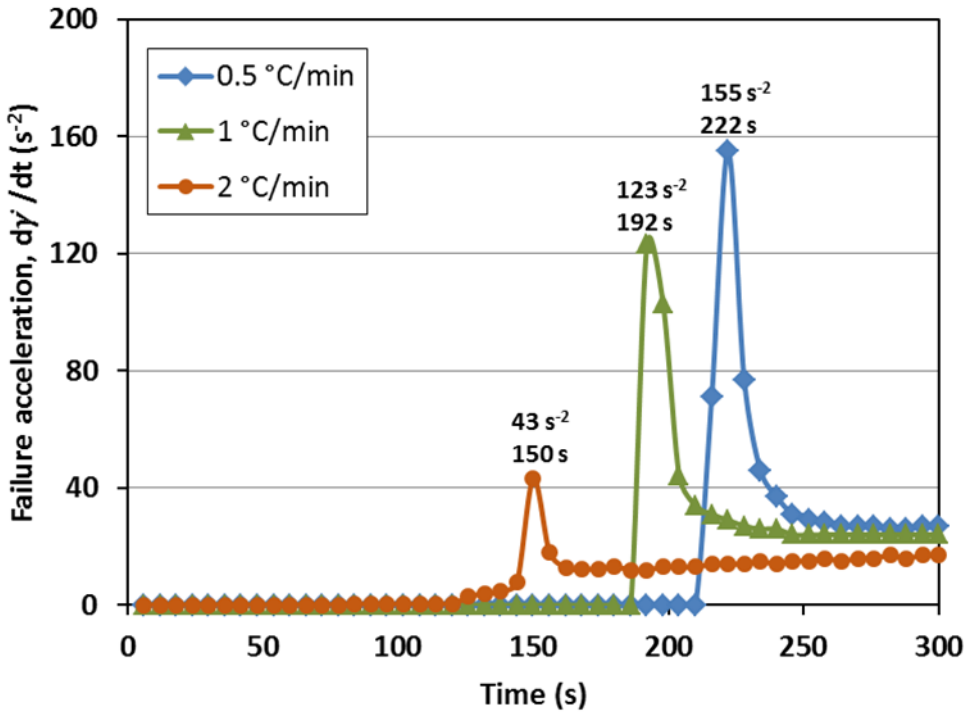

Figure 4.3.16a: Controlled stress test. Calculated failure acceleration curves of the three gelled BPO crude samples tested under the same testing conditions at testing temperature 18^{o}C and different cooling rates.

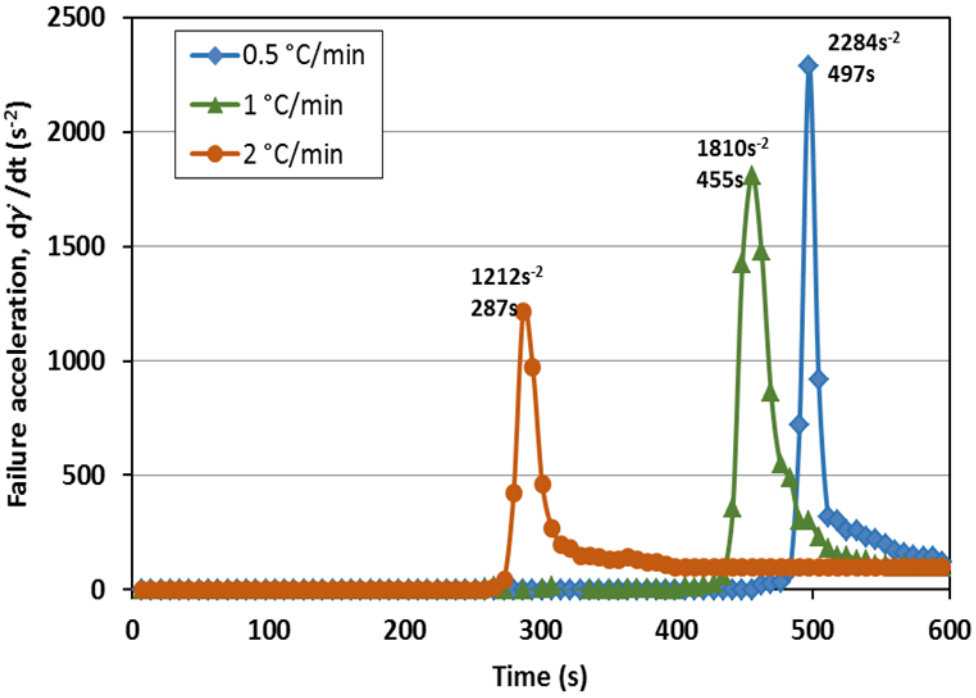

Figure 4.3.16b: Controlled stress test. Calculated failure acceleration curves of the three gelled LO crude samples tested under the same testing conditions at testing temperature 35^{o}C and different cooling rates.

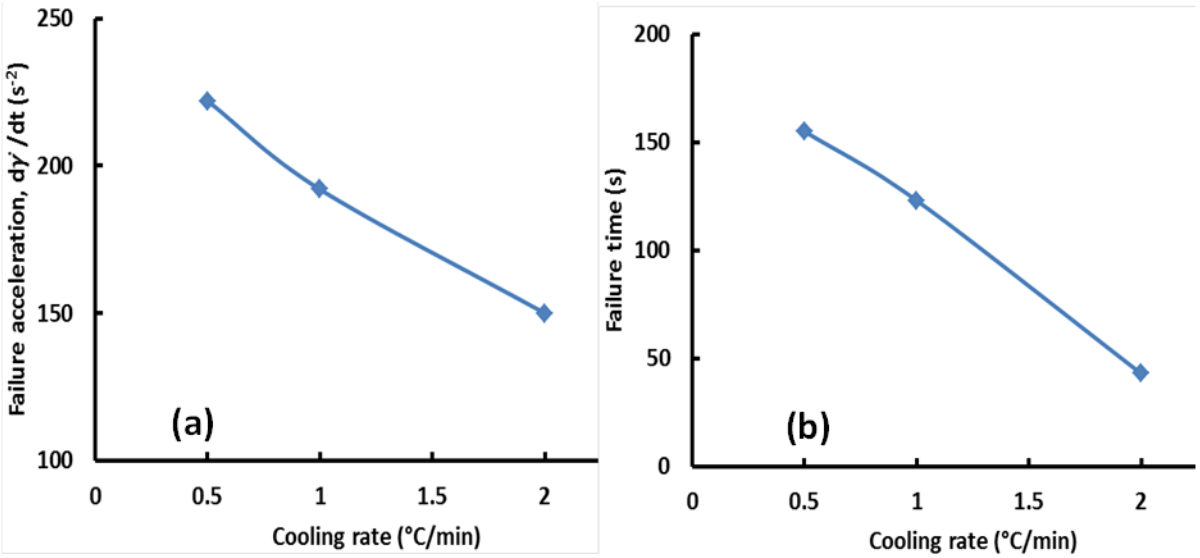

Figure 4.3.17a: Effect of cooling rate on **(a)** failure acceleration and **(b)** failure time of the three BPO crude samples tested under the same testing conditions at testing temperature 18^{o}C and different cooling rates.

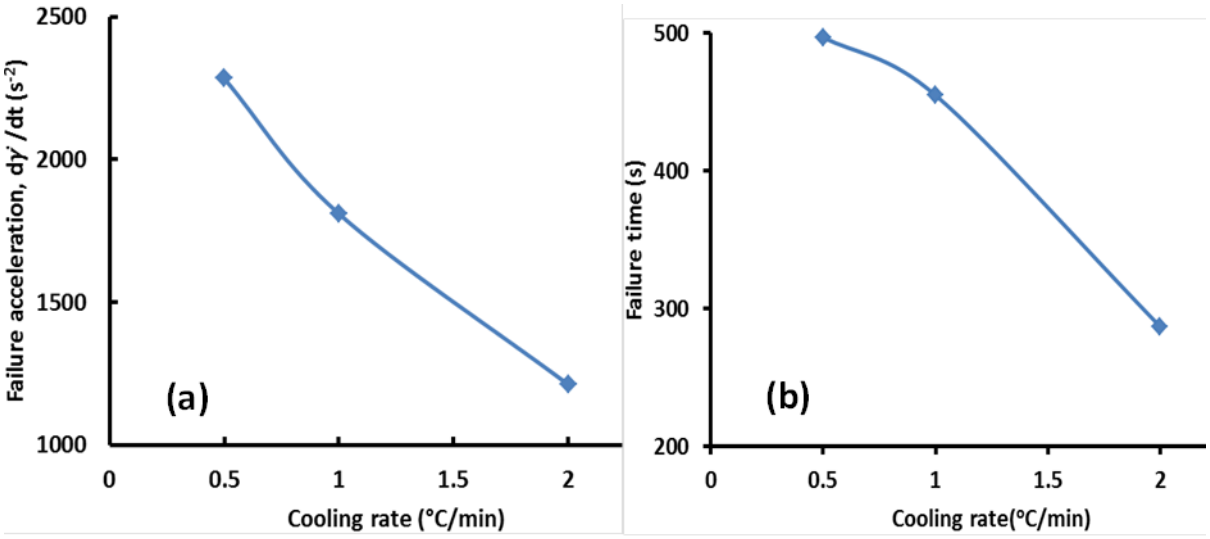

Figure 4.3.17b Effect of cooling rate on **(a)** failure acceleration and **(b)** failure time of the three LO crude samples tested under the same testing conditions at testing temperature 35^{o}C and different cooling rates.

4.3.2.5 Effect of temperature on yielding, creep and fracture processes

Temperature is the most important factor affecting the rheology of all materials. With waxy crude oil, it has a particularly strong effect as when low and below WAT it leads to the precipitation of wax. Yielding and subsequent deformations (creep and failure) and flow are thus critically dependent on temperature. Here, yielding is investigated in the temperature range of interest as discussed earlier and presented in Table 4.3.1, namely, between 13 and 30^{o}C for BPO and between 15 and 45^{o}C for LO at a fixed cooling rate of 1^{0}C/min and a fixed stress loading rate of 30 Pa/min. The data are presented in Figures 4.3.18. At the highest temperatures (30^{o}C for BPO and 45^{o}C for LO), there is essentially viscous flow only. As the temperature is reduced we observe a stronger resistance and the evidence of elastic deformation, followed by creep as observed in earlier figures. The increase of the elastic and static stresses with decreasing temperature is given in Table 4.3.4 and correlated with temperature in Figures 4.3.19. The steeper increase with decreasing temperature and larger magnitude in the yield stresses of LO compared to BPO is clearly seen in these figures, a reflection of the higher wax content of LO compared to BPO.

The effect of temperature on the static yield stress of various waxy crude oils has been studied by previous workers, Chang and Boger (2000) for example and also many others, but the variation of elastic-limit yield stress with temperatures has never been experimentally studied.

Another aspect of the important outcomes gained from this study, as it can be noticed from Figures 4.3.18 for both crude oils, the elastic reflux in elastic deformation regions was wider and higher when the sample was being cooled to a lower temperature. The elasticity of both crude oil gels cooled under static conditions was observed to increase with decreasing the testing temperature. This can be attributed to the wax structure and network growth as the behaviour of oil structure becomes more elastic than viscoelastic at a lower temperature, thus the wax network becomes more connected and the oil structure becomes stronger.

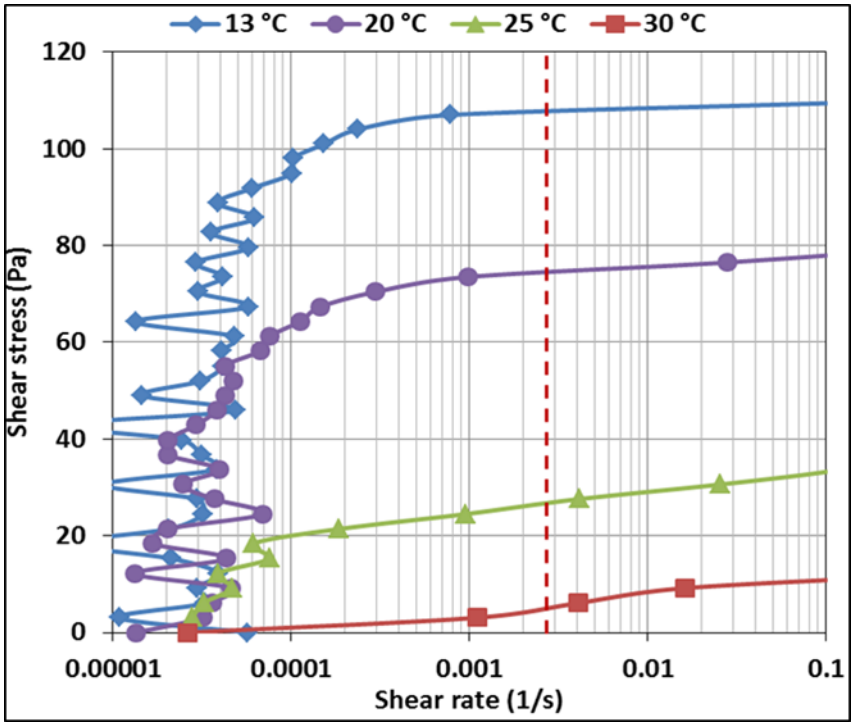

Figure 4.3.18a Controlled stress test. Yielding process curves for the four BPO samples tested under the same conditions at different temperatures below and above its PPT and cooling rate of 1°C/min.

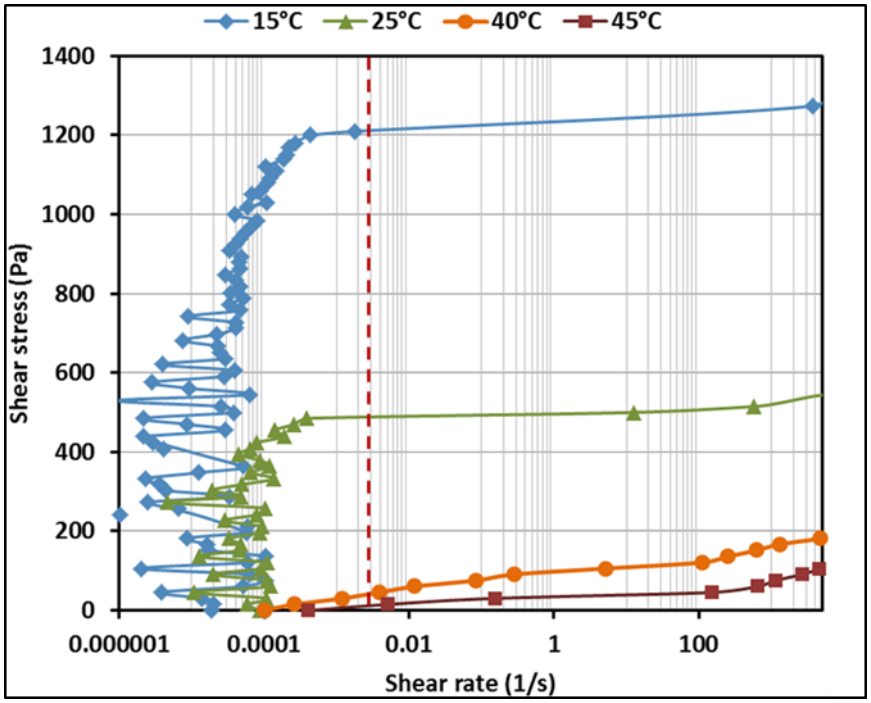

Figure 4.3.18b Controlled stress test. Yielding process curves for the four LO samples tested under the same conditions at different temperatures below and above its PPT and cooling rate of 1°C/min.

Table 4.3.4 Controlled stress test. Results of the elastic-limit and static yield stress of BPO and LO crude oils tested under the same conditions at different temperatures and cooling rate of 1°C/min.

Crude oil	Temperature (°C)	Elastic-limit yield stress (Pa)	Static yield stress (Pa)
BPO	13	73.4	107
	20	40.2	68.5
	25	18.6	24.5
	30	0.0	6.0
LO	15	773	1210
	25	333	502
	40	17.2	35.5
	45	0.0	9.0

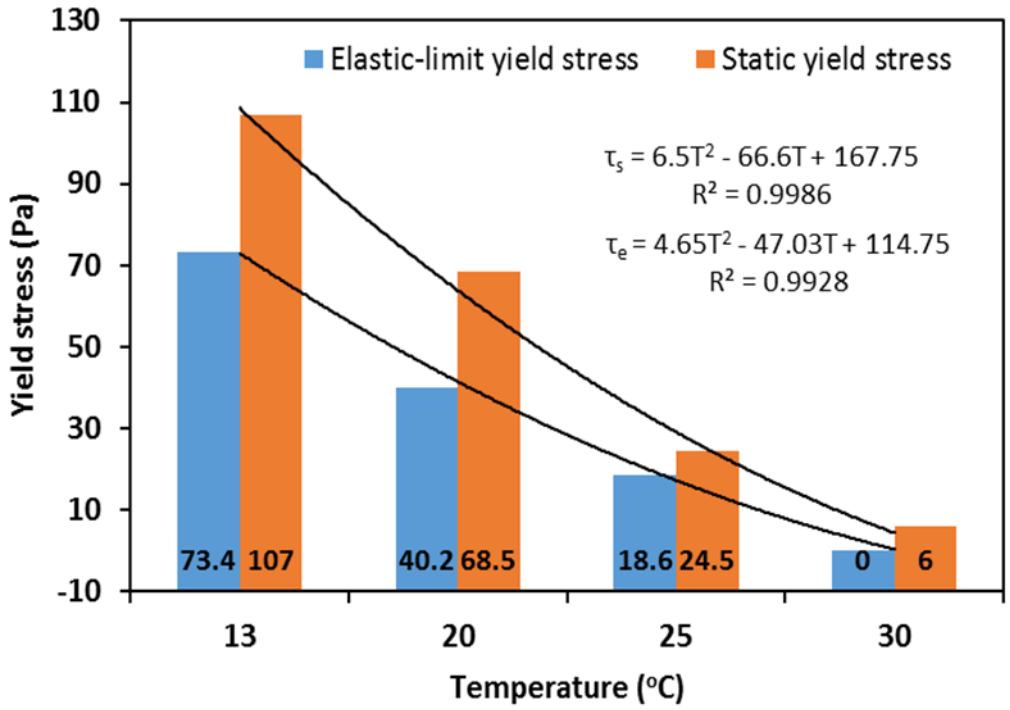

Figure 4.3.19a Effect of temperature on the elastic-limit and static yield stresses of the four BPO crude oil samples tested under the same testing conditions at different temperatures below and above its PPT and cooling rate of 1°C/min.

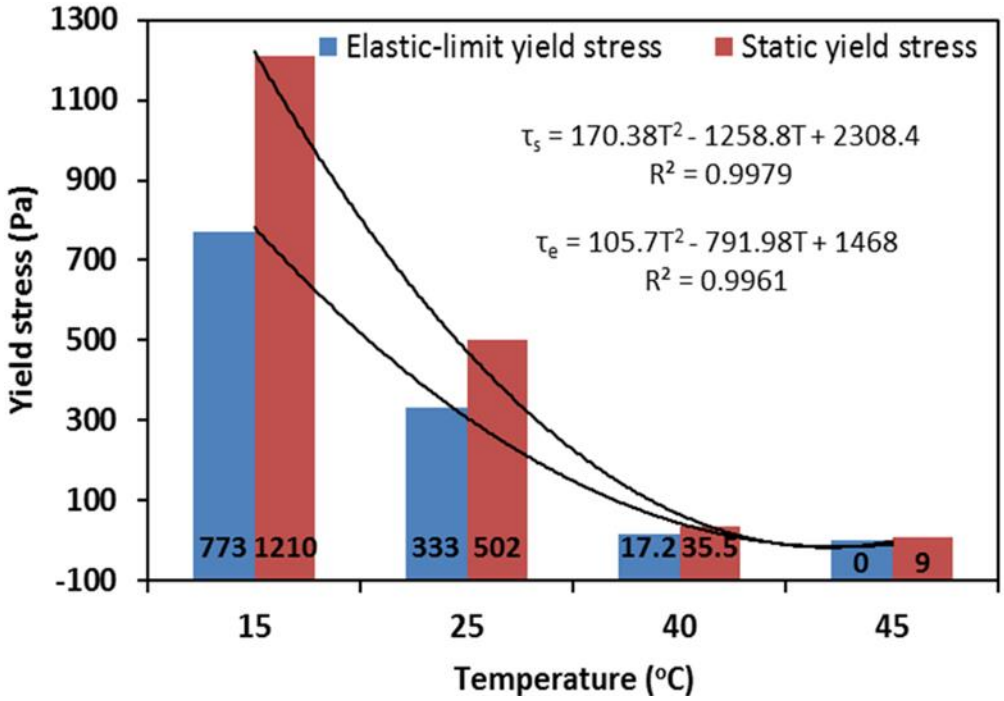

Figure 4.3.19b Effect of temperature on the elastic-limit and static yield stresses of the four LO crude oil samples tested under the same testing conditions at different temperatures below and above its PPT and cooling rate of 1°C/min.

4.3.3 Creep-Recovery Rheology

As described in the experimental method, this type of deformation consists of applying first a constant stress over a period of time and measuring the corresponding strain then removing the stress and measuring the strain recovery. Figure 4.3.20 gives a typical result obtained with BPO at 18°C, cooled from 60°C at cooling rate, 2°C/min. The creep time is 60s and four such tests are described in this figure at stresses equal to 5, 10, 15 and 25 Pa. Complete recovery is observed at the lowest stress of 5 Pa but the recovery diminishes as the stress is increased until 25 Pa when no recovery is present. Clearly the complete recovery at 5 Pa indicates that this level of stress is below the elastic limit and the sample has responded as an elastic solid with no permanent deformation. Curves 2 and 3 at 10 Pa and 15 Pa respectively, which show partial recovery indicates that both elastic and plastic deformation are involved in this stage of the creep. With this

range of applied stress the structure of the oil changes gradually from the initial solid-like state to a viscoelastic state. Curve 4 represents a completely unrecoverable state, when the stress of 25 Pa is applied to the sample, a fracture happened shortly, the structure of the oil degrades from the initial elastic solid-like state to the viscoelastic state and finally to the viscous state in less than 20s. The final range of curve 4 after the starting point of fracture represents the oil state in the fracture process in which the strain increases dramatically over time after the fracture starts even when the stress is fixed.

From the results of the creep recovery test, two stress transitions can be determined. The first transition is between curves 1 and 2 and may be defined as the elastic-limit yield stress (τ_e), an applied stress lower than this stress will only results an elastic recoverable structure while a higher stress will produce creep with recoverable and unrecoverable deformations.

The second transition is between curves 3 and 4. This transition is the static yield stress (τ_s). A stress higher than this transition will destroy the structure very quickly, in the other hand, a lower stress will not break the structure in a reasonable time. From the results in Figure 4.3.20, the elastic-limit yield stress is determined between 5 and 10 Pa, and the static yield stress is determined between 15 and 25 Pa.

The main conclusion here is the difficulty in pinpointing exactly the values for τ_e and τ_s compared with the controlled stress method by which the values for the both yield stresses can be obtained by one testing run, saving much time compared with the creep testing method. Nevertheless, this method provides a check of the controlled stress data. Clearly, reducing the steps in the stress applied can provide better resolution.

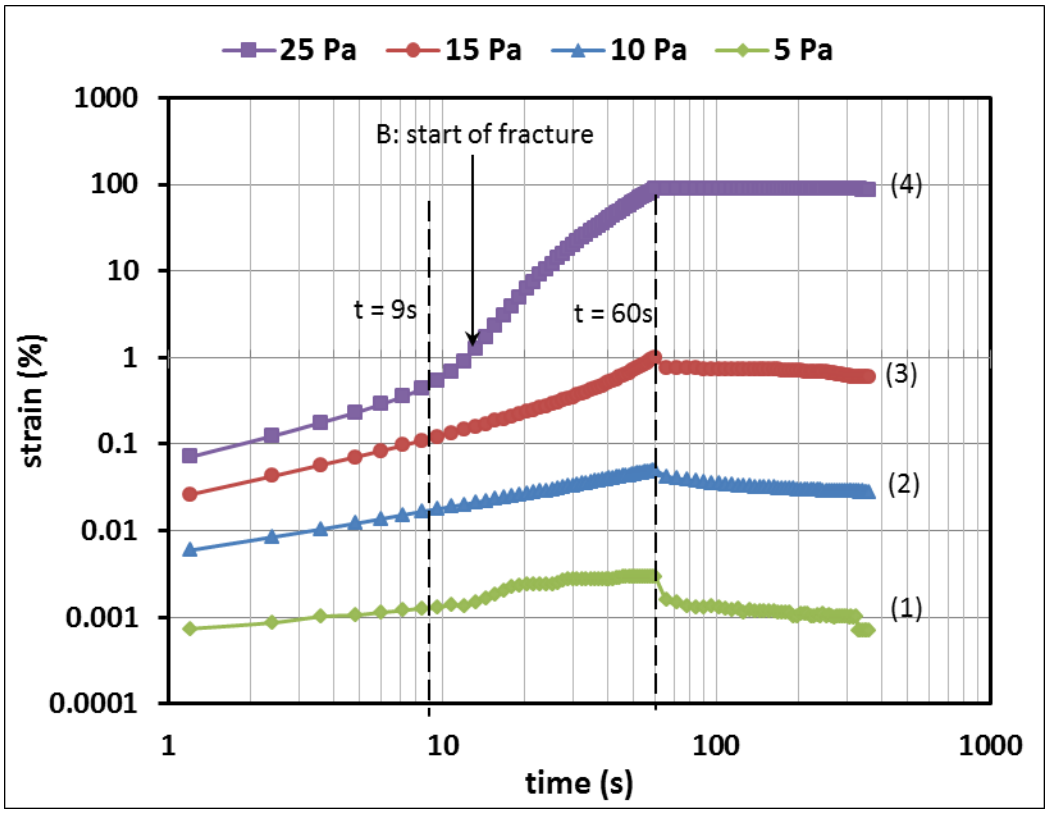

Figure 4.3.20 Creep-recovery tests. Different responses under different applied stresses for BPO crude oil samples tested at temperature 18^{o}C, cooling rate of 2^{o}C/min.

4.3.3.1 Effect of Creep Time

In the creep recovery test, the time scale of the measurement is presented as the creep time. The elastic-limit and static yield stresses are measured with an applied stress time of 1 min. The creep time on the two measured yield stresses can be observed by studying the creep curves at different applied stresses.

Curve1 in Figure 4.3.20 shows that the strain under a stress of 5 Pa increases with time and reaches a maximum at about 45s, after that the strain remains constant and does not change with time under the stress of 5 Pa. A complete strain recovery is occurred after the applied stress of 5Pa is removed. Therefore, the lower limit of the measured elastic-limit yield stress does not change with a change of time scale of the creep-recovery test.

Curves 3 and 4 show that the strain responses increase with time when the applied stress is higher than the elastic-limit yield stress. For the same creep time,

a higher applied stress causes a higher stain. Also, a higher unrecoverable stain is observed with a longer creep time when the applied stress higher than 15 Pa. The micro-structure in the oil during creep will be affected by both the stress and creep time when the applied stress is higher than the elastic-limit yield stress. The fracture may then occur at a lower stress if the creep time is a longer. The fracture occur 15s after a stress of 25Pa is applied as shown in Figure 4.3.20. If the stress was removed after only 9s of application to the sample, no fracture would occur and a partial strain recovery would be observed to follow the creep. Therefore, to produce a fracture with a creep time of 9s a higher applied stress will then be needed. On the other hand, a fracture would be observed under the stress of 10 or 15 Pa if the stress time was extended to sufficiently long since the strains under these stresses keep increasing over time while the unrecoverable strain can be observed even with a stress time of 1 min. However, no fracture can be observed under the stress of 5Pa with any extended stress time, as shown by the constant strain between 45 and 60s in curve 1.

4.3.4 Oscillatory Deformations Rheology

The purpose with oscillatory tests here is to check the yield stresses measurements carried under controlled stress. In addition, measurements will be carried out in a range of temperatures below WAT to determine the gel point (gelation temperature) of both LO and BPO as DSC is not suited to provide this data and providing WAT only.

4.3.4.1 Measurement of yield stresses

Oscillatory tests were performed for BPO crude oil sample at 18°C and for LO crude oil sample at 35^{o}C, by applying oscillations at a fixed low frequency and measuring the strain response in both linear and nonlinear regions, hence the storage ($G^{'}$) and loss modulus ($G^{''}$). The data are presented in Figures 4.3.21 when the stress amplitude was increased linearly from 1 to 75 Pa for BPO and from 1 to 120 Pa for LO, at a frequency of 1 Hz. The elastic, creep and fracture regions were identified. The corresponding G’ and G’’ data are given in Figures 4.3.22,

again clearly demarcating the yielding-creep-fracture process. However, unlike in the controlled stress tests where the shear stress is increased gradually, in the oscillatory tests the stress oscillates and the frequency at which it does throws in uncertainty as to the exact values of the static and fracture stresses. Figures 4.3.23 show clearly the dependence on frequency which can be likened to the effect of stress loading rate observed in the controlled stress rheology. As was done with the controlled stress data, an accurate way of locating the yield, static and fracture stresses is to use the change of slope in the data ($dG'/d\tau$). This is shown in Figures 4.3.24 which interestingly reveals that the static yield stress decreases as the frequency is decreased, 67.1 Pa for 6 Hz, 48.8 Pa for 1 Hz and 37 Pa for 0.3 Hz. This is an important finding in the light of previous work (see Chang and Boger, 1998) which reports the opposite as shown in the comparative Figures 4.3.25.

In order to verify the finding that the static yield stress is reduced when the frequency is reduced, three further tests were carried out on BPO at 18^{o}C with fixed stress amplitude of 65 Pa at frequencies of 1Hz, 10Hz and 20Hz. The results are shown in Figure 4.3.26 giving further proof that a lower frequency reaches a higher strain more quickly, the gel structure is destroyed more quickly at lower frequency.

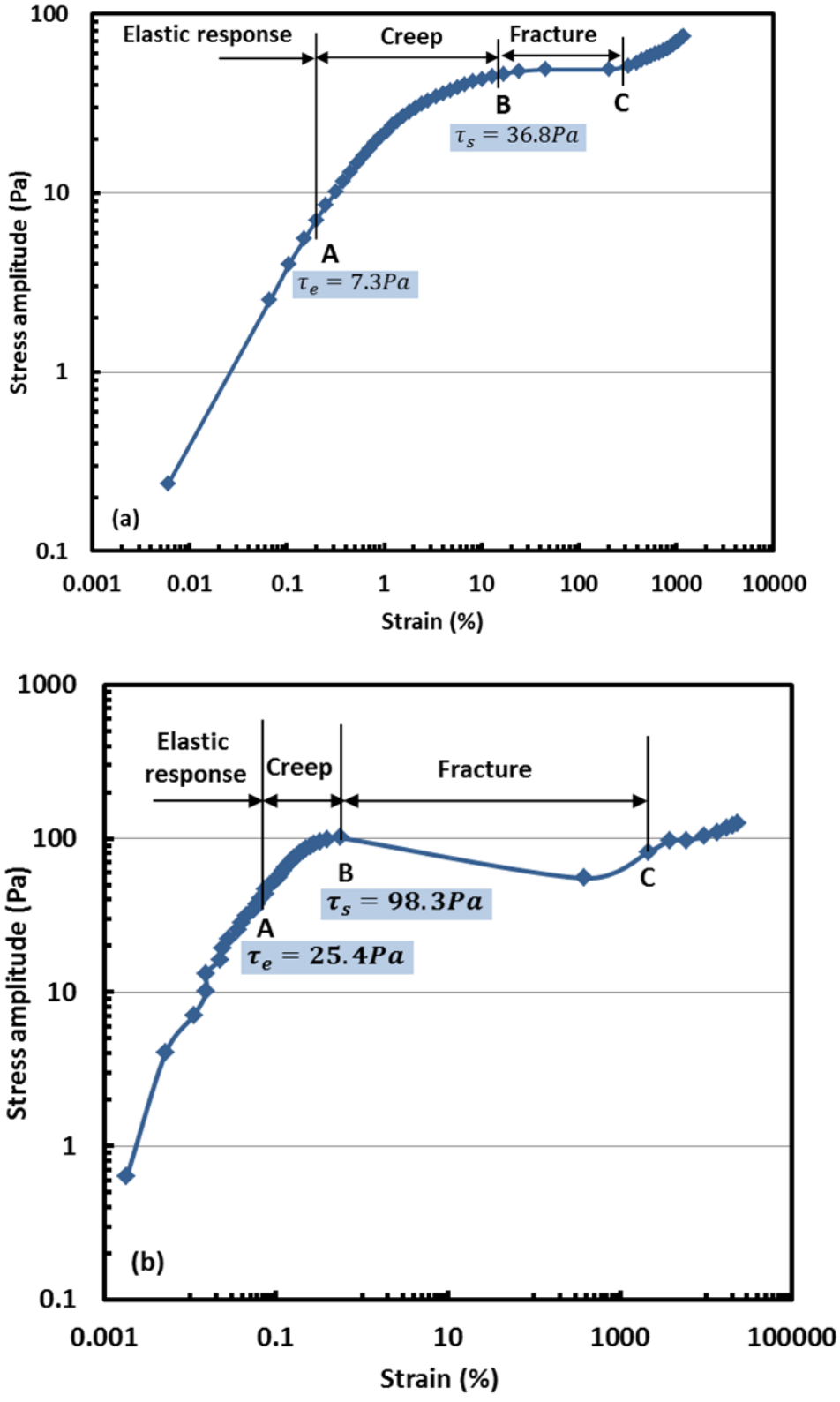

Figure 4.3.21: Oscillatory test data for BPO crude oil at temperature 18°C, cooling rate of 2°C/min and frequency of 1 Hz; stress vs. strain relationship during the yielding process **(a)** BPO **(b)** LO.

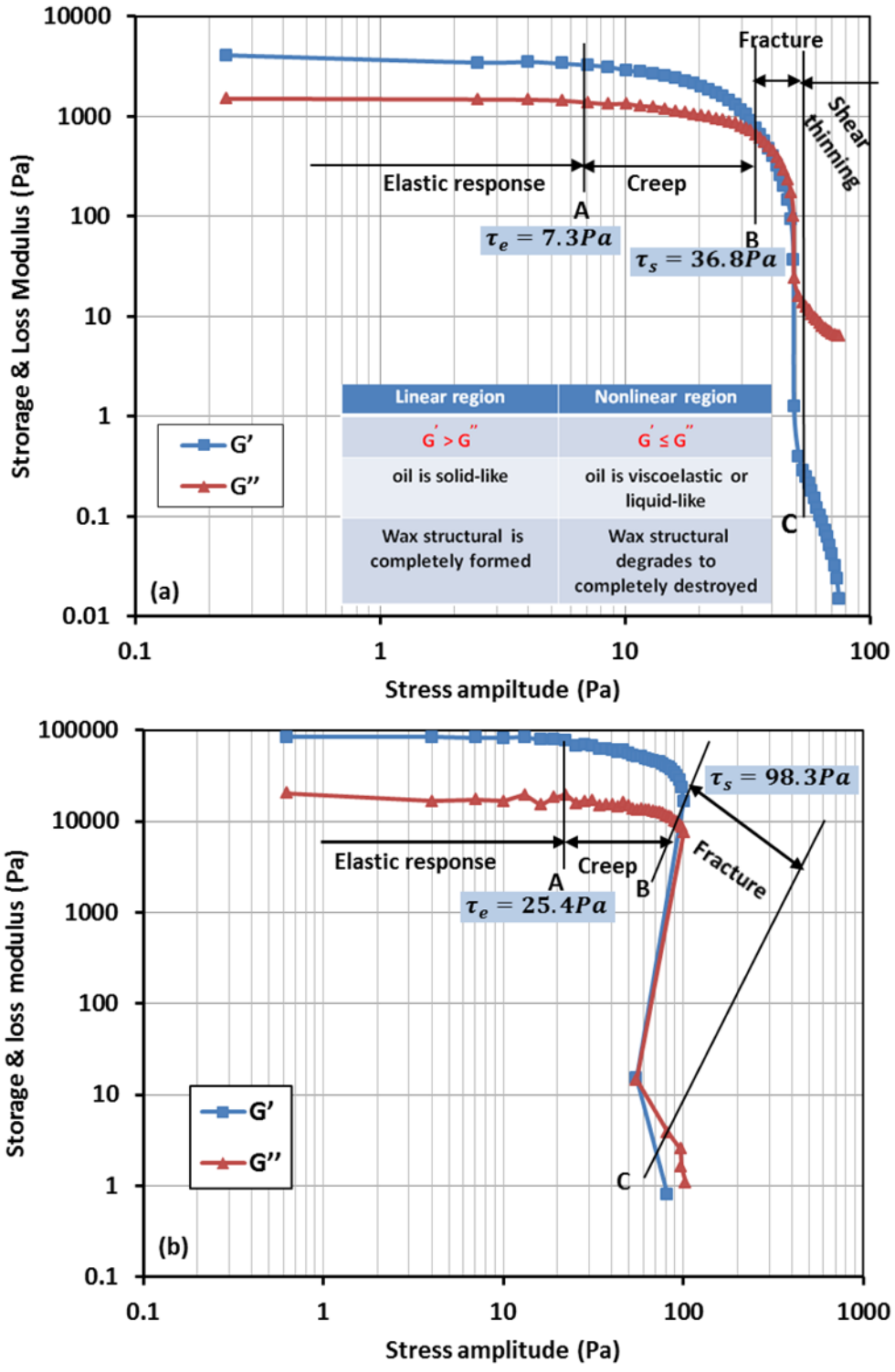

Figure 4.3.22: Oscillatory test data for BPO crude oil at temperature 18^{o}C, cooling rate of 2^{o}C/min and frequency of 1 Hz; G$^{'}$ and G$^{''}$ behaviour during the yielding process **(a)** BPO **(b)** LO.

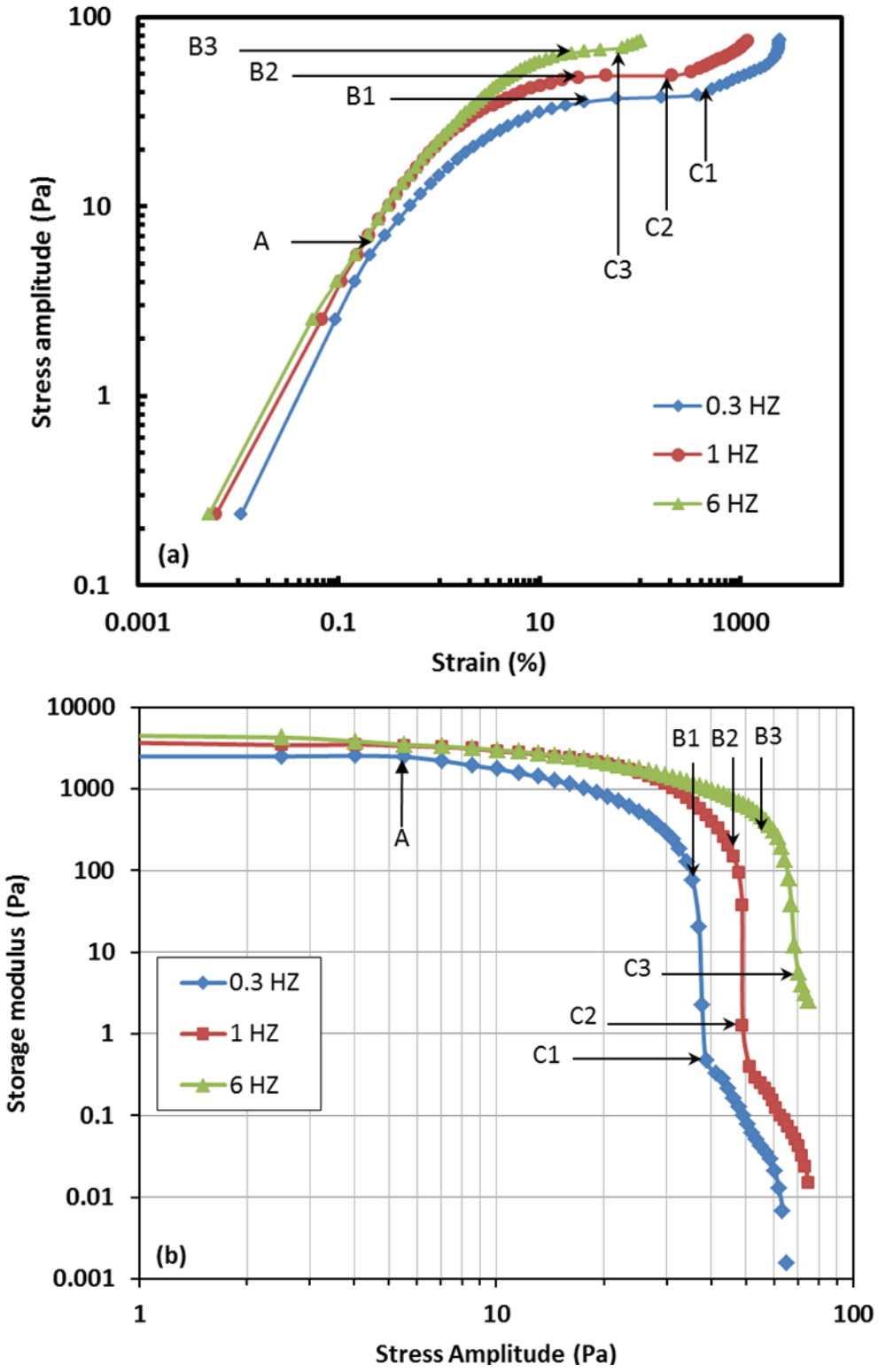

Figure 4.3.23: Oscillatory Test. Effect of frequency on yielding process of BPO crude oil samples tested at temperature 18^{o}C, cooling rate of 2^{o}C/min and under stress amplitude applied from 0 to 75 Pa at different frequencies **(a)** effect of frequency on stress vs. strain relationship during and after yielding **(b)** effect of frequency on G' during and after yielding.

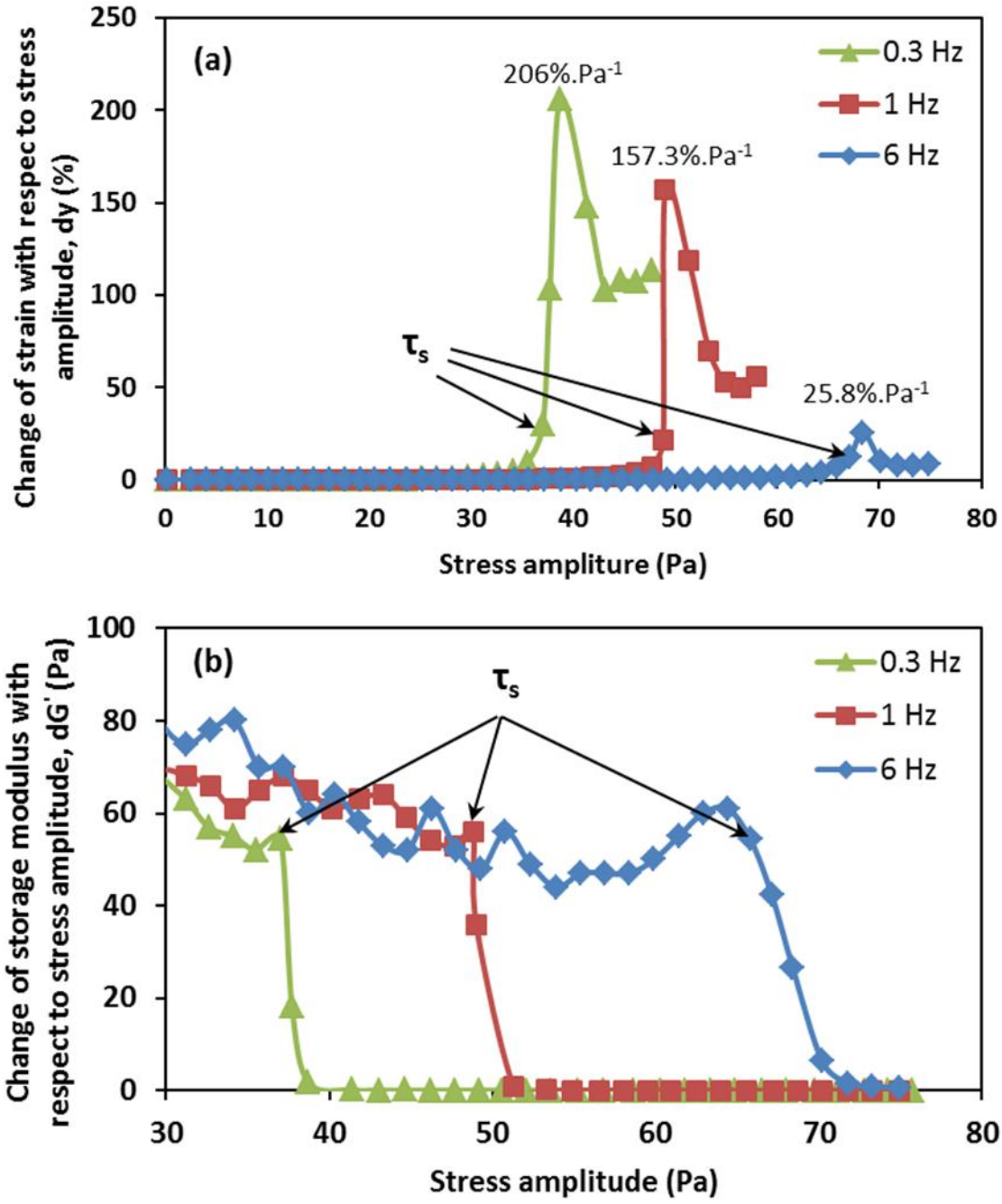

Figure 4.3.24: Effect of frequency on yielding process of BPO crude oil samples tested at temperature 18°C, cooling rate of 2°C/min and under stress amplitude applied from 0 to 75 Pa at different frequencies **(a)** effect of frequency on Δy **(b)** effect of frequency on $\Delta G'$.

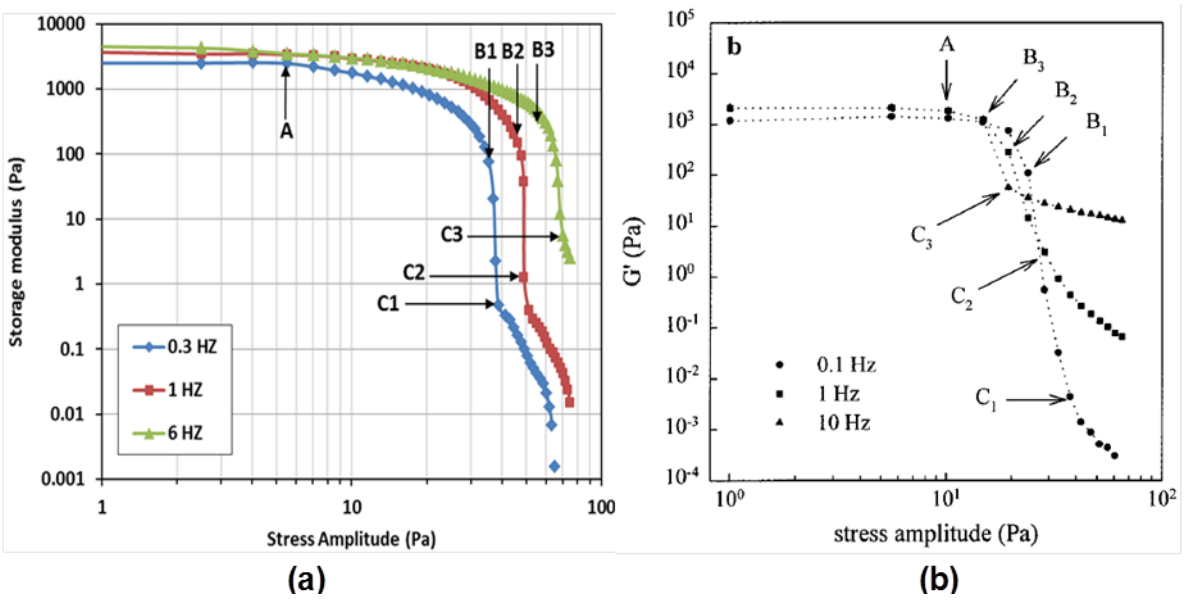

Figure 4.3.25: Oscillatory test; comparison the results of effect of frequency on stress vs. strain relationship during and after yielding **(a)** for BPO crude oil at 18°C done in this research **(b)** for DH19 crude oil at 20°C done by Chang & Boger, 1998.

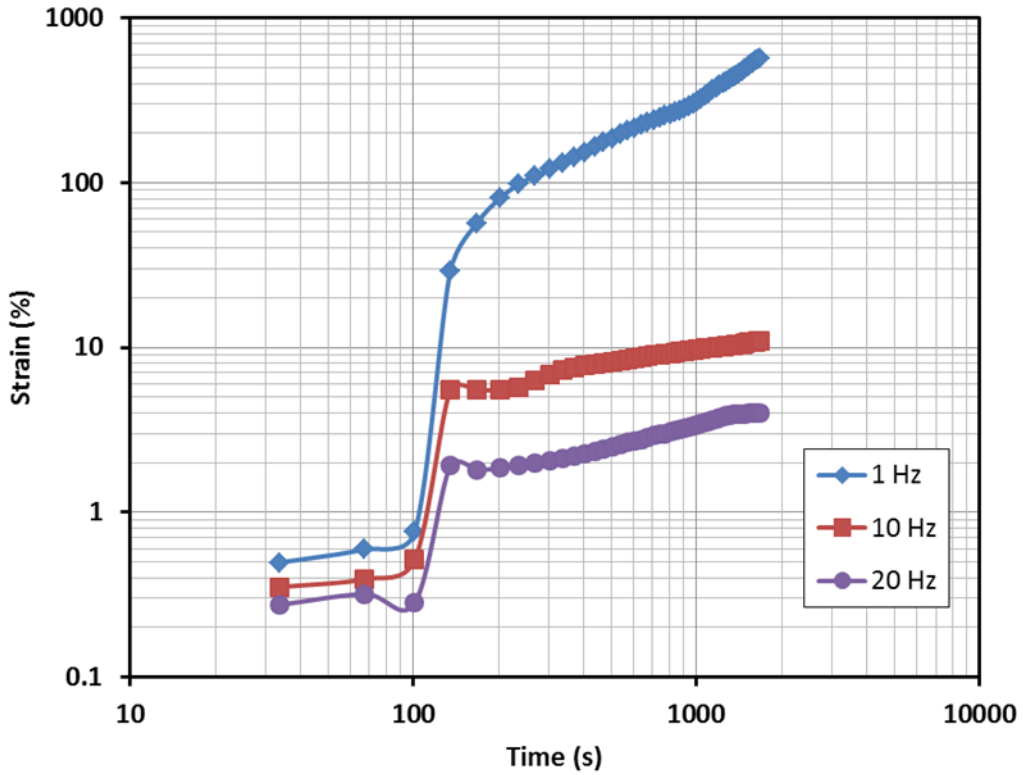

Figure 4.3.26: Oscillatory test; effect of frequency on stain vs. time relationship during the fracture of wax structure of BPO crude oil samples tested at temperature 18°C, cooling rate of 2°C/min and different frequencies.

4.3.4.2 Measurements of gelation temperature (T_{gel})

Oscillatory rheometery is uniquely suited in determining changes from viscous to viscoelastic behaviour. When temperature is the prime variable, a cross over is observed in G′ and G″ corresponding to the gel point temperature (T_{gel}). This is precisely the picture shown in Figure 4.3.27 for both BPO and LO deformed at a fixed frequency of 0.15 Hz and a strain 0.05% and cooling rate of 0.1^{o}C/min. As it can be noted from figure 4.3.27a and b, for both cases of the crude oils, that at high temperature, the oil structure responses as more viscous than elastic as G″ is higher than G′. Both G ′ and G″ increase with decreasing the temperature and at a certain temperature; G′ starts growing faster than G″. When the G′ becomes higher than G″ at a lower temperature, the crude oils behaviours start to change from viscous to mostly elastic, indicating the formation of an inflexible network. The temperature at which the G′ and G″ crossover is taken place is around 30^{o}C for BPO crude oil sample and 53^{o}C for LO crude oil sample; this point is called the *gel point or gelation temperature (T_{gel}).* Therefore, it is necessary to reach a certain amount of crystals before the viscoelastic modifications become obvious. The spread in temperatures before gel point indicates gradual precipitation of the wax.

Similar oscillatory tests were performed for BP crude oil samples at different cooling rates; 0.5, 1 and 5^{o}C/min and the results are plotted in Figure 4.3.28. As it can be noted from the figure, the G′ and G″ values are nearly independent of cooling rate in the viscous region. Figure 4.3.29 represents the gelation temperature as a function of cooling rate. As shown in the figure, there is a difference range from 29.4 to 31.3^{o}C for the gelation temperature with cooling rate range between 0.5 and 5^{o}C/min. Thus, a lower cooling rate results a higher gelation temperature for statically gelled waxy crude oil. These findings are consistent with those made by other researches (see Smith and Ramsden [128]).

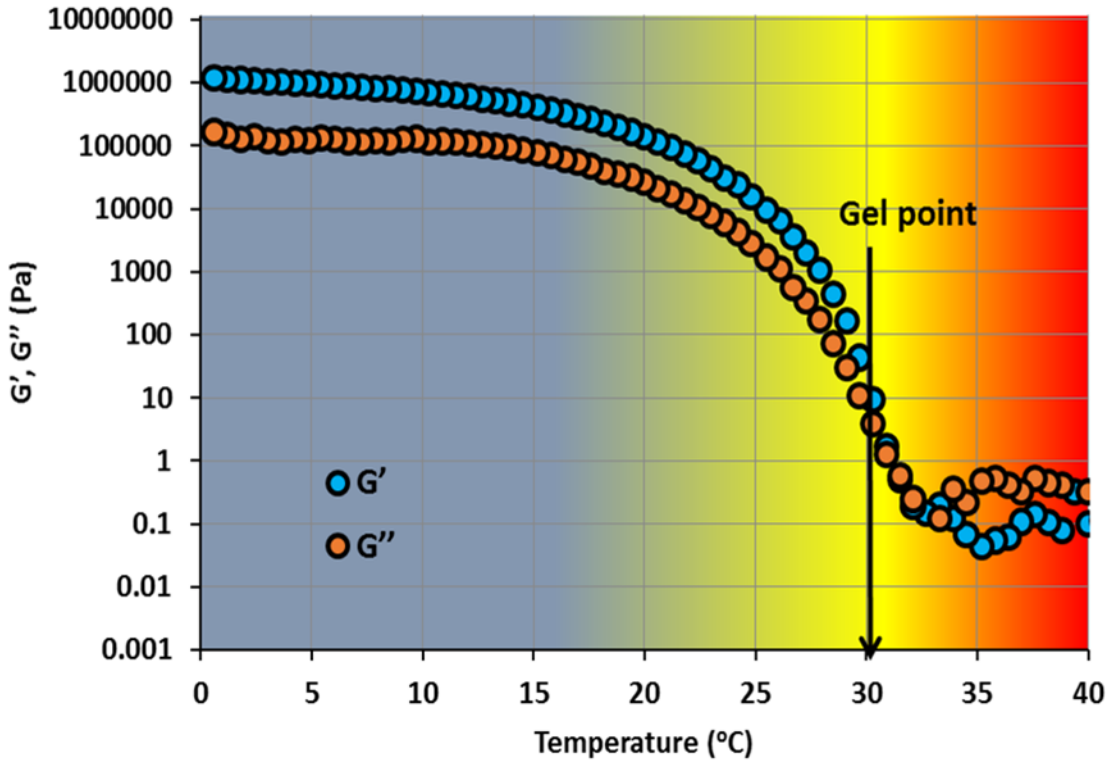

Figure 4.3.27a: The storage and loss moduli versus temperature for BPO crude oil at fixed frequency of 0.15 Hz and a strain 0.05% and cooling rate of 0.1°C/min.

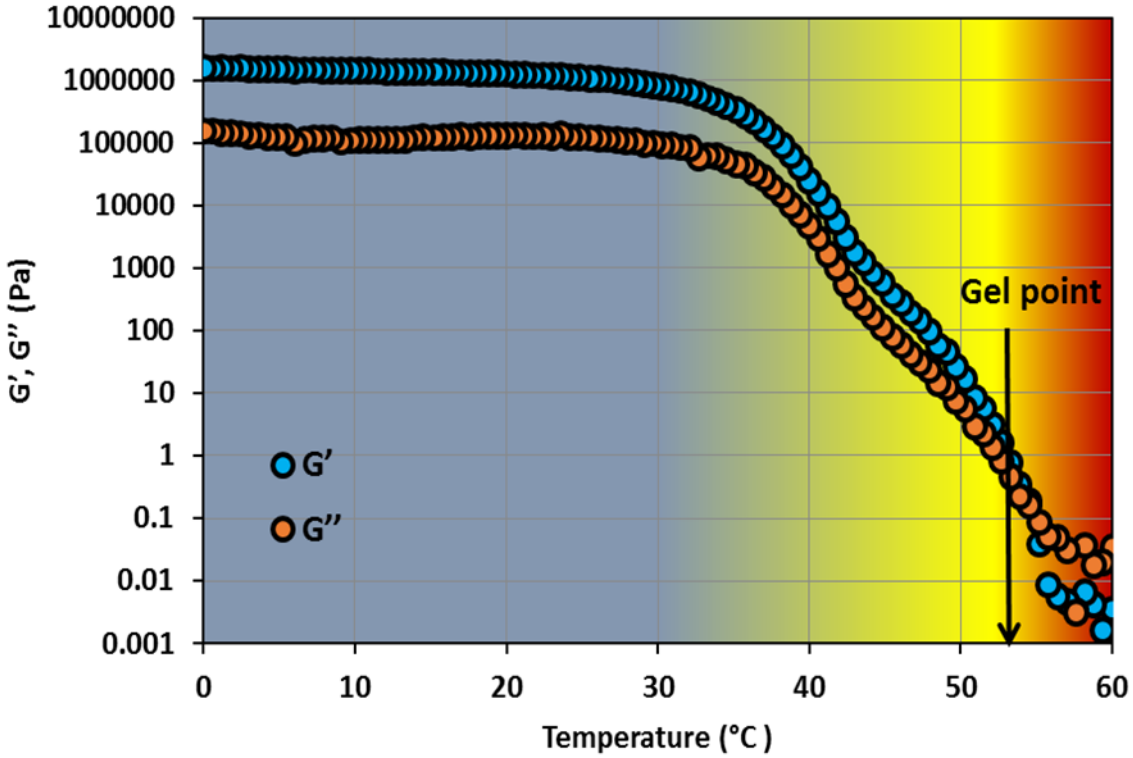

Figure 4.3.27b: The storage and loss moduli versus temperature for LO crude oil at fixed frequency of 0.15 Hz and a strain 0.05% and cooling rate of 0.1°C/min.

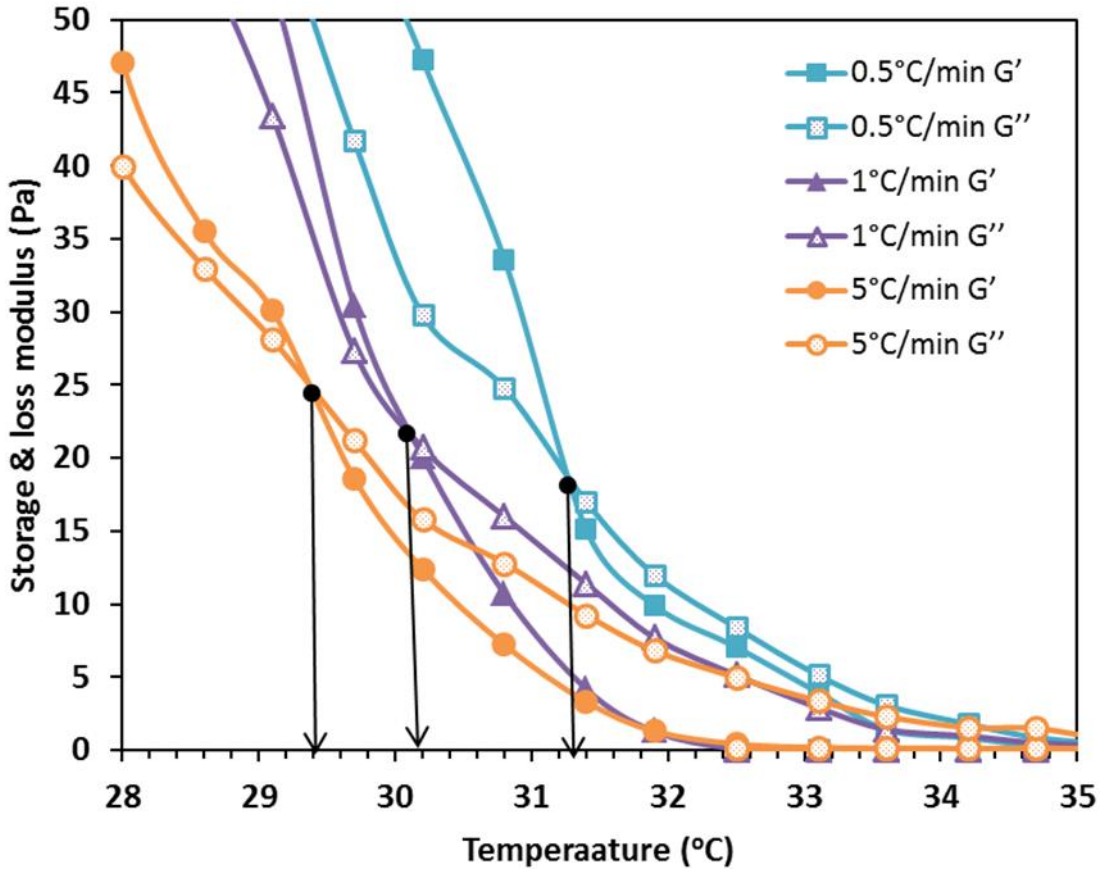

Figure 4.3.28: Variations of the gel point of BPO crude oil as a function of different cooling rates.

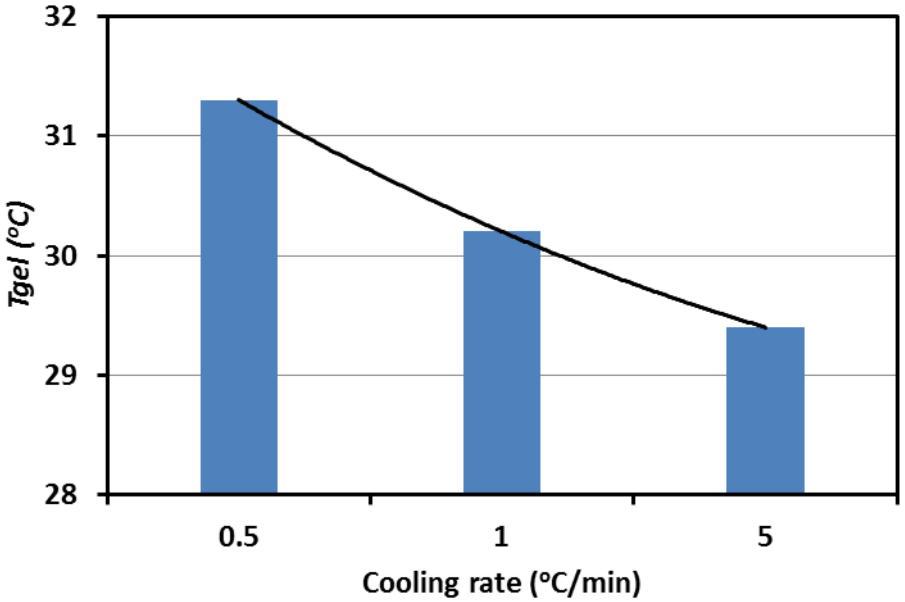

Figure 4.3.29: Dependence gelation temperature of cooling rate for BPO crude oil samples**.**

4.3.4.3 Variation of storage and loss moduli with temperature

Here, data on the variation of the storage and loss moduli with temperature are presented in Figures 4.3.30-31 for LO and BPO, respectively, in a frequency range up to 10Hz and a low strain of 0.05% to remain in the linear viscoelastic region (LVR). In all cases, the temperatures were lowered to the test temperatures at a rate of 0.1^{o}C/min and maintained constant for 15 min before each measurement. Recall that pour point temperature (PPT) is about 18^{o}C for BPO and 35 ^{o}C for LO and that in practice we are interested in behaviour at field temperatures, typically around the pour points of the oils on account climatic difference between the two oils, hence the investigated ranges of 14^{o}C - 23^{o}C for BPO and 31^{o}C - 40^{o}C for LO. As consistent with the LVR assumption, the moduli measured are essentially constant throughout the range of frequencies tested and increasing with decreasing temperature. The higher values for LO compared with BPO are on account of the larger wax content of LO and its morphology, further described in the next section.

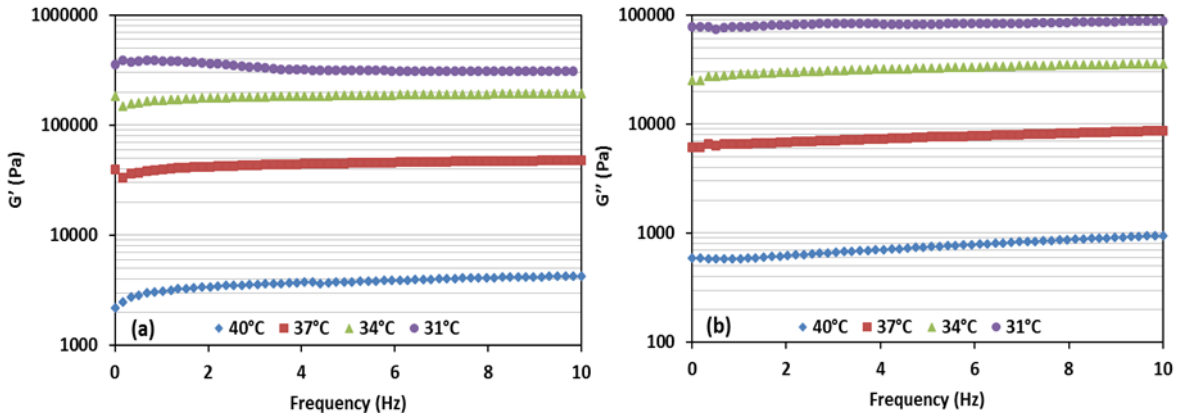

Figure 4.3.30: The storage and loss moduli for LO crude oil at different temperatures **(a)** the storage modulus, G$^{'}$ **(b)** the loss modulus, G$^{''}$.

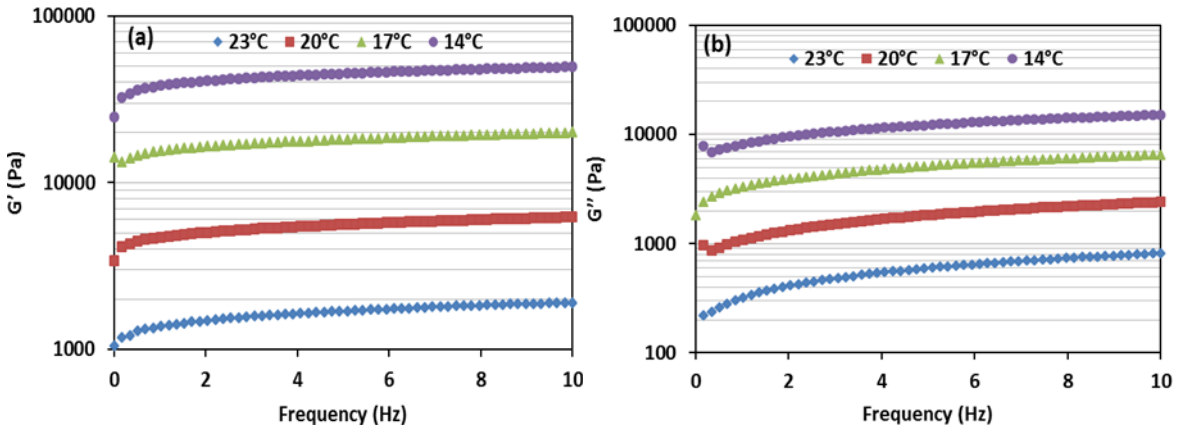

Figure 4.3.31: The storage and loss moduli at different temperatures for BPO crude oil **(a)** the storage modulus, G' **(b)** the loss modulus, G''

4.3.5 Evaluation and Comparison of Measurement Techniques

The elastic-limit yield stress is independent of the time scales of the measurements. The static yield stress and fracture yield stress, which are the important required stress values for calculating the pump pressure required to restart flow in a pipeline, are dependent of the time scale of the yielding. The dynamic yield stress, which is used in the calculation of the pressure-flow rate relationship after fracture, is also affected by the time scale of the yielding. Therefore, the obtained static yield stress from each measurement technique are not directly comparable with each other, because they are dependent on the time scale of the yielding and the time scale is totally different in the three testing techniques. However, the elastic-limit yield stress from the different tests are comparable since it is not influenced by the time scale of the test technique; thus, our results of elastic-limit yield stresses from controlled stress, creep-recovery and oscillatory tests are in a good agreement. The value of the elastic-limit yield stress was determined from the controlled stress test as 10.2 Pa for BPO crude oil at test temperature 18^{o}C and cooling rate of 2^{o}/min as presented in Table 4.3.3, between 5 and 10 Pa from the creep-recovery test and 7.3 Pa from the oscillatory test. For LO, under the same conditions, the elastic-limit yield stress measured was 22.2 Pa under controlled stress and 25.4 Pa in oscillatory deformations. However, the

testing results can also only be comparable if the pre-treatment, the cooling rate, temperature and testing are conducted by the same procedures and under the same conditions. The reproducibility and repeatability can be guaranteed by controlling all related factors of each process and removing all thermal and shear histories before the testing.

4.3.6 Effect of cooling rate on thixotropy of waxy crude oil

Thixotropy in material can be assessed by the hysteresis loop method, performed under controlled stress by increasing the shear stress from 0 to a value where viscous flow is deemed to occur (found by trial and error experiments) and then bringing the shear stress back to 0. Figure 4.3.32 shows the data obtained with LO tested at 35^{o}C, after cooling from 80^{o}C at cooling rates of 0.5, 1 and 2^{o}C/min with the shear stress ramped linearly from 0 to 150 Pa over a 5 min period then back to zero over a 1 min period. Thixotropic behaviour is evident from the hysteresis loop observed and its extent with varying cooling rate can be quantified by calculating the area inside the loop, between the upper and lower curves [121]. As it can be seen from the figure, the breadth of the loop (in the shear rate axis direction) increases with increasing cooling rates and this can be attributed to the difference in the structure strength of the oil under different cooling rates. When the cooling rate is lower, the waxy structure formed is stronger (explained earlier by the fact that the crystals are allowed to grow) and the extent of damage to the structure is less by the identified applied stress. In this condition, structure behaves as a solid or visco-plastic system when it settles back into its original consistency after the applied stress is removed. On the opposite of that, when the cooling rate is higher, the waxy structure formed is relatively weaker; the damage in wax crystal structure is relatively high under the same applied stress, the oil structure behaves as a liquid like or viscoelastic system when it settles back into its original consistency after the applied stress is removed.

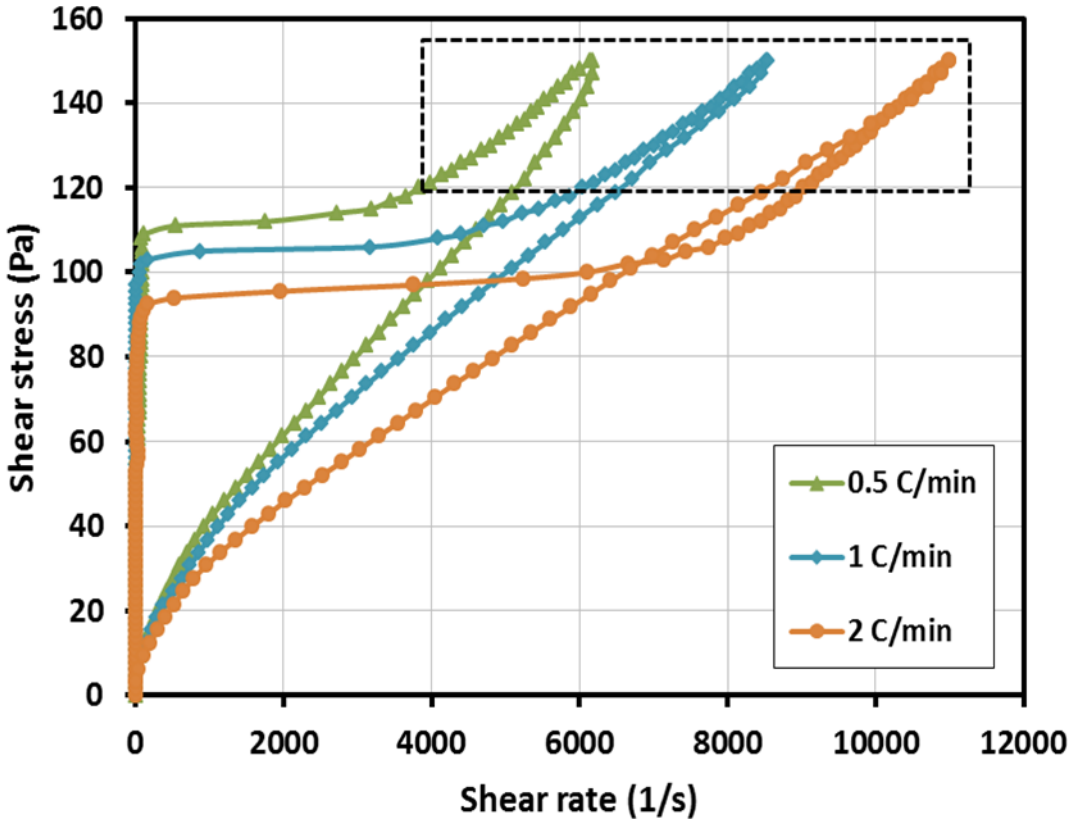

Figure 4.3.32: Effect of cooling rate on the thixotropy of LO crude oil samples tested at 35^{o}C using controlled stress test.

4.4 Microscopic Unravelling of Wax Gel Structure & Yielding

As inferred earlier from calorimetry and rheology, the precipitation of the wax upon cooling produces a gel structure strong enough to resist re-start of shut pipelines transporting waxy crude oils. Calorimetry as described earlier enables the detection of the wax appearance temperature (WAT) found to be 32 ^{0}C for BPO and 60 ^{0}C for LO but a little dependent on cooling rate as shown in Figure 4.2.2a and 4.2.4a. The wax gel structure that ensues however was found to be strongly dependent on cooling rate as established from rheological measurements of yielding. This section uses Cross Polarised Microscopy (CPM) described in the experimental method chapter to view how the structure changes upon cooling to reinforce the observations already obtained from calorimetry and rheology. Importantly, it seeks to demonstrate the apparent contradiction that it is slow

cooling which allows crystal growth, rather than fast cooling which hinders it, that leads to strong gel structures.

4.4.1 Determination of wax appearance temperature, WAT

Here**,** the morphology of pre-conditioned (i.e. with no memory) samples of BPO and LO well above WAT (65^oC for BPO and 85^oC for LO) were observed during cooling at the nominal cooling rate of 1^oC/min. The results of the microscopic observations are presented in Table 4.4.1 revealing a WAT of 31.7^oC for BPO and 59.9^oC for LO. This table is supported by Figure 4.4.1 which gives photos of the precipitating wax crystals number morphology. As explained in the experimental method chapter, CPM is based on the principle that all crystalline material rotates the plane of polarised light. Therefore, upon crossing two prisms on the opposite side of the oil sample, the oil appears black due to the blocking of light. When the wax precipitates, the crystals appear as bright spots. Note that in order to zoom in as closely as possible on WAT, the observations were made at temperature steps of 1^oC down to 35^oC for BPO and 65^oC for LO with 10 minutes holding time between temperature settings and observations and thereafter in steps of 0.1^oC with 5 minutes holding time between temperature settings and observations until the first spots of crystalline material could be seen. The temperature at which a further 5 to 10 additional crystalline material spots could be seen was taken as the WAT. From Figure 4.4.1, it is worthy of observation that the crystal size of LO are much larger than that of BPO suggesting that stronger gel structure will form in comparison with those of BPO. This validates broadly the yielding data measured rheologically and presented earlier.

Table 4.4.1: Summary of CPM observations for determining wax appearance temperature (WAT) of BPO and LO crude oils.

Crude Oil	Time (min)	Temperature (°C)	Observation
BPO	0	55	Clear
	20	35	Clear
	30	34	Clear
	40	33	Clear
	50	32	3 crystals ≈ 1 micron
	65	**31.7**	**9 crystals ≈ 4 microns**
LO	0	85	Clear
	20	65	Clear
	30	64	Clear
	40	63	Clear
	50	62	Clear
	60	61	Clear
	70	60	4 crystals ≈ 5 micron
	75	**59.9**	**15 crystals ≈ 11 micron**

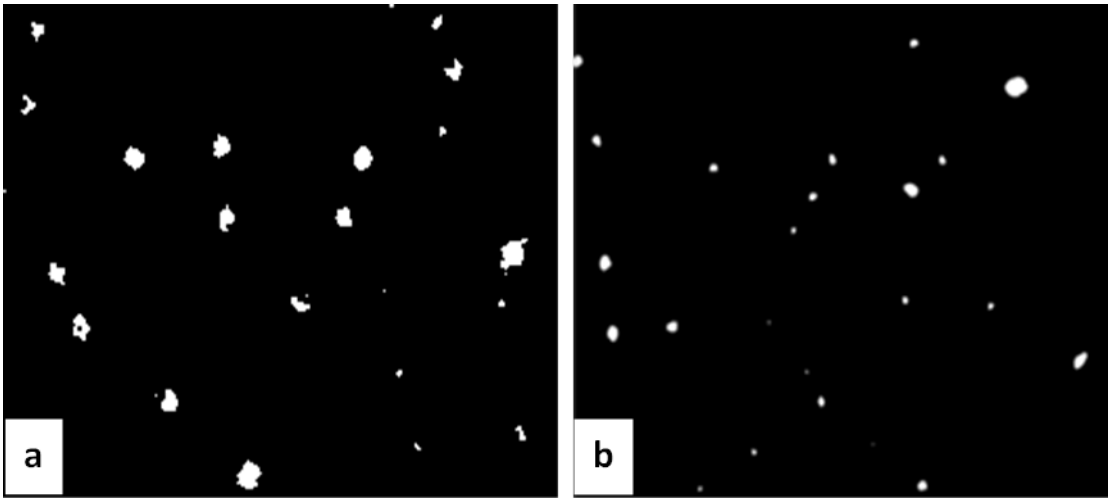

Figure 4.4.1: Wax crystals number and size at WAT for **(a)** LO and **(b)** BPO.

4.4.2 Effect of cooling rate on wax gel structure and yielding

It is well established that crystal growth upon cooling is restricted by fast cooling rates. Here CPM observations are reported for LO cooled below WAT down to 25.5^{o}C at rates of 0.5 and 5^{o}C/min. Figure 4.4.2 shows photographs of the wax crystalline structure. The difference in crystal size is easily notable and confirms the assertion that low cooling rate allows the crystals to grow. Further remarks can be made on the structure.

(i) The gel that forms consists of both solid and liquid phase with platelet-shaped wax crystallites that overlap and interlock around liquid crude oil.

(ii) At the lower cooling rate the wax crystals are larger and the shape of crystal is sheet like.

(iii) At the higher cooling rate, the number density of crystals is increased but the crystal sizes are smaller and the shape of the crystals is smaller, bead-like and compact.

(iv) As the cooling rate increases, the size of wax crystals decreases and, as a result, the network of wax-crystal structure loses its interconnectivity. At the same time, the number density of crystals increases as the cooling rate is increased.

The same results observed by Cazaunx et al. (1998) who reported that the key parameters that determine the structure of waxy-oil gel are the crystal shape (aspect ratio) and number density of wax crystals, both of which depend on the temperature and cooling rate. These observations are in fact universal to crystalline materials behaviour upon cooling, made by numerous investigators.

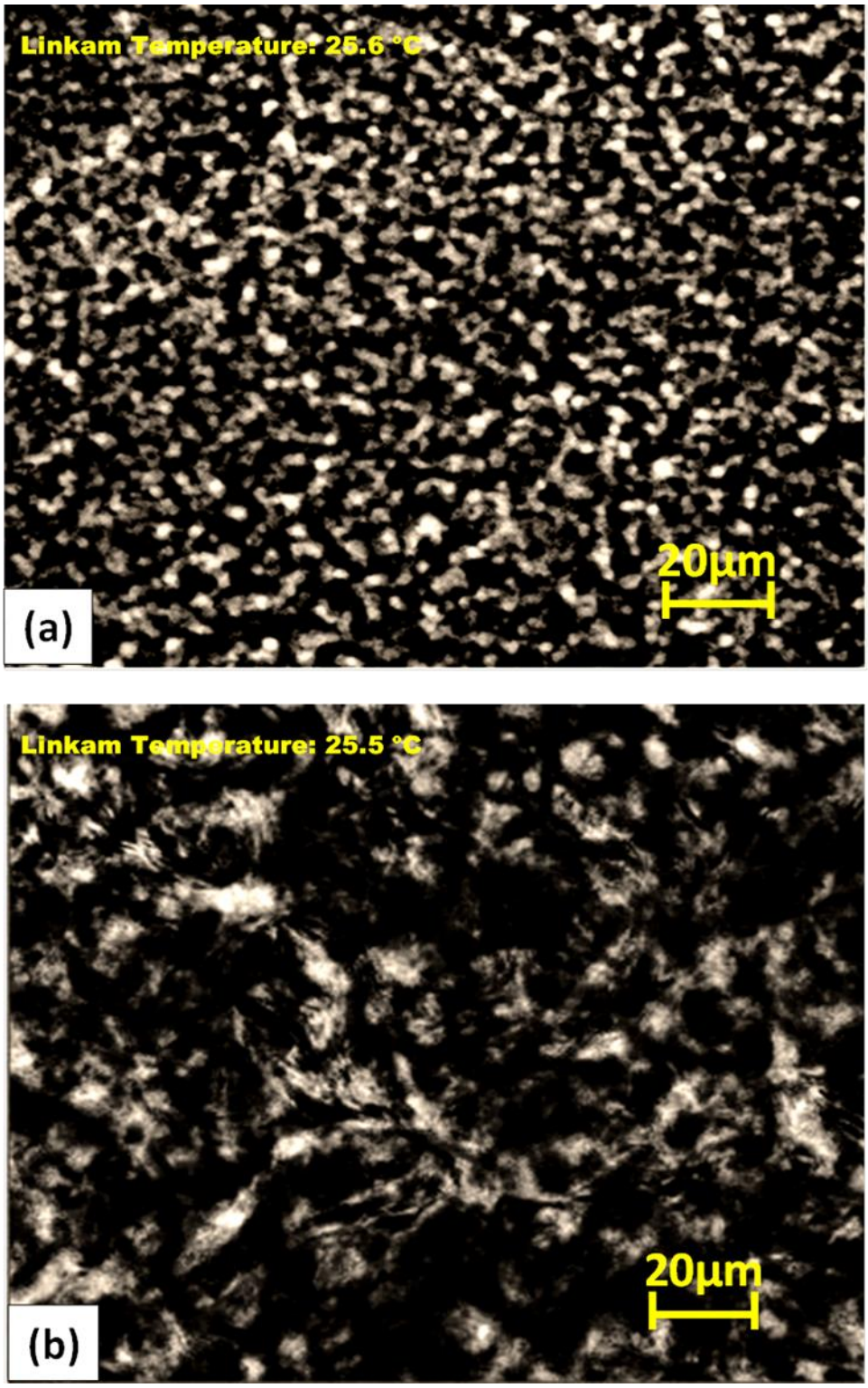

Figure 4.4.2: Cross-polarized microscope photos of LO wax-oil gel samples cooled from temperature above its WAT to 25.5^{o}C at cooling rate of (a) 5^{o}C/min (b) 0.5^{o}C/min.

4.4.3 Effect of ageing time on wax gel structure and yielding

A parameter used in the methodology is the effect of the isothermal holding time (ageing time) of the sample once it has been cooled to the desired temperature and ready for testing in the rheometer. Is this effect important? A priori, it is conceivable that this time could allow the adhesion force between the crystals to strengthen. This is however speculative as adhesive forces usually do not take time unless a chemical reaction is occurring. It is thus important to assess this effect both rheologically and via microscopy to observe if any structural change occurs.

Figure 4.4.3 presents such rheological data for two vastly differing isothermal holding time, 5 min and 2 hours, obtained under controlled stress tests performed on BPO at a temperature 15^{o}C after cooling at a cooling rate of 1^{o}C/min. The controlled stress tests were run by ramping the stress up from 0 to 150Pa at rate of 30Pa/min and then back to 0 in one minute. No change is observed in the flow curve indicating that the forces in the structure do not evolve with time. Corresponding photographs of the structure morphology viewed under the CPM are shown in Figure 4.4.4 and support that no changes has occurred for two different ageing time, 5 min and 4 hours, albeit in terms of crystal number and size, not on adhesive forces of course. The same microscopic observations and rheological results were performed for the cooled LO crude oil samples and similar results to BPO crude oil were obtained.

These results of the effect of isothermal holding time on gel strength are in agreement with previous results obtained by Chang et al. [6] on different waxy crude oils. As explained earlier, this observation follows the logic that interfacial forces between crystals do not evolve in time when the isothermal holding temperature is held constant.

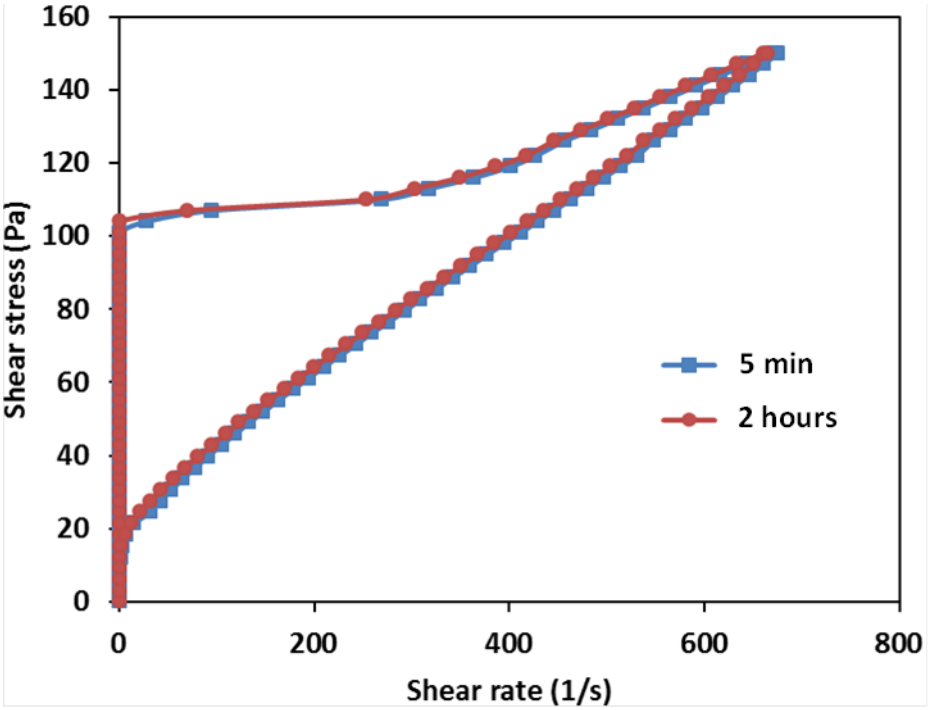

Figure 4.4.3: Controlled stress data performed on BPO showing isothermal holding time having no effect on flow curves (yielding process).

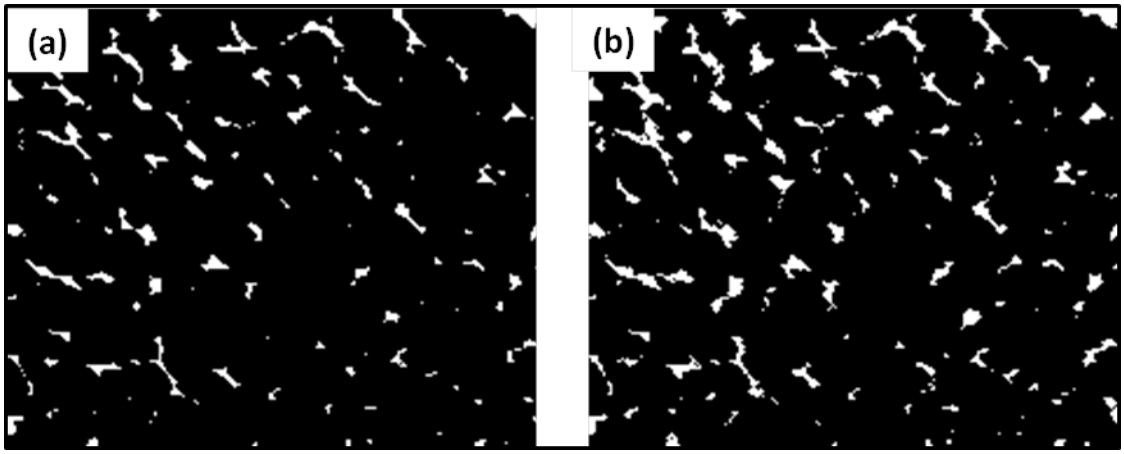

Figure 4.4.4: CPM photographs taken on BPO after isothermal holding time of **(a)** 5 minutes and **(b)** 4 hours.

4.4.4 Linking Calorimetric and Microscopic Observations to Rheological Data

Having determined WAT via calorimetry (DSC) and microscopy (CPM) and assessed the effect of cooling rate on gel morphology via microscopy and gel "strength" via rheology, here an attempt is made at establishing correlation between the three techniques.

First, photographs of microscopic observations are shown in Figure 4.4.5 for BPO and LO, at temperature below their pour points, 15.2^{o}C and 30.3^{o}C, respectively after being cooled at 1^{o}C/min. They show the crystal structure in BPO to be significantly different from that of LO. In BPO, the crystals are dispersed in the liquid crude oil, giving a loose structure. In LO the crystals are more compact suggesting a stronger interlocked network, hence requiring larger yield stress to break.

Secondly, Figure 4.4.6 depicts the correspondence between DSC data (the variation of heat flow with temperature) and structure morphology observed in the CPM photographs which show clearly a developing network as temperature is decreased, here LO is taken as an example.

Finally, Figures 4.4.7 combine calorimetric and rheological data with photographs of gel structure at different temperatures for BPO. As it can be observed from the amplitude sweep in the linear regions, the structural modulus (storage and loss modulus) increase as temperature is decreased as a result of the increasing amount of precipitated wax as indicated in the DSC heat flow variation. Correspondingly, the crystal network develops as shown in the CPM photographs and this is reflected in the rheological data which show the yielding point values in the nonlinear regions to increase with decreasing temperatures.

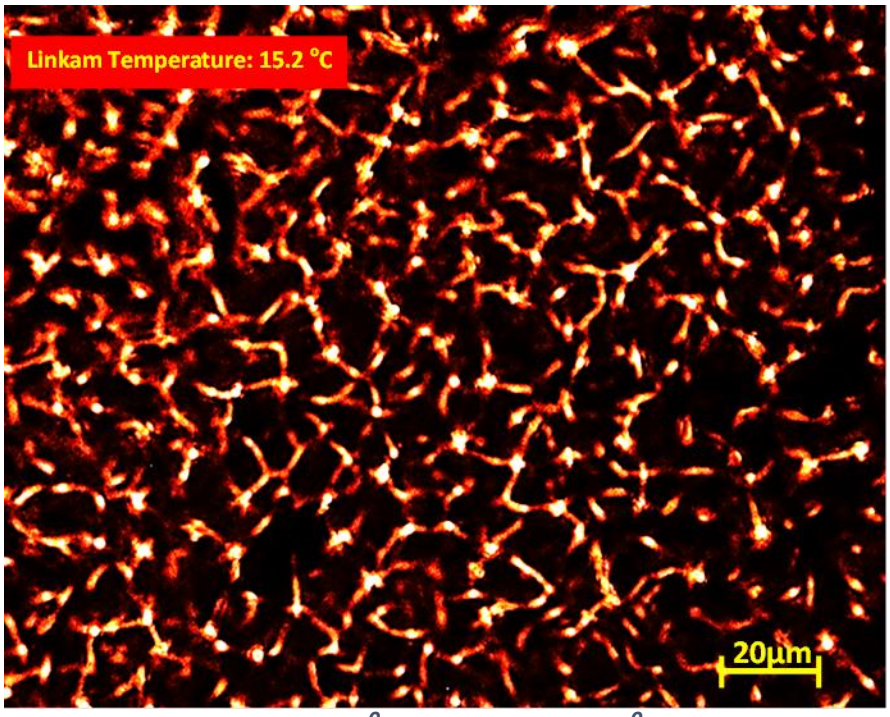

BPO @T=15.2^{0}C, cooling rate 1^{0}C/min

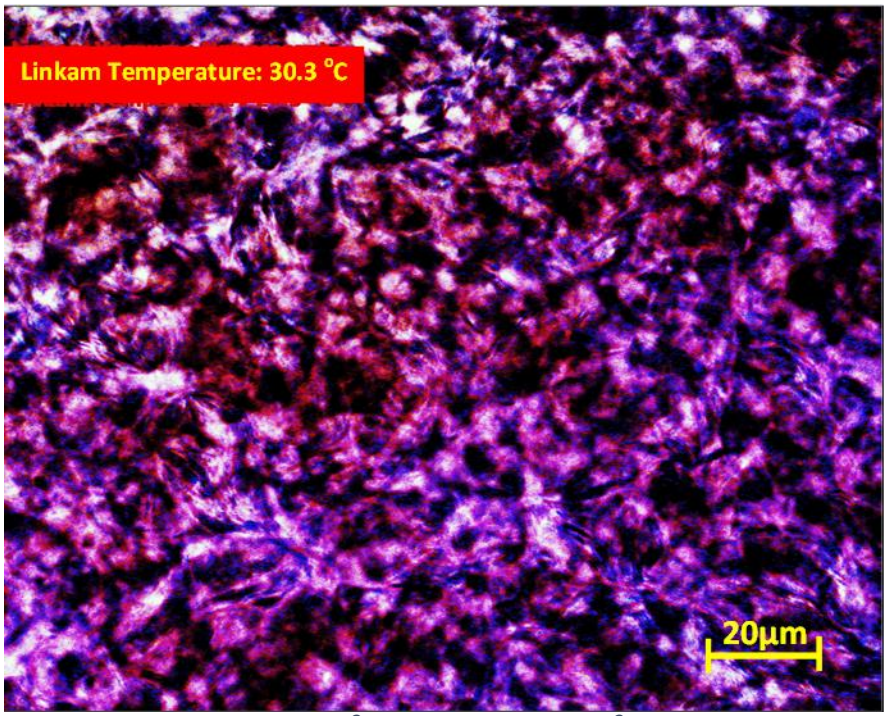

LO@T=30.3^{0}C, cooling rate 1^{0}C/min

Figure 4.4.5: CPM photos of BPO and LO waxy gels.

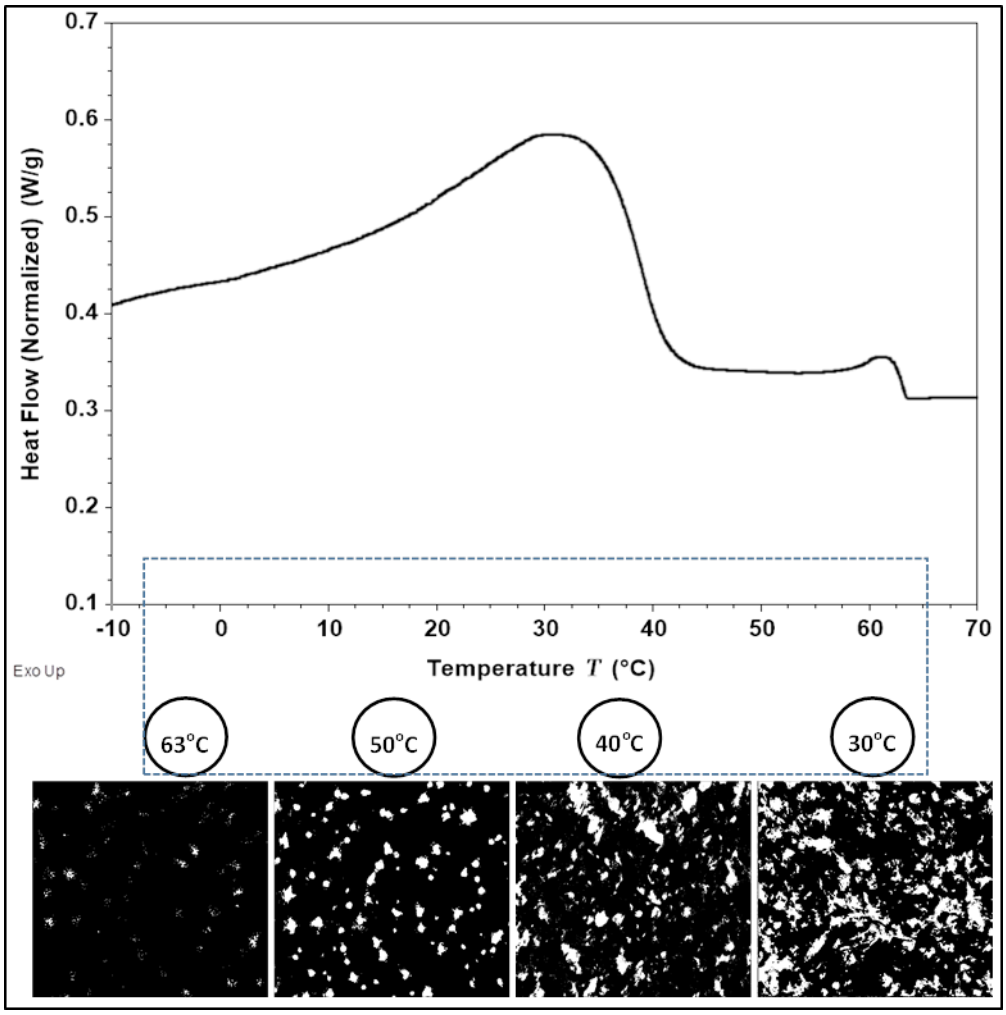

Figure 4.4.6: Correlation between crystallisation (DSC) and morphology (CPM) at various temperatures of LO crude oil statically cooled at 1°C/min.

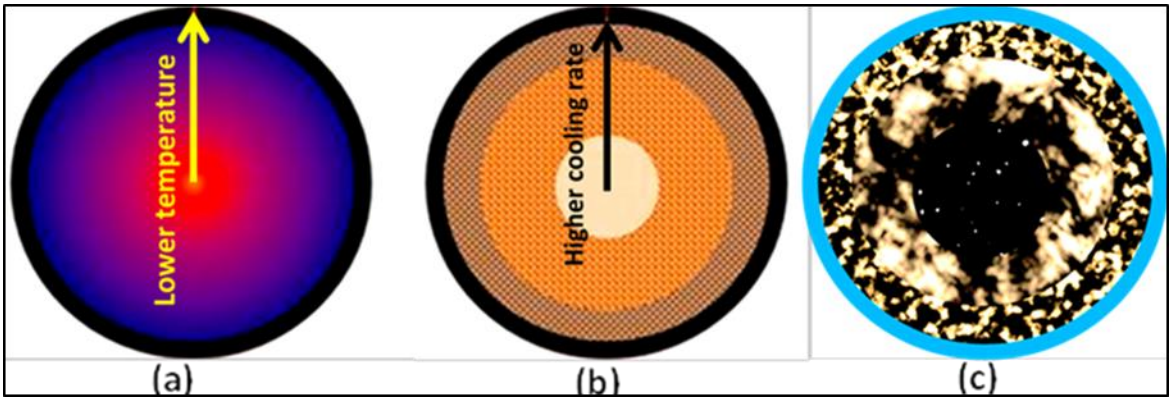

Figure 4.4.8: Cross-sectional area of pipeline under statically cooling down: **(a)** the radial temperatures **(b)** the radial cooling rates **(c)** the final radial morphology and interfaces.

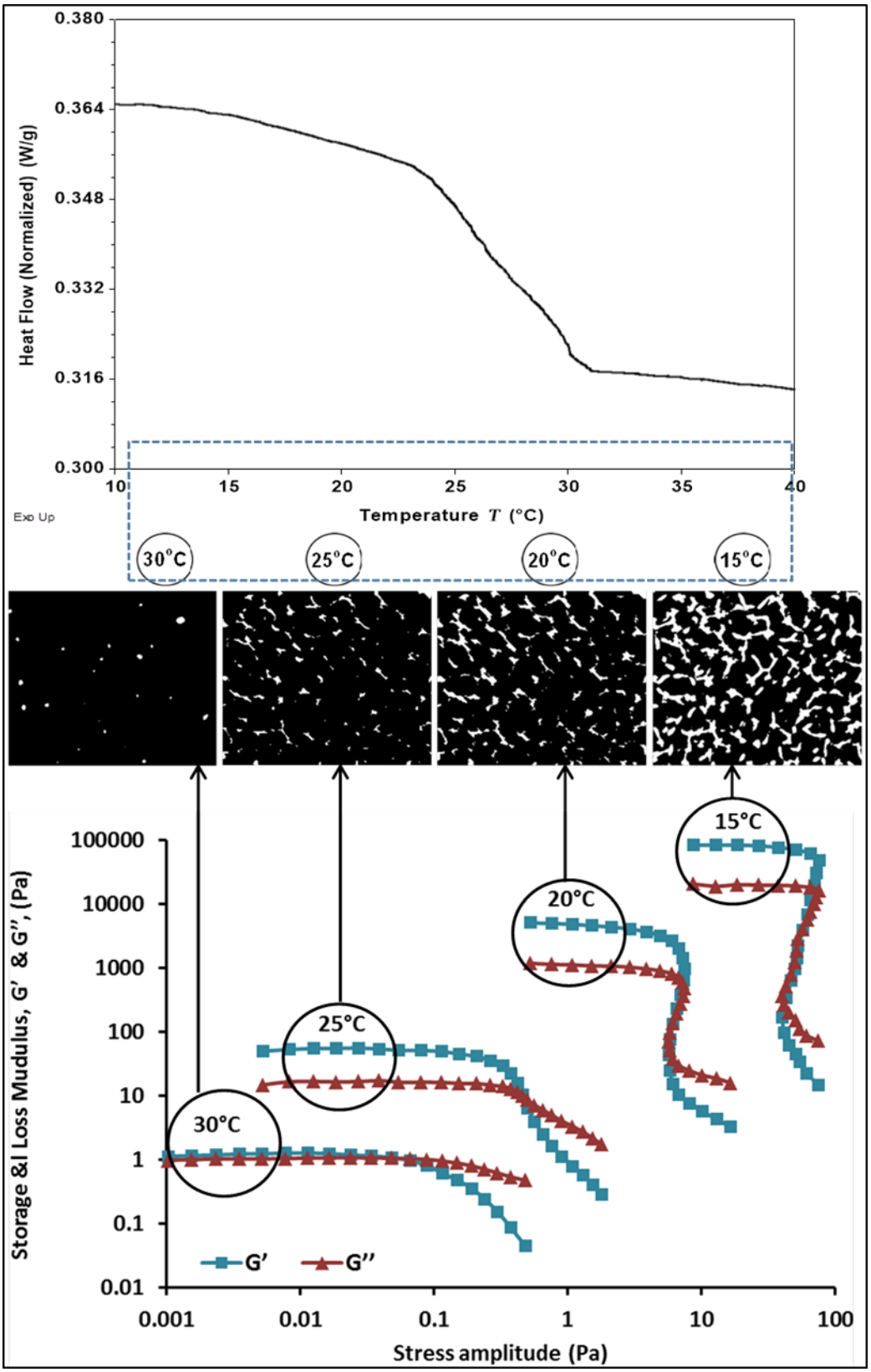

Figure 4.4.7: Correlation between crystallisation (DSC), morphology (CPM) and yielding (CSR) at various temperatures of BPO crude oil statically cooled at 1°C/min.

4.4.5 Summary

Microscopic observations of the wax gel structure as the cooling rate, holding time and temperature are varied have provided valuable information explaining and quantifying how the gel structure develops differently in BPO and LO. LO is seen as developing a strong interlocked network of large crystals whereas BPO cooling produces loose crystals dispersed in the liquid oil. These observations tally with the rheological data which showed significantly higher yield stresses in LO than BPO.

In addition, CPM data have confirmed the known fact that as the cooling rate is reduced, the crystals in the gel grow in size, leading in the case of LO to even more interlocked structure, hence larger yield stresses.

When considering, actual pipeline restart after gelling of the crude oil, it is clear that larger cooling rates will occur at the wall than towards the centre of the pipe. This will lead to a profile of crystal sizes across the diameter of the pipe. At the wall, the crystals will be many and small as a result of the larger cooling rate at the wall, and as we move towards the centre the crystals will be larger in size. This is illustrated in Figure 4.4.8. The large number of crystals at the wall will provide a large interfacial area for adhesion with the pipe wall, so it is evident that at restart, the gel will not break at the wall but somewhere towards the centre of pipe, depending on how far reaching the cooling is. A heat transfer study of waxy crude oil being cooled statically in pipeline is thus necessary to determine the temperature profile and locate the gel front, the interface where the gel will break at restart as illustrated in Figure 4.4.8.

The next section presents such heat transfer study.

4.5 Static Cooling Temperature Profile or Locating the Gel Front

In a shutdown hot pipeline which is allowed to cool at its wall it is clear that the dissolved wax will gradually precipitate and migrate towards the wall. Over time, a wax deposit region will form, leaving a core region with no dissolved wax as illustrated above in Figure 4.4.8. This is an easily understood heat transfer-mass transfer mechanism. It is precisely this situation that occurs in a pipeline pumping a hot waxy crude oil which suddenly loses pumping and heating power and begins to cool statically. As described in the experimental method chapter, we reproduce this situation most simply using an oil filled pipe section the inside and wall temperature of which can be controlled. Measuring then the temperature profile across the section of the pipe over time as the pipe is allowed to cool at controlled cooling rate at its wall will then give the gel region and front as we explain below. This information is most critical at enabling the prediction of the start-up pressure as we shall explain. Accuracy in the temperature profile measurement is important in order to be able to locate the gel front accurately.

In an effort to guide this important part of the research, a model will be first presented to evaluate the effects of the various parameters at play.

4.5.1 Modelling of Static Cooling and Wax Deposition

The situation to be analysed is depicted in Figure 2.7.1 and it is that of stagnant plug of waxy crude oil contained in a pipe the wall of which is suddenly cooled. This reproduces precisely the situation that happens in the field when heating and pumping fails. Upon cooling, several stages can be identified:

i. Transient cooling of the liquid above WAT
ii. Cooling below WAT
iii. Solid wax deposition region
iv. Gel Front movement or growth of deposit region

These stages are now analysed below.

1) Transient Cooling of liquid phase above WAT

It may be surprisingly but interestingly as observed from the data (see Figure 4.5.3), the temperature throughout the liquid phase (oil) remains uniform and the entire hot liquid temperature drops at the same rate while the liquid cooled from an initial temperature above the WAT, until reaching the wax appearance temperature (WAT) of the oil phase. To be exact, there was no radial temperature gradient during the cooling process until the bulk liquid phase changes when the temperature reaches the WAT. This suggests that the transient cooling of the hot liquid phase is by natural convection. We can express the heat transfer that occurs as:

$$m_l c_{p_l} \frac{dT_l}{dt} = -h_l A_l \left(T_l - T_{r_i}\right) \qquad at\ T_l \geq T_{WA}\ with\ 0 < r < r_i \tag{4.5.1}$$

where m_l is the mass of the liquid, T_l its temperature, A_l its area for heat transfer (interfacial area between the cooling liquid phase and the wax deposit phase) and T_{r_i} the interfacial temperature between the liquid and deposit phases. Substituting for m_l and A_l , Eq. (4.5.1) becomes:

$$\rho_l \pi {r_i}^2 L c_{p_l} \frac{dT_l}{dt} = -h_l 2\pi r_i L \left(T_l - T_{r_i}\right) \qquad at\ T_l \geq T_{WA}\ with\ 0 < r < r_i \tag{4.5.2}$$

where L here is the height of the sample held in the cylinder. Introducing thermal diffusivity α_l Eq. (4.5.2) reduces to:

$$\frac{dT_l}{\alpha_l dt} = -\frac{2h_l}{k_l} \frac{\left(T_l - T_{r_i}\right)}{r_i} \qquad at\ T_l \geq T_{WA}\ with\ 0 < r < r_i \tag{4.5.3}$$

As stated earlier, the transient cooling of the hot liquid phase is by natural convection so an appropriate expression for h_l is required. For liquids being cooled in a cylindrical vessel by natural convection, McAdams (1954) gives the equivalent Nusselt expression:

$$Nu = 0.53(Pr.Gr)^{0.25} \tag{4.5.4}$$

Such expression as Eq. (4.5.4) are not exact as they derive from experimental data and will be the first source of discrepancies between the model being developed and the measurements of the present study. However the

approach of this study is in fact to use the data to calculate the heat transfer coefficient which was found to be here equal to 0.0985 kJ m^{-2} s^{-1} °C^{-1} for LO crude oil and 0.07 kJ m^{-2} s^{-1} °C^{-1} for BPO crude oil, thus, the Nusselt number was calculated to be equal to 0.0622 and 0.042 for LO and BPO, respectively (see calculations and Excel tables in Appendix A2). This value is close to values reported by other researchers [90, 91] for convective of stagnant fluid.

2) Cooling below WAT

As indicated from the outset, the above equations assume the liquid phase to be at a temperature above wax appearance. Once the liquid temperature is reached at temperature, $T_l < T_{WAT}$, wax particles will precipitate into the liquid changing the way it will cool, effectively adding an element of conduction as the wax are solid particulates. In the process of precipitating, the mass fraction $x_{w,l}$ wax particles will release a latent heat $(\lambda_{w,l})$. Thus we will have a modified version of Eq. (4.5.1), using the effective conductivity of the oil with the precipitated wax (k_l):

- Hot liquid cooling by conduction and convection:

$$q_r = -k_l \frac{dT_l}{dr} + h_l\left(T_l - T_{r_i}\right)$$

- Heat balance:

$$q_r(2\pi rL) - q_{r+dr}(2\pi(r+dr)L) + \dot{w}_l(\pi L((r+dr)^2 - r^2)\lambda_{w,l}) = \frac{d}{dt}(\rho_l c_{p_l}\pi((r+dr)^2 - r^2)(T_l - T_{ri})$$

with the rate of wax precipitation $\dot{w}_l = \rho_l \frac{dx_{w,l}}{dt}$, $(x_{w,l})$ being the mass fraction of wax precipitated in the liquid phase.

The above equation in derivative form becomes:

$$-\frac{1}{r}\frac{d}{dr}(rq_r) + \lambda_{w,l}\rho_l \frac{dx_{w,l}}{dt} = \rho_l c_{p_l}\frac{dT_l}{dt}$$

leading to:

$$m_l c_{p_l}\frac{dT_l}{dt} = -h_l A_l\left(T_l - T_{r_i}\right) + \frac{k_l}{\pi {r_i}^2 L}\frac{1}{r}\frac{d}{dr}\left(r\frac{dT}{dr}\right) + m_l\lambda_{w,l}\frac{dx_{w,l}}{dt}$$

$$at \quad T_l < T_{WAT} \quad 0 < r < r_i \qquad (4.5.5)$$

Rearranging we obtain:

$$\frac{dT_l}{\alpha_l dt} - \frac{\rho_l}{k_l}\lambda_{w,l}\frac{dx_{w,l}}{dt} = \frac{d^2T_l}{dr^2} + \left(\frac{1}{r} - \frac{h_l}{k_l}\right)\frac{dT_l}{dr} - \frac{h_l}{rk_l}\left(T_l - T_{r_i}\right)$$

$$at \quad T_l < T_{WA} \quad with \;\; 0 < r < r_i$$

$$\frac{dT_l}{\alpha_l dt} = -\frac{2h_l}{k_l}\frac{\left(T_l - T_{r_i}\right)}{r_i} + \frac{1}{r}\frac{d}{dr}\left(r\frac{dT_l}{dr}\right) + \frac{\rho_l}{k_l}\lambda_{w,l}\frac{dx_{w,l}}{dt}$$

$$at \quad T_l < T_{WA} \quad with \;\; 0 < r < r_i \qquad (4.5.6)$$

3) Solid Wax Deposition Region

Heat transfer here for the deposit layer is governed by conduction as we have a solid phase. The treatment is the same as above but without convection and using $\dot{w}_s$ rather than $\dot{w}_l$ as the wax rate increase is now in the solid phase:

$$-\frac{1}{r}\frac{d}{dr}(rq_r) + \lambda_{w,s}\,\rho_s\frac{dx_{w,s}}{dt} = \rho_s c_{p_s}\frac{dT_s}{dt}$$

T_s , is the temperature of the solid layer in the deposit region, $\dot{w}_s = \rho_s\frac{dx_{w,s}}{dt}$ the rate of wax increase, $x_{w,s}$ the mass fraction of wax in the solid phase and $\lambda_{w,s}$ the heat of wax formation. Thus, the term $\lambda_{w,s}\,\rho_s\frac{dx_{w,s}}{dt}$ accounts for the heat released in the liquid-solid two-phase region due to the increased mass fraction in the deposit layer. Also we note here conduction only through $q_r = -k_s\frac{dT_s}{dr}$, i.e. no convective term.

By combining the conduction and energy balance terms, the equation then becomes:

$$\frac{dT_s}{\alpha_s dt} = \frac{1}{r}\frac{d}{dr}\left(r\frac{dT_s}{dr}\right) + \frac{\rho_s}{k_s}\lambda_{w,s}\frac{dx_{w,s}}{dt} \quad with \;\; r_i < r < R \qquad (4.5.7)$$

Noting that we can write $\frac{dx_{w,s}}{dt} = \frac{dx_{w,s}}{dT_s}\frac{dT_s}{dt}$ we rearrange the above equation as:

$$\left(\frac{1}{\alpha_s} - \frac{\rho_s}{k_s}\lambda_{w,s}\frac{dx_{w,s}}{dT_s}\right)\frac{dT_s}{dt} = \frac{1}{r}\frac{d}{dr}\left(r\frac{dT_s}{dr}\right) \quad with \;\; r_i < r < R \qquad (4.5.8)$$

Defining $\frac{1}{\alpha_s'} = (\frac{1}{\alpha_s} - \frac{\rho_s}{k_s}\lambda_{w,s}\frac{dx_{w,s}}{dT_s})$ we can rewrite the above equation as:

$$\frac{dT_s}{\alpha'_S dt} = \frac{1}{r}\frac{d}{dr}\left(r\frac{dT_s}{dr}\right) \quad with\ r_i < r < R \tag{4.5.9}$$

where α'_S represents a modified thermal diffusivity value for the deposit layer.

4) Growth of deposit region or movement of the interface

Gel front movement results from the particles which have precipitated in the liquid phase becoming in equilibrium with the solid phase at the interface between the two phases and being integrated by diffusion gradually within the solid phase causing in the process the interphase position (r) to move inwards. During the formation of the solid deposit (dr), heat is transferred by convection through the surface $(r_i - dr)$ followed by heat transfer by conduction in the deposit at (r). We can thus describe this movement in term of the following heat balance:

$$\lambda_{w,i}x_{w,i}\frac{\rho_l 2\pi r_i L dr_i}{dt} = k_s 2\pi r_i L\frac{dT_s}{dr} - h_l 2\pi r_i L\left(T_l - T_{r_i}\right) \qquad at\ r = r_i$$

$$\rho_l\lambda_{w,i}x_{w,i}\frac{dr_i}{dt} = k_s\frac{dT_s}{dr} - h_l\left(T_l - T_{r_i}\right) \quad at \quad r = r_i \tag{4.5.10}$$

Note here we have used $\lambda_{w,i}x_{w,i}$ to be consistent that wax is being precipitated now at the interface.

5) Solution scheme

The model just described requires solution of Equations (4.5.3), (4.5.6), (4.5.9) and (4.5.10).

<u>The initial conditions are</u>:

$t = 0 \quad r_i = R$

$t = 0 \quad T_l = T_{hot}\ \ a\ given\ fixed\ value\ \ at \quad 0 \le r \le R$

<u>The boundary conditions are:</u>

$t > 0 \qquad at\ \ r = 0 \qquad \frac{dT_l}{dr} = 0 \quad or\ symmetry$

$t > 0 \qquad at\ \ r = r_i \qquad T_l = T_{r_i} = T_s \quad or\ continuity$

$t > 0 \qquad at\ \ r = R \qquad T_s = T_{wall}\ and\ \frac{dT_{wall}}{dt} = cst\ cooling\ rate$

$\frac{dT_{wall}}{dt}$ = *1.1°C/min and from 85 to 20°C for LO, and from 60 to 10°C for BP*

It is now appropriate to non-dimensionalised all the equations above using the following dimensionless variables:

$$\xi = r/R \qquad \Theta = \frac{T-T_{WAT}}{T_{hot}-T_{WAT}} \qquad \tau = \frac{\alpha t}{R^2} \qquad Nu = \frac{h_l R}{k_l} \qquad H_w = \frac{\lambda}{c_p(T_{hot}-T_{WAT})} \qquad X_w = x_w$$

Thus, the equivalent non dimensional expressions for Equations (4.5.3), (4.5.6), (4.5.9) and (4.5.10) are:

Liquid Phase above WAT:

$$\frac{d\Theta_l}{d\tau} = -2Nu_{l^+}\frac{\left(\Theta_l - \Theta_{\xi_i}\right)}{\xi_i} \tag{4.5.11}$$

Liquid Phase below WAT:

$$\frac{d\Theta_l}{d\tau}\left(1 - \frac{dX_{w,l}}{d\Theta_l}H_{w,l}\right) = \frac{d^2\Theta_l}{d\xi^2} + \left(\frac{1}{\xi} - Nu_{l^-}\right)\frac{d\Theta_l}{d\xi} - Nu_{l^-}\frac{\left(\Theta_l - \Theta_{\xi_i}\right)}{\xi} \tag{4.5.12}$$

Solid Phase:

$$\frac{d\Theta_s}{d\tau}\left(1 - \frac{dX_{w,s}}{d\Theta_s}H_{w,s}\right) = \frac{1}{\xi}\frac{d}{d\xi}\left(\xi\frac{d\Theta_s}{d\xi}\right) \tag{4.5.13}$$

Interface Movement:

$$X_{w,i}H_{w,i}\frac{d\xi_i}{d\tau} = \frac{d(\Theta_l - \Theta_{\xi_i})}{d\xi} \tag{4.5.14}$$

The initial and boundary conditions in non-dimensional form are:

$t = 0 \quad \xi_i = 1$

$t = 0 \quad \Theta_l = 1 \quad at \quad 0 \le \xi \le 1$

$t > 0 \qquad at \;\; \xi = 0 \qquad \frac{d\Theta_l}{d\xi} = 0 \quad or\ symmetry$

$t > 0 \qquad at \;\; \xi = \xi_i \qquad \Theta_l = \Theta_{r_i} = \Theta_s \quad or\ continuity$

$t > 0 \qquad at \;\; \xi = 1 \qquad \frac{d\Theta_s}{dt} = cst \quad or\ cst\ cooling\ rate$

6) Properties required for solving the model equations

Values of all the properties required are listed in Appendix A2 and these were obtained experimentally during the course of this research.

h_l: Convective heat transfer coefficient.

Nu : Nusselt number.

ρ_l c_{p_l} k_l: Properties of the liquid above and below WAT.

ρ_s c_{p_s} k_s: Properties of the solid wax.

$x_{w,l}$, $\lambda_{w,l}$: mass fraction of wax precipitated from the liquid below WAT and corresponding heat of precipitation.

$X_{w,l}$, $H_{w,l}$: mass fraction of wax precipitated from the liquid below WAT vs. dimensionless temperature and corresponding heat of precipitation.

$x_{w,s}$, $\lambda_{w,s}$: mass fraction of wax in the solid deposit and corresponding heat of precipitation.

$X_{w,s}$, $H_{w,s}$: mass fraction of wax in the solid deposit vs. dimensionless temperature and corresponding heat of precipitation.

$x_{w,i}$, $\lambda_{w,i}$: mass fraction of wax forming at the solid-liquid interface and corresponding heat of precipitation.

$X_{w,i}$, $H_{w,i}$: mass fraction of wax forming at the solid-liquid interface vs. dimensionless temperature and corresponding heat of precipitation.

Note: The mass fraction of wax precipitated and corresponding heat of precipitation represents a challenge which is overcome using DSC experimental data in the guise of:

$$\frac{dx_w}{dt} = \frac{dx_w}{dT}\frac{dT}{dt}$$

Thus all we need is to measure $\frac{dx_w}{dT}$ in the entire temperature range of liquid above and below WAT, interface and deposit ($x_{w,l}$, $x_{w,s}$, and $x_{w,i}$).

4.5.2 Measurement Calibration and Accuracy

To ensure that the inner wall temperatures are the same around the vessel, the heat transfer equilibrium takes place across all sides of the vessel centre and the thermocouples readings are accurate, additional thermocouples were placed in the opposite side of the main measuring thermocouples and distributed at the same diameters with the same distances and angles, and they were labelled as shown in Figure 4.5.1. LO crude oil was used for static cooling in the 120mm diameter vessel from 80 to 10^{o}C at cooling rate of 1^{o}C/min. The radial

temperatures for both sides of the vessel were recorded as shown in Figure 4.5.2. The same calibration procedure was used for 60mm diameter vessel and the error associated for both vessels with these calibration measurements for each twin thermocouples is neglected as around ± 0.1^{o}C.

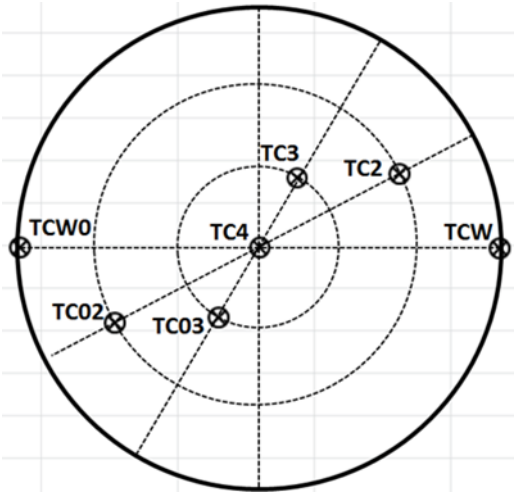

Figure 4.5.1: Radial distribution of thermocouples in the vessels for measurement calibration experiments.

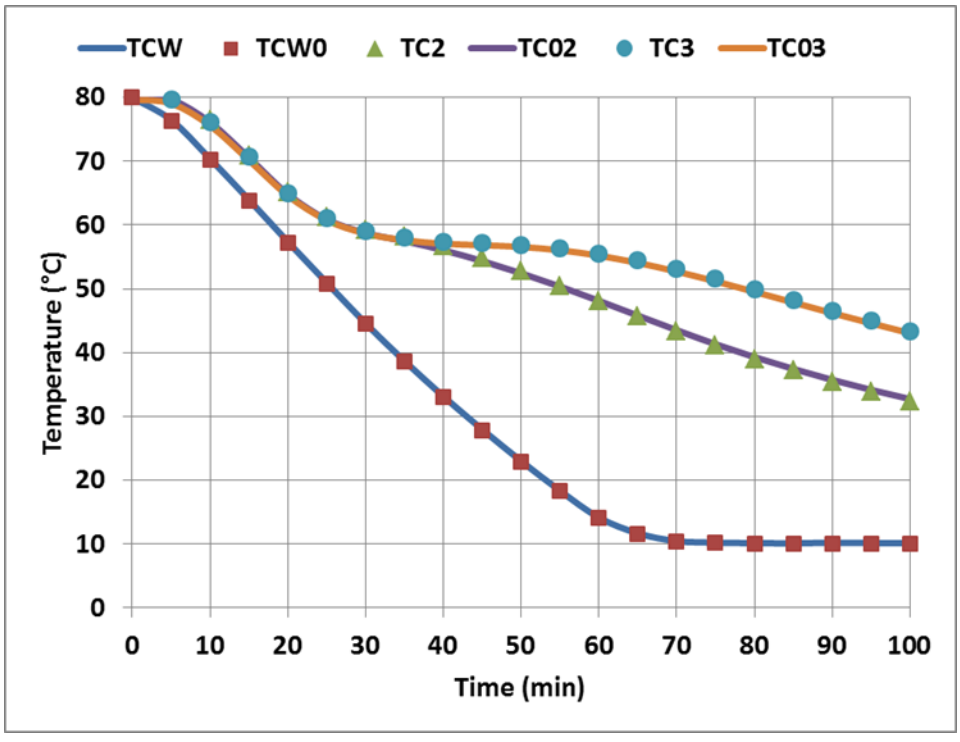

Figure 4.5.2: Static temperature experiment for measurement calibration using LO crude oil at cooling rate of 1.1^{o}C/min.

4.5.3 Radial Temperature Profiles during Static Cooling

Figures 4.5.3 and 4.5.4 give the pertinent data in the 120mm and 60 mm diameter cylinders or pipe sections for LO and BPO cooled from 80^{o}C down to 15^{o}C at a wall cooling rate (WCR) of 1.1^{o}C/min.

The first observation is that there is a period of time in which the temperature remains the same across the diameter of the pipe. For LO, this time period is 25 min in the 120mm cylinder. It is much longer, 55 min in the case of BPO. For the smaller cylinder, the time periods are 20 min and 40 min for LO and BPO respectively. These periods correspond to the situation when the temperature of the oil is above WAT as indicated in the figures. The fact that above WAT there is no radial variation in temperature is understandable as cooling here is by convection only, on account that the oil is in a liquid state with no wax having precipitated. Recall that at the low cooling rate of 1^{o}C/min, calorimetric measurements gave a WAT of 30.3^{o}C for BPO and 63.3^{o}C for LO. These values are consistent with the initial temperature profile measured here. We need however to verify this assertion that cooling here is by natural convection on account that above WAT, the oil is in liquid state with no precipitated wax particles. The results presented in Figure 4.5.5 obtained with pure non waxy lubricating oil cooled under the exact same conditions confirm the intuitive hypothesis that above WAT cooling is through convection. The second observation is that during this initial cooling period above WAT, apart from the beginning, the variation of temperature with time is linear with a gradient slightly more than that which the wall of the cylinder is being cooled.

On approaching WAT, a sudden change in the temperature profiles is observed signalling precipitation and a change in the heat transfer situation. Below WAT, the evolution in time of the temperatures diverges with the temperature nearest the wall dropping at a faster rate than those away from the wall. Clearly, below WAT, here the precipitation of the wax hampers convective cooling with conduction and heat of precipitation contributing to heat transfer. Note in these figures the steeper variation of TC1 (close to the cooling wall) backed by visual observation of the gel front near this location. It is clear that the sudden change in

the temperature profiles in Figures 4.5.3 and 4.5.4 corresponds to the gel front appearing as recorded by the various thermocouples TC1, TC2, TC3 and TC4 after a certain period of times as presented in Table 4.5.1. As noted the temperatures in Table 4.5.1 are very close to WAT but slightly decreasing as we move toward the centre of the vessel. This is due to the fact of the ongoing precipitation of the wax, depleting the bulk (centre) of wax hence leading to a lower gel front temperature at TC4. Clearly, the depletion will occur more quickly in smaller diameter pipes and this is reflected in the 60mm diameter cylinder data. The differences are minor.

When comparing LO with BPO, the data collected from the 120mm diameter cylinders in Figure 4.5.3 a-b show the BPO temperatures to drop faster in time than those of LO as presented comparatively in Figure 4.5.6a and shown more clearly in Figures 4.5.6b, c and d which gives comparison for the single positions TC2, TC3 and TC4. This can be attributed to the lower wax content of BPO compared to that of LO. Also when comparing the data collected from the 120mm and 60 mm diameter cylinders for BPO, it is evident that the temperature profiles in the 60mm cylinder will be steeper as presented comparatively in Figure 4.5.7a and shown more clearly in Figures 4.5.7b, c and d which gives comparison for the single positions TC2, TC3 and TC4.

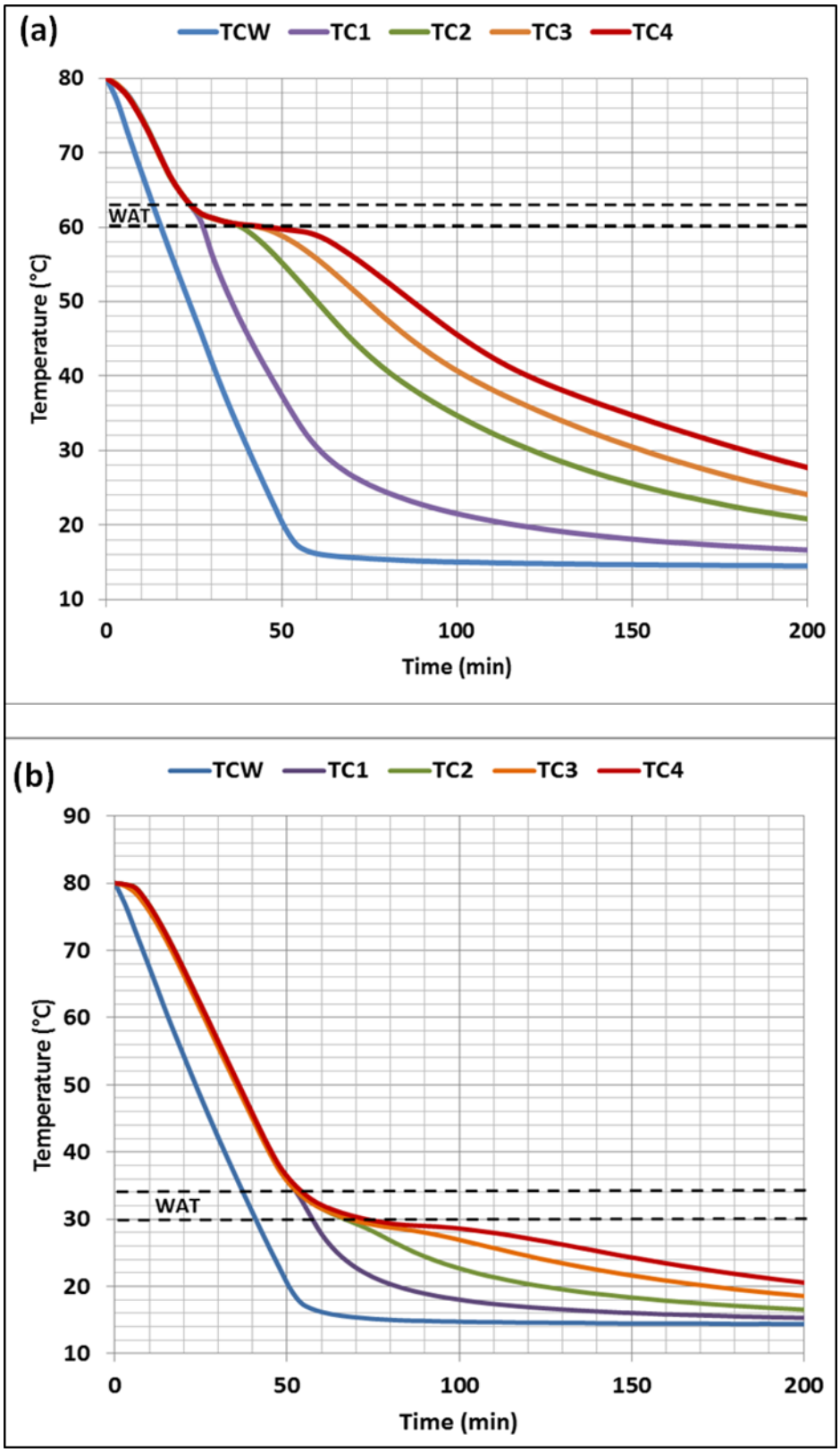

Figure 4.5.3: Radial temperature profile during static cooling in the 120 mm diameter vessel for **(a)** LO and **(b)** BPO with cooling rate at 1.1^{o}C/min.

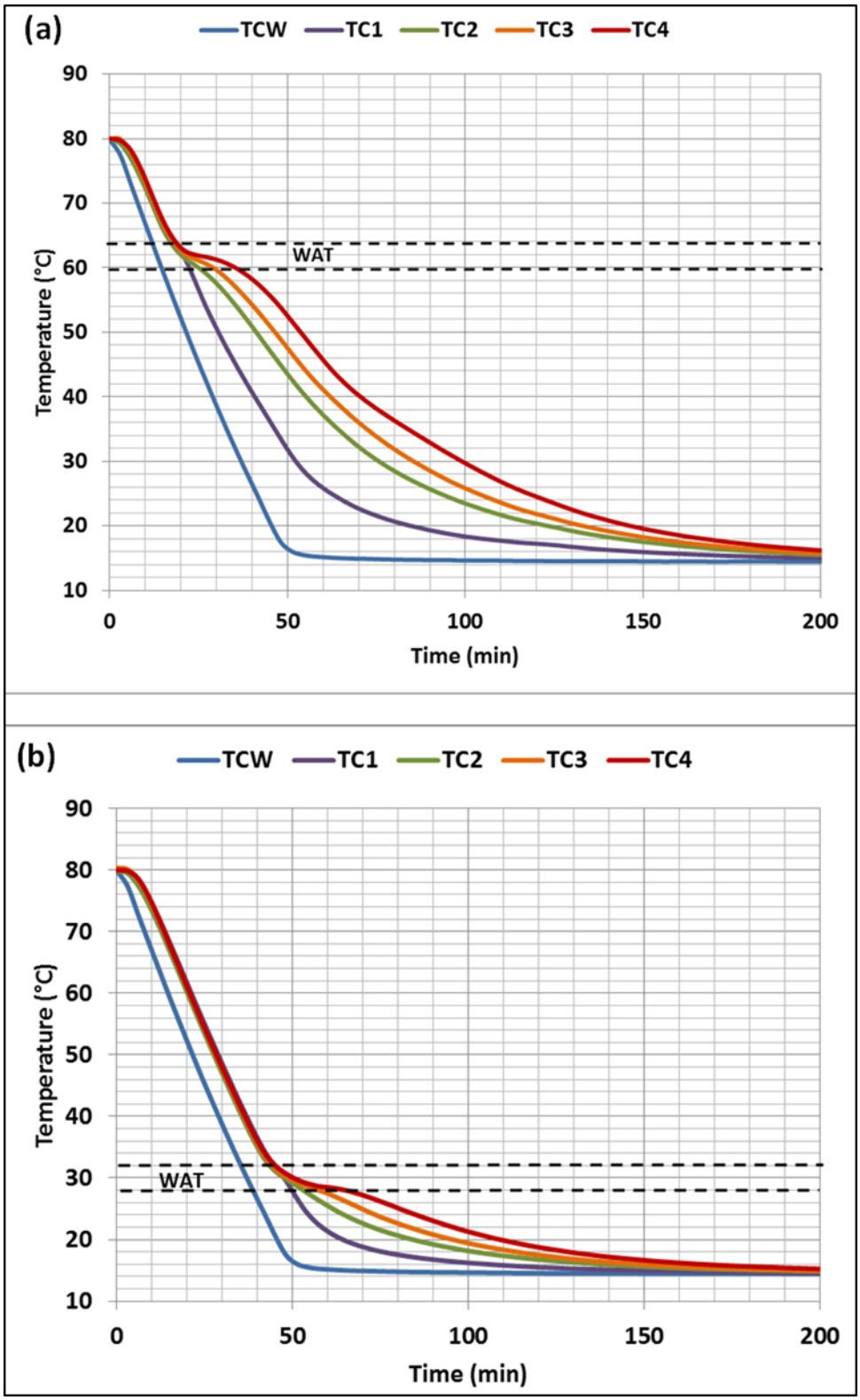

Figure 4.5.4: Radial temperature profile during static cooling in the 60 mm diameter vessel for **(a)** LO and **(b)** BPO with cooling rate at 1.1^{o}C/min.

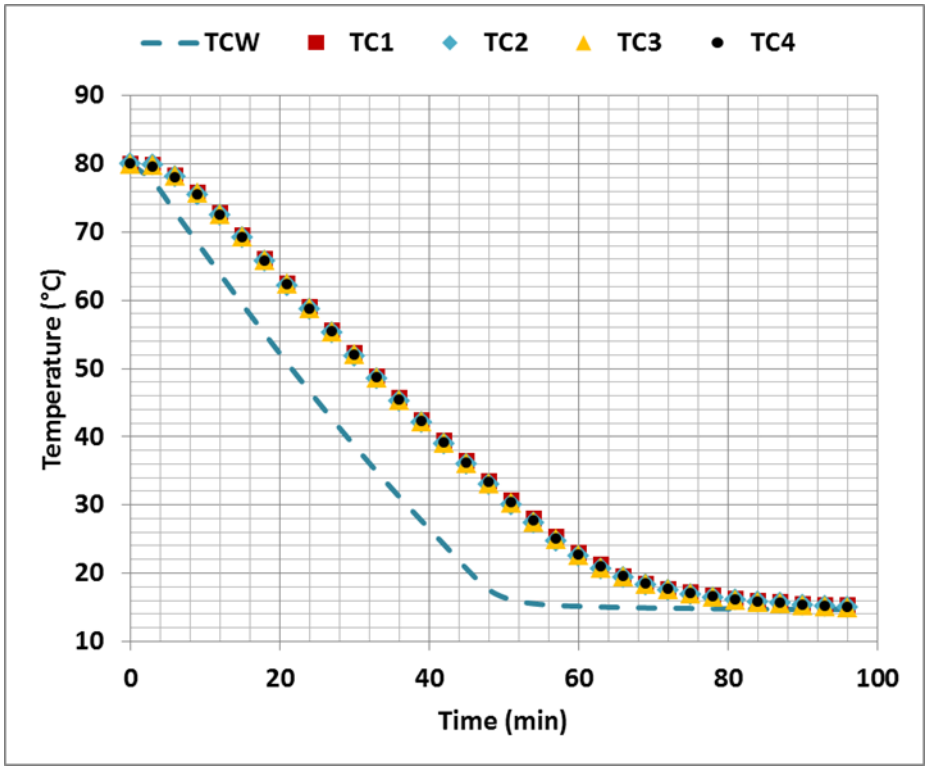

Figure 4.5.5: Radial temperature profile during static cooling for Millers oil (Millmax 68) in the 120 mm diameter vessel with cooling rate at 1.1°C/min.

Table 4.5.1: Gel front or liquid-deposit interface temperature results for the static cooling for BPO and LO crude oils from 80°C to 15°C at 1.1°C/min.

Crude oil	Wax content (%wt.)	Cylinder diameter size (mm)	TC1		TC2		TC3		TC4	
			T_d (°C)	Time (min)	T_d (°C)	Time (min)	T_d (°C)	Time (min)	T_d (°C)	Time (min)
LO	39.6	**120**	61.5	25	60.4	35	60.3	41	60.1	45
BPO	15.7	**120**	32.2	55	31.4	69	30.1	84	29.2	95
		60	31.3	46	30.2	48	29.1	54	28.7	60

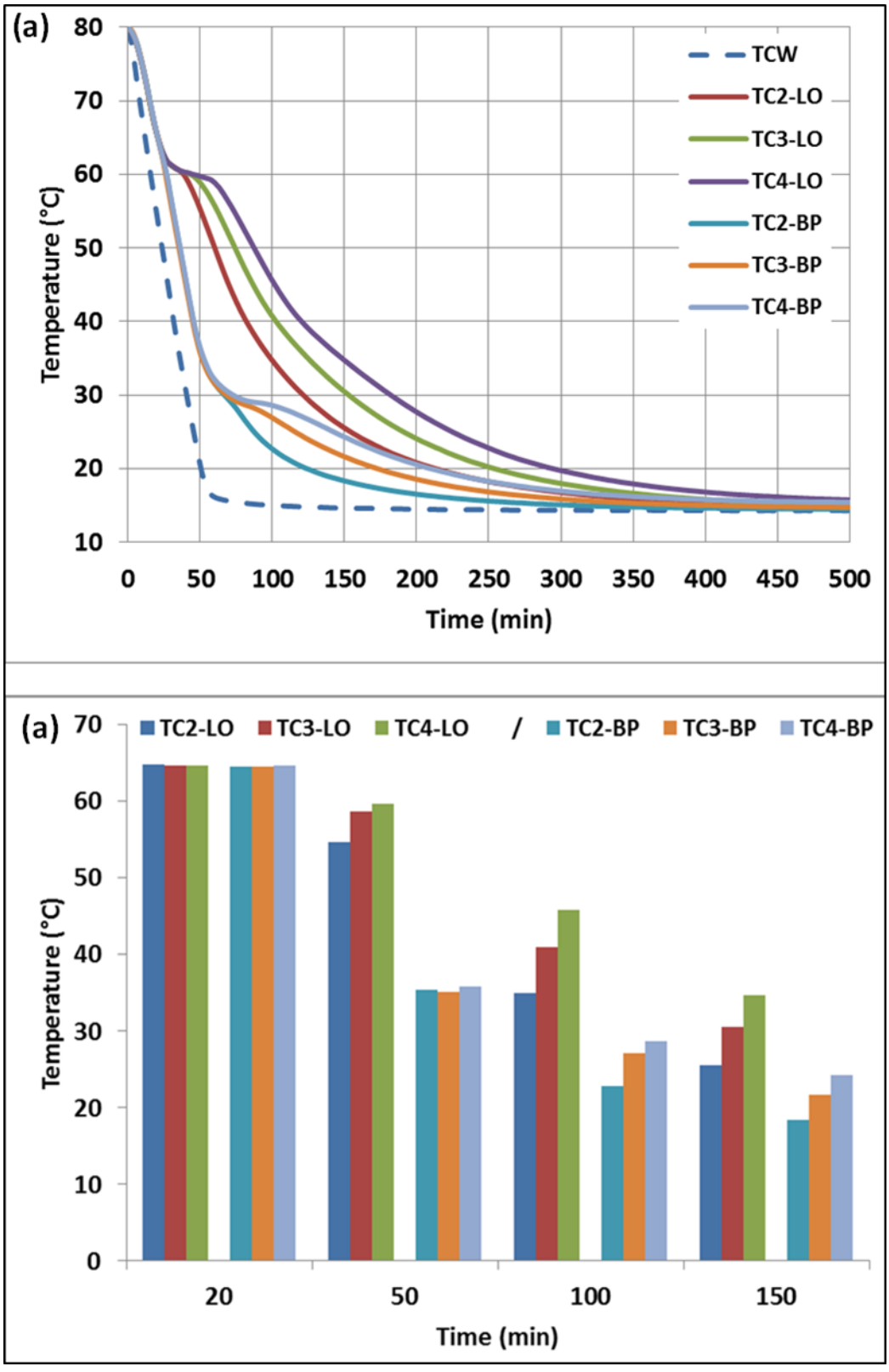

Figure 4.5.6a: Comparison of temperature profile with the three radial locations for LO and BP crude oils cooled statically in 120mm diameter vessel.

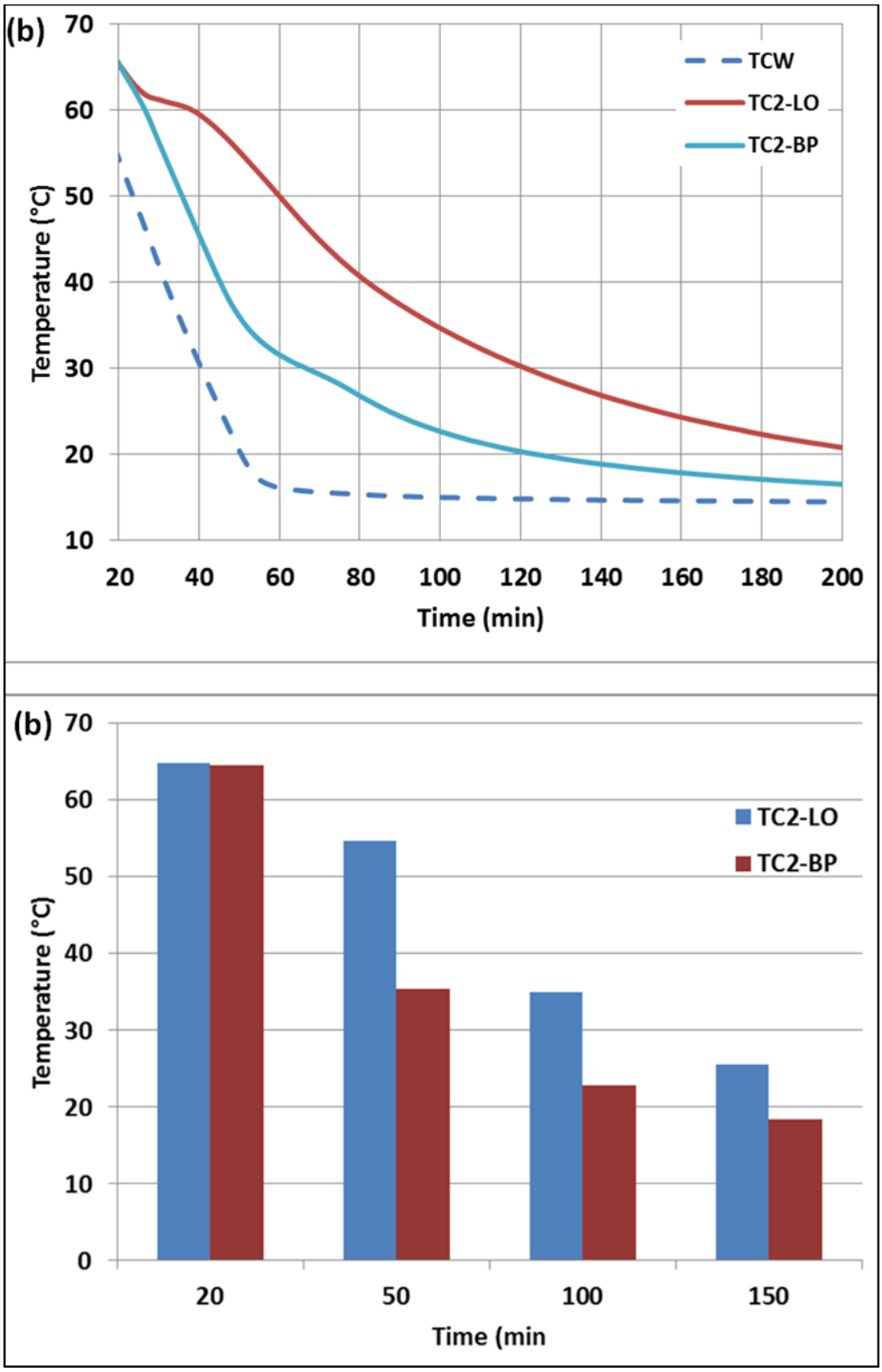

Figure 4.5.6b: Comparison of temperature profile of the TC2 for LO and BP crude oils cooled statically in 120mm diameter vessel.

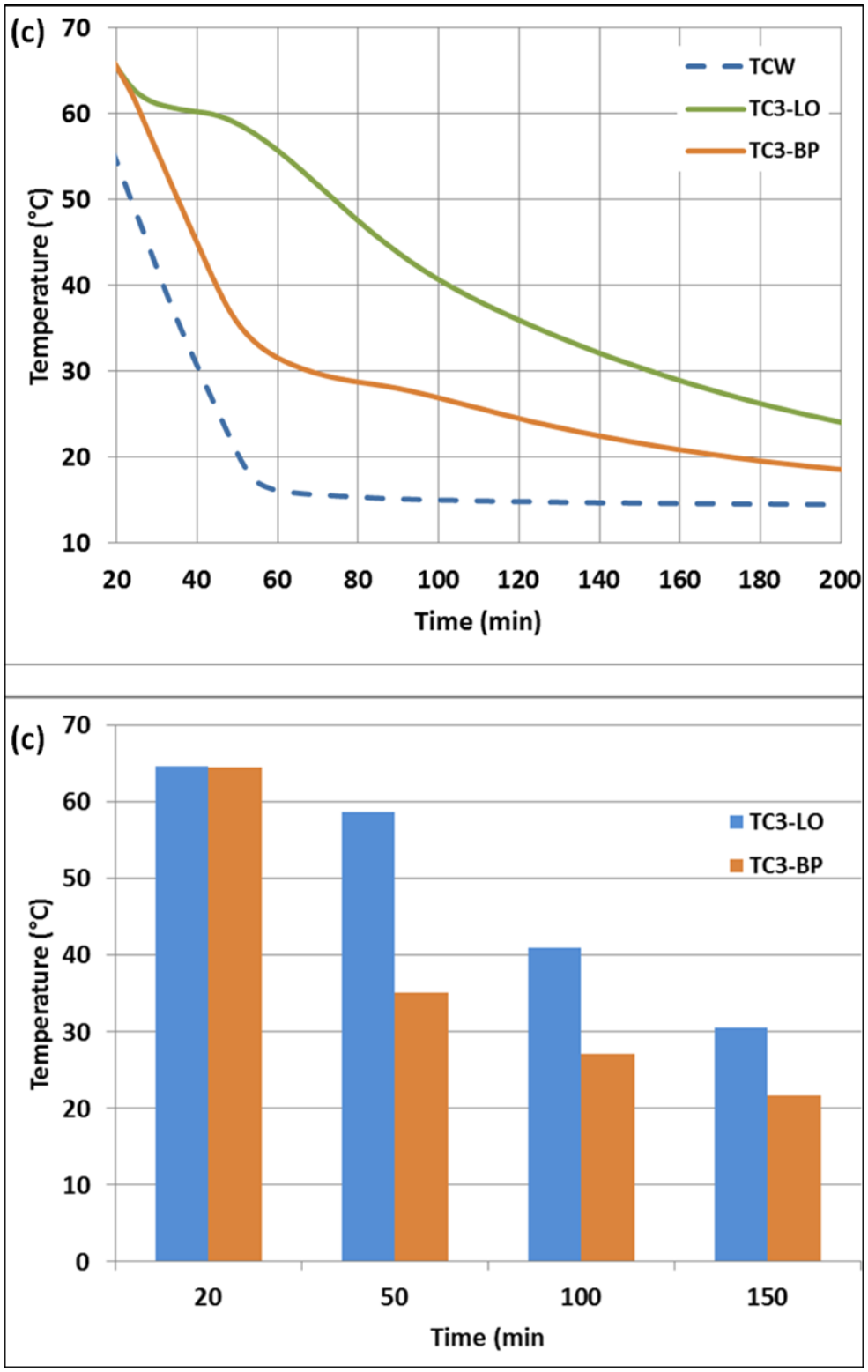

Figure 4.5.6c: Comparison of temperature profile of the TC3 for LO and BP crude oils cooled statically in 120mm diameter vessel.

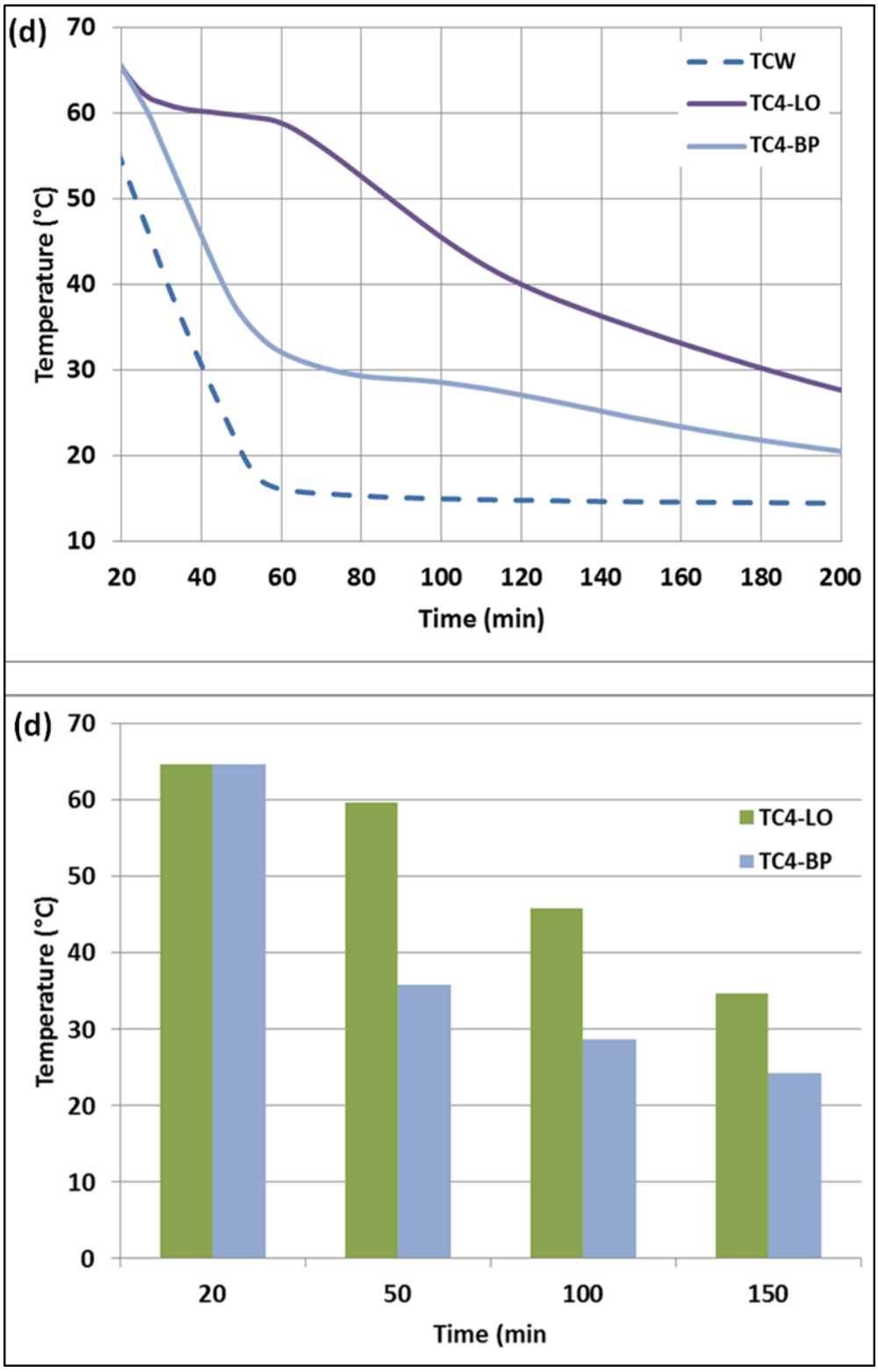

Figure 4.5.6d: Comparison of temperature profile of the TC4 for LO and BP crude oils cooled statically in 120mm diameter vessel.

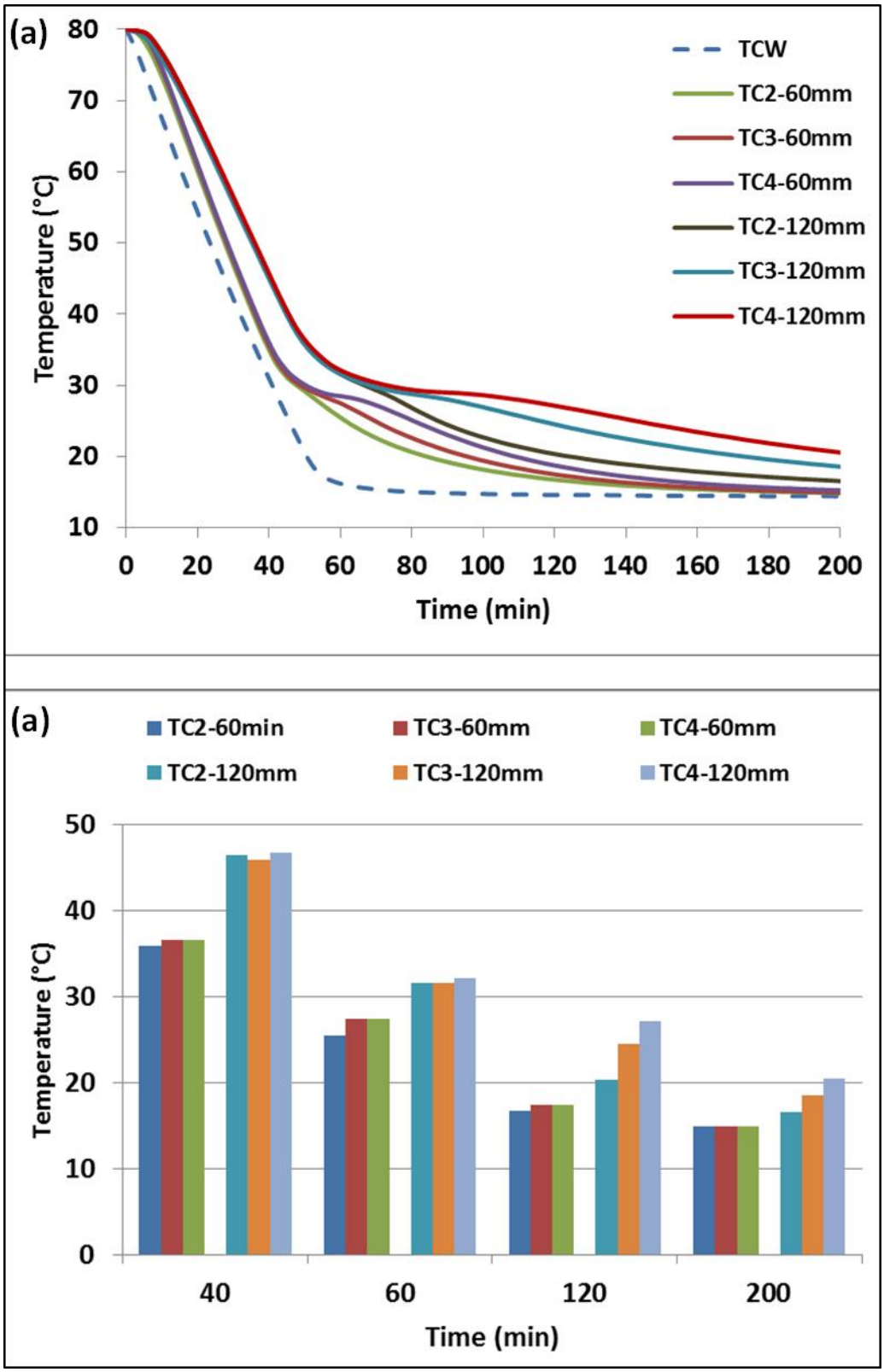

Figure 4.5.7a: Comparison of temperature profile of the three radial locations for BPO crude oil cooled statically in 60 and 120 mm vessels.

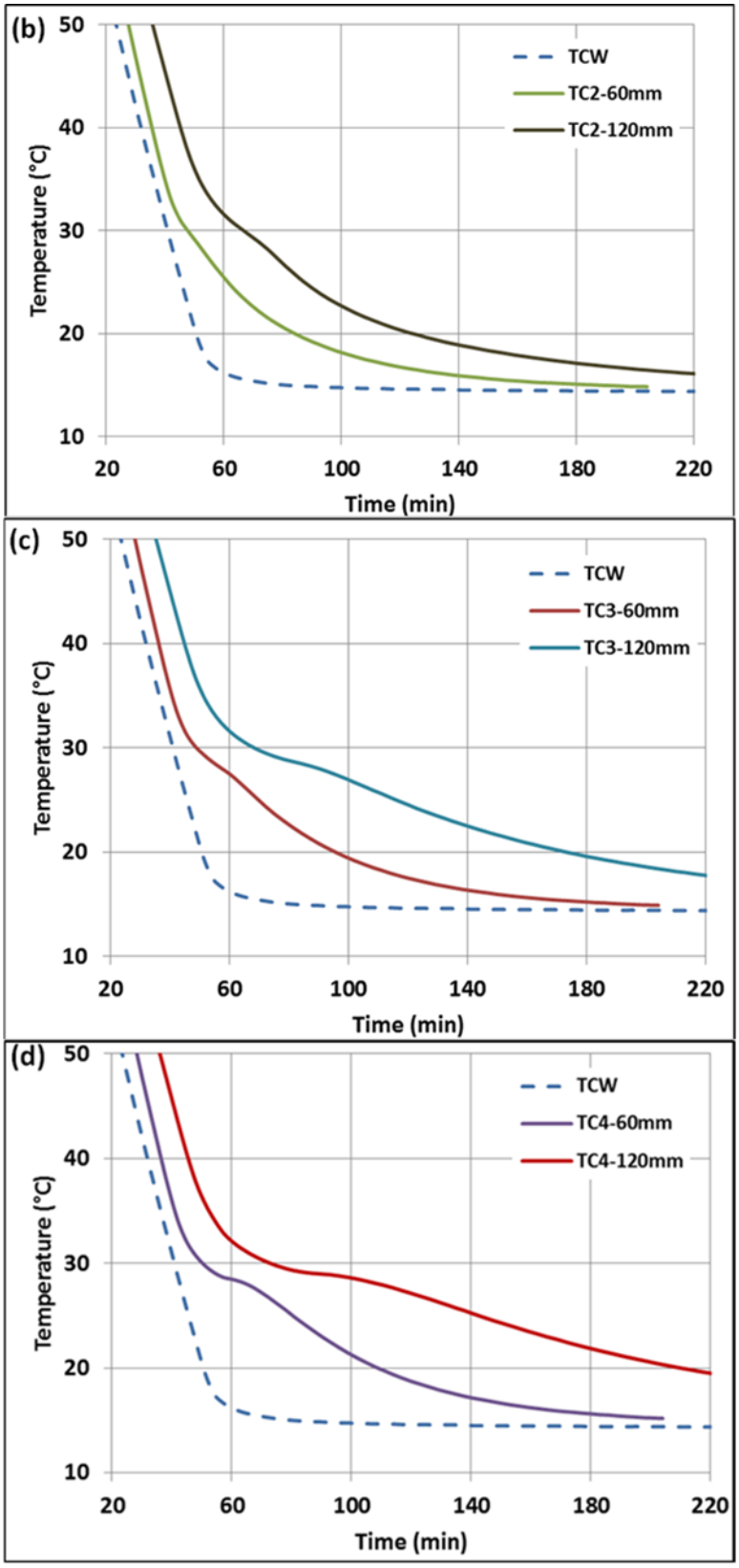

Figure 4.5.7b, c & d: Comparison of temperature profile of **(b)** TC2 **(c)** TC3 **(d)** TC4 for BPO crude oil cooled statically in 60 and 120 mm vessels.

4.5.4 Determination of the Gel front or Liquid-Deposit interface location

As explained above, the divergence in the temperature profiles is the indicator of the gel front. Thus, the time at which the rate of change of temperature at a particular thermocouple location started to deviate from those of other thermocouples was taken to indicate the interface position, at the surface of the thermocouple, at that radial location. Mathematically, this is expressed by plotting this change *dT/dt* against time at each thermocouple location. Figure 4.5.8a-b show the plots of the calculations of the data obtained from the 120mm diameter cylinder for LO and BPO, respectively, and Figure 4.5.8c shows the plot of calculations of the data obtained from the 60mm diameter for BPO. In all the plots of Figure 4.5.8, *dT/dt* is initially the same for all thermocouple locations and when the value of each thermocouple reaches a maximum and starts to deviate, indicative of the inflexion in the temperature profiles curves, the interface is reached to the location of the thermocouple, corresponding with the time taken for the thermocouple to be completely immersed in the deposit layer. Figure 4.5.8 presents such data, further expressed in Table 4.5.2 and Figure 4.5.9 to give the evolution of the deposit thickness in time. As Figure 4.5.9 shows, the gel front develops more quickly in LO than in BPO and in the 60 mm than the 120mm diameter cylinder, a complete gel in 120 mm diameter vessel occurring in 45 mins with LO and 95 mins with BPO, The difference is due mainly to LO having larger wax content than BPO. The deposit-layer thickness grew faster with cooling in 60 mm diameter vessel than 120mm diameter vessel, which is attributed to a higher depositing rate due to the higher radial cooling rates as the radial locations of TC1, TC2, TC3 and TC4 in 60mm diameter vessel are closer to each other than those radial locations in 120mm diameter vessel as they were placed proportionally to their diameter size (δ/R) in both cases. These indirect (via temperature) measurements conform to visual observations of the gel formation in the cylinders.

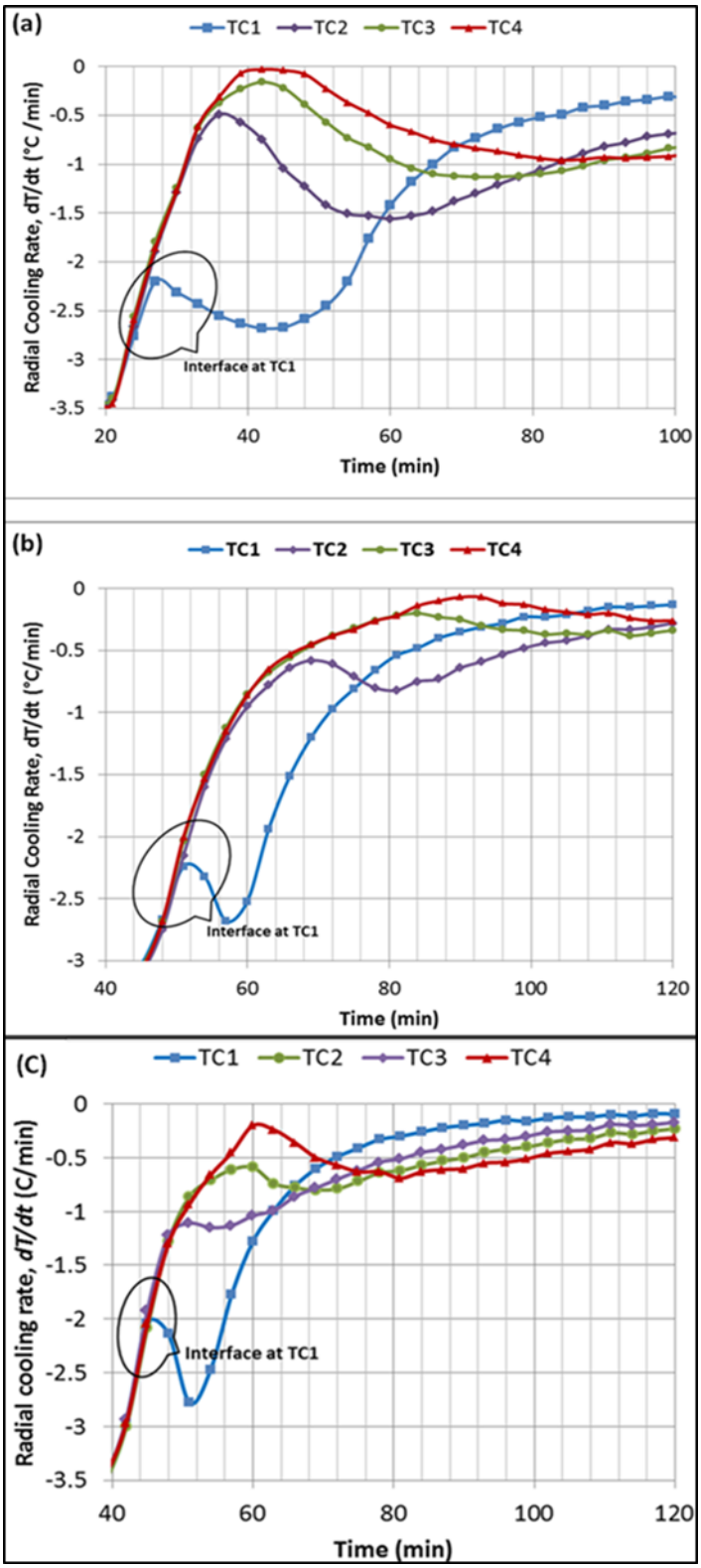

Figure 4.5.8: Determining the interface location from rate of change of the temperature profile for **(a)** LO in the 120mm cylinder and **(b)** BPO in the 120mm cylinder **(c)** BPO in the 60mm cylinder. All the experiments cooled statically at cooling rate of 1.1^{o}C/min.

Table 4.5.2: Deposit thickness with time for static cooling experiments for LO and BPO crude oils in the 60mm and 120mm diameter vessels.

TC no.	Deposit thickness (δ/R)	Time (min)		
		LO	BPO	
		120mm	120mm	60mm
TC1	0.17	25	55	46
TC2	0.33	35	69	48
TC3	0.67	41	84	54
TC4	1	45	95	60

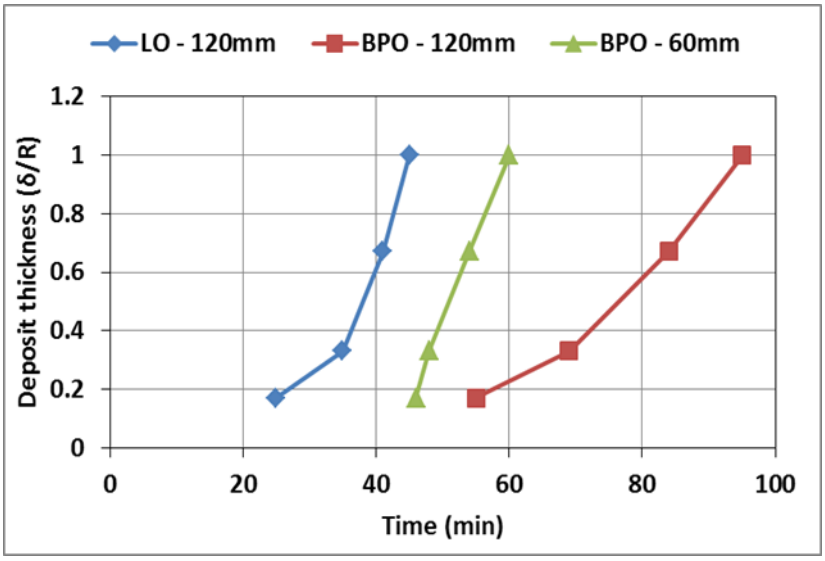

Figure 4.5.9: Effect of wax content and diameter size on the rate of deposit growth for LO and BPO crude oils in the 60mm and 120mm diameter vessels.

4.5.5 Effect of cooling rate on radial cooling process

4.5.5.1 Variation of temperature profiles

Figures 4.5.10 present data to assess the important effect of cooling rates decreased here from 1.1^{o}C/min and 0.05^{o}C/min. Data are given for BPO cooled in the 120 mm diameter vessel from 80^{o}C to 15^{o}C. The difference, as expected, shows a more pronounced drop in temperature with time in the larger cooling rate. As shown earlier, above WAT, the temperature profiles coincide and below WAT, they diverge.

As to actual values, the expanded Figures 4.5.11 show a maximum difference in the radial temperatures measured at TC2, TC3 and TC4 in the WAT region of only 0.5^{o}C with cooling rate of 0.05^{o}C/min compared with 6.5^{o}C for a cooling rate of 1.1^{o}C/min, the maximum variation being between TC2 and TC3 at the cooling temperature of 15^{o}C (see tabulated temperatures in Figure 4.5.11).

It is also to be noted from Figure 4.5.11, the temperature differences between the wall, TCW, and the other radial locations. It is much larger at the high cooling rate, on average about 16.5^{o}C compared to 3^{o}C at the low cooling rate. Table 4.5.5 summarises the temperatures of the radial locations, TC1 – TC4, obtained from similar static cooling experiments for BPO cooled in the 120 mm diameter vessel from 60^{o}C to 10^{o}C at 0.05 and 1^{o}C/min. Four specified wall temperatures (TCW) in range between the WAT and the final cooling temperature were studied as presented in the Table. Figure 4.5.16 shows the difference in the cooling temperature between the wall and the centre of the vessel (TCW and TC4) for both cooling rate experiments. As it can be seen, the higher the cooling rate, the wider deviation for the centre temperature trend line from the wall temperature trend line. From the linear trend lines of the temperature profiles and their displayed equations, the average difference value in temperature between the wall and the centre for the cooling experiment with cooling rate at 0.05^{o}C/min is 5.3^{o}C, while it is 23.9^{o}C for the cooling experiment with cooling rate at 1^{o}C/min.

4.5.5.2 Variation of gel front

Following from the above observations in Figures 4.5.10-11, the variation of the gel front or interface location can be obtained as done earlier by plotting the change *dT/dt* against time at each thermocouple location and find when it reaches a maximum and starts to deviate. Figure 4.5.12 gives such data with Table 4.5.3 giving the corresponding deposit thickness and Figure 4.5.13 showing the evolution of the gel front with time. Comparing the data at the different cooling rates, it is seen that at cooling rate of 1.1^{o}C/min, 95min only are required for complete gelling whereas at 0.05^{o}C/min 1130min or nearly 19 hours are required.

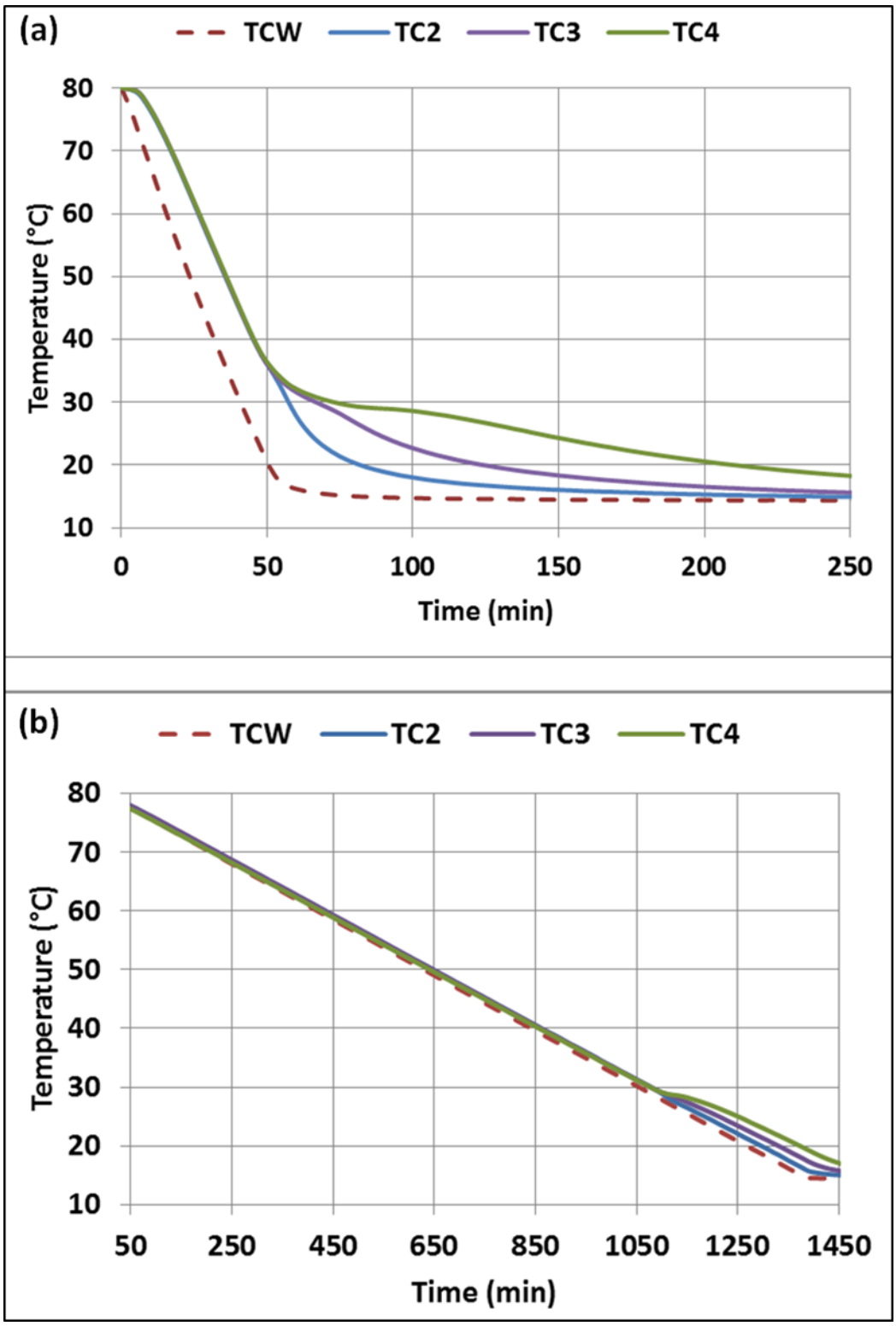

Figure 4.5.10: Comparison of temperature profiles for BPO crude oil cooled statically in the 120 mm vessel from 80 to 15^{o}C at **(a)** 1.1^{o}C/min **(b)** 0.05^{o}C/min.

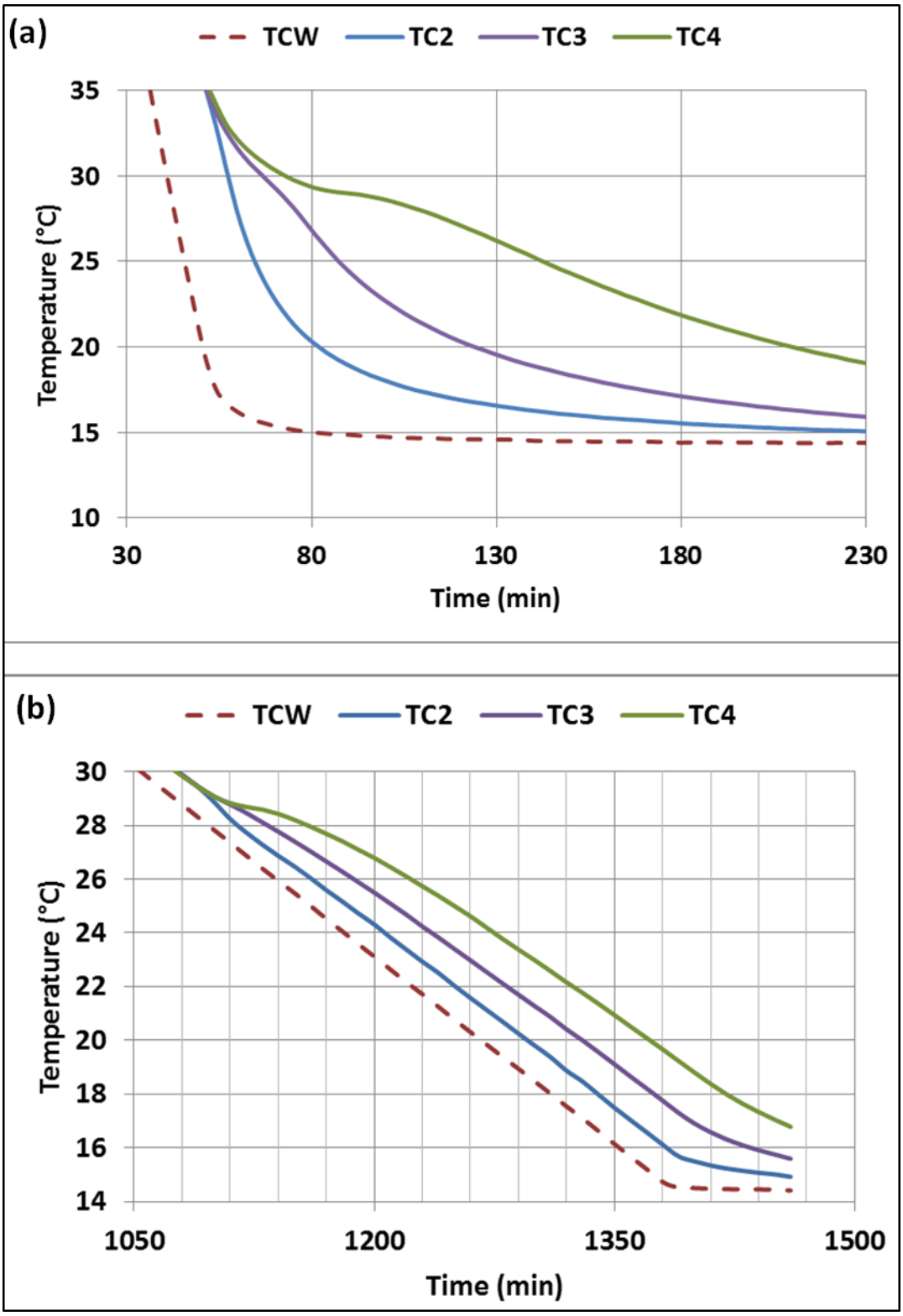

Figure 4.5.11 (a & b): Comparison of temperature profiles near to WAT region for BPO crude oil cooled statically in the 120 mm vessel from 80 to 15^{o}C at **(a)** 1.1^{o}C/min **(b)** 0.05^{o}C/min.

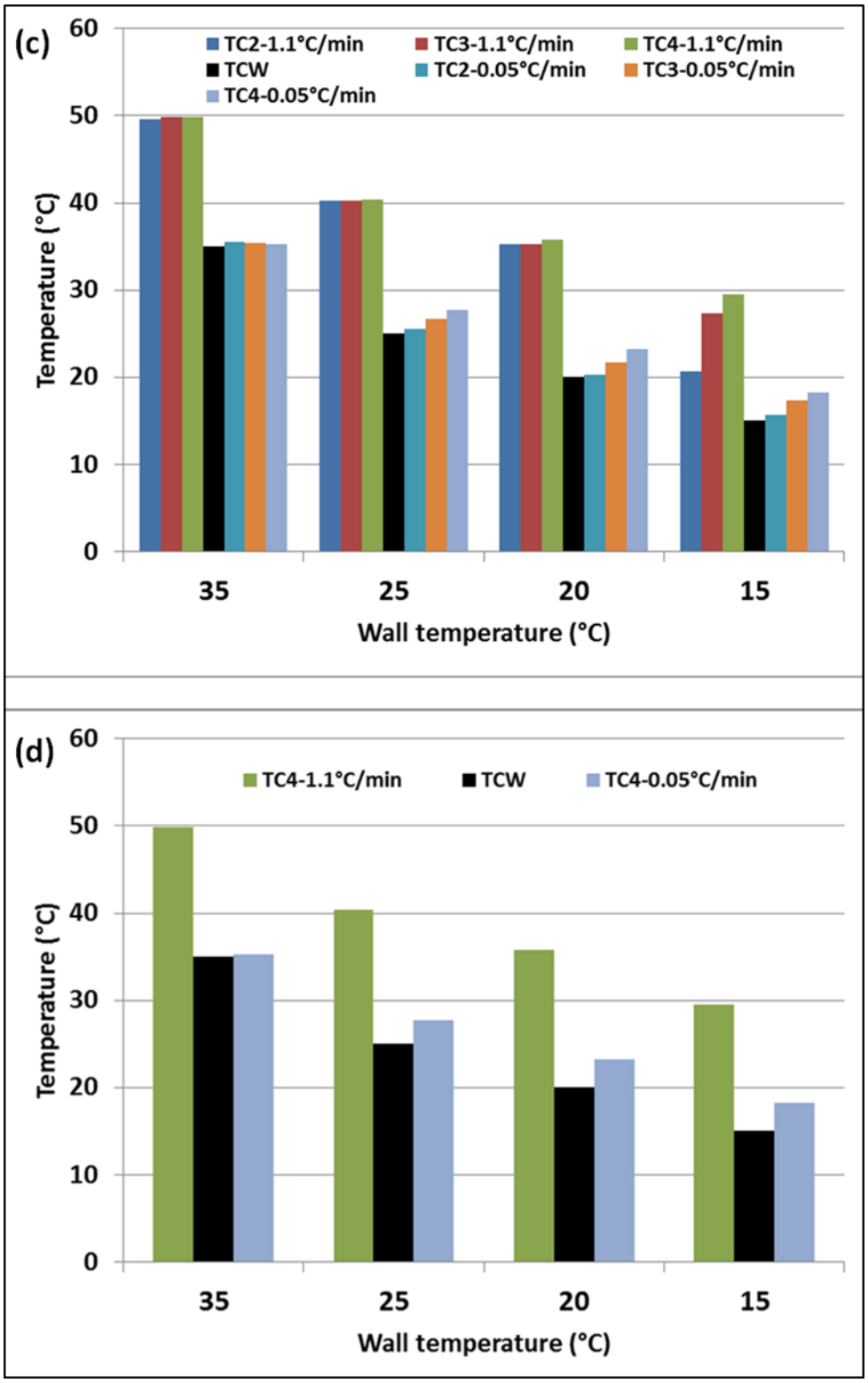

Figure 4.5.11 (c & d): Comparison the variation of the radial temperature around WAT region for BPO crude oil cooled statically in the 120 mm vessel from 80 to 15^{o}C at 1.1 and 0.05^{o}C/min **(c)** the radial temperatures with wall temperature **(d)** the centre temperature with the wall temperature.

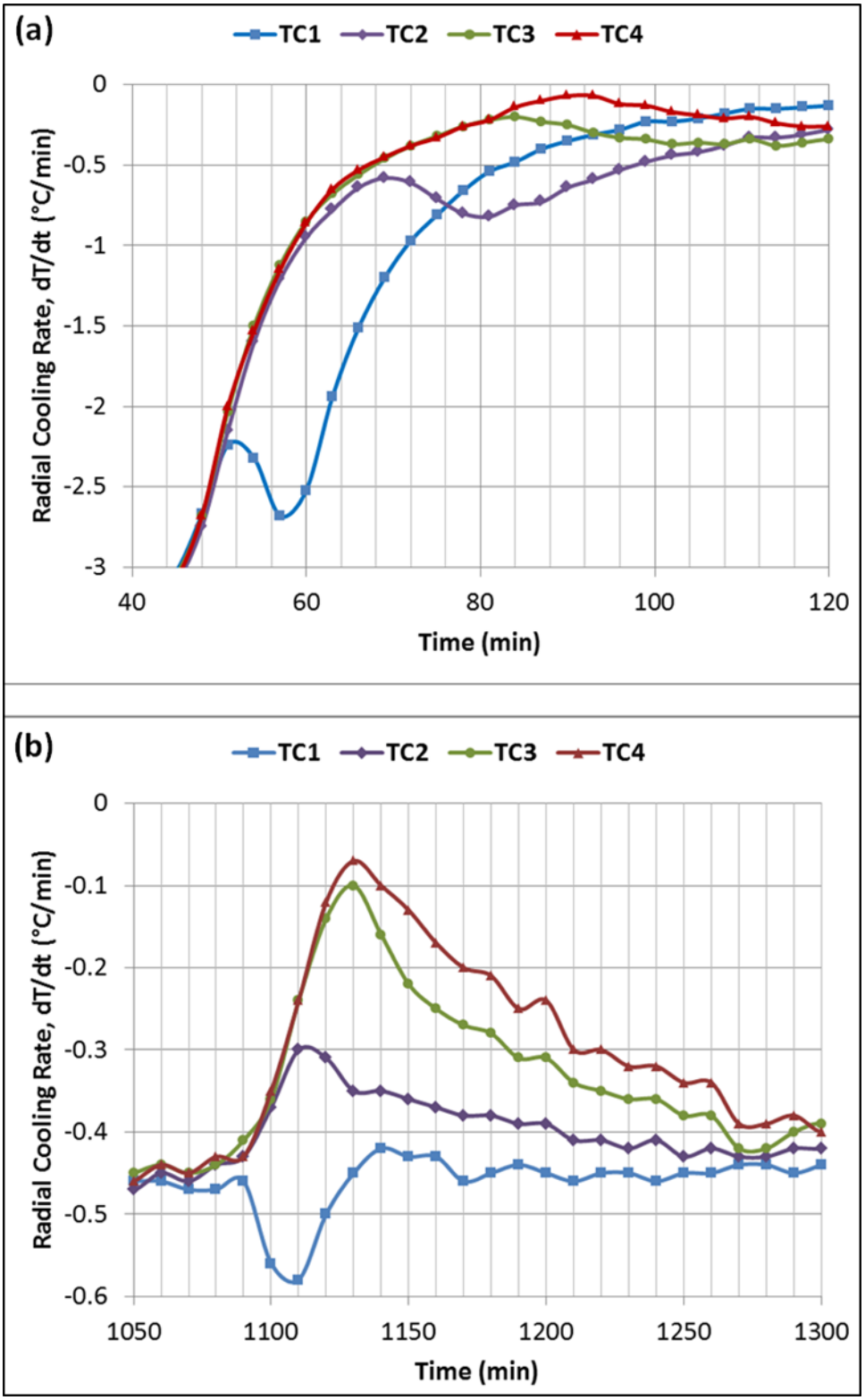

Figure 4.5.12: Determining the interface location from rate of change of the temperature profile for BPO crude oil cooled from 80 to 15^{o}C/min with cooling rate at **(a)** 1.1^{o}C/min **(b)** 0.05^{o}C/min.

Table 4.5.3: Deposit thickness with time for static cooling experiment for BPO crude oil cooled from 80 to 15°C at various cooling rates in the 120mm diameter vessel.

TC no.	Deposit thickness (δ/R)	Time (min)		
		0.05°C/min	0.11°C/min	1.1°C/min
TC1	0.17	1090	400	55
TC2	0.33	1110	420	69
TC3	0.67	1120	430	84
TC4	1	1130	440	95

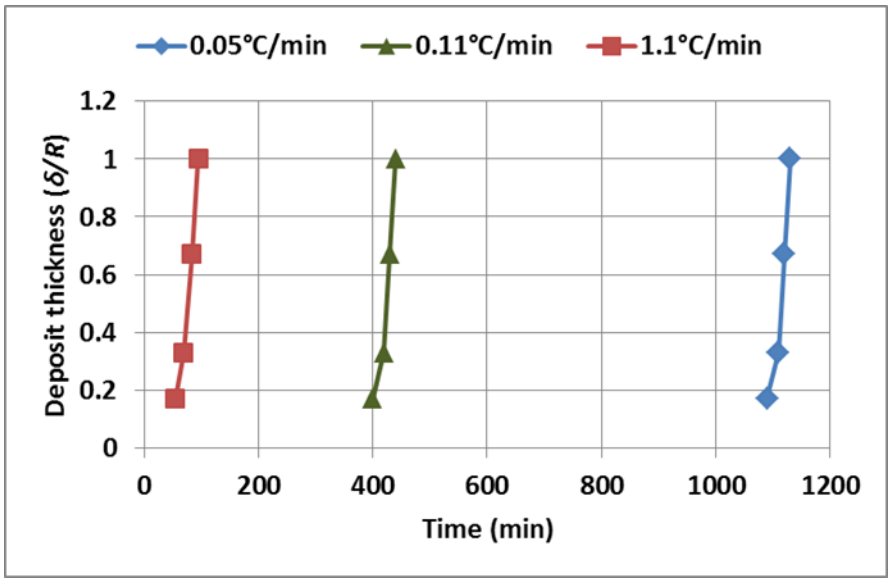

Figure 4.5.13: Effect of cooling rate on the rate of deposit growth for BPO crude oil cooled from 80 to 15°C at various cooling rates in the 120mm diameter vessel.

4.5.5.3 Variation of liquid-deposit interface temperature, T_d

Following the procedure described in Figure 4.5.12, the time taken for the interface to reach each of TC1–TC4 locations was determined. The corresponding average temperature at that radial location was taken to be the interface temperature, T_d. These calculations and estimations were performed for both crude oils experiments with cooling from 80^{o}C to 15^{o}C at 1.1^{o}C/min, 0.11^{o}C/min, and 0.05^{o}C/min in 120mm diameter size vessel, and all the results are summarized in Table 4.5.4. Figures 4.5.14a and b show the changes in T_d with respect to time and Figure 4.5.15a and b also show the changes in T_d but with respect to the thickness of the deposit layer (δ/R, which also represents the radial location of the interface) for the static cooling measurements for BP and LO crude oils, respectively. The region labelled as WAT in the figures indicates the upper and lower values of the WAT.

As mentioned previously, when the liquid temperature reached the WAT, the liquid became a two-phase mixture, with solid crystals suspended in the liquid phase. Due to the formation of waxy solid particles, the wax concentration in the associated liquid phase would be less than the original concentration. The precipitation of a fraction of wax from the waxy crude oils would cause a lowering of the WAT of the liquid phase. In other words, the gel front (interface) temperatures slightly decrease as we move toward the centre of the vessel. This is due to the fact of the ongoing precipitation of the wax, depleting the bulk (centre) of wax hence leading to a lower gel front temperature around the centre line. This hypothesis is demonstrated in Figures 4.5.14-15. Also, it is interesting to note that, the higher the cooling rete, the faster the movement of the interface (or growth of the deposit layer). For the results in both plots of Figure 4.5.14, the interface temperatures are close together because of a gradually decreasing of interface area due to the inward deposit growth and more closer in the case of LO crude oil than those in the case of BP crude oil, this can be attributed to the difference in wax concentration between the crude oils which influence the interface movement.

Table 4.5.4: Liquid-Deposit interface temperature results of the static cooling for BPO and LO crude oils from 80^{o}C to 15^{o}C with various cooling rates.

Crude oil	Cooling rate ^{o}C/min	TC1		TC2		TC3		TC4	
		T_d (^{o}C)	Time (min)	T_d (^{o}C)	Time (min)	T_d (^{o}C)	Time (min)	T_d (^{o}C)	Time (min)
LO	1.1	61.5	25	60.6	35	60.3	41	60.1	45
	0.11	60.7	150	60	165	59.7	170	59.6	180
	0.05	60	410	59.7	425	59.6	435	59.5	440
BPO	1.1	31.3	55	30.8	69	29.9	84	29.2	95
	0.11	30.7	400	29.4	420	29.2	430	29.1	440
	0.05	30.1	1090	29.2	1110	29	1120	28.9	1130

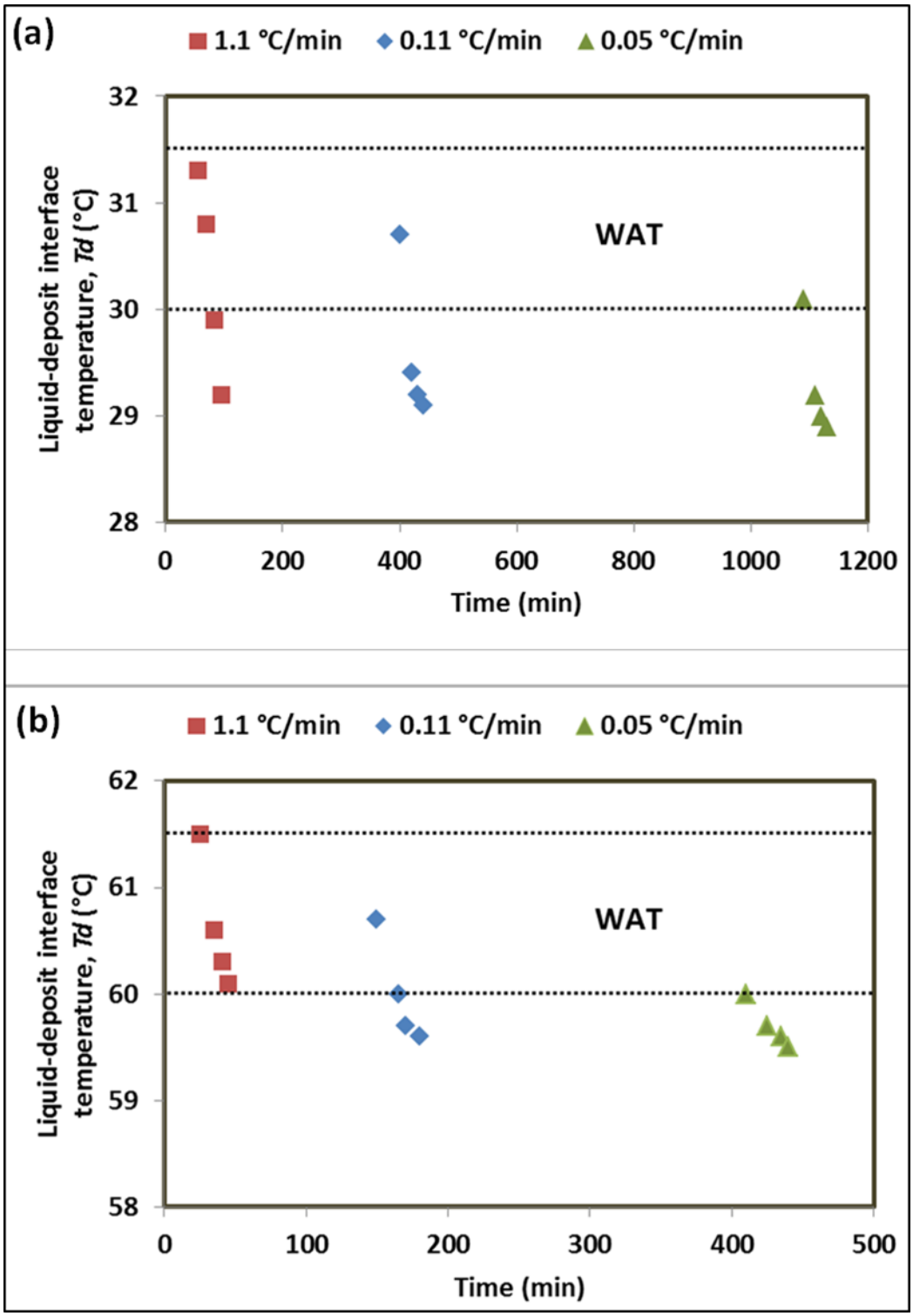

Figure 4.5.14: Variation in Interface temperature, T_d, with respect to time for Static Cooling from 80°C to 15°C at various cooling rates for **(a)** BP crude oil **(b)** LO crude oil.

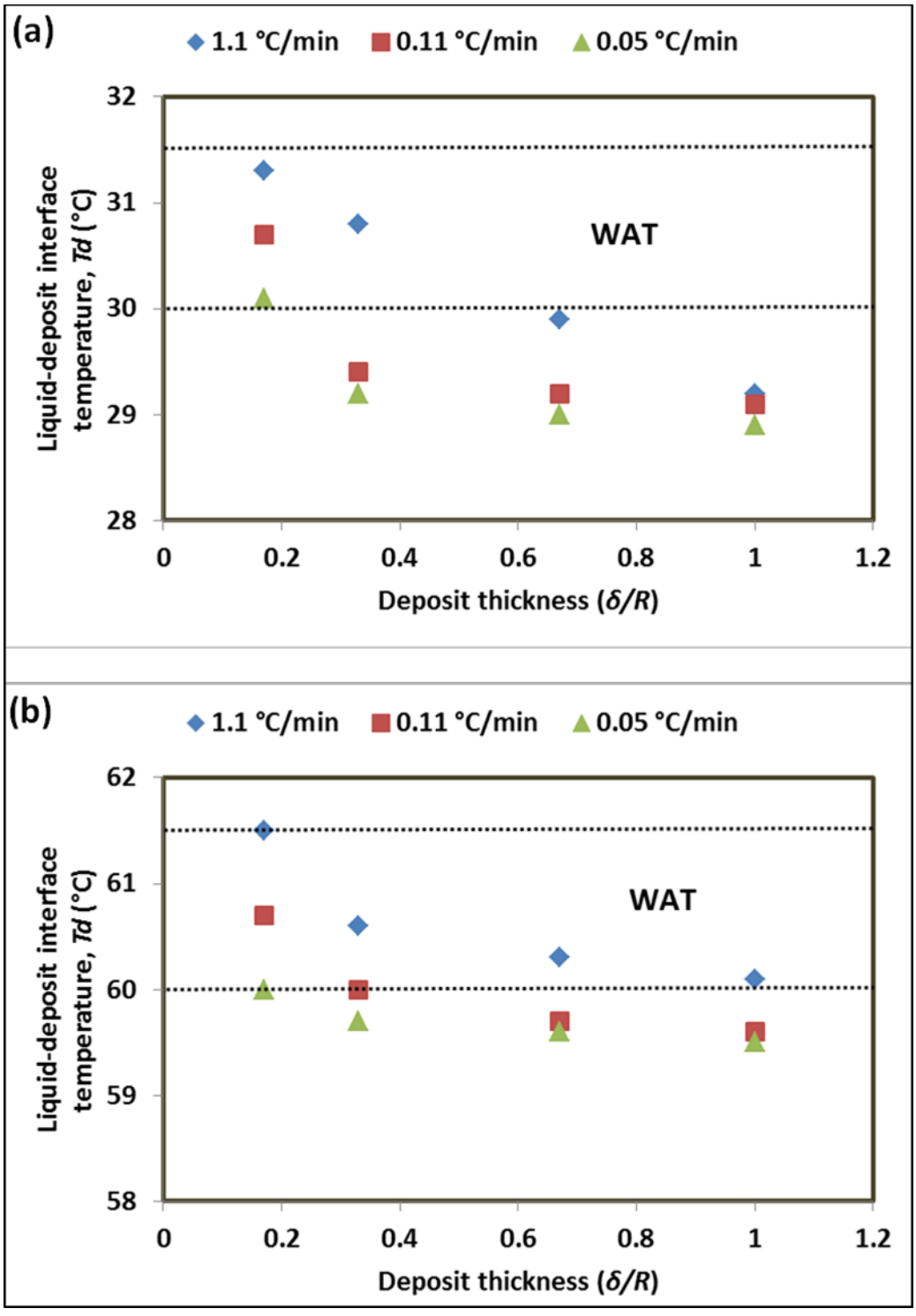

Figure 4.5.15: Change in interface temperature, T_d, with respect to radial location for static cooling from 80°C to 15°C at various cooling rates for **(a)** BP crude oil **(b)** LO crude oil.

Table 4.5.5: Results of the radial temperature with wall temperature around WAT region for BPO crude oil cooled statically from 60 to 10°C at 1 and 0.05°C/min.

TCW (°C)	Cooling rate (°C/min)	TC1 (°C)	TC2 (°C)	TC3 (°C)	TC4 (°C)
35	1	49.6	49.8	49.8	49.9
	0.05	35.5	35.4	35.3	35.5
25	1	40.2	40.2	40	40.4
	0.05	25.6	26.7	27.7	28.1
20	1	38.3	38.3	38.1	38.8
	0.05	20.3	21.7	23.3	23.8
10	1	24.4	28.7	32.8	34.7
	0.05	11.9	13.1	13.7	14.7

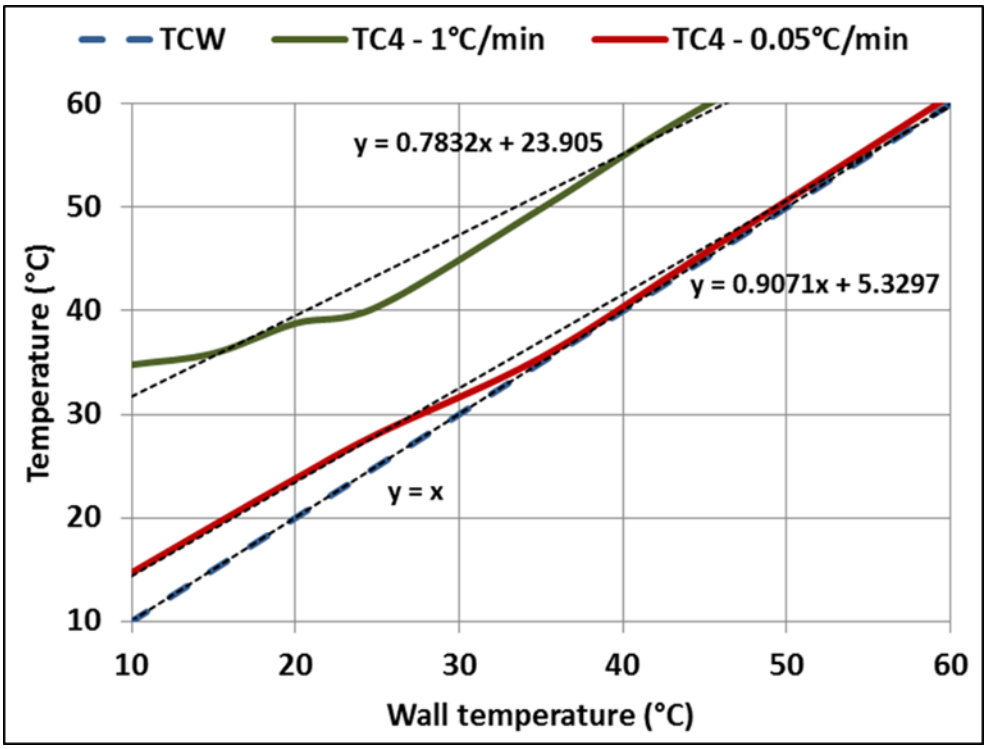

Figure 4.5.16: Effect of cooling rate on the thermal equilibrium between the wall and centre of the vessel under static cooling process for BPO crude oil cooled statically from 60 to 10°C at 1 and 0.05°C/min.

4.5.6 Summary

An experimental evaluation of the heat transfer that occurs in a hot pipeline carrying waxy crude oil suddenly shut and allowed to cool statically has been presented. The prime parameter as expected is the cooling rate which controls the evolution of the gel front in the pipeline. Initially, as the oil is above WAT, the cooling is found to be uniform throughout the pipe that is no radial variation is measured. This was explained as being due to the fact that natural convection only controls cooling above WAT. At the point of wax precipitation that is at WAT a sudden change in the temperature profile was observed indicative of a different heat transfer mechanism at play. Heat of wax precipitation and conduction is now playing a part as well as convection. This change in the temperature profile is the condition that enables the location of the gel front to be measured and its evolution in time to be obtained as illustrated in Figures 4.5.17 and 4.5.18 below. These figures show measured temperatures across a 120 mm diameter pipeline containing LO and being cooled from 85 to 20^0C at cooling rate of 1^0C/min. In the first 29 min no variation in temperature across the pipe is measured. At minute 30, the temperature profiles diverge, indicating that the wax at position TC1 near the wall has precipitated. At minute 40, the wax has precipitated at position TC2. At minute 60, the temperatures TC1, TC2, TC3 and TC4 are all equal or below WAT (taken here to be 60^0C) indicating that oil across the entire pipeline has gelled and cooled further thereafter. As expected, the cooling rate will affect this situation, accelerating it when it is faster. Equally the diameter of the pipeline has the effect of delaying the penetration of the gel front towards the centre.

Although intuitive, these observations provide the foundations to help develop mathematical models to determine temperature profiles in these situations. To be successful, the model must capture this phase change due to the precipitation of the wax and the ensuing different heat transfer mechanism from that (natural convection) prevailing at the beginning of cooling. As the data show the change to be *sudden* and *confined* near WAT, accurate properties (wax concentration, heat of precipitation of wax, kinetics of wax precipitation, thermal

conductivity of wax) are required if there is any hope of making accurate predictions.

Once the gel front location and its temperature have been obtained, a corresponding yield stress (static) as determined earlier (see Section 4.3) can be found and the start-up pressure calculated by a simple force balance on the non-gelled plug (see Figure 4.5.18). In the situation where the pipe is completely gelled, re-start- scenarios can be proposed as illustrated in Figure 4.5.17.

This takes us conveniently to the next section which deals with the data obtained from re-start pressure measurements.

It should be noted that the testing temperature used to measure the yield stress for a waxy crude oil by rheometer is corresponding to the final cooling temperature at a pipeline wall under static cooling to a certain temperature. From Table 4.5.5, the final cooling temperature (10^{o}C) at the vessel wall (TCW), is obtained at 60 min as shown in Figure 4.5.10a, while, the temperatures at the other radial locations throughout the vessel were still around 28^{o}C and at the centre line was still 35^{o}C. However, thermal equilibrium throughout the cross-section of the vessel can be obtained at around 500min at which the temperatures from the wall to the centre of the vessel become uniform. Hence, for a large size diameter as in the actual field pipeline, this gap of temperature between the pipeline wall and the centre would be bigger and this causes larger errors in prediction of the required restart pressure for the pipeline after a certain period of shutdown. It would take much longer time after shutdown before a thermal equilibrium throughout the pipeline can be obtained for larger diameter pipes.

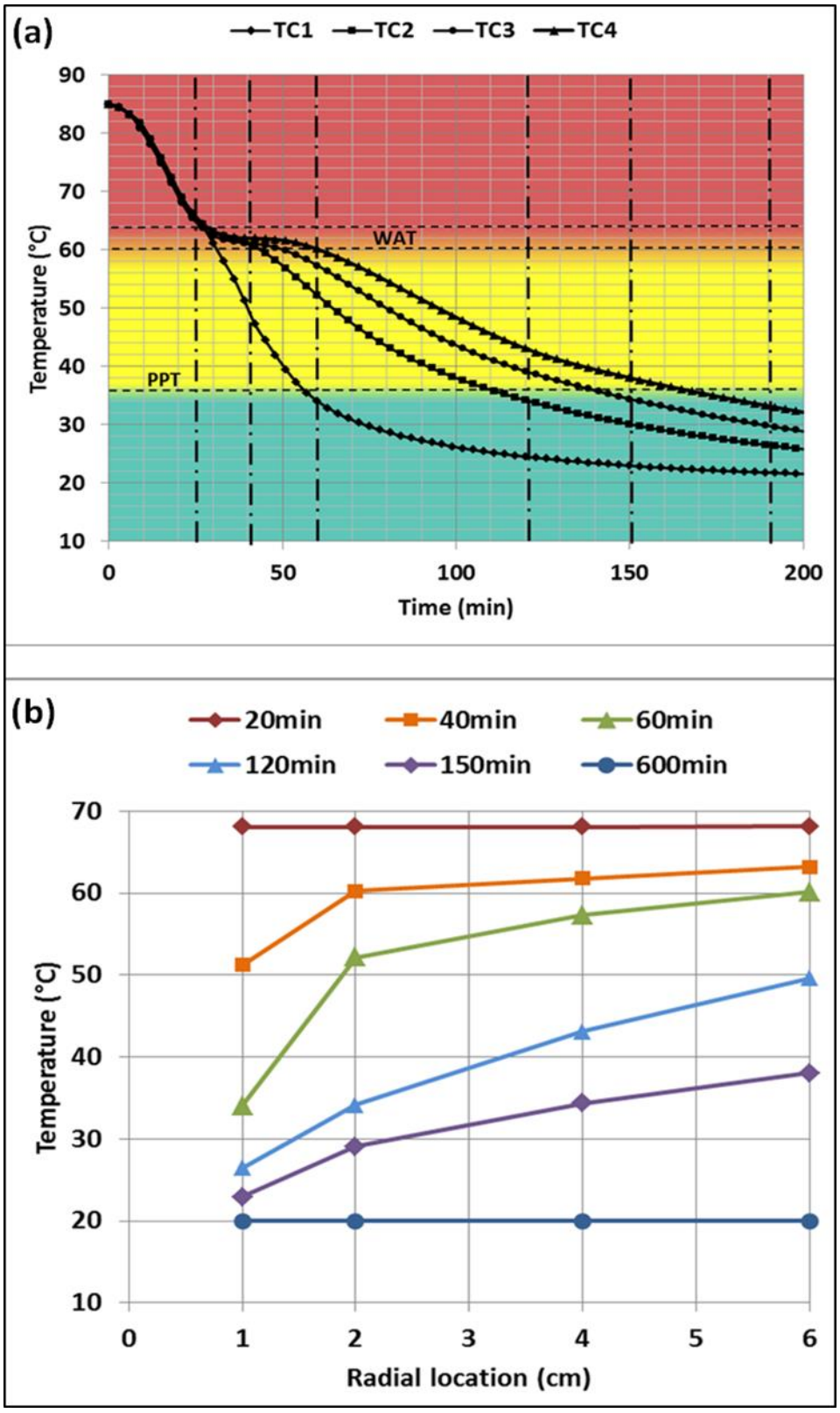

Figure 4.5.17: Static cooling durations of LO crude oil cooled from 85 to 20°C at 1°C/min in 120mm D **(a)** radial temperature profile **(b)** change of temperature with radial location.

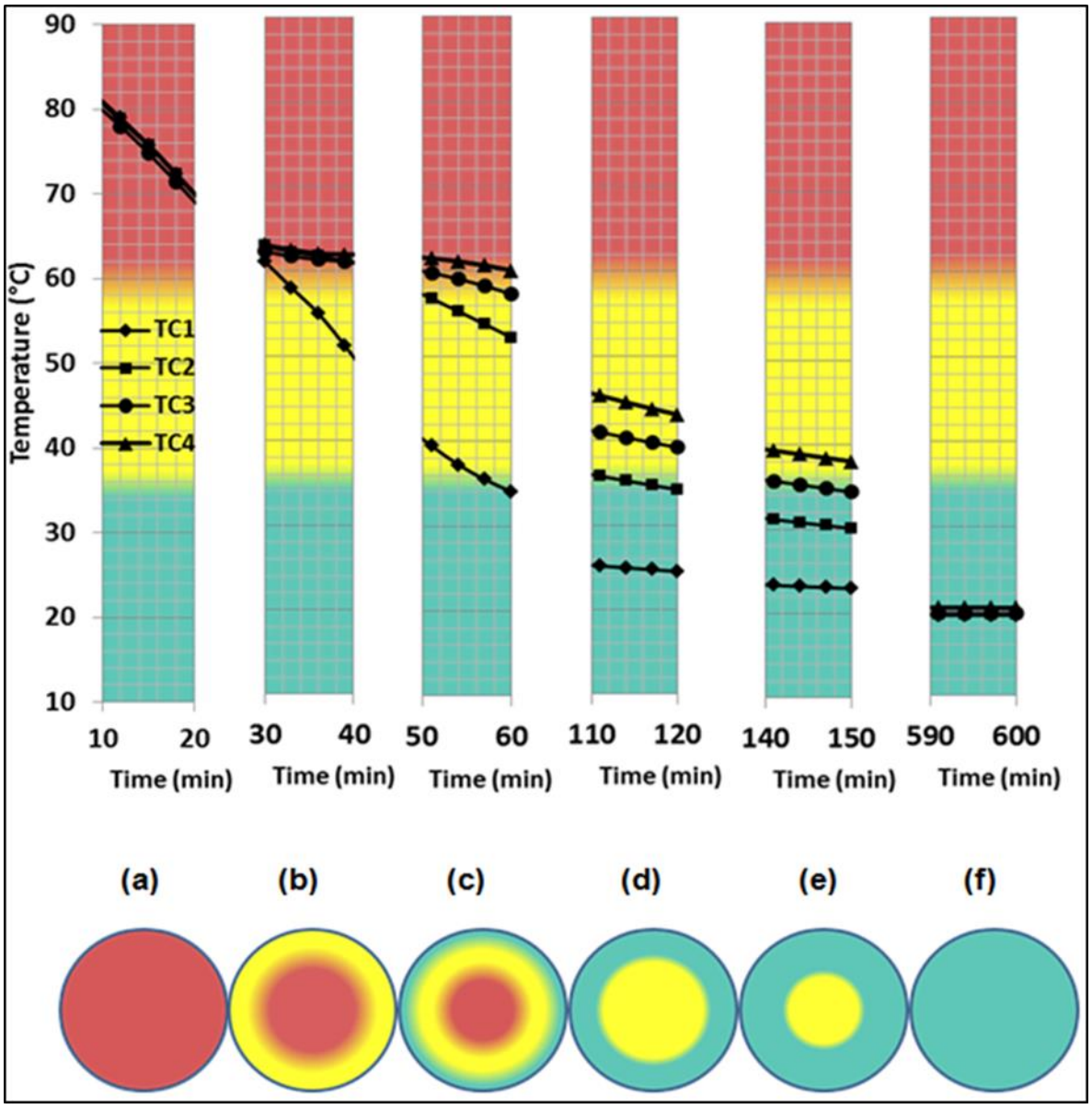

Figure 4.5.18: Evolution of wax deposit and changing of radial homogeneity inside a cross-section of the 120 mm diameter vessel for LO crude oil at different cooling durations.

4.6 Re-start of cooled waxy crude oil pipelines

The previous sections have assembled all the information necessary to predict re-start pressures as just explained in the concluding part of Section 4.5. DSC enabled the calculation of WAT and wax concentration, CPM revealed how in sufficiently wax rich crude oil (LO), low cooling rates allowed crystal growth and interlocking leading to structures with yield stresses as measured rheologically. Here re-start pressures of the waxy crude oils characterised BPO and LO are presented. The experimental method, described in the Experimental Chapter, consists essentially of a laboratory size pipeline, initially filled with a hot pre-conditioned waxy crude oil. The pipe is set at a similarly hot temperature to begin with, and then cooled through a jacketed pipeline around it. After a sufficient length of time, the oil inside the pipe will gel. A pressure (Nitrogen gas) is then applied at the pipe entry and increased gradually until flow was seen to commence at the outlet end of the pipeline. Two such pipelines were tested, with diameter 6.5mm and 13.5mm anticipating that with the smaller diameter pipeline, the temperatures across it after cooling would be more uniform leading to a more uniform crystal structure. In comparison, the 13.5mm would reveal effects associated with a comparatively less uniform temperature profile/crystal structure. The effect of interest is whether the gel fails and restarts at the wall or somewhere in the centre. As explained in Section 4.5.5, in actual large diameter pipeline, there will always be a temperature variation/crystal structure across the diameter throwing uncertainty where the gel breaks, albeit predictable on theoretical grounds from yield stress (static) values. This put into context the importance of the heat transfer study described in Section 4.5. The correct temperature/gel front must be located in order to be able to infer from rheological data the re-start pressure. This relationship is an essential aspect without which in large pipeline no prediction is possible.

4.6.1 Effect of Temperature on Re-Start Pressures

First, the baseline data on the 6.5mm pipeline are reported for BPO and LO cooled respectively from 60^{o}C to 15^{o}C and 80^{o}C to 35^{o}C at cooling rate of 2^{o}C/min. In order to ensure that the gel developed, the oils were held for 3 hours in the

pipeline after which the pressure was increased in 0.5 psi steps every 5 min until flow commenced at 19 psi for BPO and 26.6 psi for LO respectively. For this condition, the yield stress calculated was $\tau_y = \Delta PD/4L$ = 85 Pa and 105 Pa for BPO and LO respectively. Variations in the hold temperature were then tested and the data presented in Figure 4.6.1 and Table 4.6.1. As expected, LO required higher yield stresses for restart than BPO, typically by a factor of 10 and the yield stresses increased with decreasing temperatures. It is clear from this data, that the effect of temperature is very strong.

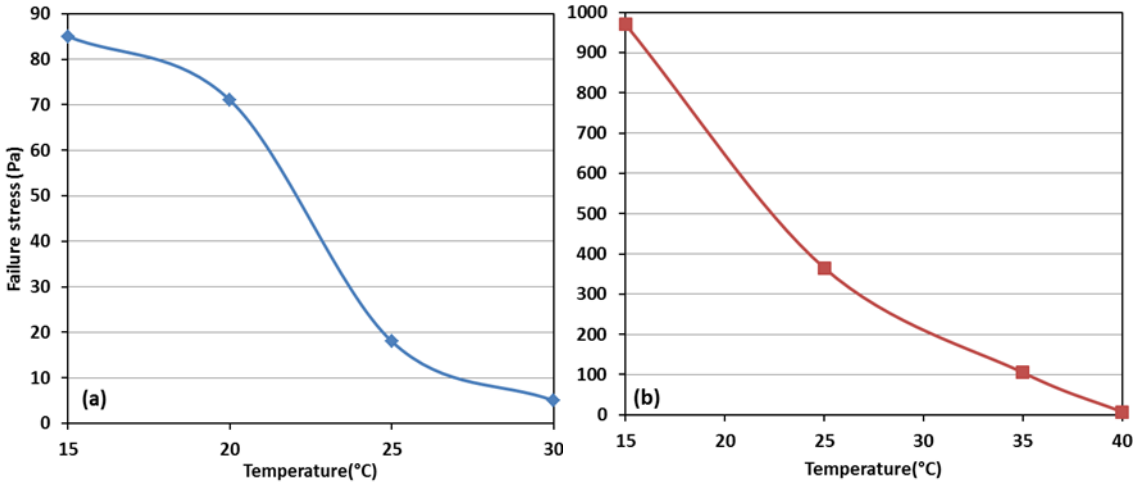

Figure 4.6.1: Effect of temperature on yield stress values of the crude oils measured by 6.5mm diameter model pipeline and cooled to test temperatures at cooling rate of 2°C/min with aging time of 3 hours **(a)** BPO crude oil **(b)** LO crude oil.

Table 4.6.1: Model 6.5mm pipeline experiments; Results of the failure stress of BPO and LO crude oils samples cooled at 2°C/min and tested under the same conditions at different temperatures.

Crude Oil	Test Temperature (°C)	Failure Stress (Pa)
BPO	15	85
	20	71
	25	18
	30	5
LO	15	970
	25	365
	35	105
	40	7

4.6.2 Effect of Cooling Rates on Re-Start Pressures

In the previous section, the correspondence between rheological data and start-up pressure was validate in situation where the cooling/gelling was uniform, thus leading to a similar break at the wall of the pipe. Here the cooling is increased in an attempt to provoke the setting of a non-uniform cooling/crystal gel structure. The data are shown in Figure 4.6.2 and Table 4.6.2 for the two pipe diameters at cooling rate sweep from 0.05 to 5^{o}C/min for LO crude oil. We see immediately (at 0.2^{o}C/min) the departure in the correspondence between the data measured rheologically and the re-start pressures data for the larger pipe of 13.5 mm diameter, a delineation point is existed between cohesive and adhesive failures at cooling rate of about 0.2^{o}C/min, i.e., beyond this point, the measured yield strength by the rheometer fails to predict the exact required pressure to restart this pipeline as the gel breaking will occur somewhere along the radial structure as cohesive failure. Validation of these results can be proved from Figure 4.6.3 which show the data of the failure stress values of LO crude oil with respect to temperature, measured by the rheometer and the both model pipelines with the same testing conditions previously used in obtaining the data in Figure 4.6.2, but at constant cooling rate of 0.2^{o}C/min which is the cooling rate equivalent to the delineation point in Figure 4.6.2 and testing temperature ranging from 15 to 40^{o}C. The data in Figure 4.6.3 is corroborated perfectly and for the two pipes when bringing in the yield stresses measured rheologically at the same temperatures. The data in this figure show that even with the large pipe diameter (13.5 mm), little or no discrepancy (Table 4.6.3) is observed with the rheological data, suggesting in both situations the cooling/gelling remain uniform. This is not surprising and indeed intentional as the cooling rate was kept very low in this situation.

4.6.3 Effect of Holding Time on Re-Start Pressures

The data shown in Figure 4.6.4 and Table 4.6.2 were obtained for LO crude oil from similar experiments of Figure 4.6.2, the only difference is a longer holding time of 4 hours was applied to the model pipelines experiments before testing. These experiments were performed to investigate effect of holding time on the

uniformity of the oil structure throughout the pipelines cross-section. As can be seen from Figure 4.6.4a-b, excellent agreement between the data measured rheologically and the re-start pressures data by applying longer holding time before testing. The holding time period needed to assure the gel uniformity of a pipeline is dependant on the pipe diameter, cooling rate and wax content of the oil.

4.6.4 Effect of Roughness on Re-Start Pressures

As previously mentioned, in the case of the data in Figure 4.6.2, the gel in the pipe is non-uniform in structure and has not broken at the wall (the stronger *adhesive* resistance) but somewhere towards the bulk flow where the *cohesive* resistance is weaker. By adhesive it is meant that near the wall, the crystals are smaller in size and numerous because they experience rapid cool adjacent to the cool wall. As such crystal structure will offer a large interfacial area to the wall pipe resulting in a strong adhesive force, made even stronger as pipe roughness is increased (greater interfacial area, the delineation point changes with changing the roughness). This is indicated in the data of Figure 4.6.5 and Table 4.6.2, which show the cohesive failure at lower stress as roughness is decreased. When the roughness of the rheometer plate and inner pipe wall increased from 0.002 to 0.03 mm the delineation point is changed from exist at 0.2^{o}C/min to 0.1^{o}C/min.

Table 4.6.2: Comparison of the yield stress values of LO crude oil obtained from the controlled stress rheometer and the model pipelines and all tests performed at 33^{o}C.

Cooling rate (^{o}C/min)	Failure stress (Pa)							
	Rheometer		6.5mm pipe		13.5mm pipe			
	Ra (mm)		holding time		holding time		Ra (mm)	
	0.002	0.03	5min	4hrs.	5 min	4hrs.	0.002	0.03
0.05	182	286	174	174	170	179	170	273
0.1	158	252	158	155	155	159	155	248
0.2	152	233	148	148	145	145	145	178
0.5	127	183	132	132	91	126	91	98
1	114	132	109	113	41	105	41	52
2	102	116	82	101	23	98	23	35
5	86	79	66	87	16	83	16	27

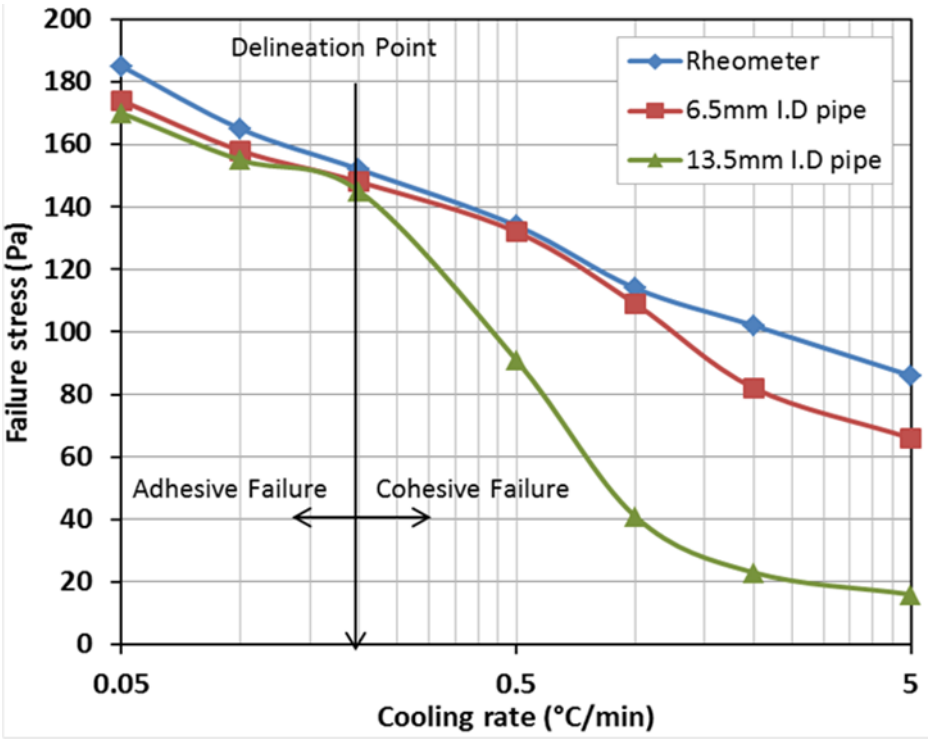

Figure 4.6.2: Comparison between the yield stress values of LO crude oil obtained from the controlled stress rheometer and different diameter model pipelines and measured with holding time of 5 min at 33^{o}C with respect to cooling rate.

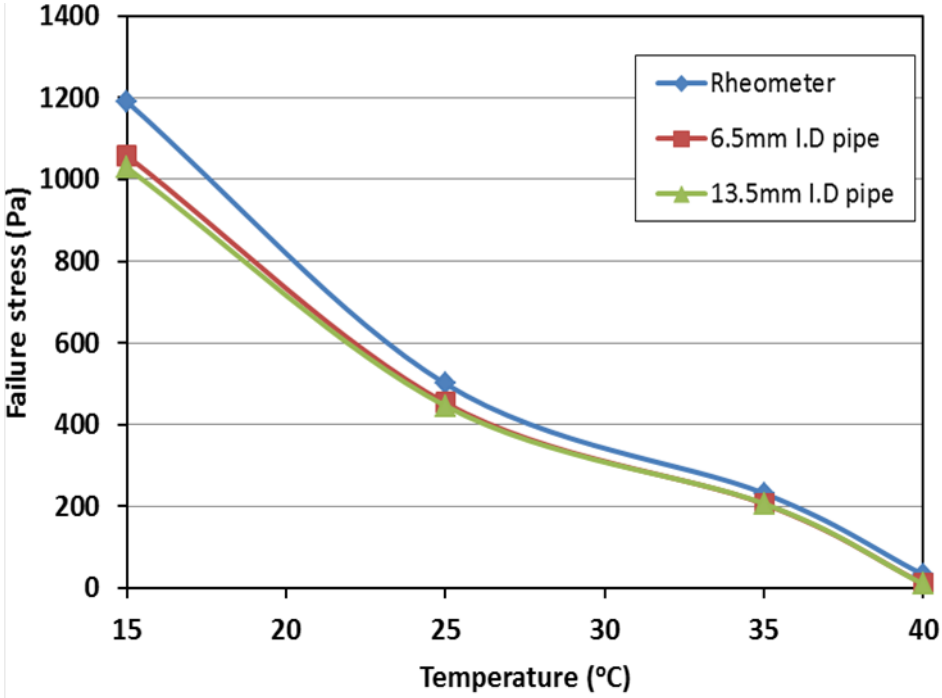

Figure 4.6.3: Comparison between the yield stress values of LO crude oil obtained from the controlled stress rheometer and different diameter model pipelines and measured with holding time of 5 min at 0.2^{o}C/min with respect of temperatures.

Table 4.6.3: Comparison of the yield stress values of LO crude oil cooled at cooling rate of 0.2°C/min and measured by the controlled stress rheometer and the model pipelines.

Temperature (°C)	Failure stress (Pa)				
	Rheometer	6.5mm pipe	Deviation %	13.5mm pipe	Deviation %
15	1190	1058	-11.1	1029	-13.5
25	500	453	-9.4	446	-10.8
35	232	206	-11.2	207	-10.7
40	33	11	-66.7	10	-69.7

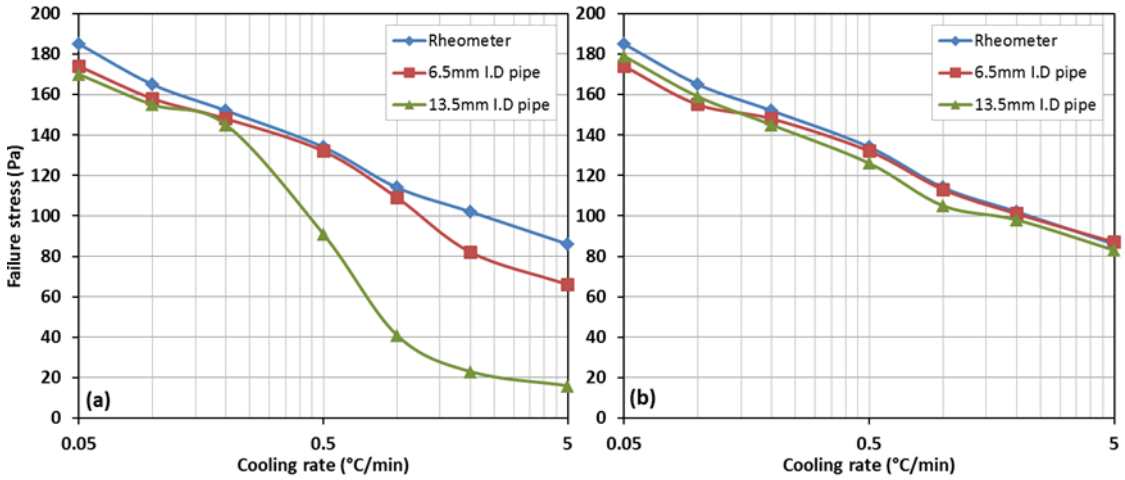

Figure 4.6.4: Effect of holding time on the failure stress values with respect of cooling rate of LO crude oil measured at 33°C in 6.5 and 13.5 mm diameter pipelines, with holding time of **(a)** 5 min **(b)** 4 hours.

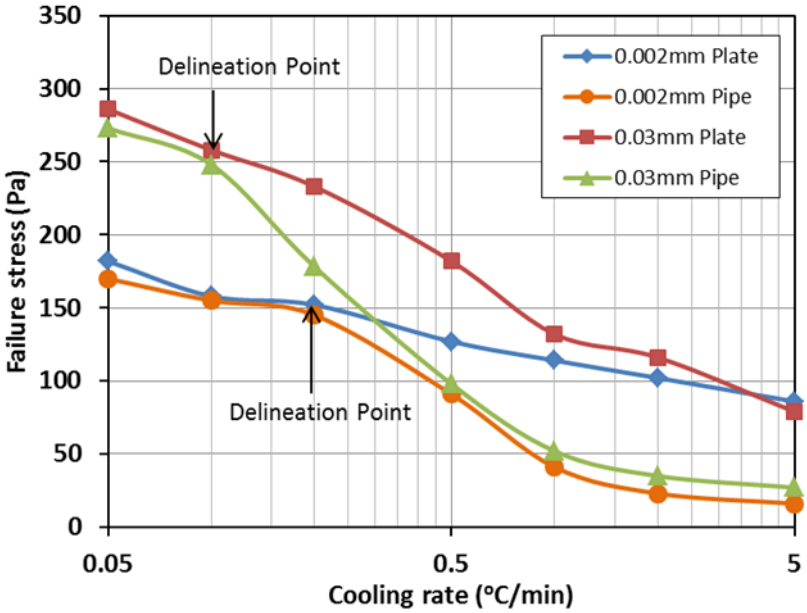

Figure 4.6.5: Gel failure stress vs. cooling rate of LO crude oil measured at 33°C; effect of the plate and pipeline roughness on the delineation point between adhesive and cohesive failures, by the controlled stress rheometer and 13.5 mm diameter model pipeline.

4.6.5 Prediction of Start-up Pressure for Non-uniformly Pipelines

As it can be seen from Figures 4.5.17-18 in the previous section, at t = 20 min, i.e. before the interface reaches TC1, the temperature of the liquid region was the same and thermal equilibrium takes place throughout the cross-section of the vessel. The structural state and yielding strength of the crude oil should be uniform and homogeneous at this time as shown in Figure 4.5.18a. The required pressure to restart the pipeline at this point can be successfully predicted by the rheometer measurement as that the breakage of the crude oil structure will occur at the pipe wall (adhesive failure). At t = 40 min, the interface was reached TC1 and the temperature at this location was close to the WAT. At this point the radial cooling process becomes un-uniform resulting different radial temperatures, radial cooling rates and radial structural strengths. Therefore, different state regions should be considered throughout the cross-section as shown in Figure 4.5.18b. Thus, prediction of failure strength by the rheometer measurement becomes more complicated at this stage, as the breakage of the structure can be happened at any radial location as cohesively failure depends on the radial temperatures. Recall that experiments was done using the rheometer, DSC and Cross-Polarized Microscope in section 4.4 of this chapter, Figure 4.4.6-7 show a correlation between the calorimetry, morphology and yielding at various temperatures for LO and BPO crude oils cooled statically at 1^{o}C/min. These results describe the effect of the temperature and cooling rate on the structural modulus of the crude oils (storage and loss modulus) and the corresponded crystal structure observed by the microscope. Thus, the yielding point depends on the weakest point in the radial structures and this would be corresponded to the radial location with highest temperature, Hence, the yield stress measured by the rheometer should be corresponded to this temperature and the required restart pressure should be recalculated according to this radial location, “effective” yielding radius (r_{ye}), which can be determined from liquid-deposit interface as presented in Table 4.15. At t = 60 min, the temperature at TC2 and TC3 reached the WAT while TC1 dropped below the WAT as it immersed in the deposit layer which works as insulator and this causes higher differences in the radial cooling rates and so in the radial

temperatures. At this point, the temperature in the liquid region was still above the WAT, thus, three state regions can be resulted; deposit, precipitate and liquid regions, as shown in Figure 4.5.18c. At t = 150 min, the temperature in the liquid region was still in range of the WAT, while TC2 and TC3 followed TC1 respectively with different speed and became immersed in the deposit layer, thus, two different structural regions were obtained throughout the cross-section as shown in Figure 4.5.18d. After this time, the temperature TC4 decreased to below the WAT. The deposit occupied the entire vessel at about 190 min as TC4 reached the lower limit of WAT. Beyond this time point, further cooling of the deposit layer took place with the transfer of sensible heat as well as the latent heat corresponding to the gradual solidification of the liquid phase within the deposit as shown in Figure 4.5.18e. The centre temperature (TC4) reached the Pour Point Temperature of the crude oil (PPT) at t =165 min. At t = 600 min, the deposit temperature throughout the cross-section became back uniform and equal to the wall temperature resulting homogeneous gel structure as shown in Figure 4.5.18f. Thus, direct application of rheometer measurement to predict the restart pressure in a pipeline will be successful at this stage. The data in Table 4.6.4 summarised the above sex specified shutdown durations with classification of the structure failure mechanism and this depend on the diameter of a pipeline and the cooling rate at the wall. This data are plotted in columns chart for easy comparisons as shown in Figure 4.5.19

In conclusion, predicted restart pressure obtained from the rheometer measurement can be applied directly to a statically cooled waxy crude oil pipeline only when the radial structure is uniform and the effective yielding radius is equal to the actual radius of a pipeline (r_{ye} = R) and this can be used to calculate the required a pressure for adhesive restart. At a restart point when the radial temperature and the radial structure throughout a pipeline cross section are not uniform, the required restart pressure should be recalculated using the effective yield stress (τ_{ye}) and effective yielding radius (r_{ye} = R - δ) for cohesive restart.

The effective yielding temperature (T_{ye}) for each cooling duration were determined from the radial temperatures at the specified radial locations and the effective yield stresses were measured by rheometer at the corresponding effective

yielding temperatures using the controlled stress test. Then the restart pressure was calculated using the radial location of the effective diameter and the length of a pipeline (L) as presented in Table 4.6.4, the effective yield stresses with respect of the cooling (shutdown) durations, *t*, is plotted in Figure 4.5.20. As it can be seen from the figure, good linear relation was obtained between the effect yield strength τ_{ye} (Pa) and the corresponding shutdown durations *t* (min) for LO crude oil cooled at cooling rate of 1^{o}C/min in cross-section diameter of 120mm. This relationship can be expressed as Equation 4.6.1 with a correlation coefficient of R^2 = 0.9847.

$$\tau_{ye} = 2.2148t - 93.743 \qquad (4.6.1)$$

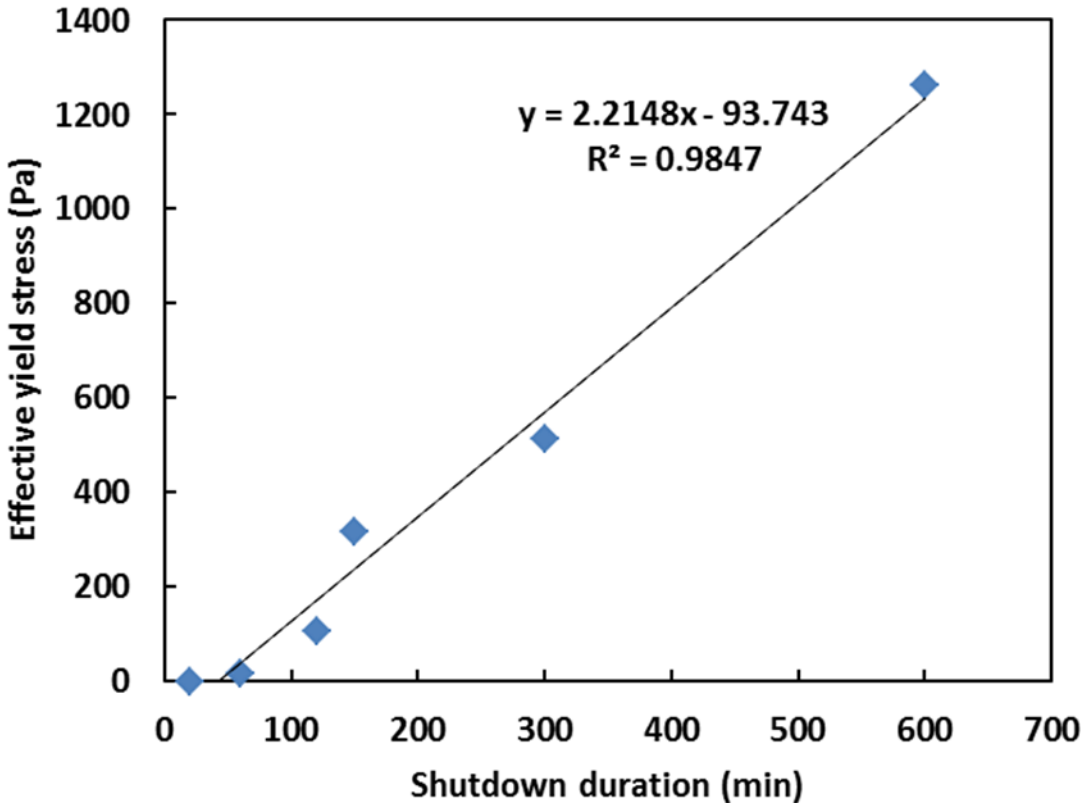

Figure 4.5.20: The relationship between the shutdown duration and the effective yield stress.

Table 4.6.4: Results of effective yield stress and restart pressure after different shutdown durations for **LO** crude oil pipeline cooled from 85°C to 20°C at 1°C/min.

Shutdown duration (min)	Radial temperatures (°C)				Effective yielding temp. T_{ye} (°C)	Effective yield stress, τ_{ye} (Pa) (*Rheometer*)	Effective yielding radius, r_{ye} (m)	Restart pressure, (kPa) (*Pipeline*)	Restart failure mechanism
	TC1	TC2	TC3	TC4					
20	68.1	68.1	68.1	68.1	68.1	0	0.06	0	Newtonian
60	34.1	52.2	57.3	60.1	52.2	15	0.05	0.5*L	Cohesive
120	26.5	34.2	43.2	49.6	43.2	105	0.04	5.25*L	Cohesive
150	22.9	29.1	34.4	38.1	38.1	315	0.02	31.5*L	Cohesive
600	20	20	20	20	20	1260	0.06	42*L	Adhesive

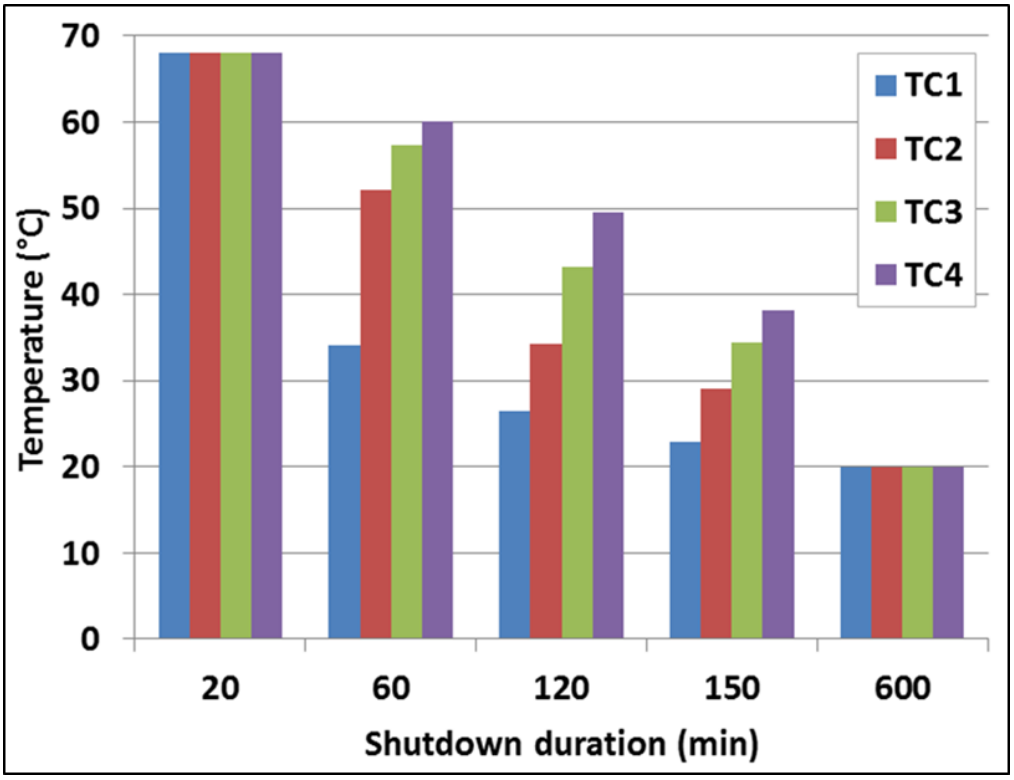

Figure 4.5.19: : Comparison of radial temperature values at the specified cooling durations for LO crude oil cooled statically in 120 mm vessels from 85 to 20°C at 1°C/min.

4.6.6 Summary

The measurements taken on the laboratory scale pipeline have confirmed many of the findings developed earlier in this chapter, mainly that:

a. Re-start in large diameter pipelines cannot be predicted on the basis that failure occurs at the wall. This is because there will always be a temperature variation, hence a crystal structure variation causing the gel breaks at its weakest *cohesive* section away from the strong *adhesive* region near the wall
b. Adhesive strength is defined in relation to fast cooling rates leading to a large number of tiny crystals forming near the wall of pipeline, offering their large interfacial area for adhesion with the wall. This hypothesis can be demonstrated from the data collected from the experiments of the model pipelines with different diameters at varying cooling rate.
c. Data collected with pipes of different roughness further complemented the above hypothesis as it was seen that as the roughness was increased, the departure from the yield stress measured in rheology occurred at lower cooling rates.
d. Finally, for any correct prediction of re-start pressure one must carry out a heat transfer analysis to determine the temperatures at which the gel front occurs and these will depend particularly strongly on cooling rate but evidently on the pipe diameter and cooling temperature.

5. CONCLUSIONS

5.1 Introduction

The objectives of this research were to develop a fundamental understanding of the yielding mechanism of gelled waxy crude oils, their wax deposition in pipelines and the minimum pressure required to restart such gelled oils in pipelines through both experimental and theoretical means. These objectives have been largely met and the conclusions can be summarised as follows:

1. The yielding stages have been unravelled through constant stress rheology with an advanced instrument capable of resolving deformation at very low stresses not attained by previous workers.
2. The yielding stages were found to require a 4-yield stress model, these stresses being the *elastic* yield stress, followed by the *end of creep* yield stress, the *end of fracture* yield stress and an *"imaginary" dynamic* yield stress relating to viscous flow.
3. The rheological data obtained were checked against pressure drop measurements in laboratory pipelines at two diameters (6.5mm and 13.5mm) in an effort to mimic both the instrument rheological condition (isothermal cooling through the sample) and the actual in field situations (non-isothermal cooling because of the normally very large diameters of industrial pipelines).
4. These comparative tests have been complemented with microscopic observations of gel formation during cooling in an effort to understand how the wax crystals that form affect interfacial stresses (bulk liquid oil-wax crystals interface and pipeline metal wall-wax crystals interface). These observations have shown that when the cooling rate is very low, the crystals grow in size whereas at large cooling rates many more crystal forms but are of smaller size.

5. The implication of this structure formation is that in actual operations, the cooling rate are larger at the wall than at the centre thus creating crystals that are finer at the wall than towards the centre (a gradient of size forms). Naturally a wax free oil plug will form at the centre. Thus two interfaces form: a bulk liquid oil-*large* wax crystals interface and a pipeline metal wall-*small* wax crystals interface. Consequently, larger interfacial stresses form at the wall (adhesive forces) and weaker ones (cohesive forces) at the oil plug. To restart the pipeline, the cohesive force only needs to be overcome. The problem is that the location of this interface is unknown.
6. The last part of the research addressed the latter point by investigating effect of cooling in large sections of pipes (60 and 120mm diameter), measuring temperature profiles to locate the gel front, i.e. the position of this interface which is necessary to verify the force balance $\Delta p \pi r_i^2 = 2\pi r_i \tau_y$ thus completing the information necessary for restart.

5.2 On the thermal (DSC) measurements

They have provided the necessary data to guide the rheological work in that the critical temperature at which the wax begins to precipitate (WAT) is obtained unequivocally. Also, this data revealed how WAT and WDT showed opposite variation with cooling rate indicating the importance of cooling rate on the structure (strength) of the wax network (crystal size and by implication number). Importantly, this data provides also a direction for the rheological measurements and a preliminary estimation of the yielding mechanism of these structures.

5.3 On the microscopic (CPM) observations

CPM proved to be very informative at explaining the mechanism of formation of wax crystals upon cooling. As expected, high cooling rates have produced wax structures formed of many small crystals which because of their large surface area adhere strongly to the pipe wall where cooling is at its largest. On the other hand, low cooling rates which must develop away from the

wall, led to the formation of large wax crystal offering smaller interfacial areas with the oil plug at the centre thus weaker cohesive forces. This data explains the discrepancy between the yield stress measured in the controlled stress rheometer and the laboratory pipeline of large diameter. Only data at the smaller diameters mimic the rheological instrument where cooling is uniform. Large diameter pipe cools non-uniformly and are “poor rheometers” for waxy crude oils.

Finally, in the context of comparing various oils, the microscopic observations revealed the differences between the BPO and LO, the latter forming strong interlocked network compared with the looser more dispersed structure of BPO with clear implications on the magnitude of the yield stresses measured.

5.4 On the rheological data

As this part of the work required comprehensive coverage on the effect of cooling rate, temperature and stress loading rate using controlled stress principally but also oscillatory and creep tests, a number of conclusions can be drawn:

i. The entire yielding process of BPO and LO waxy crude oils was successfully characterised as a model of four yield stresses by controlled stress test, creep-recovery and oscillatory tests. Four yield stresses were qualitatively indicated using different analytical methods for the data such as shear rate, dynamic fluidity and failure acceleration. The elastic-limit yield stress (τ_e), static yield stress (τ_s) and fracture yield stress (τ_f) were directly determined as single values by the controlled stress test and supported also by range of values obtained from oscillatory and creep-recovery tests. The dynamic yield stress (τ_d) in controlled stress test was extrapolated from the high shear range after the fracture to the zero-shear rate limit, according to Bingham equation.

ii. In the controlled stress tests, a lower stress loading rate produces a lower static yield stress, a lower dynamic yield stress, and as a result a higher dynamic fluidity and a lower apparent viscosity. The dependence of the static yield stress on the stress loading rate may indicate that the pressure required to restart a

pipeline flow is also dependent on how quickly the pipeline is started, in addition to that it being already controlled by the strength of the wax structure of the oil in the pipeline. It is then for the best operation that the pump pressure in restarting a gelled waxy crude oil pipeline should be increased as slowly as possible, since a slower operation will need a lower pump pressure not only in starting the flow but also in transporting the oil in the final broken state after the pipeline restarts and this will reduce the cost of the operation.

iii. The yielding strength of BPO and LO crude oil gels cooled under static conditions was observed to increase with decreasing the cooling rate and vice versa. A lower cooling rate results in a higher elastic-limit yield stress, a higher static yield stress and a higher dynamic yield stress. Furthermore, the effect of cooling rate on the yielding strength for both crude oils was investigated by means of the failure acceleration. Earlier failures were observed with higher cooling rates and later failures with lower cooling rates, so this means that the yielding strength is higher in the case of lower cooling rates and vice versa.

iv. Temperature is a very important factor as it has a strong effect on the yielding process and other rheological properties of waxy crude oils. The flow curves of the waxy crude oils at temperature above their PPT are almost plateau at low shear rate, indicating that the crude oils behave like a Newtonian fluid. Also, there is no clear distinction between the yielding process stages. Consequently, there is no significant difference between the elastic-limit yield stress and the static yield stress. When the temperature is reduced below the PPT, waxy crude oils behave as non-Newtonian fluids and display distinct yield characterise with large differences between the elastic-limit yield stress and the static yield stress. In general, the yielding strength of BPO and LO crude oil gels cooled under static conditions is observed to increase with decreasing temperature and vice versa. A lower temperature produces a clear yielding behaviour and a stronger wax structure, thus, a higher elastic-limit yield stress, a higher static yield stress and a higher dynamic yield stress.

v. The elasticity and elasticity-limit of waxy crude oil gels cooled under static conditions was observed to increase with decreasing temperature and lower

cooling rate. This can be attributed to the wax structure and network growth as the behaviour of oil structure becomes more elastic than viscoelastic, thus the wax network becomes more connected and the oil structure becomes stronger. As noticed from the results of this study, the elastic reflux in the elastic deformation region was wider and higher when the sample was tested at a lower temperature or a lower cooling rate. Furthermore, the refluxing of oil structure, for a given test at given temperature and cooling rate, is wider at the beginning of the elastic deformation when the structure and the interlocking system are strong at low shear stress. When the applied stress increases, the vibration narrows with time because the oil structure changes from elastic like to viscoelastic until, with increasing deformation, the structure is completely destroyed.

vi. The variation of the elastic-limit yield stress and the extent of creep with different stress loading rates, temperatures and cooling rates were investigated in this study. By using unique analytical methods for the data through the change of strain and storage modulus with respect to applied stress, the elastic-limit yield stress and static yield stress were directly determined as single values from oscillatory tests. These unique points provide description of the yielding of waxy crude oils and the effect of the investigated factors on the yielding process. They also enabled a further appreciation of the failure behaviour and failure acceleration of gel structure of waxy crude oils over the whole range of shear stress and shear rate.

vii. The elastic-limit yield stress obtained from the different testing techniques have been found to be comparable since it is not influenced by the time scale of the test; thus, our results of elastic-limit yield stresses from controlled stress, creep-recovery and oscillatory tests are in a good agreement.

viii. One yield stress is not sufficient to describe the yielding process of the oil, a four yield stresses model should be used for designing pipelines and pumps in different stages of yielding (shear stress vs. shear rate relationship calculation through elastic, creep, fracture and flow processes). The elastic-limit yield stress should be used to determine if the yielding could start, the static yield

stress can be used to determine if fracture starts and fracture yield stress can be used if fracture occurs. After the fracture, the dynamic yield stress should be used in the calculations of the flow from the shear stress-shear rate relationship.

ix. Waxy crude oil is a complicated material because in addition to its dependence of shear-thinning and thermal history, the results obtained from both oscillatory and controlled stress tests indicate that the rheological properties of waxy crude oil, such as viscosity, G' and G'', at the final broken state are also shear history dependent. This must be attributed to the wax structure in the oil. The repeatability can be guaranteed by controlling all related factors of each process and reducing effect of presence thermal and shear histories of the sample before testing.

5.5 On non-uniform cooling and pipeline restart

i. In the static cooling experiments, the temperature of the waxy crude oils decreased rapidly to the WAT much before the gel started to form at the pipe (vessel) wall. Initially, as the oil is above WAT, the cooling is found to be uniform throughout the pipe (vessel cross-section) that is no radial variation is measured. This can be explained as being due to the fact that the cooling above WAT is only controlled by natural convection. At the point of wax precipitation (that is at WAT), a change in the temperature profile was observed, indicative of a different heat transfer mechanism taking place, heat of wax precipitation and conduction now playing a part in conjunction with convection.

ii. The wax deposit is found to add a layer of insulation to the system and reduce the thermal gradient. Consequently, diffusion effect begins to reduce as more crystals are deposited. Therefore, a stronger gel is formed at the wall and a weaker one at the pipe centre. As a result of the increasing thermal insulation, the temperature at the oil-deposit interface was found to decrease as the layer of deposit grows and this was attributed to a lowering of the WAT of the liquid phase with lower wax content.

iii. Variations in temperature profile with radial locations and deviation from the wall temperature were observed beyond WAT. These variations were higher with higher wax content, higher cooling rate, and larger diameter and vice versa. Thus, the lower wax content of crude oil, the lower cooling rate and the smaller diameter, the better the thermal equilibrium and radial homogeneity throughout the vessel cross section.

iv. The predicted restart pressure obtained from the rheometer measurement can be applied directly to a statically cooled waxy crude oil pipeline only when the radial wax structure (i.e. cooling) is uniform. Under such conditions, the effective yielding radius is equal to the actual radius of a pipeline ($r_{ye} = R$) and this radius can be used to calculate the required pressure for adhesive restart. When the radial temperature and the radial structure throughout a pipeline cross-section are not uniform, the required restart pressure should be recalculated using the effective yield stress (τ_{ye}) and effective yielding radius ($r_{ye} = R - \delta$) for cohesive restart where δ is the wax annulus thickness.

v. In all the cases of the experiments, an agreement between the controlled stress rheometer data and the required pressure for breakage of the gel in a pipeline can be obtained when the temperature between the wall and centre line is uniform (thermal equilibrium throughout the cross section). Experimentally, this requires applying a holding time until a uniform temperature is obtained This is obtained by taking a holding time of duration from the time when the wall temperature (TCW) reaches the final range of cooling process (i.e. corresponding the testing temperature in the rheometer measurement) up to the time when the temperature between the wall and centre line becomes uniform. The required holding time is dependent on the cooling rate, wax content and diameter size. For example, for the cooling of BPO and LO crude oils from 80^{o}C to 15^{o}C with cooling rate at 1.1^{o}C/min in the 120mm diameter vessel, the wall temperature was reached to the final cooling range in 60min, while the thermal equilibrium was obtained in 400min and 600min for BPO and LO crude oils respectively. For the same crude oils with the same cooling conditions in the 60mm diameter vessel, the thermal equilibrium was obtained

in 200min and 300min for BPO and LO respectively. Hence, for a very large (industrial) diameter pipeline, much longer time would be used before thermal equilibrium is reached.

vi. Thermal equilibrium throughout the media between the wall and the centre line during the cooling process is found to be dependent on cooling rate. The higher the cooling rate, the wider the deviation will be for the centreline temperature from the wall temperature. For the low cooling rate, no significant differences were observed in the temperature between the radial locations and the wall, i.e., the oil-gel interface reached TC1-TC4 at the same time approximately and the radial temperatures of the cooled crude oil were always close to the wall temperature. Thus, thermal equilibrium had taken place throughout the cross-section of the vessel during the whole of the cooling time. The state and yielding strength of the cooled crude oil were uniform and homogeneous throughout the cross-section at any time of the cooling process as well. For low cooling rate therefore, in this case, the yield stress measured by the rheometer at the wall temperature at any time can be used directly to predict and calculate the required pressure to restart the cooled crude oil pipeline, using the actual diameter. This is because the breakage of the gelled oil structure will occur at the pipe wall (adhesive failure) as the shear stress exerted at the wall is the highest when applying the restart pressure.

vii. The data collected from the model pipelines of different roughness show that as the roughness was increased, there was a departure from the yield stress measured in the rheometer which occurred at a lower cooling rate. In other words, the adhesive strength increases as the surface roughness is increased because of the greater contact area between the wax crystals and the wall. An additional increase in roughness can prevent any adhesive failure caused by slip at the surface. The failure will then only be cohesive elsewhere in the pipeline cross-section.

5.6 Overall Conclusion

The research undertaken here aimed at reconciling rheometric data with start-up pressure data in order to define an appropriate yield stress and effective start-up pressure. In order to achieve this, four important points had to be considered:

1. The oil sample must be conditioned prior to the rheometric and the start-up pressure experiments.
2. The rheometer used must be able to resolve both very small stresses ($< 10^{-5}$ Pa) and small shear rates ($< 10^{-4}\ s^{-1}$)
3. The cooling of the sample was the determinant factor and must be controlled carefully in both the rheometric and the start-up pressure experiments. Critically, only when cooling was uniform in the start-up pressure experiments would the rheometric data predict the correct yield start-up pressure.
4. When the cooling rate was non uniform across the sample in the start-up pressure experiments, the temperature must be determined to calculate the position and cooling rate of the gel front and then obtain the effective start-up pressure.

Sections 5.1-5.5 in this concluding chapter detailed these key points and should be read together with this brief overall conclusion.

6. RECOMMENDATION AND FUTURE WORK

The research described in this thesis points to several topics worthy of future research, in particular to:

(1) For prediction of re-start pressure in a waxy crude oil pipeline, a heat transfer analysis must be carried out to determine the temperatures at which the gel front occurs. The observations of this work provide the foundations to help develop mathematical models to determine temperature profiles in these situations. The model must capture this phase change due to the precipitation of the wax and the following different heat transfer mechanism from that (natural convection) prevailing at the beginning of cooling. Accurate properties (wax concentration, heat of precipitation of wax, kinetics of wax precipitation, thermal conductivity of wax) are required for accurate predictions. Once the gel front location and its temperature have been obtained, a corresponding yield stress can be measured and the start-up pressure calculated by a simple force balance.

(2) Investigate the correspondence of the wax compositions and types contained in BPO and LO crude oils, by using modified model samples; by mixing different percentages of quantities from BPO and LO crude oils, using the rheometer and DSC to measure viscosity, yield stress, solid fraction, wax content, WAT and WDT at various cooling rates and comparing to the results of the same parameters for the original crude oil samples at the same testing conditions. Also, one of the objectives of such investigation would be to find a correlation between the wax percentage and the values of these parameters.

(3) Study the effect of stress loading rate on the viscous behaviour and flow of waxy crude oils beyond the fracture process by using controlled stress test and applying wider ranges of shear stress at various stress loading rates, for example from 1 to 500Pa instead of 1 to 150Pa which was used in this thesis research. In addition, oscillatory tests can be done for the same purpose, by applying larger

ranges of stress amplitude at various frequencies, covering the behaviour of the elastic and viscous modulus beyond the fracture process at the final state of the oil flow.

(4) Investigate the impact of inhibitors on wax precipitation. These are frequently injected to reduce or prevent wax deposition. Such work can be approached using the same techniques as the one developed in this research using say BPO and LO in conjunction with inhibitors added at various doses, the aim being to establish the cost-benefit compared to restart/pumping without inhibitors.

(5) Further rheological measurement to be done using the concentric cylinder viscometer technique to measure yield stress. Then, comparing the data obtained by this technique to the cone and plate technique data at the same cooling rates and testing conditions, and analyse which of the two methods is more reliable and appropriate to predict the start-up pressure in model pipelines.

(6) Develop from the rheological data, models in terms of the 4 yield stresses τ_e, τ_s, τ_f and τ_d to describe yielding, creep, fracture and flow of waxy crude oils.

(7) Importantly, solve the static cooling heat transfer model to predict the gel front for various cooling scenarios and test its prediction against data obtained in this research.

(8) Use the predicted gel front position and the fracture yield stress τ_f to predict restart pressures in gelled pipelines.

Indeed, recommendations (6) and (7) combined will provide the definitive model to predict restart pressure accurately, an aim that has eluded previous research.

7. REFERENCES

[1] Encyclopedia Britannica, 2008. Encyclopedia Britannica Online, [http://www.britannica.com/bps/search?query=crude+oil].

[2] Fan Zhang and Guo-qun Chen, 2007. Viscoelastic properties of waxy crude oil. Journal of Central South University of Technology, Volume 14, Supplement 1, 445-448.

[3] Speight, J. G. 1999. Petroleum Chemistry and Refining, Western Research Institute, Laramie. Wyoming, USA.

[4] Barry, E.G., 1971. Pumping Non-Newtonian Waxy Crude Oils. *J. Inst. Pet.* 57(554): 74 - 85.

[5] Singh, P., and Fogler, H.S. 1999. Prediction of the Wax Content of the Incipient Wax-Oil Gel in a Pipeline: An Application of the Controlled-Stress Rheometer. *J. Rheol.* 43 (6): 1437 – 1459.

[6] Singh, P., Venkatesan, R., Fogler, H.S., and Nagarajan, N. 2000. Formation and Aging of Incipient Thin Film Wax-oil Gels. *AIChE J.* 46 (5): 1059-1074.

[7] L. T. Wardhaugh, L.T. and D. V. Boger (1991). The Measurement and Description of the Yielding Behaviour of Waxy Crude Oil.

[8] Cheng Chang, David V. Boger and Q. Dzuy Nguyen, 1998. Yielding of Waxy Crude Oils. *Industrial and Engineering Chemistry,* 37:1551–1559, 1998.

[9] Harvey, A.H., Briller, R. and Arnold, M.D. 1971. Pipeline Design for Gelling Oils: part 1 – Preliminary Calculations. *Oil and Gas J* 96.

[10] Ells, J.W., and Brown, V.R.R. 1971. Designing of Pipelines to Handle Waxy Crude Oils. *J. Inst. of Petr.* 555: 175-183.

[11] Irani, C., and Zajac, J. 1982. Handling of High Pour Point West African Crude Oils. JPT: 289-298.

[12] Ronningsen, H.P. 1992. Rheological Behavior of Gelled, Waxy North Sea Crude Oils. *J. Petr.Sci. and Eng.* 7: 177-213.

[13] Chang, C., Nguyen, Q.D., and Rønningsen, H.P., 1999. Isothermal Start-Up of Pipeline Transporting Waxy Crude Oil. *J. Non-Newtonian Fluid Mech.* 87: 127–154.

[14] Davidson, M.R., Nguyen, Q.D., Chang, C., and Hans Petter Ronningsen. 2003. A Model for Restart of a Pipeline with Compressible Gelled Waxy Crude Oil. *J. Non-Newtonian Fluid Mech.* 123: 269–280.

[15] Davidson, M.R., Nguyen, Q.D., and Hans Petter Ronningsen. 2003. Restart Model for a Multi-plug Gelled Waxy Oil Pipeline. *J. Pet. Sci. Eng.* 59: 1–16.

[16] Alboudwarej, H., Huo, Z., Kempton E., 2006. Flow Assurance Aspects of Subsea Systems Design for Production of Waxy Crude Oils. Paper SPE 103242 presented at the ATCE in San Antonio, 24-27 Sept.

[17] Thomason, W.H. 2000. Start-Up and Shut-In Issues for Subsea Production of High Paraffinic Crudes. Paper OTC 11967 presented at the Offshore Technology Conference, Houston, 1- 4 May.

[18] Ronningsen, H.P., Bjorndal, B., Hansen, A.B., and Pedersen, W.B. 1991. Wax Precipitation from North Sea Crude Oils. 1. Crystallization and Dissolution Temperatures and Newtonian and Non-Newtonian Flow Properties. *Energy & Fuels*. 5: 895 – 908.

[19] Hamouda, A.A., Viken, B.K. 1993. Wax Deposition Mechanism Under High-Pressure and in Presence of Light Hydrocarbons. Paper SPE 25189 presented at the SPE International Symposium on Oil filed Chemistry in New Orleans, 2-5 March.

[20] Pan, H., Firoozabadi, A., and Fotland, P. 1997. Pressure and Composition Effect on Wax Precipitation: Experimental Data and Model Results. *SPEPF*: 250 – 259.

[21] Elsharkawy, A.M., Al-Sahhaf, T.A., and Fahim, M.A. 2000. Wax Deposition from Middle East Crudes. *Fuel* 79: 1047-1055.

[22] Cazaux, G., Barre, L., and Brucy, F., 1998. Waxy Crude Cold Start: Assessment through Gel Structural Properties. Paper SPE 49213 presented at the SPE Annual Technical Conference and Exhibition in New Orleans, 27-30 September.

[23] Calange, S., Ruffier-Meray, V., Hehar, Emmanuel. 1997. Onset Crystallization Temperature and Deposit Amount for Waxy Crudes: Experimental Determination and Thermodynamic Modelling. Paper SPE

37239 presented at the SPE International Symposium on Oilfield Chemistry in Houston, TX, 18-21 Feb.

[24] Bordalo, S.N., and Oliveira, R.C., 2007. Experimental Study of Oil/Water Flow with Paraffin Precipitation in Subsea Pipelines. Paper SPE 110810 presented at the ATCE in Anaheim, Carlifornia, 11-14 Nov.

[25] Chang, C., Boger, D.V., and Nguyen, Q.D., 2000. Influence of Thermal History on the Waxy Structure of Statically Cooled Waxy Crude Oil. *SPE Journal* 5 (2): 148 – 157.

[26] Ekweribe, C. K. 2008. Quiescent Gelation of Waxy Crudes and Restart of Shut-In Subsea Pipelines. Ms. Thesis, University of Oklahoma.

[27] Venkatesan, R., Nagarajan, N.R., Paso, K., Yi, Y.-B, Sastry, A.M., Fogler, H.S. 2005. The Strength of Paraffin Gels Formed Under Static and Flow Conditions. *Chem. Eng. Sci*. 60 (13): 3587 – 3598.

[28] Chen, J., Zhang, J., and Li, H. 2004. Determining the Wax Content of Crude Oils by using Differential Scanning Calorimetry. Thermochimica Acta 410: 23-26.

[29] Hansen, A.B., Larsen, E., Pedersen, W.B., and Nielsen, A.B. 1991. Wax Precipitation from North Sea Crude Oils. *Energy Fuels*, 1991, *5* (6), pp 924–932. DOI: 10.1021/ef00030a022.

[30] Claudy, P., Letoffe, J. M., Benoit, C., and Jean, O., 1988. Crude oils and their Distillates: Characterization by Differential Scanning Calorimetry. *Fuel* 67: 58-61.

[31] Bhat, N. V. and Mehrotra, A. K. 2004. Measurement and Prediction of the Phase Behaviour of Wax– Solvent Mixtures: Significance of the Wax Disappearance Temperature. Industrial and Engineering Chemistry Research, 43: 3451-3461.

[32] Fong, N. and Mehrotra, A. K. 2007. Deposition under Turbulent Flow of Wax-Solvent Mixtures in a Bench-Scale Flow-Loop Apparatus with Heat Transfer. Energy and Fuels, 21, 1263.

[33] Holder, G. A., and J. Winkler, 1965a. Wax Crystallization from Distillate Fuels: I. Cloud and Pour Phenomena Exhibited by Solutions of Binary n-Paraffin Mixtures. *J. Inst. Petrol.*, 51, 228 _1965a.

[34] Holder, G.A., and Winkler, J. 1965b. Wax Crystallization from Distillate Fuels: II. Mechanism of Pour Depression. *J. Inst. Petrol.* 51: 235.

[35] Letoffe, J.M., Claudy, P., Kok, M.V., Garcin, M., and Volle, J.L. 1995. Crude Oils: Characterization of Waxes Precipitated on Cooling by D.S.C. and Thermomicroscopy. *Fuel.* 74: 810.

[36] Kane´, M., Djabourov, M., Volle, J., Lechairec, J., and Frebourg, G. 2003. Morphology of Paraffin Crystals in Waxy Crude Oils Cooled in Quiescent Conditions and Under Flow. *Fuel*. 82: 127–135.

[37] Dirand, M., Chevallier, V., Provost, E., Bouroukba, M., and Petitjean, D. 1998. Multicomponent Paraffin Waxes and Petroleum Solid Deposits: Structural and Thermodynamic State. *Fuel*. 77 (12): 1253-1260.

[38] Ferris, S. W.; Cowles, H. C. 1945. *Ind. Eng. Chem.* 37: 1054.

[39] Visintin, R.F.G., Lapasin, R., Vignati, E., D"Antona, P., and Lockhart, T.P. 2005. Rheological Behavior and Structural Interpretation of Waxy Crude Oil Gels. *Langmuir*. 21: 6240 – 6249.

[40] Radlinski, A. P.; Barre´, L.; Espinat, D. J. 1996. *Mol. Struct.* 51: 383.

[41] Henaut. I., Vincke, O., and Brucy, F. 1999. Waxy Crude Oil Restart: Mechanical Properties of Gelled Oils. Paper SPE 56771 presented at the SPE Annual Technical Conference and Exhibition, Houston, 3 -6 October.

[42] Vignati, Roberto Piazza, Ruben F G Visintin, Romano Lapasin, Paolo D Antona and Thomas P Lockhart. 2005. Wax crystallization and aggregation in a model crude oil. *J. Phys.: Condens. Matter* 17:S3651–S3660.

[43] Van den Tempel, M.J. 1958. Rheology of Plastic Fats. *Rheol. Acta* 1: 115-118.

[44] Van den Tempel, M. 1961. Mechanical Properties of Plastic-disperse Systems at Very Small Deformations. *J. Colloid Sci*. 16: 284-296.

[45] Venkatessan R. 2004. The Deposition and Rheology of Organic Gels. PhD Dissertation, Uni of Michigan.

[46] Paso, K.G. 2005. Paraffin Gelation Kinetics. PhD Dissertation, University of Michigan.

[47] Lopes-da-Silva, J.A., and Coutinho, J.A.P. 2004. Dynamic Rheological Analysis of the Gelation Behaviour of Waxy Crude Oils. *Reol. Acta* 43: 433 – 441.

[48] Lopes-da-Silva, J.A., and Coutinho, J.A.P. 2007. Analysis of the Isothermal Structure Development in Waxy Crude Oils under Quiescent Conditions. *Energy & Fuels*. 21 (6): 3612 – 3617.

[49] Venkatesan, R., Singh, P., and Fogler, H.S. 2002. Delineating the Pour Point and Gelation Temperature of Waxy Crude Oils. SPE J. 349 – 352.

[50] LiC, Yang Q, Lin M. 2009. Effects of Stress and Oscillatory Frequency on the Structural Properties of Daqing Gelled Crude oil at Different Temperatures. J Pet Sci Eng 65:167–170.

[51] Bingham, E. C., Green, H. P., 1919. A Plastic Material and not a Viscous Liquid; The Measurement of its Mobility and Yield Value. *Proc. Am. Soc. Test Mater* 20 (2), 640-675.

[52] Gill, F., and Russell, R.J. 1954. Pump Ability of Residual Fuel Oils. *Ind. Eng. Chem*. 46(6): 1264 -1278.

[53] Davenport, T. C. and R. J. Russell. 1960. The Full-Scale Pumping of Admiralty Fuel Oil and its Relation to Laboratory Tests. *J. Inst. Petroleum.* 46 (437), 143-160.

[54] Russell, R. J. 1960. The Yield Value of Admiralty Fuel Oil. *J. Inst. Pet.* 46 (438), 199-208.

[55] Davenport, T. C. and Somper, R. S. H. 1971. The Yield Value and Breakdown of Crude Oil Gels. *J. Inst. Pet.* 57 (554), 86-105.

[56] Verschuur, E., Verheul, C. M., and Hartog, A. P. D. 1971. Pilot-Scale Studies on Restarting Pipelines Containing Gelled Waxy Crudes. *J. Inst. Pet.* 57 (555): 139-146.

[57] Carniani, C., and Merlini, SM., 1996. Basic Design of Waxy Oil Transportation through Improved Lab Testing. Paper SPE 36836 presented at the SPE European Petroleum Conference in Milan, Italy, 22 -24 October.

[58] Borghi, G. P., Correra, S., Merlini, M., and Carniani, C., 2003. Prediction and Scale-up of Waxy Oil Restart Behavior. Paper SPE 80259 presented at the SPE International Symposium on Oilfield Chemistry, Houston, 5 – 8 February.

[59] Lee, H.S., Singh, P., Thomason, W.H. and Fogler, H.S. 2007. Waxy Oil Gel Breaking Mechanisms: Adhesive versus Cohesive Failure. *Energy & Fuels* 22: 480–487.

[60] Amhamed, A. I., 2009. Rheology and Pipelines Start up Pressures of Waxy Crude Oils. PhD Thesis, School of Engineering, Design and Technology, University of Bradford.

[61] Karan, K., Ratulowski, J., & German, P. 2000. Measurement of Waxy Crude Properties Using Novel Laboratory Techniques. Society of Petroleum Engineers. DOI: 10.2118/62945-MS.

[62] Abdelrahim, A.M.A., 2011. Rheology and Pumping of Waxy Crude Oils. School of Engineering. PhD thesis Design and Technology, University of Bradford.

[63] Perkins, T. K. and Turner, J. B. 1971. Starting Behavior of Gathering Lines and Pipelines Flied with Gelled Prudhoe Bay Oil. *J. Pet. Technol*. 23: 301-308.

[64] Russell, R.J. and Chapman, E.D. 1971. The Pumping of 85°F Pour Point Assam (Nahorkatiya) Crude Oil at 65°F. *J. Inst. Pet.* 57: 117.

[65] Sifferman, T.R. 1979. Flow Properties of Difficult-To-Handle Waxy Crude Oils. JPT: 1042-1050.

[66] Cawkwell, M.G., and Charles, M.E., 1989. Characterization of Canadian Arctic “Thixotropic Gelled Crude Oils Utilizing an Eight-Parameter Model”. *J. Pipelines* 7: 251-264.

[67] Paso, K. G., and Fogler H. S. 2004. Bulk Stabilization in Wax Deposition Systems. *Energy & Fuels 18*: 1005-1013.

[68] Coutinho, J.A.P., Lopes da Silva, J.A., Ferreira, A., Soares, M.R., Daridon, J.L. 2003. Evidence for the Aging of Wax Deposits in Crude Oils by Ostwald Ripening. *Petrol Sci Technol* 21:381–39.

[69] Pedersen, K.S., Skovborg, P., and Ronningsen, H.P. 1991. Wax Precipitation from North Sea Crude Oils. 4. Thermodynamic Modeling. *Energy Fuel*. 5: 924 – 932.

[70] Kriz P., Anderson, S.I. 2005. Effect of Asphaltenes on Crude Oil Waxy Crystallization. Energy & Fuels 19: 948 – 953.

[71] R. F. G. Visintin, T. P. Lockhart, R. Lapasin, P. D´Antona 2008. Structure of waxy crude oil emulsion gels. Journal of Non-Newtonian Fluid Mechanics 149, 2008 34-39.

[72] Petrellis, N.C., and Flumerfelt, R.W. 1973. Rheological Behavior of Shear Degradable Oils: Kinetic and Equilibrium Properties. *Can. J.Chem. Eng.* 51: 291 - 301.

[73] Fung, G., W.P. Backhaus, S. McDaniel, and M. Erdogmus, 2006. To Pig or Not To Pig: The Marlin Experience with Stuck Pig. Offshore Technology Conference, Houston, TX (2006).

[74] Ghedamu, M., Watkinson, A. P., Epstein, N. 1997. Mitigation of Wax Buildup on Cooled Surfaces, In Fouling Mitigation of Industrial Heat-Exchange Equipment. Panchal, C. B., Bott, T. R., Somerscales, E. F. C., Toyama, S., Editors. Begel House: New York, p 473489.

[75] Cordoba, A. J. and Schall, C. A. 2001b. Solvent Migration in a Paraffin Deposit. Fuel, 80, 1279-84.

[76] Bidmus, H.O. and Mehrotra, A.K. 2012. Comments on: The effect of operating temperatures on wax deposition (by Huang et al.). Energy & Fuels, 26(6), 3963-3966.

[77] Bidmus, H. O., and Mehrotra, A. K. 2009. Solids Deposition during “Cold Flow” of Wax-Solvent Mixtures in a Flow-loop Apparatus with Heat Transfer. Energy & Fuels, 23, 3184– 3194.

[78] Bidmus, H. and Mehrotra, A. K. 2008a. Measurement of the Liquid-Deposit Interface Temperature during Solids Deposition from Wax-Solvent Mixtures under Static Cooling Conditions. Energy and Fuels, 22(2), 1174-82.

[79] Bidmus, H. and Mehrotra, A. K. 2008b. Measurement of the Liquid–Deposit Interface Temperature during Solids Deposition from Wax–Solvent Mixtures under Sheared Cooling. Energy and Fuels, 22(6), 4039-48.

[80] Bidmus, H. O. 2003. A Thermal Study of Wax Deposition from Paraffinic Mixtures. M.Sc. Thesis, Department of Chemical and Petroleum Engineering, University of Calgary.

[81] Bidmus, H.O. and Mehrotra, A. K. 2004. Heat-Transfer Analogy for Wax Deposition from Paraffinic Mixtures. Industrial and Engineering Chemistry Research, 43: 791-803.

[82] Mehrotra, A. K. and Bidmus, H. O. 2005. Heat-Transfer Calculations for Predicting Solids Deposition in Pipeline Transportation of “Waxy“ Crude Oils. In Heat Transfer Calculations, M. Kutz (ed), McGraw-Hill: New York, NY, Chapter 25.

[83] Bhat, N. V. and Mehrotra, A. K. 2005. Modeling of Deposit Formation from "Waxy" Mixtures via Moving Boundary Formulation: Radial Heat Transfer under Static and Laminar Flow Conditions. Industrial and Engineering Chemistry Research, 44, 6948.

[84] Bhat, N. V. and Mehrotra, A. K. 2006. Modeling of Deposition from "Waxy" Mixtures in a Pipeline under Laminar Flow Conditions via Moving Boundary Formulation. Industrial and Engineering Chemistry Research, 45(25), 8728-37.

[85] Bhat, N.V. and Mehrotra, A.K. 2008. Modeling the effect of shear stress on the composition and growth of the deposit layer from “waxy” mixtures under laminar flow in a pipeline. Energy & Fuels, 22(5), 3237-3248.

[86] Mehrotra, A. K. and Bhat, N. V. 2007. Modeling the Effect of Shear Stress on Deposition from “Waxy” Mixtures under Laminar Flow with Heat Transfer. Energy and Fuels, 21, 1277.

[87] Mehrotra, A. K. and Bhat, N. V. 2010. Deposition from 'waxy' mixtures under turbulent flow in pipelines: Inclusion of a viscoplastic deformation model for deposit aging. Energy & Fuels, 24(4), 2240-2248.

[88] Parthasarathi, P. and Mehrotra, A. K. 2005. Solids Deposition from Multicomponent Wax-Solvent Mixtures in a Benchscale Flow-Loop Apparatus with Heat Transfer. Energy and Fuels, 19:1387-1398,

[89] Tiwary, R. and Mehrotra, A. K. 2009. Deposition from wax–solvent mixtures under turbulent flow: Effects of shear rate and time on deposit properties. Energy & Fuels, 23(3), 1299-1310.

[90] Arumugam, S., Kasumu, A.S. and Mehrotra, A.K. 2012. Modeling the static cooling of wax-solvent mixtures in a cylindrical vessel. Proceedings of 9th International Pipeline Conference, Calgary, Alberta, Canada, Sept 24-28, 2012, IPC2012-90691.

[91] Arumugam, S., Kasumu, A. S. and Mehrotra, A. K. 2013. Modeling of solids deposition from "waxy" mixtures in "hot flow" and "cold flow" regimes in a pipeline operating under turbulent flow. Energy & Fuels, 27, 6477-6490,

[92] Kasumu, A. S. and Mehrotra, A. K. 2013. Solids deposition from two-phase wax–solvent–water “waxy” mixtures under turbulent flow. Energy & Fuels, 27, 1914-1925.

[93] Cordoba, A. J. and Schall, C. A. 2001a. Application of a Heat Transfer Method to determine Wax Deposition in a Hydrocarbon Mixture. Fuel, 80, 1285-91.

[94] Burger, E. D.; Perkins, T. K.; Striegler, J. H. 1981. Studies of Wax Deposition in the Trans-Alaska Pipeline. J. Pet. Tech. 1981, 33, 1075.

[95] Creek, J. L.; Lund, H. J.; Brill, J. P.; Volk, M. 1999. Wax Deposition in Single Phase Flow. Fluid Phase Equilib. 1999, 801, 158.

[96] Ramirez-Jaramillo, E.; Lira-Galeana, C.; Manero, O. 2004. Modeling Wax Deposition in Pipelines. Pet. Sci. Tech. 2004, 22, 821.

[97] Singh, P.; Venkatesan, R.; Fogler, H. S.; Nagarajan, N. 2001. Morphological Evolution of Thick Wax Deposits during Aging. AIChE J. 2001, 47,6.

[98] Weingarten, J. S. and Euchner, J. A. 1986. Methods for Predicting Wax Precipitation and Deposition. SPE paper 15654.

[99] Svendson, J. A. 1993. Mathematical Modeling of Wax Deposition in Oil Pipeline Systems. AIChE Journal, 39, 1377.

[100] Brown, T. S., Niesen, V. G. and Erickson, D. D. 1993. The Effects of Light Ends and High Pressure on Paraffin Formation. SPE paper 28505.

[101] Erickson, D. D., Niesen, V. G., Brown, T. S. 1993. Thermodynamic Measurement and Prediction of Paraffin Precipitation in Crude Oil. SPE Paper No. 26604, 933-948.

[102] Hsu, J. J. C. and Brubaker, J. P. 1995. Wax Deposition Measurement and Scale-Up Modeling for Waxy Live Crudes under Turbulent Flow Conditions. SPE paper 29976.

[103] Merino-Garcia, D.; Margarone, M.; Correra, S. 2007. Kinetics of Waxy Gel Formation from Batch Experiments. Energy Fuels. 2007, 21, 1287.

[104] Clavell-Grunbaum, D., Strauss, H. L., Snyder, R. G. 1997. Structure of Model Waxes: Conformational Disorder and Chain Packing in Crystalline Multicomponent n-Alkane Solid Solutions. Journal of Physical Chemistry B, 101, 335-343.

[105] Hammami, A. and Raines, M. A. 1999. Paraffin Deposition from Crude Oils. Comparison of Laboratory Results with Field Data. SPE J., 4 (1), 9-18.

[106] Patton, C. C. and Casad, B. M. 1970. Paraffin Deposition from Refined Wax-Solvent Systems. SPE paper 2503.

[107] Woo, G. T., Garbis, S. J., Gray, T. C. 1984. Long-Term Control of Paraffin Deposition. SPE Paper No. 13126.

[108] Misra, S., Baruah, S. and Singh, K. 1995. Paraffin Problems in Crude Oil Production and Transportation: A Review. SPE Prod. Facil. 10 (1), 50.

[109] Meray, R. V., Volle, J.L., Schranz, C. J. P., Le Marechal and Behar, E. 1993. Influence of Light Ends on the Onset Crystallization Temperature of Waxy Crudes Within the Frame of Multiphase Transport. SPE paper 26549.

[110] Agrawal, K.M., Khan, H.U., Surianarayanan, M. and Joshi, G.C. 1990. Wax Deposition of Bombay High Crude Oil under Flowing Conditions. Fuel, 69, 794-796.

[111] Wu, C. H., Wang, K. S., Shuler, P. J., Tang, Y., Creek, J. L., Carlson, R. M. and Cheung, S. 2002. Measurement of Wax Deposition in Paraffin Solutions. AIChE Journal, 48:2107-2110.

[112] Cole, R. J. and Jessen, F. W. 1960. Paraffin deposition. Oil & Gas J., 58 (38), 87-91.

[113] Jorda, R. M. 1966. Paraffin Deposition and Prevention in Oil Wells. SPE paper 1598.

[114] Majeed, A., Bringedai, B. and Overa, S. 1990. Model Calculates Wax Deposition for N. Sea Oils. Oil & Gas J., 18, 63-69.

[115] Kok, M. V., Saracoglu, O. 2000. Mathematical Modelling Of Wax Deposition in Crude Oil Pipelines (Comparative Study). SPE Asia Pacific Oil and Gas Conference, SPE Paper No. 64514.

[116] Mehrotra, A. K. 1990. Comments on: Wax deposition of Bombay high crude oil under flowing conditions. Fuel, 69, 1575-1576.

[117] Kraynik, A.M., 1990. ER fluid standards: comments on fluid rheology. In: Carlson, J.D., Sprecher, A.F., Conrad, H. (Eds.), Proceedings of the Second International Conference on ER Fluids. Raleigh, 1990. Technomic Publishing Company.

[118] Houwink, R., 1958. Elasticity, Plasticity and Structure of Matter. Cambridge University Press, New York.

[119] Venkatesan, R., Östlund, J., Chawla, H., Wattana, P., Nydén, M., and Fogler, H.S. 2003. The Effect of Asphaltenes on the Gelation of Waxy Oils. *Energy & Fuels*.

[120] Smith PB, Ramsden, RMJ, 1978. The Prediction of oil Gelation in Submarine Pipelines and the Pressure Required for Restarting Flow. Eur. Offshore Pet. Conf. doi:http://dx.doi.org/10.2118/8071-MS.

[121] Guo, L.P., Wang, Y., Shi, S., Yu, X.Y. and Chen, X. 2015. Study on Thixotropic Properties of Waxy Crude Oil Based on Hysteresis Loop Area. Engineering, 7, 469-47.

APPENDIX

Thermal Properties and Parameters for Wax Deposition Model Equations

Calculation of the heat transfer coefficient (h_l) and Nusselt number (Nu)

For LO crude oil;

$$h_l = \rho_l c_{p_l} (\frac{dT_l}{dt}) \frac{r_i}{-2(T_l - T_{r_i})} = 813 \text{ x } 2.1(-0.0177) \frac{0.06}{-2(9.2)}$$

= 0.0985 kJ m^{-2} s^{-1} °C^{-1}

$$Nu_l = -\frac{d\Theta_l}{d\tau} / \frac{2(\Theta_l - \Theta_R)}{R}$$

= 0.94 / 2 x 7.65 = 0.0614 (see the table below for LO data)

Calculating of $\boldsymbol{Nu_l}$ using the expression of $\boldsymbol{h_l}$

$$Nu = \frac{h_l R}{k_l} = \frac{0.0985 \times 0.06}{0.095} = 0.0622$$

For BP crude oil;

$$h_l = \rho_l c_{p_l} \left(\frac{dT_l}{dt}\right) \frac{r_i}{-2(T_l - T_{r_i})} = 808 \text{ x } 2.1(-0.0166) \frac{0.06}{-2(12.1)}$$

= 0.07 kJ m^{-2} s^{-1} °C^{-1}

$$Nu_l = -\frac{d\Theta_l}{d\tau} / \frac{2(\Theta_l - \Theta_R)}{R}$$

= 0.032 / 2 x 0.37 = 0.043 (see the table below for BPO data)

Calculating of $\boldsymbol{Nu_l}$ using the expression of $\boldsymbol{h_l}$

$$Nu = \frac{h_l R}{k_l} = \frac{0.07 \times 0.06}{0.1} = 0.042$$

Table of static cooling data and dimensionless variables for BPO at 1.1°C/min.

Time min	Time s	TW T (°C)	TW T (K)	TL (°C)	TL (K)	ΘL	dΘL	Θi	ΘL-Θi	τ	dτ	α	ξi	dΘL/dτ	ΘL-Θi/ξi	Nu
0	0	60.0	333.2	60.0	333.2	1.00	0.00	1.00	0.00	0	0	0.000059	1	0.00	0.00	0.000
3	180	58.2	331.4	59.8	333.0	0.99	-0.01	0.94	0.06	3	3	0.000059	1	0.00	0.06	0.019
6	360	55.0	328.1	59.3	332.4	0.97	-0.02	0.82	0.15	6	3	0.000059	1	-0.01	0.15	0.021
9	540	51.8	325.0	58.2	331.3	0.93	-0.04	0.70	0.23	9	3	0.000059	1	-0.01	0.23	0.031
12	720	48.6	321.7	56.2	329.4	0.86	-0.07	0.59	0.27	12	3	0.000059	1	-0.02	0.27	0.043
15	900	45.2	318.4	53.8	326.9	0.77	-0.09	0.47	0.31	15	3	0.000059	1	-0.03	0.31	0.047
18	1080	41.9	315.0	51.5	324.7	0.69	-0.08	0.34	0.35	18	3	0.000059	1	-0.03	0.35	0.040
21	1260	38.5	311.7	48.9	322.0	0.60	-0.10	0.22	0.37	21	3	0.000059	1	-0.03	0.37	0.044
24	1440	35.2	308.3	46.1	319.3	0.50	-0.10	0.10	0.39	24	3	0.000059	1	-0.03	0.39	0.042
27	1620	31.9	305.0	43.3	316.5	0.40	-0.10	-0.02	0.41	27	3	0.000059	1	-0.03	0.41	0.041
30	1800	28.6	301.7	40.5	313.6	0.29	-0.10	-0.14	0.43	30	3	0.000059	1	-0.03	0.43	0.040
33	1980	25.4	298.5	37.8	311.0	0.20	-0.10	-0.25	0.45	33	3	0.000059	1	-0.03	0.45	0.036
36	2160	22.3	295.5	35.7	308.8	0.12	-0.08	-0.36	0.48	36	3	0.000059	1	-0.03	0.48	0.027
39	2340	19.4	292.6	34.0	307.1	0.06	-0.06	-0.47	0.53	39	3	0.000059	1	-0.02	0.53	0.020
42	2520	16.6	289.7	32.3	305.5	0.00	-0.06	-0.57	0.57	42	3	0.000059	1	-0.02	0.57	0.017

Table of static cooling data and dimensionless variables for LO at 1.1°C/min.

Time min	Time s	TW T (°C)	TW T (K)	TL (°C)	TL (K)	ΘL	dΘL	Θi	ΘL-Θi	τ	dτ	α	ξi	dΘL/dτ	ΘL-Θi/ξi	Nu
0	0	85	358.15	85.0	358.2	23.3	0.0	23.3	0.0	0	0	0.000062	1	0.00	0.00	0.000
3	180	82.7	355.85	84.4	357.5	22.7	-0.6	21.0	1.7	3	3	0.000062	1	-0.20	1.67	0.061
6	360	79.14	352.29	83.2	356.4	21.5	-1.2	17.4	4.1	6	3	0.000062	1	-0.38	4.06	0.046
9	540	75.53	348.68	81.0	354.2	19.3	-2.2	13.8	5.5	9	3	0.000062	1	-0.70	5.47	0.064
12	720	71.64	344.79	78.4	351.6	16.7	-2.6	9.9	6.8	12	3	0.000062	1	-0.82	6.76	0.061
15	900	67.75	340.9	75.4	348.6	13.7	-3.0	6.0	7.7	16	3	0.000063	1	-0.94	7.65	0.061
18	1080	63.68	336.83	72.1	345.2	10.4	-3.3	2.0	8.4	19	3	0.000063	1	-1.02	8.42	0.061
21	1260	59.6	332.75	68.5	341.7	6.8	-3.6	-2.1	8.9	22	3	0.000063	1	-1.09	8.90	0.062
24	1440	55.42	328.57	66.0	339.2	4.3	-2.5	-6.3	10.6	25	3	0.000064	1	-0.75	10.63	0.035
27	1620	51.38	324.53	64.1	337.3	2.4	-1.9	-10.3	12.7	29	3	0.000064	1	-0.59	12.73	0.023
30	1800	47.74	320.89	62.4	335.6	0.7	-1.7	-14.0	14.7	32	3	0.000064	1	-0.51	14.69	0.017
33	1980	43.69	316.84	61.2	334.3	-0.6	-1.3	-18.0	17.5	35	3	0.000064	1	-0.38	17.48	0.011

Data of mass fraction vs. temperature (T) and dimensionless temperature (Θ) cxx

For LO crude oil;

$x_w = -7E\text{-}10T^5 + 1E\text{-}06T^4 - 0.0007T^3 + 0.1981T^2 - 29.331T + 1728.9$

$X_w = -0.0059\Theta^5 - 0.0404\Theta^4 - 0.0579\Theta^3 + 0.082\Theta^2 + 0.0084\Theta - 0.0035$

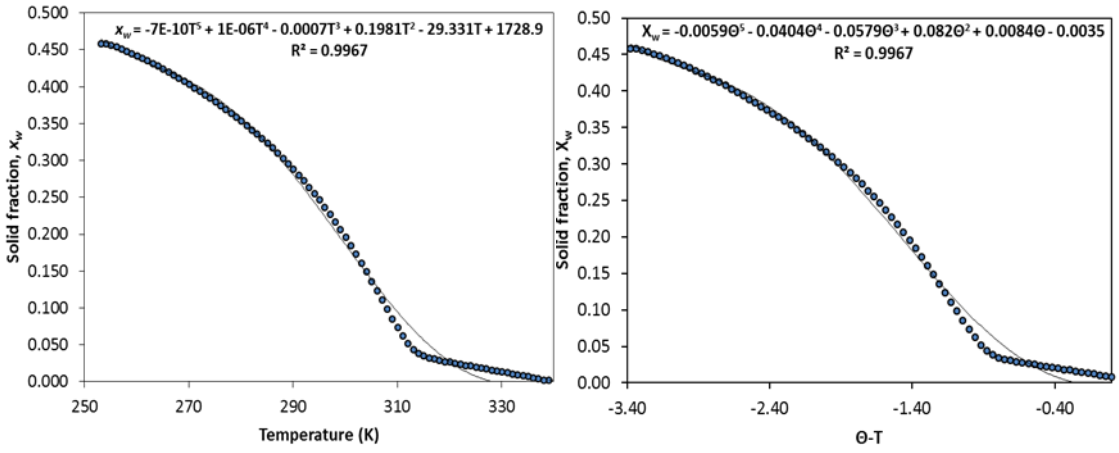

For BP crude oil;

$x_w = -6E\text{-}10T^5 + 9E\text{-}07T^4 - 0.0005T^3 + 0.1482T^2 - 20.993T + 1185$

$X_w = -0.011\Theta^5 - 0.0359\Theta^4 + 0.002\Theta^3 + 0.0806\Theta^2 - 0.043\Theta + 0.0048$

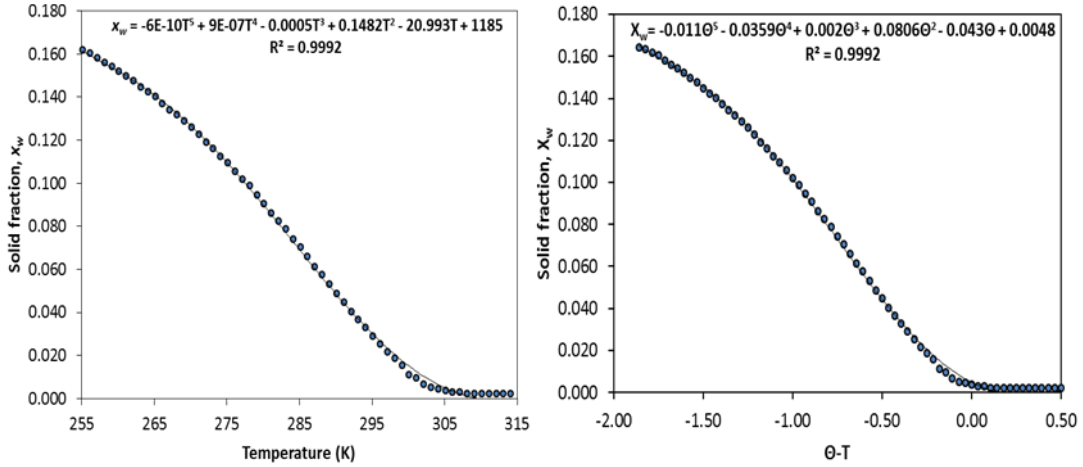

Data of latent heat of wax vs. temperature (T) and dimensionless temperature (Θ)

For LO crude oil;

Enthalpy = overall latent heat at -20^{o}C = 48.605 J/g (from the figure in next page).

λ = -1E-07T^{5} + 0.0001T^{4} - 0.0887T^{3} + 26.413T^{2} - 3910.9T + 230514

H_w = -9.2417Θ^{5} - 64.778Θ^{4} - 97.998Θ^{3} + 132.49Θ^{2} + 16.842Θ - 9.4972

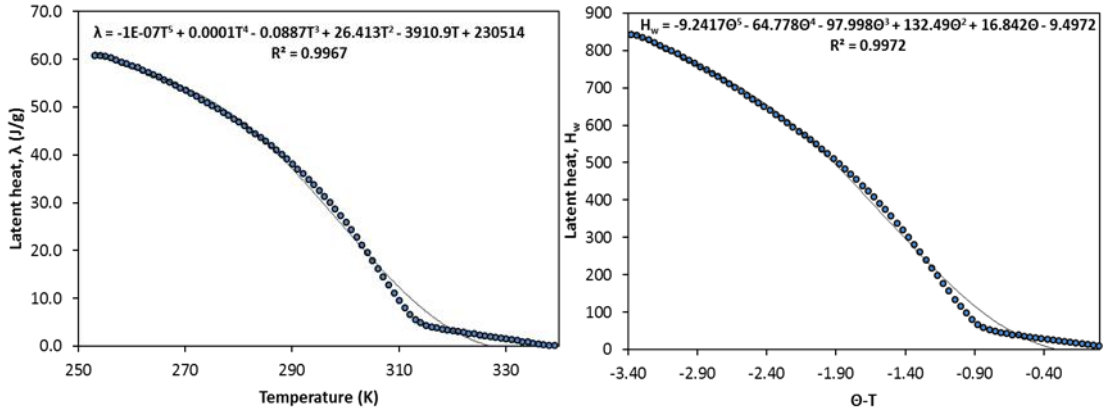

For BP crude oil;

Enthalpy = overall latent heat at -20^{o}C = 14.481 J/g (from the figure in next page).

λ = -8E-08T^{5} + 0.0001T^{4} - 0.0695T^{3} + 19.764T^{2} - 2799.1T + 158002

H_w = -19.847Θ^{5} - 67.883Θ^{4} - 1.8794Θ^{3} + 157.96Θ^{2} - 82.069Θ + 4.9909

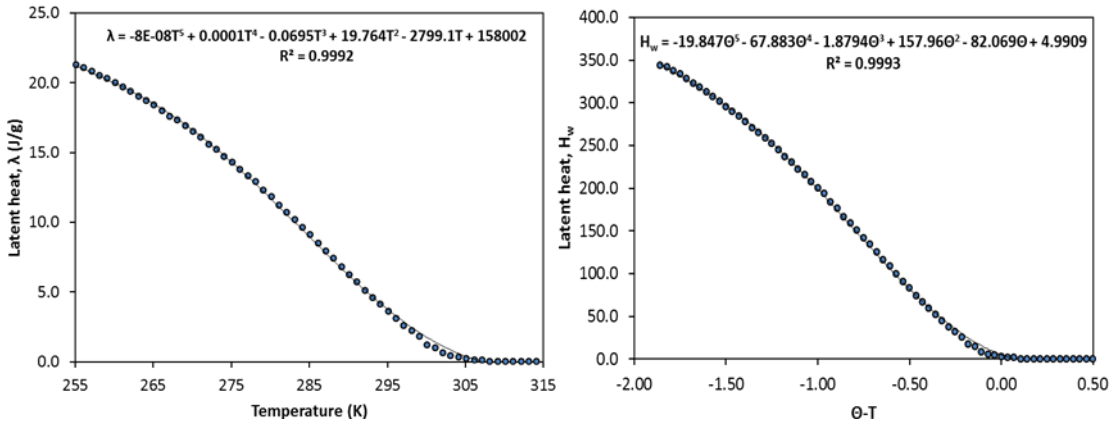

Data of specific heat capacity (C_p) vs. dimensionless temperature (Θ);

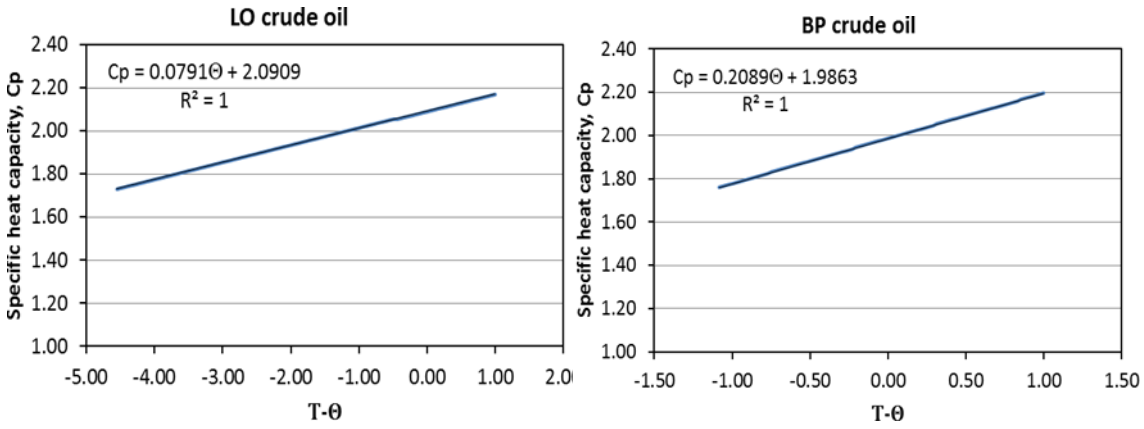

For LO crude oil;

$$C_p = 0.0791\,\Theta + 2.0909$$

For BP crude oil;

$$C_p = 0.2089\Theta + 1.9863$$

Data of thermal conductivity (k) vs. dimensionless temperature (Θ);

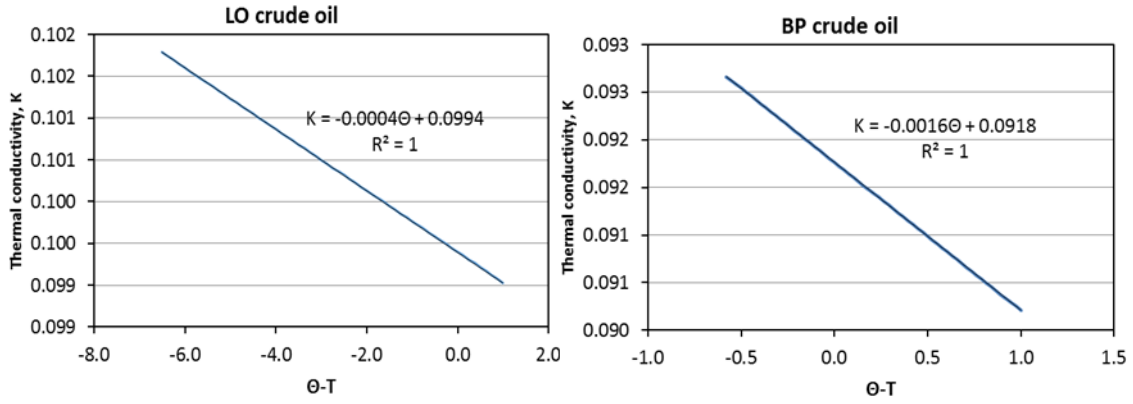

For LO crude oil;

K = -0.0004Θ + 0.0994

For BP crude oil;

K = -0.0016Θ + 0.0918

Note: Typical thermal conductivity values for crude oils reported in literature range from 0.10 to 0.42 $Wm^{-1}K^{-1}$ (Stryker and Sparrow, 1990; Bidmus, 2003; Fong and Mehrotra, 2007).

Density and specific gravity

Table of density and specific gravity for the crude oils at different temperatures

Temperature (^{o}C)	Volume of Oil (mL)		Mass of Oil (g)		Density (kg/m^3)		Specific Gravity	
	BP	LO	BP	LO	BP	LO	BP	LO
15.6 (60^{o}F)	50	50	42	43	840	860	0.841	0.861
20	50.3	50.1	42	43	835	858	0.836	0.859
25	50.4	50.4	42	43	833	853	0.834	0.854
30	50.7	51	42	43	828	843	0.829	0.844
35	51	51.2	42	43	824	840	0.825	0.841
40	51.2	51.5	42	43	820	835	0.821	0.836
45	51.4	51.8	42	43	817	830	0.818	0.831
50	51.5	52.2	42	43	816	824	0.817	0.825
55	51.7	52.5	42	43	812	819	0.813	0.820
60	51.9	52.7	42	43	809	816	0.810	0.817
65	52	52.9	42	43	808	813	0.809	0.814
70	52	52.9	42	43	808	813	0.809	0.814

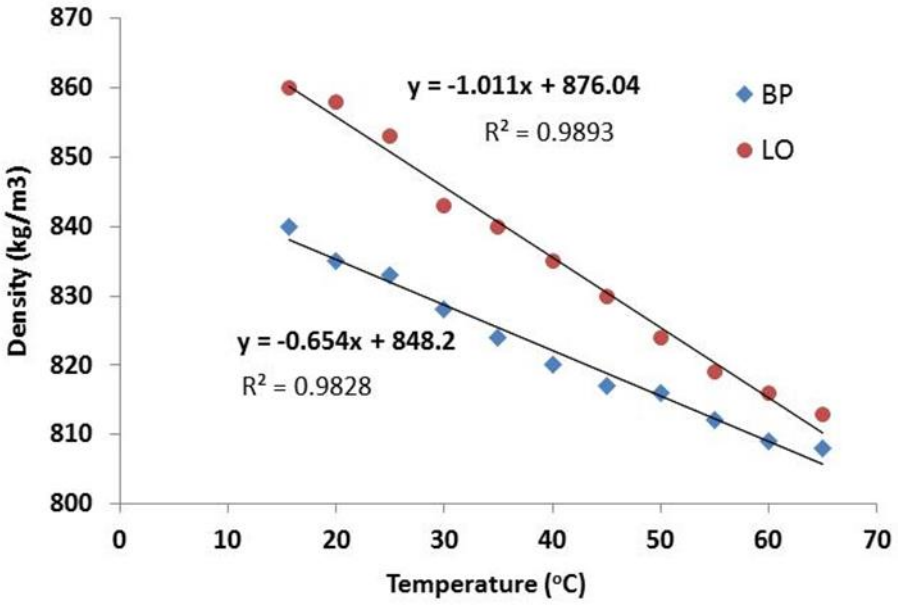

Figure of density and specific gravity variation with temperature for the crude oils

Note: The small variation in densities with temperatures of the crude oils may be neglected.